Post-Polymerization Functionalization Of Conjugated Polymer Backbones And Its Applications

Shengyu Cong

Submitted in partial fulfilment of the requirements for the degree of

Doctor of Philosophy in Chemistry

Department of Chemistry, Imperial College London

October 2019

“Every scientist dreams of doing something that can help the world”

TU Youyou (Nobel Prize in Physiology and Medicine awarded in 2015)

Declaration

This thesis is about my research work at the Department of Chemistry, Imperial College London, from October 2015 to March 2019, under the supervision by Professor Martin Heeney. The contents in this thesis are all my original work, unless stated otherwise.

Shengyu Cong

Copyright Declaration

The copyright of this thesis rests with the author and is made available under a Creative Commons Attribution Non-Commercial No Derivatives license. Researchers are free to copy, distribute or transmit the thesis on the condition that they attribute it, that they do not use it for commercial purposes and that they do not alter, transform or build upon it. For any reuse or redistribution, researchers must make clear to others the license terms of this work.

Contributions

With the help of people below, I can finish this thesis.

Here, I want particularly to give my thanks to the following people for their contributions in this thesis:

Contact angle measurement was tested by Sam Hillman at the Department of Materials.

Organic solar cell devices were fabricated and tested by Dr. Shahid at the Department of Chemistry.

Polymer light emitting diode devices were fabricated and tested by YAN Hao at the Department of Physics.

Dynamic light scattering measurement was tested by Chicheng Huang at the Department of Materials.

X-ray photoelectron spectroscopy measurement was tested by Dr Gwilherm Kerherve at the Department of Materials.

Acknowledgements

The past four years from 2015 to 2019 in London was really a great experience for me. The research at Imperial College was really interesting and I would like to thank the following people for their help and support:

I give my thanks to the CSC-Imperial scholarship which provided the funding for me to carry out research at Imperial College London. Without it, I could not come to London in 2015 and there will be no story I can tell here.

I give my thanks to my supervisor, Professor Martin Heeney who gave me the opportunity to carry out PhD research in his group. Martin is always helpful and he gave me so many useful suggestions which I really appreciated, as well as the freedom he have given me to try different ideas. I learnt many good characteristics from him and I firmly believe this will be so useful in my whole life.

I give my thanks to Dr Zhuping Fei, who is now a professor in Tianjin University (China). He gave me so much useful advice on lab work and I will always remember the days we watched premier league together.

Working in the Harwood lab was a really wonderful experience and I want to give my thanks to the members from the Heeney and McCulloch groups, who I have worked with over the last four years: Zhuping Fei, Yang Han, Munazza, Haojie, Pierre, Jess, Adam Creamer, Iain, Simeng, Brett, Adam Marsh, Tingmang, Peter, Notina, Tom, Charlotte, Qiao, Bowen, Wenmin, Florian, Filip; Cameron, Wan Yue, Petruta, Alex, Matt, Mark, James and many other members. Forgive me for not giving everyone's name, but I will always remember the days we spent together. I want to give my thanks to Shahid, Hao Yan, Sam who made a contribution to my thesis. A big thank to Huang, who did the dynamic light scattering measurement for me effectively. Thanks for being so supportive over the last few days, it has been invaluable.

Finally, I give my thanks to my family, Mum, Dad, my grandparents and my twin brother, you always give me the support whenever I need. You support the decision I made every

time and give me very helpful advice. Without your help, I could not go through the difficulties. More importantly, I know whenever I need the help and support, you are all there and always there for me, which lets me feel what love is.

Abstract

A wide range of polymerization methods for the synthesis of polymers with functional groups have been well investigated. However, there are some functional groups which may prevent polymerization or lead to side reactions. Post-polymerization modification, also named as polymer-analogous modification, is an alternative method to overcome such limitations. The synthesis of functional polymeric materials by post-polymerization modification is generally based on the polymerization monomers containing functional groups which are inert in the polymerization conditions but can be quantitatively converted into other functional groups subsequently.

Recently, the fluorinated polymers have been widely used to synthesize diverse polymers with functional groups. This thesis focuses on synthesizing different functional polymers by post-polymerization via fluorinated polymers. From Chapter 2 to Chapter 5, the fluorinated polymers were synthesized first, then different functional groups were grafted to the conjugated backbones by post-polymerization.

Based on this strategy, several functional polymers have been synthesized and investigated in this thesis. To improve the hydrophilicity of conjugated polymers, **F8BT-OC$_8$**, **F8BT-m** (m=2, 3, 4, 5, 6) and **F8BT-PEG** with hydrophilic side chains were synthesized by post-polymerization in Chapter 2. The contact angle measurement demonstrated that the hydrophilicity was improved by grafting hydrophilic side chains. Conjugated polyelectrolytes with modulated density of ionic groups have been synthesized in Chapter 3**.** The performances of OPV and OLED devices were both improved using the conjugated electrolytes as interfacial layers. Also, the effect of ionic density on conjugated polyelectrolytes used in OPV and OLED devices was investigated. A new thermo-, pH/CO_2-responsive fluorescent graft copolymer was synthesized in Chapter 4. The approach of post-polymerization via fluorinated polymer substitution gives us a very effective strategy to synthesize multi-stimuli-responsive polymers. Water soluble and pH responsive conjugated polyampholytes were synthesized in Chapter 5. With changing pH, the

polyampholytes showed intermolecular interactions via electrostatic complexation between positive and negative moieties.

Contents

Declaration 3

Copyright Declaration 4

Contributions 5

Acknowledgements 6

Abstract 8

Contents 10

Publications 15

Abbreviations 16

1 Introduction 19

1.1. Conjugated polymers 19

1.2. Characterizing polymer molecular weights 20

1.3 Synthesis of conjugated polymers 21

1.4 Post-polymerization modification 24

1.5 Post-polymerization modification reactions 26

1.5.1 Post-polymerization modification via thiol-ene addition 27

1.5.2 Post-polymerization modification of epoxides, anhydrides, oxazolines, isocyanates 27

1.5.3 Post-polymerization modification via active esters 28

1.5.4 Post-polymerization modification via Diels-Alder reactions 29

1.5.5 Post-polymerization modification via thiol-disulfide exchange 29

1.5.6 Post-polymerization modification via Michael-type addition 30

1.5.7 Post-polymerization modification via azide alkyne cycloaddition reactions 31

1.5.8 Post-polymerization modification of ketones and aldehydes 32

1.6 Post-polymerization modification of nucleophilic fluoride substitution 32
1.7 Graft copolymers synthesized by post-polymerization 34
1.7.1 The grafting-onto strategy 35
1.7.2 The grafting-through strategy 36
1.7.3 The grafting-from strategy 37
1.8 Thesis aims and overview 38
2 Hydrophilicity control of conjugated polymers by post-polymerization modification 40
2.1 Introduction 40
2.2 Synthesis of monomers and polymers 41
2.3 Optical properties 45
2.3.1. Absorption spectra 45
2.3.2. Emission spectra 47
2.4 Electronic properties 48
2.5 Air photoemission spectroscopy measurements 51
2.6 Thermal properties 53
2.7 Hydrophilicity 55
2.8 Contact angle measurement 57
2.9 Conclusions 59
2.10 Experimental methods 60
2.10.1 CV measurement 60
2.10.2 APS measurement 60
2.10.3 Contact angle measurement 60
2.10.4 Materials 61
2.10.5 Synthesis 61

3 Conjugated polyelectrolytes with modulated density of ionic groups as an interfacial layer in OPVs and OLEDs 69
3.1 Introduction 69
3.2 Synthesis 72
3.2.1 Synthesis routes 72
3.2.2 NMR analysis 74
3.2.3 Fourier-transform infrared spectroscopy 75
3.2.4 X-ray photoelectron spectroscopy 76
3.3 CPEs in polar solvents 77
3.4 Optical properties 78
3.4.1 Absorption spectra 78
3.4.2 Emission spectra 79
3.5 Electronic properties 81
3.6 OPV performance 82
3.7 OLED performance 87
3.8 Conclusions 93
3.9 Experimental methods 94
3.9.1 OPV device fabrication 94
3.9.2 OLED device fabrication 94
3.9.3 Materials 95
3.9.4 Synthesis 95
4 A new thermo-, pH and CO_2-responsive fluorescent graft copolymer 98
4.1. Introduction 98
4.2. Synthesis of monomers and graft copolymers 101

4.2.1 Synthesis routes 101
4.2.2 NMR analysis 104
4.2.3 UV-Vis absorption 105
4.3 Solution behavior of graft copolymers 106
4.3.1 Effect of polymer concentration. 108
4.3.2 Effect of isotopic solvent 110
4.3.3 ^{1}H-NMR analysis at different temperatures 112
4.3.4 Effect of addition NaCl 113
4.3.5 Effect of Urea. 114
4.3.6 pH response 115
4.3.7 CO_2 response 119
4.4 Conclusions 122
4.5. Experimental methods 122
4.5.1 Characterization 122
4.5.2 Dialysis process 123
4.5.3 Materials. 123
4.5.4 Synthesis 123
5. pH-responsive optical properties of water soluble conjugated polyelectrolytes 129
5.1. Introduction 129
5.2. Synthesis of polyampholytes 130
5.2.1 Synthesis routes 130
5.2.2 X-ray photoelectron spectroscopy 131
5.2.3 Fourier-transform infrared spectroscopy 132
5.2.4 UV-Vis absorption analysis 133

5.2.5 NMR analysis 134
5.3 Solubility 135
5.4. Optical properties of CPAs 135
5.4.1 UV-Vis absorption and photoluminescence spectra 135
5.4.2 Photoluminescence as function of pH 138
5.4.3 Photoluminescence changes with concentrations 140
5.5 Dynamic light scattering 141
5.6. Conclusions 142
5.7 Experimental methods 142
5.7.1 Laser light scattering 142
5.7.2 Synthesis 143
6. Conclusion 146
7. References 148
8. Appendix 166
8.1 Chapter 2 166
8.2 Chapter 3 172
8.3 Chapter 4 176
8.4 Chapter 5 185
9 Permissions 191

Publications

1. Adam Creamer, Christopher S. Wood, Philip D. Howes, Abby Casey, **Shengyu Cong**, Adam V. Marsh, Robert Godin, Julianna Panidi, Thomas D. Anthopoulos , Claire H. Burgess, Tingmang Wu, Martyn A. McLachlan, Molly M. Stevens, Martin Heeney*, Post-polymerisation functionalisation of conjugated polymer backbones and its application in multifunctional emissive nanoparticles.
Nature Communications, | (2018) 9:3237 | DOI: 10.1038/s41467-018-05381-4

2. Emmanuel Reichsöllner, Adam Creamer, **Shengyu Cong**, Abby Casey, Simon Eder, Martin Heeney and Florian Glöcklhofer*,
Fast and selective post-polymerization modification of conjugated polymers using dimethyldioxirane.
Frontier in Chemistry, | (2019) 7:123| DOI: 10.3389/fchem.2019.00123

3. Manuscripts for the work carried out in Chapter 2 and 4 have been drafted.

Abbreviations

°	Degree
δ	Chemical Shift
μ	Micro
λ	Wavelength
Δλ	Stokes Shift
APS	Air Photoemission Spectroscopy
BHJ	Bulk Heterojunction
BT	2,1,3-Benzothiadiazole
CA	Contact Angle
CB	Chlorobenzene
CF	Chloroform
CV	Cyclic Voltammetry
CPA	Conjugated Polyampholyte
CPE	Conjugated Polyelectrolyte
$Đ_M$	Dispersity Index
DLS	Dynamic Light Scattering
DMF	*N,N*-dimethylformamide
DMSO	Dimethyl Sulfoxide
DSC	Differential Scanning Calorimetry
E_g	Band Gap
$E_{g(opt)}$	Optical Band Gap
$E_{g(elec)}$	Electrical Band Gap
EIL	Electron Injection Layer
EQE	External Quantum Efficiency
eV	Electron Volt
ETL	Electron Transport Layer
FF	Fill Factor
FTO	Fluorine Doped Tin Oxide
FTIR	Fourier-Transform Infrared Spectroscopy

GPC	Gel Permeation Chromatography
h	Hour
HOMO	Highest Occupied Molecular Orbital
HTL	Hole Transport Layer
ICT	Intramolecular Charge Transfer
ID	Ionic Density
ITO	Indium Tin Oxide
J_{SC}	Short Circuit Current
kDa	KiloDalton
LCST	Lower Critical Solution Temperature
LE	Luminous Efficiency
LUMO	Lowest Unoccupied Molecular Orbital
M_n	Number Averaged Molecular Weight
M_w	Weight Averaged Molecular Weight
min	Minute
nm	Nanometre
NMR	Nuclear Magnetic Resonance
OFET	Organic Field-Effect Transistor
OLED	Organic Light Emitting Diode
OPV	Organic Photovoltaic
PCE	Power Conversion Efficiency
$Pd(PPh_3)_4$	Tetrakis(triphenylphosphine) Palladium
PEG	Polyethylene Glycol
PEO	Poly(2-ethyl-2-oxazoline)
PL	Photo Luminescence
PNIPAM	Poly-N-Isopropyl Acrylamide
PVEA	Poly(N-(4-vinylbenzyl)-N,N-diethylamine)
PPO	Poly(2-propyl-2-oxazoline)
S_NAr	Nucleophilic Aromatic Substitution
THF	Tetrahydrofuran
UV-Vis	Ultraviolet–Visible

v:v	Volume Ratio
V_{oc}	Open Circuit Voltage

1 Introduction

1.1. Conjugated polymers

Conjugated polymers are a class of organic materials with π-electron conjugation along the polymer backbone. They show unique chemical and physical properties for a wide range of applications.[1,2] Conjugated polymers are materials which combine the electronic properties of inorganic semiconductors and the mechanical and physical properties of organic polymers.[3–6] Due to their solubility in organic solvents, conjugated polymers with extended conjugation length can be processed to form thin and lightweight films though high throughput methods such as roll-to-roll printing, inkjet printing, and spray-coating.[7] Such effective processing methods are advantageous to potentially develop low-cost organic electronic devices, like solar cells, transistors, light-emitting diodes, memory devices and sensing probes.[8–11] Some conventional structures of conjugated polymers are listed in the Figure 1.

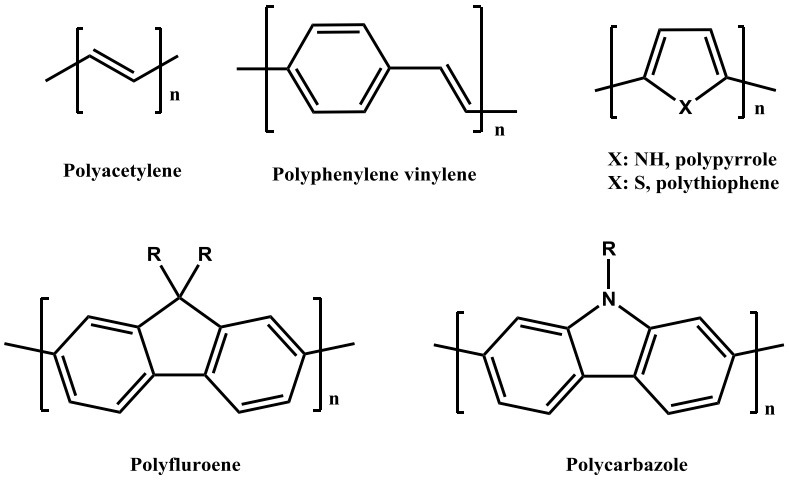


Figure 1. Structures of some conventional conjugated polymers[12]

To fulfil the needs of a wide range of applications, tailor-made conjugated polymers are usually designed and synthesized. For example, in order to modulate optical, electronic or physical properties, conjugated aromatic backbones are designed with electron-donating or electron-withdrawing moieties.[13–15] Besides, non-conjugated side-chains are generally used to improve solubility or impart additional functionalities.[16–18] The importance of conjugated

polymer research was emphasized when Shirakawa, MacDiarmid, and Heeger were awarded the Nobel Prize of Chemistry for their work on conductive polymers in 2000.

1.2. Characterizing polymer molecular weights

The 'molecular weight' of the polymer chains can influence their chemical and physical properties. But polymers are different from small molecules which have a defined molecular weight, polymers do not have a mono-disperse molecular weight. The molecular weight of polymer mainly depends on the polymerization methods and reaction conditions. The distribution of molecular weights can vary with different polymerization batches, which means different polymerization batches lead to different polymer 'molecular weight'. A conventional method to characterize the molecular weight distribution in a particular batch is to average the molecular weights of the polymer chains. The number average molecular weight (M_n) equals the total weight of the polymer chains divided by the number of polymer chains. For example, if n_i is the number of polymer chains and 'i' is the repeating unit with molar mass M_i. Then the M_n can be calculated from the following equation.

Equation 1:

$$M_n = \frac{\sum_{i=1}^{\infty} n_i M_i}{\sum_{i=1}^{\infty} n_i}$$

In addition to M_n, we also use the weight averaged molecular weight (M_w). This method takes into account the fact that larger polymer chains contribute more to the total mass of the polymer. The M_w can be calculated from the following equation.

Equation 2:

$$M_w = \frac{\sum_{i=1}^{\infty} n_i {M_i}^2}{\sum_{i=1}^{\infty} n_i M_i}$$

These two different ways are usually used to describe the molecular weight of a polymer sample. Besides, the dispersity, or width of the distribution of molecular masses can be defined as below:

Equation 3: The molar mass dispersity $Đ_M$.

$$Đ_M = \frac{M_w}{M_n} \geq 1$$

The $Đ_M$ has a value above 1. If the $Đ_M$ of a polymer sample equals 1, which means all the polymer chains are exactly the same length. These three parameters (M_n, M_w, $Đ_M$) are the conventional three parameters which are used to characterize the polymers synthesized and discussed in this thesis. As we know, the polymer properties depend on chemical structures of the monomers. In addition to chemical structures, the molecular weight and $Đ_M$ of the polymers can influence the polymer properties. For example, the mechanical properties,[19] physical properties[20] and optoelectronic properties[21] are all influenced by the molecular weights of the polymers.

1.3 Synthesis of conjugated polymers

The molecular weight and $Đ_M$ are usually influenced by the types of polymerization methods. There are two main types of polymerization reactions: step-growth[22] and chain growth.[23] Conjugated polymers in this thesis were synthesized by the step-growth polymerization. In step-growth polymerization, monomers with bi-functionality (for linear polymer chains) react initially to form dimers, then trimers followed by small oligomers. Oligomers then begin to react with other oligomers to form longer polymer chains. The step-growth reaction mechanism means high molecular weight polymer can only be formed at high conversion when long chains begin to react with other long chains.

For organic electronic applications, device performances are influenced by the molecular weight of active layers.[24,25] As polymer with high molecular weight is only obtained under high reaction conversions (> 99% yield), clearly it is not easy to obtain high molecular weights by step-growth polymerization. Besides, the stoichiometry of the two monomers must be equivalent in order to obtain high reaction yield. So the monomers in step-growth polymerization should be as pure as possible. Based on such factors effecting step-growth polymerization reactions discussed above, it is difficult to obtain conjugated polymers with high molecular weights by step-growth polymerization.

Unlike step-growth polymerizations, we can obtain polymers with very high molecular weight by chain-growth polymerization. Besides, chain-growth polymerization also gives a narrow $Đ_M$ which is desirable as the polymer chains will have consistent molecular properties.[26] In chain-growth polymerizations, an initiator reacts with a monomer to form the reactive species and the resulting reactive species react with another monomer. Monomers continue to add to the end of the growing polymer chain before a termination step stops the polymerization. In chain-growth polymerizations, a polymer with high molecular is obtained at very early stage, which is different with step-growth polymerizations (Figure 2). The molecular weight of the polymer can be controlled by the initial ratio of monomer/initiator. Chain-growth polymerizations can be used to synthesize homo-polymers (A-A-A-A-A…) or block co-polymers (A-A-A-B-B-B…) by adding a different monomer at each stage. However, alternating co-polymers (i.e. A-B-A-B-A…) cannot be synthesized using chain-growth polymerization while it is an obvious advantage of step growth polymerization. The conjugated polymers in this thesis are alternating co-polymers (A-B-A-B-A…), so all the polymers discussed are synthesized by step-growth polymerization.

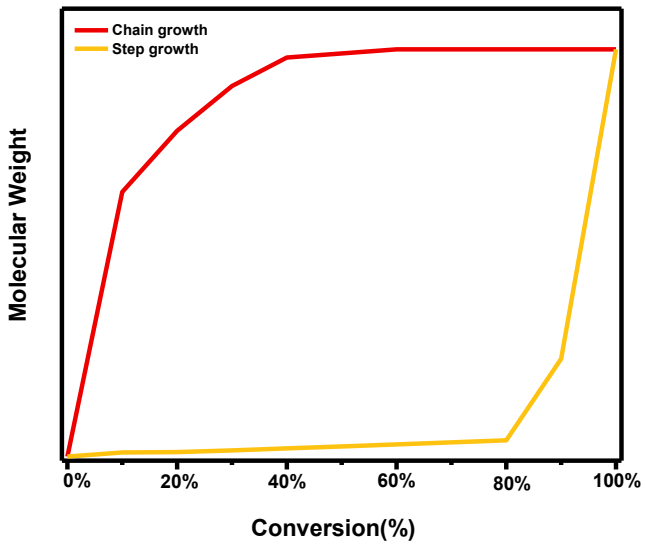


Figure 2: Molecular weight varies with conversion depending on polymerization mechanism.

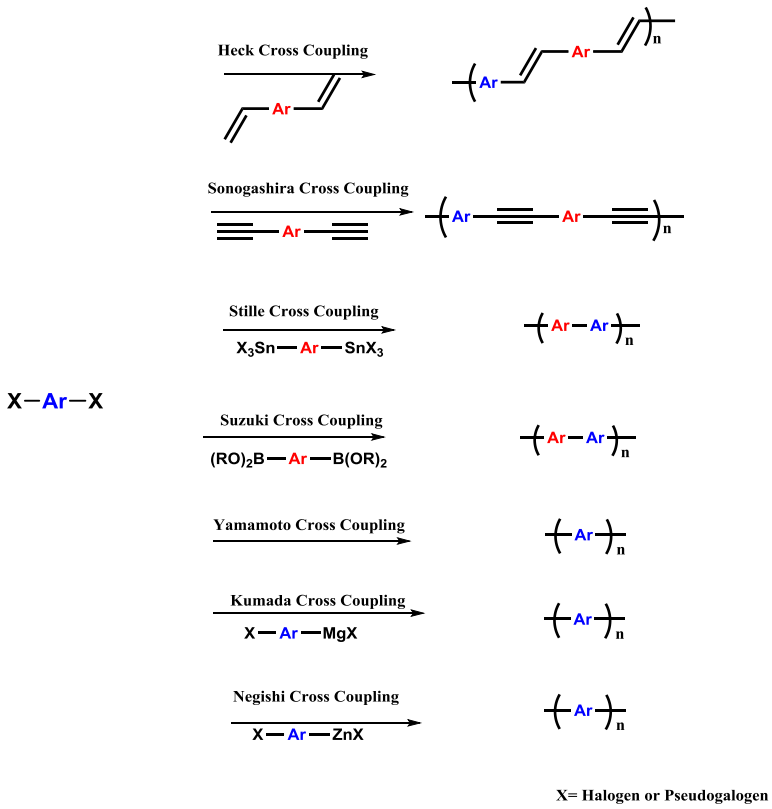


Figure 3: Traditional C–C coupling techniques for the preparation of π-conjugated materials.[3]

To obtain diverse polymeric structures, reliable formation of C–C bonds is needed. Palladium (e.g., Stille, Suzuki) and nickel-catalyzed (e.g., Kumada, Negishi) cross-coupling reactions have proven to be very useful synthetic methods in polymer synthesis (Figure 3). As all the polymers synthesized in this thesis are through palladium catalysed cross-coupling reactions, the palladium-catalysed mechanism is discussed herein. The most common way to synthesize conjugated alternating co-polymers by palladium catalyst are Suzuki and Stille coupling reactions.[27,28] Most palladium-catalysed cross-coupling reactions involve three main steps (Figure 4). First, oxidative addition in which the metal centre is oxidised as the metal inserts into the aryl-halide (R_1-X) bond. Then followed by transmetallation in which the halide on the palladium is replaced with another aryl group, and finally reductive elimination in which the palladium is reduced back to Pd(0) and the coupled aryl groups (R_1-R_2) are eliminated. In Stille reactions, the organostannane ($SnBu_3$ or $SnMe_3$) functionalised aryl groups are used in transmetallation step.[29] As the Stille reaction can be carried out under neutral conditions, a wide range of functional polymers are synthesized by Stille reactions, especially for the polymers with sensitive groups. However, a disadvantage of Stille reaction is that the organostannane reagents are highly toxic, which means Stille

reactions are generally carried out on a laboratory-scale only. Suzuki coupling reactions are carried out under basic conditions, and they use generally non-toxic boronic esters or acids ($R\text{-}B(OH)_2$) in the transmetallation step. However, the reaction mechanism of Suzuki couplings is far more complex than that of Stille couplings. This can often result in the need to optimise Suzuki coupling conditions, which may not be possible if limited monomer is available. In addition, basic conditions are unsuitable for some functional groups. All of the conjugated polymers in this thesis were synthesised under typical Suzuki coupling reactions.

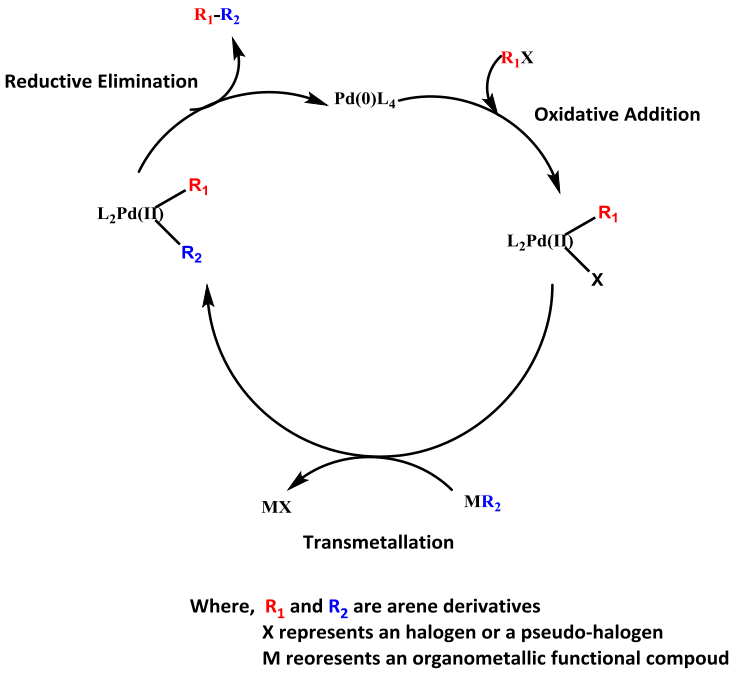


Figure 4: Catalytic cycle of palladium cross-coupling reactions (isomerism of Pd^{II} complexes ignored for simplicity)

1.4 Post-polymerization modification

The concept of post-polymerization modification was developed by Staudinger, which he termed as ''polymer analogous reactions.''[30] Many functional polymers have been synthesized based on the post-polymerization modification concept. The Serniuk group reported the functional butadiene polymers by thiol-ene addition reaction in 1948.[31] Later, the modification of halogenated poly(meth)acrylates was investigated in 1960s and the Iwakura group synthesized polymers bearing pendant epoxide groups by post-polymerization modification. Although many functional polymer synthesis were synthesized

by post-polymerization modifications, the variety of chemical reactions allowing quantitative post-polymerization modification was limited. With the development of polymerization techniques such as atom transfer radical polymerization (ATRP),[32] reversible addition fragmentation chain transfer (RAFT)[33] and single-electron transfer living radical polymerization (SET-LRP),[34] functional group tolerance has been improved by these techniques. With functional group tolerance improved, a wide variety of functional groups can be quantitatively and selectively modified under mild reaction conditions.

The synthesis of functional polymers through post-polymerization modification is illustrated in Figure 5. Post-polymerization modification is based on the polymerization of monomers with functional groups which are inert towards the polymerization conditions but which can be quantitatively converted in a subsequent reaction step into other functional groups. One obvious advantage of post-polymerization polymerization modification is that it allows access to functional polymers which cannot be prepared by direct polymerization of the corresponding functional monomers. Besides, this strategy is very attractive for combinatorial materials discovery. However, it is important that such reactions need to proceed in close to quantitative yield, otherwise complex mixtures can form. This can be difficult on polymers due to high number of functional groups and steric accessibility problem.

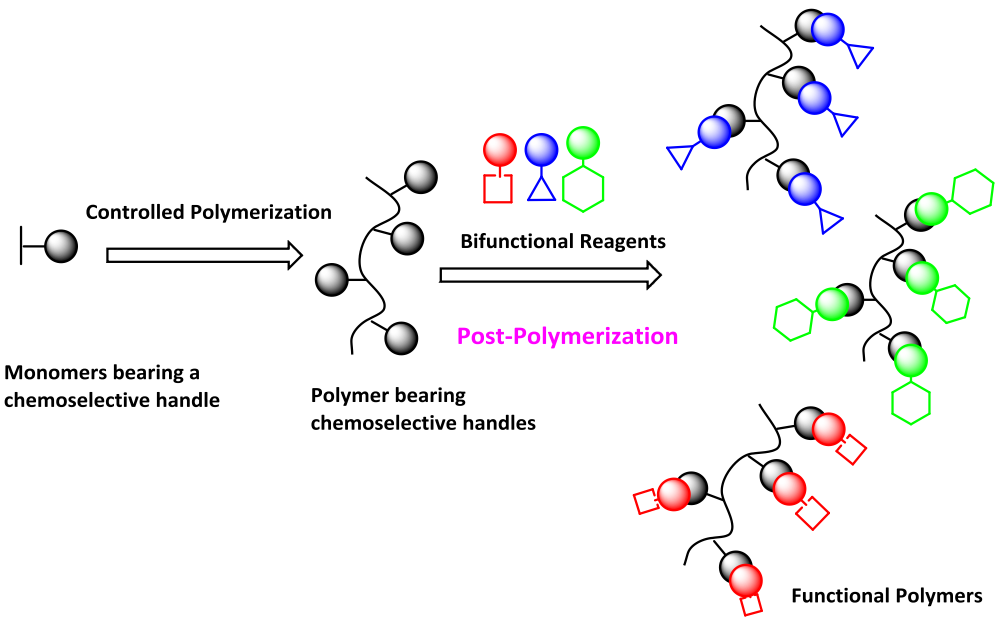


Figure 5. Synthesis of polymers by post-polymerization modification

1.5 Post-polymerization modification reactions

The research on post-polymerization modification increased as a result of development of functional group tolerance polymerization techniques. This part will discuss eight of the most frequently used reactions for the post-polymerization modification for conjugated polymers briefly. They are post-polymerization modification via (1) thiol-ene addition, (2) epoxides, anhydrides, oxazolines, isocyanates, (3) active ester, (4) Diels-Alder reaction, (5) thiol-disulfide exchange, (6) Michael-type addition, (7) azide alkyne cycloaddition reactions, (8) ketones and aldehydes. The main classes of reactions used for post-polymerization modification are shown in Figure 6.

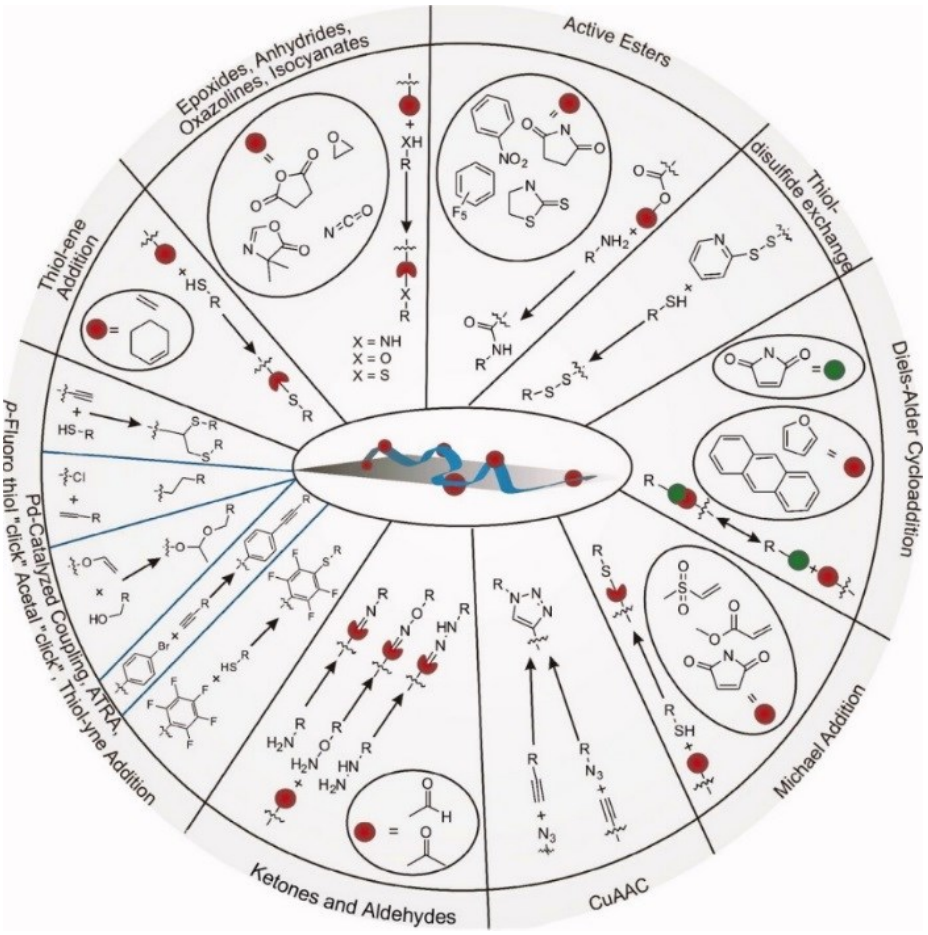


Figure 6 Main classes of reactions that used for synthesis of functionalized polymers via post-polymerization modification[35]

1.5.1 Post-polymerization modification via thiol-ene addition

The thiol-ene reaction is an organic reaction between a thiol and an alkene to form a thioether. Thiol-ene chemistry was widely used as a method for forming crosslinked networks. There are many advantages of thiol-ene addition for polymer synthesis: tolerance to many different reaction conditions/solvents, defined reaction path ways/products, and a range of easily obtained starting materials. These advantages have led to thiol-ene addition being used increasingly in polymer functionalization, macromolecular synthesis, and functionalized biomaterials.[36] For example, the Martin group[37] investigated the post-polymerization modification of poly(3,4-propylenedioxythiophene) (PProDOT) surfaces by using a dialkene functionalized variant (ProDOT-diene) (Figure 7).

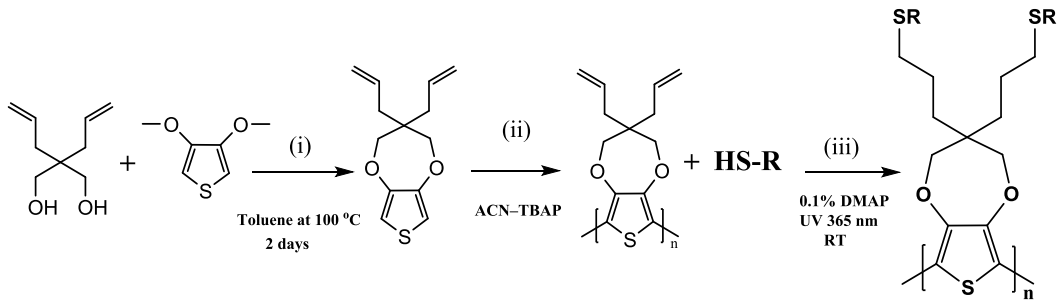


Figure 7: Functional polymer synthesized by post-polymerization via thiol-ene addition[37]

1.5.2 Post-polymerization modification of epoxides, anhydrides, oxazolines, isocyanates

Epoxides, anhydrides, oxazolines, and isocyanates are a class of functional groups which have a long history in polymer synthesis. A common advantage of such groups is that they are tolerant toward radical based polymerization techniques. Here, take isocyanates for example. The isocyanate group is an attractive group which allows post-polymerization modification with amines, alcohols, and thiols. The post-polymerization functionalization of hydroxyl functional polymers (both end group and side chain) by hydrolysis-stable carbamate formation with a wide range of functional isocyanate derivatives yielding a high degree of conversion was reported by the Scherman group.[38] (Figure 8)

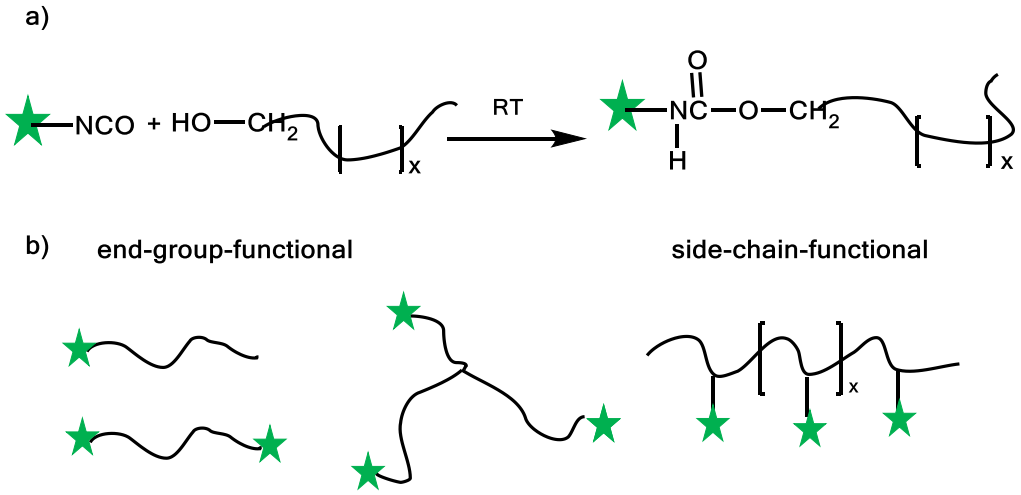


Figure 8: Functionalization of hydroxyl end groups polymers with Isocyanates by post-polymerization[38]

1.5.3 Post-polymerization modification via active esters

The synthesis and post-polymerization modification of active ester polymers was developed by Batz et al.[39] The reaction of active ester polymers with amines is the most commonly used post-polymerization modification strategy. Amines are most frequently used for the post-polymerization modification of active ester polymers as they can react selectively even in the presence of weaker nucleophiles, such as alcohols.

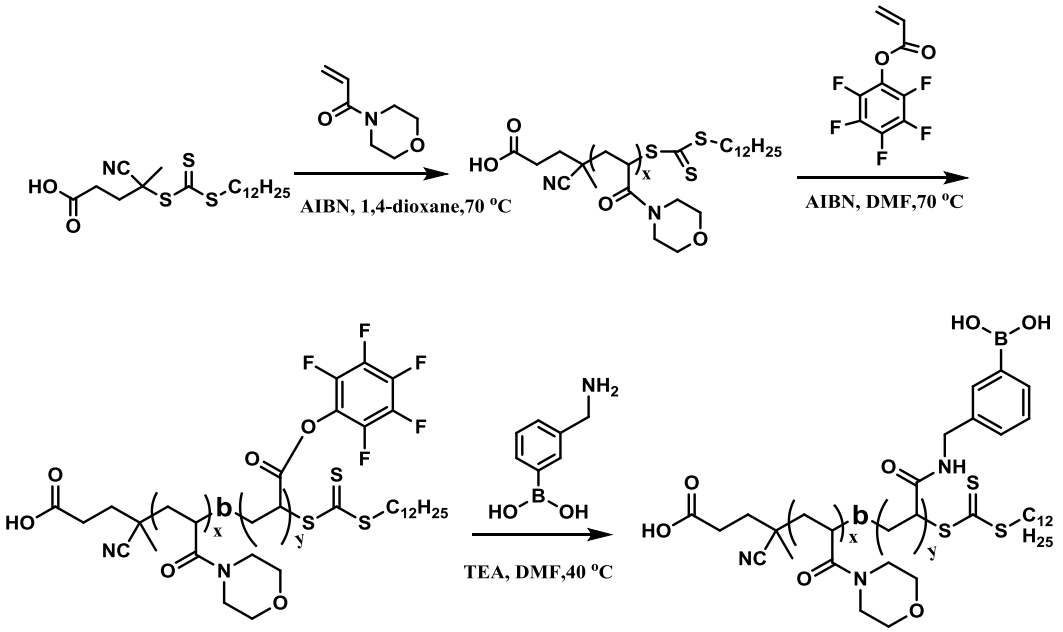


Figure 9: Functional polymer synthesized by post-polymerization via active eater[40]

The Patrick Theato group reported a well-defined diblock copolymer synthesized by sequential RAFT polymerization and post-polymerization modification via active-ester. The self-assembly of these diblock copolymers was responsive to the change in pH and the presence of sugar.[40] (Figure 9)

1.5.4 Post-polymerization modification via Diels-Alder reactions

The cycloaddition reaction between a diene and a substituted alkene, which was discovered by Diels and Alder, has emerged as an attractive method for post-polymerization modification.[41,42] The Diels- Alder reaction can proceed with quantitative yields without any side reactions and is tolerant to a wide range of functional groups. Besides, many Diels-Alder reactions are reversible and the Diels-Alder adduct can decompose into the starting diene and dienophile at higher temperatures. The Sanyal group reported poly(ethylene glycol) methacrylate-based hydrogels containing thiol reactive maleimide functional groups synthesized by post-polymerization via a novel Diels-Alder cycloaddition.[43] (Figure 10)

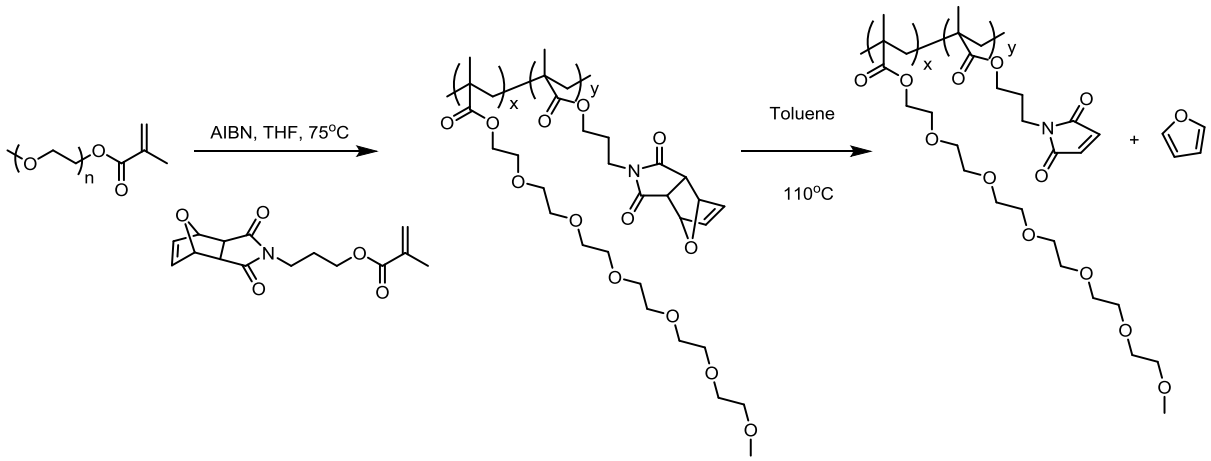


Figure 10: Functional polymer synthesized by post-polymerization via Diels-Alder reaction[43]

1.5.5 Post-polymerization modification via thiol-disulfide exchange

Disulfides are attractive reactive groups for post-polymerization modification, as they can be readily exchanged with thiol compounds in high yields. Based on this method, diverse pyridyldisulfide-functionalized acrylates and methacrylates have been developed which can

be polymerized using conventional free-radical polymerization. One of the advantages of the thiol-disulfide exchange reaction is that it allows the introduction of functional groups via a disulfide bond. The Zugates group demonstrated the reduction of pyridyl disulfide containing poly(b-amino ester)s modified with glutathione in intracellular media, which led to a 50% decrease in the DNA binding capacity of the polymer[44] (Figure 11).

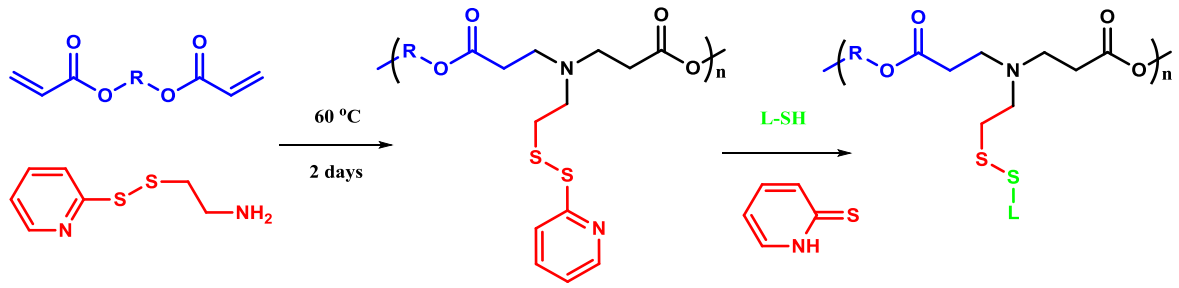


Figure 11: Functional polymer synthesized by post-polymerization via thiol-disulfide exchange[44]

1.5.6 Post-polymerization modification via Michael-type addition

Michael-type addition reactions have been generally utilized in polymer research to synthesize a variety of macromolecular structures including polymers, dendrimers, and crosslinked networks. Michael-type addition reactions were also utilized to prepare side chain functional polymers bearing Michael acceptors, such as acrylates, maleimides, and vinyl sulfones. Post-polymerization modification of these polymers with thiols is very attractive, as this reaction can proceed quantitatively and selectively in aqueous media at room temperature.[45] The Zhong group prepared vinyl sulfone functionalized poly(ester carbonate)s by ring-opening copolymerization of a vinyl sulfone carbonate monomer with ε-caprolactone, lactone, or trimethylene carbonate. Post-polymerization modification was reported to proceed quantitatively even with bulky thiols at room temperature[46] (Figure 12).

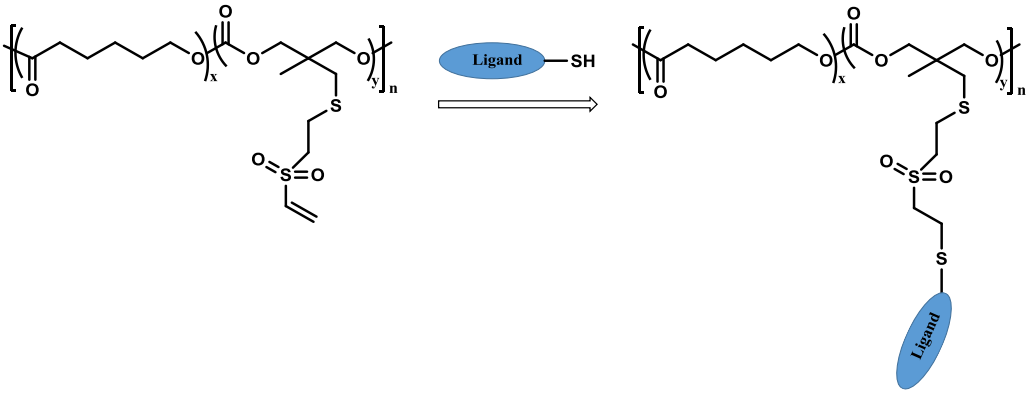


Figure 12: Functional polymer synthesized by post-polymerization via Michael-Type addition[46]

1.5.7 Post-polymerization modification via azide alkyne cycloaddition reactions

Azide alkyne cycloaddition reactions have been used for post-polymerization, as they can give high yields under mild conditions in aqueous or in organic media. This type of reactions requires the preparation of polymers containing azide or alkyne functional groups, which can be obtained by various polymerization techniques. An advantage of post-polymerization modification using the azide alkyne cycloaddition reactions is that almost all functional groups have been reported to be tolerant to this type reaction.[47] Quantitative modification of the alkyne groups was achieved with an azide-functionalized PEG (M_n = 1100 g/mol) in stoichiometric conditions at 80 °C when $CuSO_4 \cdot 5H_2O/Na_{asc}$ was used as a catalyst by Parrish group[48] (Figure 13).

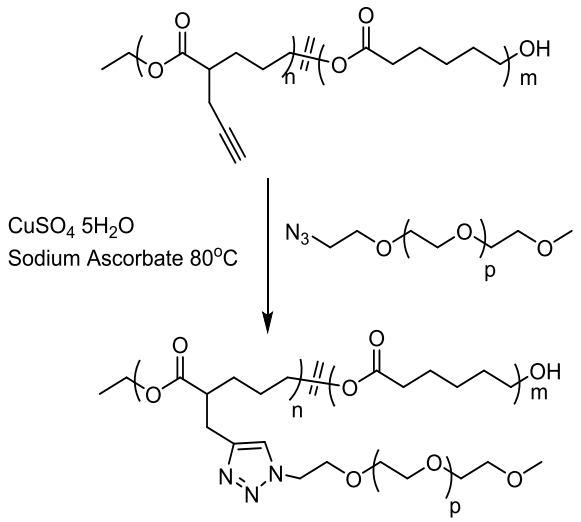


Figure 13: Functional polymer synthesized by post-polymerization via azide alkyne cycloaddition reaction[48]

1.5.8 Post-polymerization modification of ketones and aldehydes

Ketones and aldehydes can selectively react with primary amines, alkoxyamines, and hydrazines to form imines, oximes, and hydrazones, respectively. While imines are prone to hydrolysis, oximes and hydrazones are hydrolytically stable between slightly acidic to neutral pH. However, imines can be further converted to stable secondary amines via reductive amination under the presence of a reducing agent, such as borohydride derivatives. Barrett and Yousaf prepared a library of poly(ketoester)s, which contain ketone groups as part of the backbone of the polymer. Post-polymerization modification of these backbone ketone groups proceeded quantitatively with a library of oximes at room temperature[49] (Figure 14).

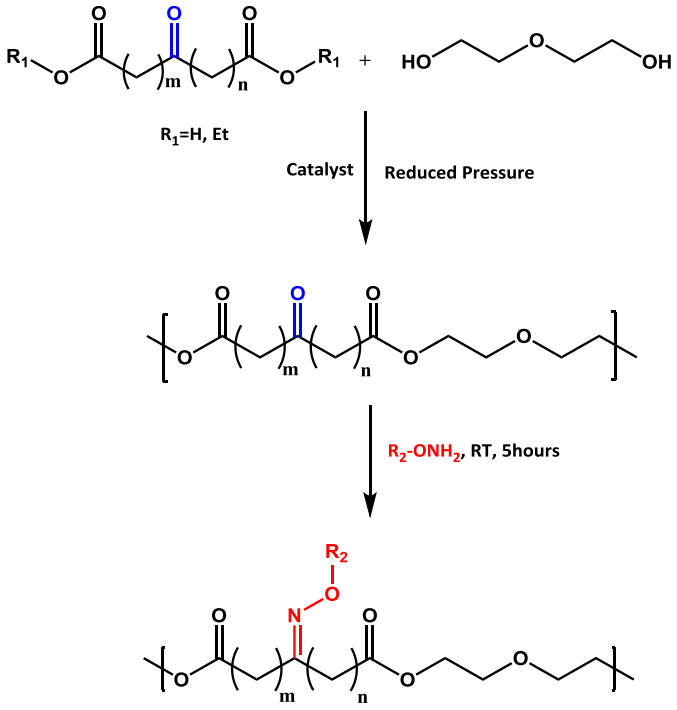
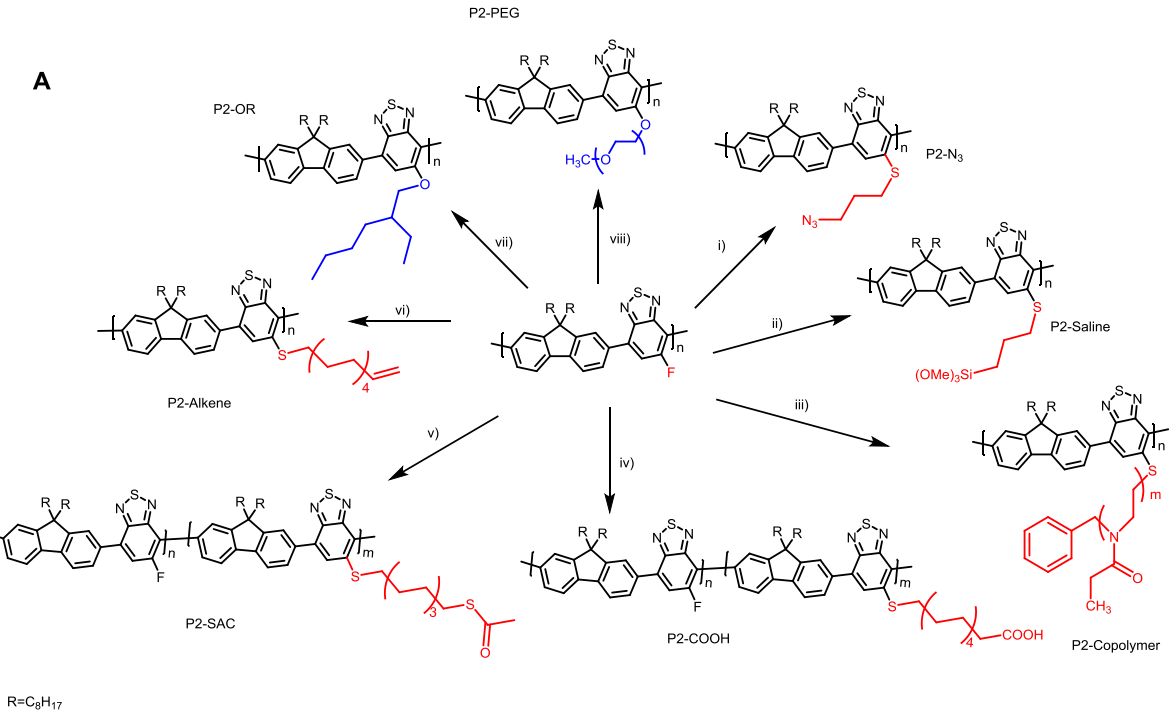


Figure 14: Synthesis and functionalization of poly(ketoester)s by post-polymerizatio[49]

1.6 Post-polymerization modification of nucleophilic fluoride substitution

The eight conventional post-polymerization modification reactions have been discussed briefly above. Although successful, none of these approaches directly modifies a conjugated polymer backbone. We are interested in such an approach which can be used to tune

polymer energetics. During the course of this thesis, we developed the nucleophilic fluoride substitution as an effective approach to functionalize conjugated polymer backbones with a wide range of functional groups under highly controlled and mild conditions. This approach allows for facile tuning of the physical and optoelectronic properties within a batch of consistent molecular weight and dispersity. The nucleophilic fluoride substitution also enables the introduction of multiple different functional groups onto the polymer backbone in a controlled manner. Such functionalisation results in significant changes to the optoelectronic and physical properties of the polymer. Besides, it enables the quantitative introduction of functional groups on conjugated backbone. To demonstrate the versatility of this fluoride substitution reaction, we designed and synthesized a range of emissive poly(9,9- dioctylfluorene-alt-benzothiadiazole) (F8BT)-based polymers for the creation of mono and multifunctional semiconducting polymer.[50] Most of the polymers were synthesized by my colleague, Adam Creamer, and some polymers were synthesized by me (Figure 15). This thesis fully develops this work.



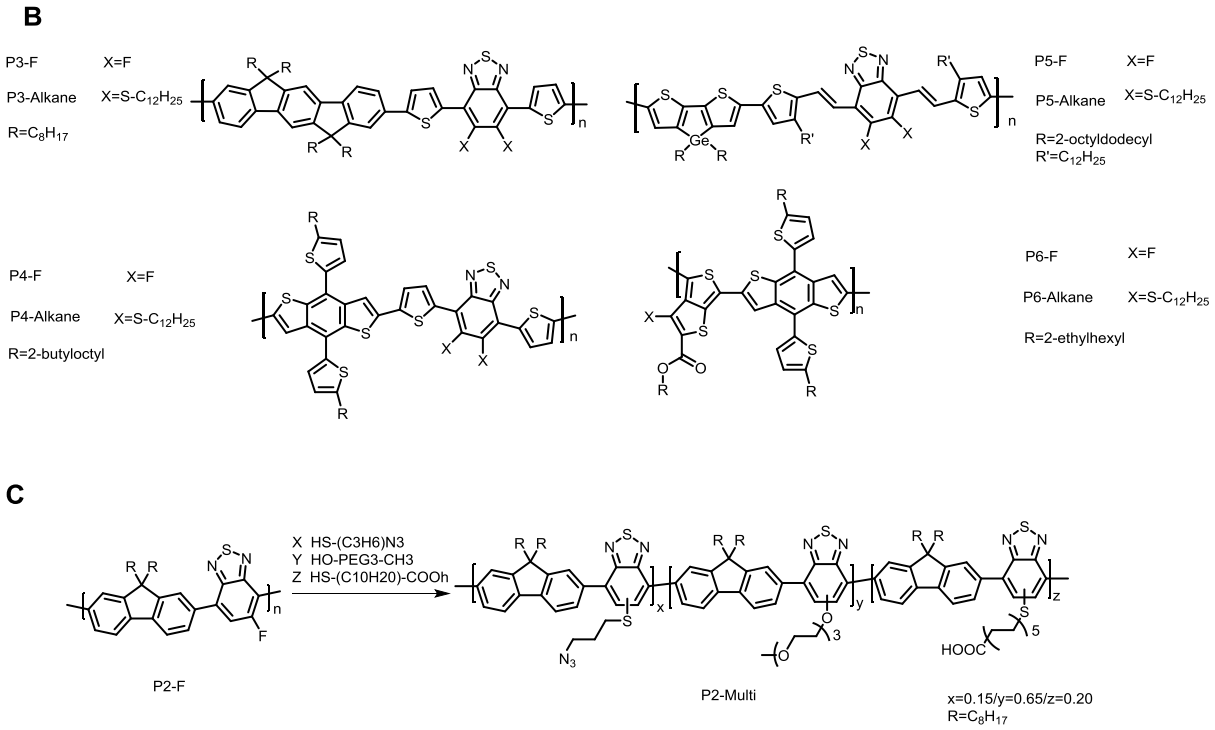


Figure 15: Scope of the nucleophilic fluoride substitution reactions[50]

1.7 Graft copolymers synthesized by post-polymerization

After discussion about generally used reactions in post-polymerization, a wide range of reactions that have proven to be effective and powerful to synthesize diverse functional polymers via post-polymerization. These simple reactions can greatly facilitate the synthesis and modification of functional polymers. The advantage of post-polymerization strategy lies in the fact that one reactive scaffold can be transformed into multiple derivatives simply upon changing the chemical identity of the functionalizing moiety. There are diverse materials which have been prepared by various post-polymerization reactions, including: terminal- and pendant-functional polymers; copolymers and micelles; complex architectures such as star, brush, graft, hyperbranched, and dendritic polymers; gels and networks; and polymers conjugated to nanomaterials.[51,52] As the polymers synthesized in this thesis are all graft copolymers, the preparation of functional graft copolymers by post-polymerization is briefly reviewed here.

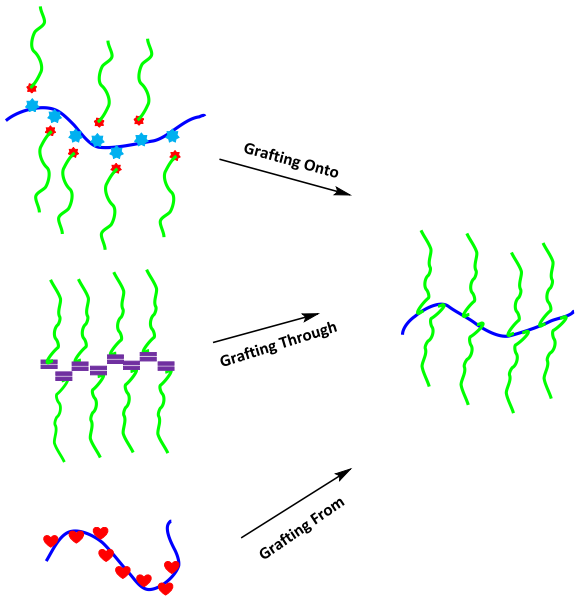


Figure 16: Three main strategies for synthesizing the graft copolymers by post-polymerization[53]

Graft copolymers containing side chains chemically attached onto a linear backbone are endowed with unique properties including wormlike conformation, compact molecular dimension and notable chain end effects.[54] Much attention has been paid to the synthesis of graft copolymers with desired functional groups, chemical compositions and lengths of side chains. The graft copolymers due to their unique molecular structures have a wide range of applications from biology to nanoscience.[55–57] According to the features of synthetic approaches, three main strategies: grafting through, grafting-from and grafting-onto, are mainly utilized to synthesize the graft copolymers[53] (Figure 16).

1.7.1 The grafting-onto strategy

The grafting-onto strategy is based on attaching side chains onto a linear backbone by a coupling reaction. As the linear backbone and side chains are synthesized independently, they can be obtained by appropriate pathways and the chain lengths can be readily tuned. The key in the synthesis of graft copolymers via the grafting-onto strategy is to utilize an efficient coupling reaction of functionalized backbones with side chains. Based on this strategy, the Nuyken group synthesized poly[2-(4-methoxybenzylsulfanyl)ethyl-2-oxazoline] co-poly- (ethyl-2-oxazoline) bearing potential thiol groups (Figure 17). After quantitative deprotection of thiol groups and thiol-ene coupling reaction of those SH groups of the copolymer with acrylamide or maleimide in the end of poly(2-methyl-2-oxazoline)s,

different graft copolymers containing poly(2-oxazoline)s as both backbone and side chains with different lengths of side chains were prepared with a quantitative conversion.[58]

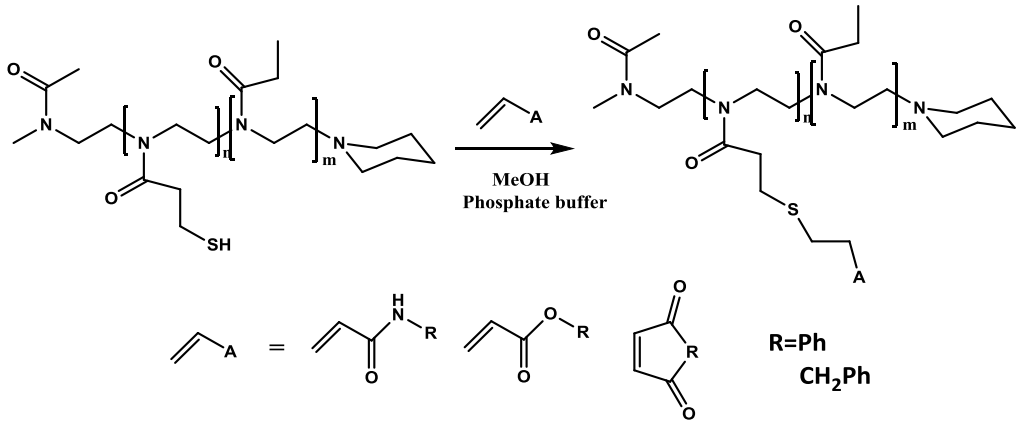
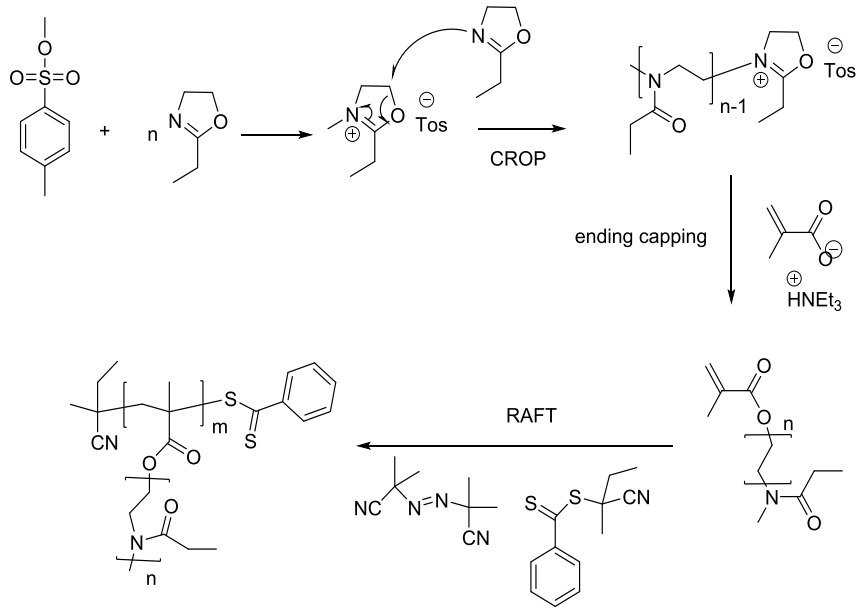


Figure 17 : Functional polymer synthesized by grafting-on strategy[58]

1.7.2 The grafting-through strategy

The grafting-through strategy to synthesize graft copolymers is to polymerize the macromonomers with a polymerizable end group. Based on this strategy, the length of side chains and the grafting density can be controlled by adjusting the degree of polymerization of side chains and backbone, respectively. Due to such advantages, many graft copolymers have been obtained by the combination of different polymerization approaches. For example, the Weber group prepared methacrylate-terminated oligo-(2-ethyl-2-oxazoline) via living cationic ring-opening polymerization followed by synthesizing the graft copolymers containing oligo(2-ethyl-2-oxazoline) side chains.[59] (Figure 18)



CROP: cationic ring-opening polymerization.
RAFT: reversible addition-fragmentation chain transfer polymerization.

Figure 18: Functional polymer synthesized by grafting-through strategy[59]

1.7.3 The grafting-from strategy

This strategy involves polymerising the side chains from an initiation group on the polymer backbone, thus can be obtained directly from the initiation-group-containing monomer or by the introduction of initiating functional groups on a precursor polymer. With the living polymerization technique, this strategy is an attractive method to synthesize graft copolymers. Many graft copolymers with various backbones and side chains have been synthesized via this ‘‘grafting-from’’ strategy. Based on this strategy, he Huang group reported the synthesis of well-defined graft copolymers consisting of PtBA backbone and poly(methyl acrylate) (PMA) side chains.[60] (Figure 19)

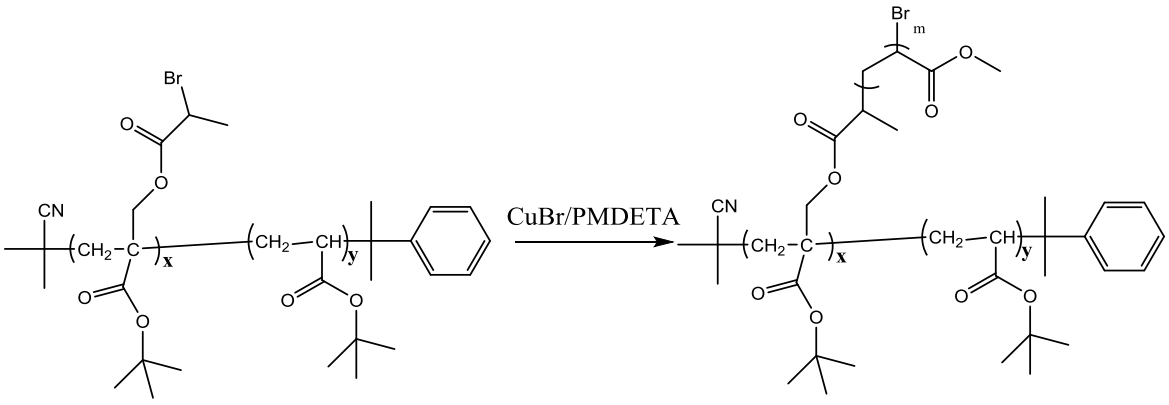


Figure 19: Functional polymer synthesized by grafting-from strategy[60]

1.8 Thesis aims and overview

Backbone functionalization of conjugated polymers is important to optimize their performances in many applications, from optoelectronic devices to nanoparticle biosensors. So, it is important to introduce diverse functional groups to backbones by effective approaches. To address this challenge, we develop an approach for the direct modification of the aromatic backbone of conjugated polymer by post-polymerisation. This approach concerns fluoride displacement via an aromatic backbone substitution reaction. The aim of this thesis (from Chapter 2 to Chapter 5) focuses on synthesizing different functional conjugated polymers by post-polymerization and investigation of their chemical and physical properties. In Chapter 2, conjugated polymers with same aromatic backbone but increasingly hydrophilic side chains were synthesized by post-polymerization (Figure 20). The hydrophilicity of conjugated backbone was improved by grafting hydrophilic side chains.

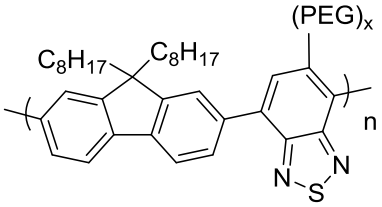
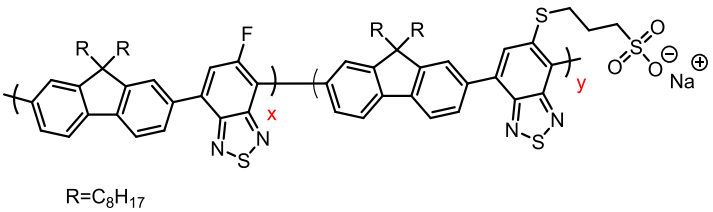


Figure 20: Conjugated polymer with hydrophilic side chains

In Chapter 3, conjugated polyelectrolytes with same conjugated backbone but different ionic densities were synthesized by post-polymerization (Figure 21). The conjugated polyelectrolytes with same conjugated backbones but different ionic densities can aid the understanding of relationship between ionic densities and device performance.



R=C_8H_{17}

x=0.5, y=0.5

x=0.25, y=0.75

x=0, y=1.0

Figure 21: Conjugated polyelectrolytes with different ionic densities

As multi-stimuli-responsive polymeric materials respond to different external factors, such as temperature, pH, light. How to synthesize multi-stimuli-responsive in a facile way has received much attention. In chapter 4 a thermo-, pH- and CO_2-responsive fluorescent graft copolymer has been synthesized by post-polymerization (Figure 22). This facile synthesis strategy gives us an effective approach to design and synthesize multi-stimuli responsive polymers.

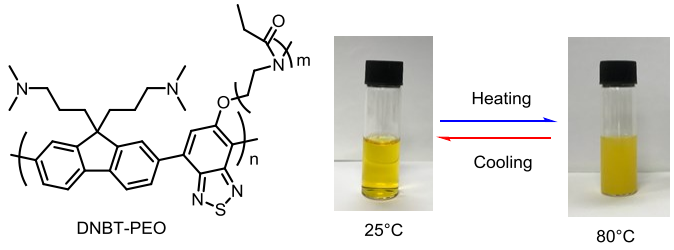


Figure 22: A multi-stimuli-responsive polymer synthesized by post-polymerization

The Chapter 5 focuses on the synthesis of water soluble conjugated polyampholytes (Figure 23). The two conjugated polyampholytes are all water soluble and pH responsive. With changing pH, the polyampholytes demonstrated intermolecular interactions via electrostatic complexation between positive and negative moieties. This study suggests that the pH sensitive CPAs can be used as a useful signaling platform for design of various fluorescent biological assays.

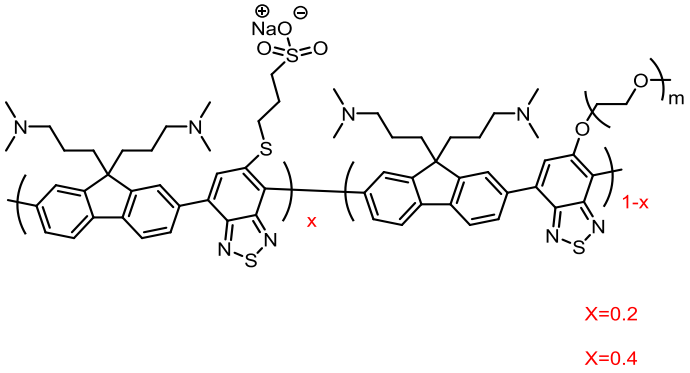


Figure 23: Structures of two water soluble conjugated polyampholytes

2 Hydrophilicity control of conjugated polymers by post-polymerization modification

2.1 Introduction

Conjugated polymers are a class of organic materials which have unique physical and chemical properties.[43–45] Conjugated polymers have been widely used in material industry and played a very important role as they have many obvious advantages. The advantages are the biocompatibility, flexibility, and tunability of their optical, electronic and mechanical properties which can be modulated by chemical functionalizations.[64–68] Conjugated polymers' hydrophilicity has a large impact on the efficiency of many practical applications, because hydrophilicity affects conjugated polymers' wettability, paintability, biocompatability, anti-electrostatic properties.[69–72] For example, as conjugated polymers have excellent light-harvesting and light-amplifying properties, they have been applied as promising fluorescent probes in biology fields.[73,74] Conjugated polymers are used as probes which can detect biomacromolecules such as proteins, antibodies, and DNA via electrical, electrochemical, photoluminescent and chemoluminescent responses.[75–78] Clearly the solubility in aqueous solution of conjugated polymers is essential for interfacing with the biomacromolecules which are only soluble in aqueous media. Improving the hydrophilicity of conjugated polymers to enable dissolution in aqueous media is fundamental to fulfil the biological applications.[79–81]

In addition, water/alcohol soluble conjugated polymers have been used in organic optoelectronic devices.[82–84] The excellent solubility of conjugated polymers in highly polar solvents is desirable for fabricating multilayer devices without interface mixing through the deposition of different layers from orthogonal solvents.[85,86] Improving polymer hydrophilicity can ensure that conjugated polymers dissolve in highly polar solvents. Besides, the issues of bonding and finishing of many conjugated polymers are mainly due to the low hydrophilicity of their surfaces.[69] Take conjugated polymer membranes for an example and a problem is fouling which is caused by undesired interactions, generally of colloids, with the membrane materials. The consequence is a sharp decrease in permeate flux and changing solute selectivity over operation time, which has detrimental effects on

the efficiency of the membrane process. To improve the anti-fouling ability of the membrane, an effective method is needed to impart hydrophilic groups in conventional hydrophobic membrane materials.[81,87,88]

Poly(ethylene glycol) methyl ether (PEG) is very hydrophilic and commonly used to impart hydrophilicity to a hydrophobic surface.[89–91] Also, the antifouling abilities of PEG have been reported in many research papers.[92] In this chapter, we report an effective and facile approach to modify the conjugated polymers hydrophilicity by grafting PEG and its analogues to a hydrophobic conjugated backbone by post-polymerization (Figure 24). A series of side chains with increasing hydrophilicity were grafted to the conjugated backbone, and the hydrophilicity of resulting conjugated polymers was improved gradually. The contact angle of starting **F8FBT** was 101.4°, however, after grafting PEG (M_n= 10,000 g/mol) to conjugated backbone, the contact angle of **F8BT-PEG** decreased dramatically to only 31.0°. Furthermore, the solubility of **F8BT-PEG** in polar solvents (like methanol, DMSO, water) increases as expected while the starting **F8FBT** is only soluble in non-polar solvents.

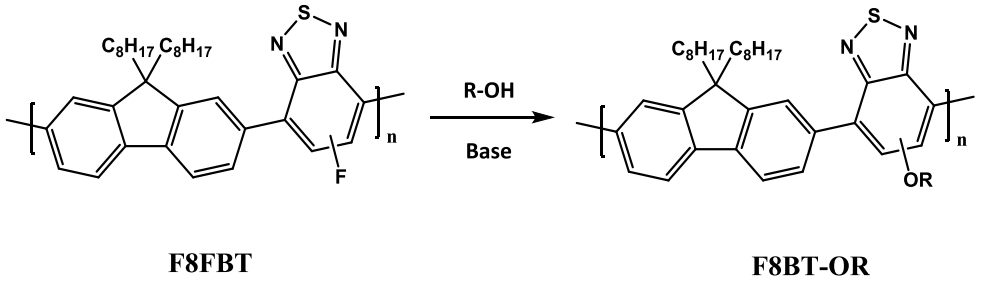


Figure 24 Nucleophilic substitution reaction by post-polymerization

2.2 Synthesis of monomers and polymers

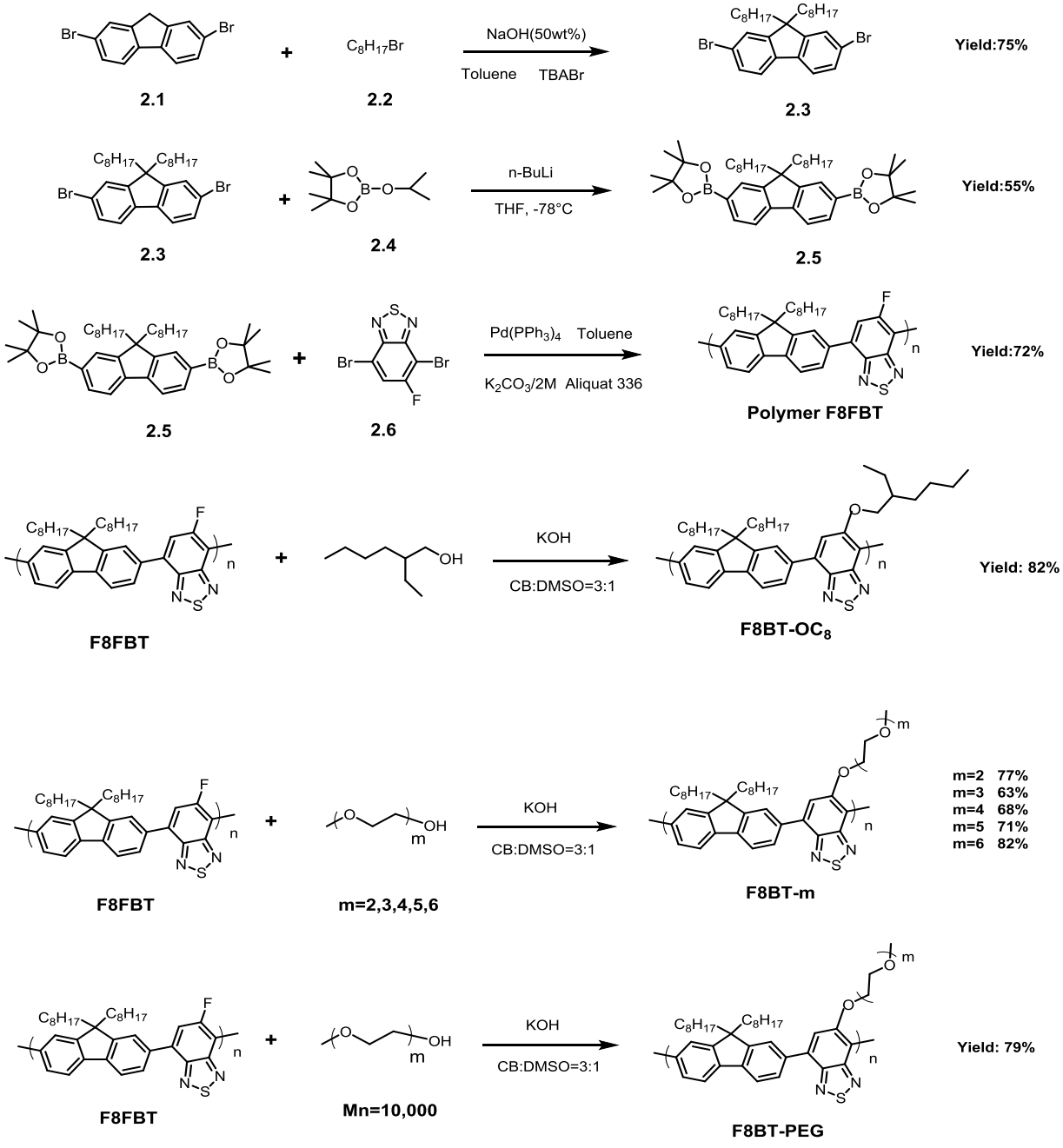
First, 2, - 7- dibromofluorene was reacted with 1-bromooctane in a two-phase system composed of toluene and NaOH aqueous solution (50 wt%). As toluene and NaOH aqueous solution are immiscible systems, tetrabutylammonium bromide was used as the phase-transfer catalyst in this reaction. After reaction, the crude product was purified by column chromatography using hexane as the eluent to give pure monomer **2.3** (yield 75%). The dibromide was converted into the required boronic ester by treatment with n-Buli, followed by quenching of the dianion with 2-isopropoxy-4, 4, 5, 5-tetramethyl-1, 3, 2

dioxaborolane. The crude product was recrystallized from acetone to give pure monomer **2.5** (yield 55%). Using typical Suzuki reaction condition, equimolar quantities of monomer **2.5** were reacted with 4, 7-dibromo-5-fluoro-2, -1, -3-benzothiadiazole to give **F8FBT** (yield 72%). After reaction, the polymer was purified by Soxhlet washing with methanol first, then acetone, followed by hexane and chloroform for 24 hours each respectively. The Soxhlet extraction removes lower molecular weight oligomers and catalyst residues to afford **F8FBT** with lower polydispersity and higher molecular weight.

The synthesized **F8FBT** (M_n= 38,500 g/mol, M_w= 65,100 g/mol, PDI= 1.69) was soluble in typical organic solvents, such as toluene, THF, chloroform and chlorobenzene at room temperature. Following successful synthesis of **F8FBT**, the fluoride displacement reactions were optimized. Typically aprotic solvents perform best for S_NAr reactions, but the polymer was not soluble in DMSO alone. Therefore, a mixed solvent of chlorobenzene and DMSO was utilized in presence of KOH at 120°C. The nucleophilic aromatic substituted reactions were all monitored by ^{19}F-NMR spectroscopy. We checked that the **F8FBT** did not react with KOH alone under these conditions. The substituted reactions were complete when ^{19}F-NMR did not demonstrate any fluorine signal, typically after 48 h. After reaction, the products were precipitated into methanol, then purified by Soxhlet washing with acetone (24 hours) to give the substituted polymers. However, **F8BT-PEG** was soluble in methanol due to the grafted hydrophilic side chain, PEG. For this polymer, the reaction solvent was removed when reaction was complete, then the remaining polymer was dissolved in deionized water. The excess PEG was removed by dialysis for 2 days and pure **F8BT-PEG** was obtained. All substituted polymers are characterized by ^{1}H and ^{19}F-NMR.

Diffusion ordered spectroscopy (DOSY) has been successfully used to evaluate the purity of copolymers and the proportion of residual homopolymers.[93] **F8BT-PEG** was also confirmed by DOSY NMR. In DOSY NMR, each component in a mixture can be pseudo-separated, based on its own diffusion coefficient.[94] The DOSY NMR of **F8FBT** and PEG mixtures were investigated (Appendix Figure 12). Clearly, the proton signals consisted of three parallel signal lines, and the first signal line belonged to the deuterated solvent ($CDCl_3$). The second and third signal lines were PEG and **F8FBT** respectively. Clearly in the mixture different diffusion coefficients were found for **F8FBT** and PEG from the two separated signal lines. The DOSY NMR of the **F8BT-PEG** graft was also investigated (Appendix Figure 13). As

expected, there was only one signal line which meant all the protons were from **F8BT-PEG**, indicating the high purity of **F8BT-PEG**.



Scheme 1: Synthesis of monomers and substituted polymers.[95]

Table 1: Molecular weights of polymers (polystyrene as standards, chlorobenzene as solvent)

Polymer	M_n (KDa)	M_w (KDa)	DP_n[a]	DP_w[b]	$Đ_M$[c]
F8FBT	38.5	65.1	71	120	1.69
F8BT-OC_8	37.5	74.2	57	113	1.98
F8BT-2	45.4	78.3	70	121	1.72
F8BT-3	54.1	89.3	78	129	1.65
F8BT-4	55.2	88.1	75	120	1.60
F8BT-5	50.8	83.9	66	110	1.65
F8BT-6	49.9	85.4	62	107	1.71
F8BT-PEG	-	-	-	-	-

[a]Degree of polymerisation calculated from M_n.
[b]Degree of polymerisation calculated from M_w.
[c]$Đ_M$ calculated from M_w/M_n.

The molecular weights of the polymers were all determined using gel permeation chromatography (GPC) in chlorobenzene and are summarized in **Table 1**. As the substituted polymers are all from the same batch of **F8FBT**, we would expect similar M_w and dispersity for all polymers. Some small variance may be due to the work-up and purification. Inspection of **Table 1** shows that the observed M_n and M_w gradually increase as the length of the hydrophilic chain increased from diethylene glycol monomethyl ether (m= 2) to tetraethyleneglycol monomethyl ether (m= 4), before slightly decreasing for 2, 5, 8, 11, 14 pentaoxahexadecan-16-ol (m= 5) and hexaethylene glycol (m= 6). The hydrophilic ethylhexanol chain exhibits a similar profile to the starting polymer. Therefore, we believe the changes observed are due to a change in hydrodynamic radius in chlorobenzene solution. We note that we could not measure **F8BT-PEG** molecular weight by GPC under these conditions. This may be due to the adsorption of **F8BT-PEG** onto the surface of GPC stationary phase, which limits the reproducibility and separation efficiency.[96,97]

2.3 Optical properties

2.3.1. Absorption spectra

The UV-Vis absorption spectra of **F8FBT**, **F8BT-OC$_8$**, **F8BT-m** (m= 2, 3, 4, 5, 6) and **F8BT-PEG** at room temperature in chloroform solution and thin films are shown in Figure 25 and the data of optical properties is summarized in **Table 2**. Clearly, both in solution and thin films, all polymers demonstrate two absorption bands, a high energy band corresponding to the π-π* transition around 330 nm and a low energy band of 450 nm corresponding to intramolecular charge transfer (ICT) between the electron donating unit and electron accepting unit.[50,98] In chloroform solution, the starting **F8FBT** has a high energy band with peak at 319 nm and a low energy band with peak at 440 nm.

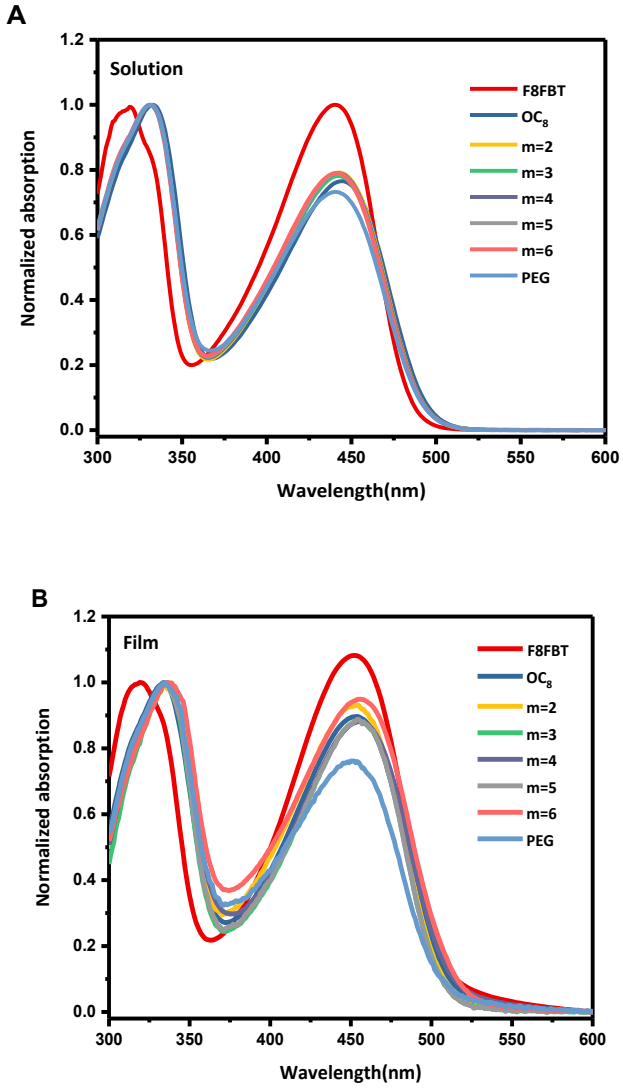


Figure 25 UV-Vis absorption spectra of polymers in chloroform solution (A) and thin film (B)

After the fluorine on the conjugated backbone is substituted by a series of increasingly hydrophilic side chains, the two absorption bands of synthesized polymers both demonstrate a slight red shift in chloroform solution. For the absorption maxima (λ_{max}) of the high energy band of **F8BT-OC$_8$**, **F8BT-m** (m= 2, 3, 4, 5, 6) and **F8BT-PEG,** they demonstrate a 12 nm red shift in chloroform solution compared with **F8FBT**. Unlike the absorption maxima (λ_{max}) of the high energy band, the absorption maxima (λ_{max}) of the low energy band of **F8BT-OC$_8$**, **F8BT-m** (m= 2, 3, 4, 5, 6) and **F8BT-PEG** demonstrate a smaller red shift, around 2-5nm. The shifts can be related to a change in the nature of the backbone substituent, from electron withdrawing fluorine to an electron donating oxygen.

The two absorption bands of **F8FBT** have almost same absorption intensity in chloroform solution. However, the intensity of ICT of **F8BT-OC$_8$**, **F8BT-m** (m= 2, 3, 4, 5, 6) and **F8BT-PEG** is clearly weaker than the high energy band absorption intensity, which is very different from **F8FBT**. The intensity difference in the ICT is related to the change in electron accepting ability of the BT comonomers as the electron deficient fluorine is replaced by electron donating oxygen. Noticeably, from short side chain 2-ethyl-1-hexanol to very long side chain PEG, the length of side chain has little influence on absorption in chloroform solution, suggesting the electronics are similar.

In the solid state, the substituted polymers demonstrate similar trends as in chloroform solution. First, the substituted polymers all demonstrate a slight red shift both in high energy band and low energy band compared with **F8FBT**. Second, the intensity of ICT is also weaker than high energy band intensity, which has been discussed in chloroform solution. From the 2-ethyl-1-hexayloxyl to the hexaethylene glycol, clearly the length of side chain has little influence on absorption in solid state. However, when the side chain is PEG (M_n= 10,000 g/mol), the intensity of the ICT band is noticeably lower. There are many studies about the effect of side chain on optical properties, but to my knowledge, the side chain as long as PEG (M_n= 10,000 g/mol) is not reported. The reduction in the low energy band absorption intensity is maybe due to the weaker interchain interactions with the very long side chain.[99] The **F8FBT**, **F8BT-OC$_8$**, **F8BT-m** (m= 2, 3, 4, 5, 6) and **F8BT-PEG** have the following optical band gaps (measured from the absorption onset in thin film): 2.45 eV, 2.44 eV, 2.44 eV, 2.45 eV, 2.44 eV, 2.45 eV, 2.44 eV, 2.46 eV. Clearly, all the polymer have almost same band gap. From the data from absorption in solid states, the effect of side chain length on optical band gap is limited.

2.3.2. Emission spectra

The photoluminescence (PL) spectra of polymers in chloroform solution and thin films are shown in Figure 26. The emission maxima ($\lambda_{em,\ max}$) of the polymer solution and thin film PL spectra are summarized in **Table 2**. All polymers demonstrate broad emission profiles with emission maxima in the green region of the spectrum. All polymers were excited at the absorption maximum of the low energy band.

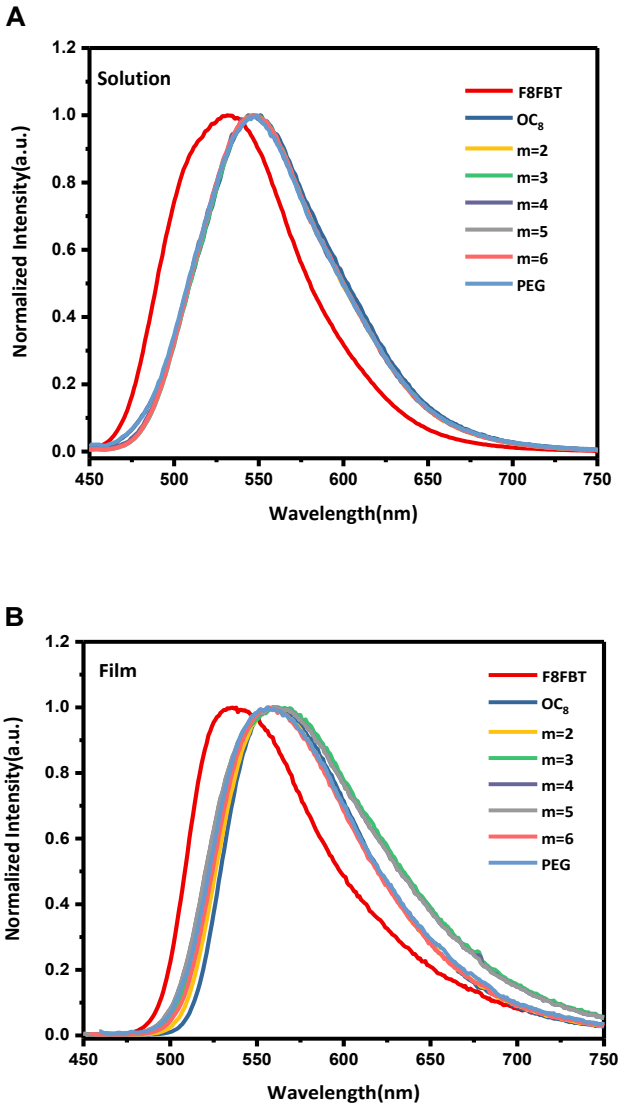


Figure 26 Emission spectra of polymers in chloroform solution (A) and thin film (B).

In chloroform solution, the $\lambda_{em,\ max}$ of **F8FBT** is 532 nm. For **F8BT-OC$_8$**, **F8BT-m** (m= 2, 3, 4, 5, 6) and **F8BT-PEG**, they have an almost same $\lambda_{em,\ max}$ of 546 nm in chloroform solution, which is a large solution Stokes shift ($\Delta\lambda_{(sol)}$) of 104 nm. However, the thin film emission maximum of **F8FBT** (538 nm) is slightly red shifted in comparison to solution (532 nm). Also, the solid

state $\lambda_{em,\ max}$ (550-556 nm) of substituted polymers were slightly red shifted in comparison to chloroform solution (546 nm).

The absorption and emission of polymers in toluene solution were also investigated. (Appendix Figure 1, 2) The emission maxima of **F8FBT** is 506 nm, while the emission maxima of **F8BT-OC$_8$**, **F8BT-m** (m= 2, 3, 4, 5, 6) and **F8BT-PEG** is 535 nm. The emission maxima of all the polymers are blue shifted in toluene compared to chloroform solution. The red shift of the emission maxima ($\lambda_{em,\ max}$) in the more polar solvent (chloroform) suggests a polar excited state that is stabilized through interactions with a polar solvent. In more polar solvents, the ICT state is stabilized and therefore more likely to be the lowest in energy.[100]

Table 2 Optical properties of polymers in chloroform solution and thin film

Polymer	$\lambda_{abs,\ max}$ (sol) nm	$\lambda_{abs,\ max}$ (film) nm	$E_{g(opt)}$ eV	$\lambda_{em,\ max}$ (sol) nm	Δ λ (sol) nm	$\lambda_{em,\ max}$ (film) nm	Δ λ (film) nm
F8FBT	319[a], 440[b]	319[a],452[b]	2.45	532	92	538	88
F8BT-OC$_8$	331[a], 445[b]	334[a],454[b]	2.44	548	103	554	100
F8BT-2	331[a], 442[b]	335[a],454[b]	2.44	546	104	556	102
F8BT-3	331[a], 442[b]	335[a],455[b]	2.45	546	104	556	101
F8BT-4	331[a], 442[b]	336[a],455[b]	2.44	546	104	555	100
F8BT-5	331[a], 442[b]	335[a],456[b]	2.45	546	104	556	100
F8BT-6	331[a], 442[b]	336[a],455[b]	2.44	546	104	554	99
F8BT-PEG	331[a], 442[b]	335[a],454[b]	2.46	546	104	550	96

[a] λ_{max} of high energy band.
[b] λ_{max} of low energy band.
$\lambda_{abs,\ max}$(sol) nm, $\lambda_{em,\ max}$ (sol) nm and Δλ (sol) nm were all investigated in chloroform solution.

2.4 Electronic properties

To investigate the electronic properties of substituted polymers, the solid state electronic properties of **F8FBT**, **F8BT-OC$_8$**, **F8BT-m** (m= 2, 3, 4, 5, 6) were investigated using cyclic voltammetry (CV).

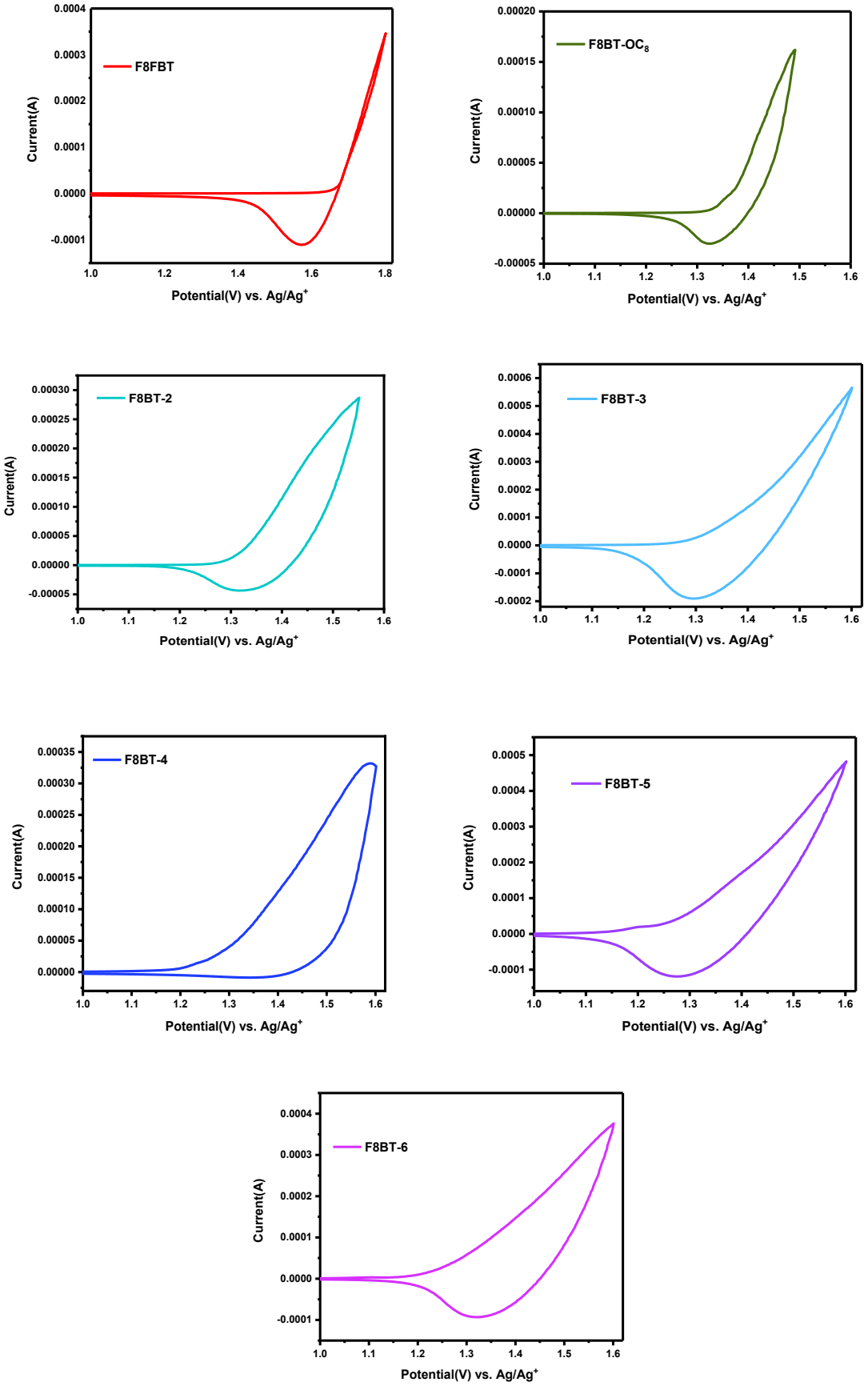


Figure 27: CV of thin films of **F8FBT**, **F8BT-OC$_8$** and **F8BT-m** (m= 2, 3, 4, 5, 6) in acetonitrile/ [n–Bu$_4$N]PF$_6$ solutions (0.1 M) at a scan rate of 0.1 V/s.

Samples were prepared by drop-casting solution on the Pt rod surface. Samples were measured in anhydrous, degassed solutions of acetonitrile with tetrabutylammonium hexafluorophosphate (0.1 M) electrolyte using an Ag/Ag^+ as reference electrode. The cyclic voltammograms of all polymers are demonstrated in Figure 27 and the electronic properties are summarized in **Table 3**. The HOMO level of each polymer was estimated from the onset of oxidation, assuming that the ferrocene/ferrocenium reference redox system is 4.8 eV below the vacuum level.[101,102] The LUMO levels are approximated by adding the optical band gap to the HOMO levels estimated using CV.

The HOMO energy level of polymers can be calculated from the onset oxidation potential $E_{ox(onset)}$, based on the reference energy level of ferrocene (4.8 eV below the vacuum level). The molecular orbital energy levels are calculated from the cyclic voltammetry and E_{op} according to the following equations:

$$\boldsymbol{E_{HOMO} = -(E_{ox(onset)} + 4.8 - E_{FOC})}$$

$$\boldsymbol{E_{LUMO} = E_{HOMO} + E_{op}}$$

E_{FOC} is the potential of external standard, ferrocene/ferricenium ion (F_{oc}/F_{oc+}) couple. The solution of ferrocene in acetonitrile (0.01 M) was used as the external standard (Appendix Figure 4). The HOMO level of **F8FBT** is -6.09 eV, which is very similar to the literature value (-6.01 eV).[103] As fluorine is more electron deficient than alkoxy substituted side chains, the HOMO level of the **F8FBT** is deeper than the alkoxy polymers. As the substituted polymers only differ by the length of side chains, it is not surprising that they demonstrate very similar electronic properties. The HOMO level of **F8BT-OC_8** and **F8BT-m** (m= 2, 3, 4, 5, 6) are -5.77 eV, -5.73 eV, -5.73 eV, -5.72 eV, -5.69 eV, -5.67 eV respectively. As **F8BT-PEG** is soluble in acetonitrile, it could not be measured by CV as a thin-film, and was therefore measured by air photoemission spectroscopy (APS).

Table 3: Electronic properties of polymers

Material	HOMO[a] eV (CV)	LUMO[b] eV (CV +$E_{g(opt)}$)	I.P.,eV[c] (APS)	'LUMO' eV[d] (APS +$E_{g(opt)}$)	$E_{g(opt)}$ eV
F8FBT	-6.09	-3.68	-6.07	-3.65	2.45
F8BT- OC_8	-5.77	-3.38	-5.82	-3.41	2.44
F8BT-2	-5.73	-3.33	-5.67	-3.24	2.44
F8BT-3	-5.73	-3.33	-5.67	-3.24	2.45
F8BT-4	-5.72	-3.29	-5.71	-3.28	2.44
F8BT-5	-5.69	-3.31	-5.73	-3.31	2.45
F8BT-6	-5.67	-3.31	-5.81	-3.40	2.44
F8BT-PEG			-5.82	-3.36	2.46

[a] Measured by CV, error ± 0.05 eV[104]
[b] Estimated by adding $E_{g(opt)}$
[c] Ionisation potentials measured from APS, error ± 0.05 eV[105]
[d] Estimated by adding $E_{g(opt)}$

2.5 Air photoemission spectroscopy measurements

APS exploits the photoelectric effect by measuring the number of photoelectrons that are emitted from a sample illuminated by tuneable monochromatic UV light. Photoelectrons are only emitted from the sample if the photon energy is greater than the depth of the HOMO, and so the HOMO level can be determined by scanning the excitation photon energy and measuring the photocurrent.[105] The ionisation potential levels of substituted polymers are investigated by APS (Figure 28). The ionisation potential level of **F8FBT** is – 6.07 eV by APS, which is very close to the HOMO level measured by CV. The ionisation potential levels are -5.82 eV, -5.67 eV, -5.67 eV, -5.71 eV, -5.73 eV, -5.81 eV and -5.82 eV for **F8BT-OC_8**, **F8BT-m** (m= 2, 3, 4, 5, 6) and **F8BT-PEG** respectively. A rough estimate of the LUMO levels of each polymer can be calculated by adding the optical band gap $E_{g(opt)}$ onto the ionisation potential levels measured by APS. However, the optical band gap does not take into account the exciton binding energy, so the LUMO levels in **Table 3** using this method are approximations.

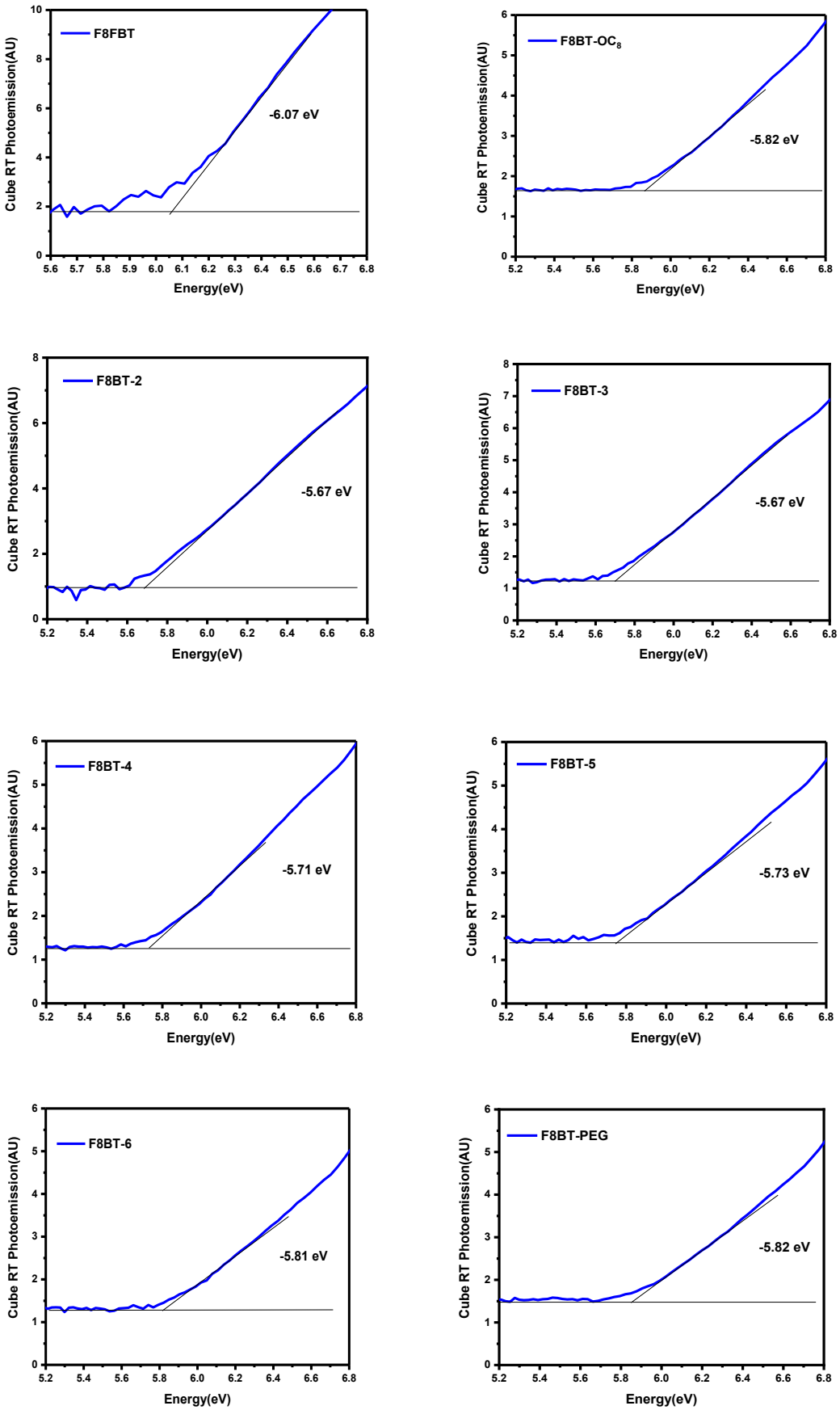
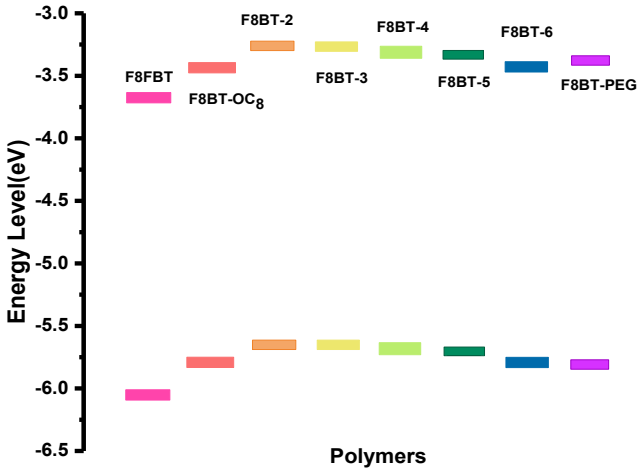


Figure 28 Ionisation potentials of polymers measured by APS

In order to have a better understanding of energy levels of substituted polymers, the energy levels of substituted polymers are demonstrated in **Scheme 2** (data from APS and E_g). Compared with **F8FBT**, the HOMO and LUMO energy levels of substituted polymers both increase. This is maybe due to the alkoxy substituted polymers being more electron rich than the fluorine substituted polymer. Previous work on fluorine substituted polymers has shown that fluorine stabilizes both the HOMO and LUMO energy levels equally.[106] This work appears to validate these previous observations.



Scheme 2 Energy levels diagram of the polymers (calculated from APS and $E_{g(opt)}$).

2.6 Thermal properties

Differential scanning calorimetry (DSC) has been widely applied to explore the crystallinity and thermal behaviours of polymers. The thermal behaviours of **F8FBT**, **F8BT-OC$_8$**, **F8BT-m** (m= 2, 3, 4, 5, 6) and **F8BT-PEG** were investigated using DSC on powder samples under nitrogen (Figure 29). For **F8FBT**, there is one relatively strong and broad endothermic transition measured, which onsets at around 226 °C and peaks at 262°C. This transition is likely the result of the polymer melting. Upon cooling, the side chain solidify, giving one exothermic transition. The transition onsets at 154 °C and peaks at 138 °C. This transition is due to the polymer crystallization.

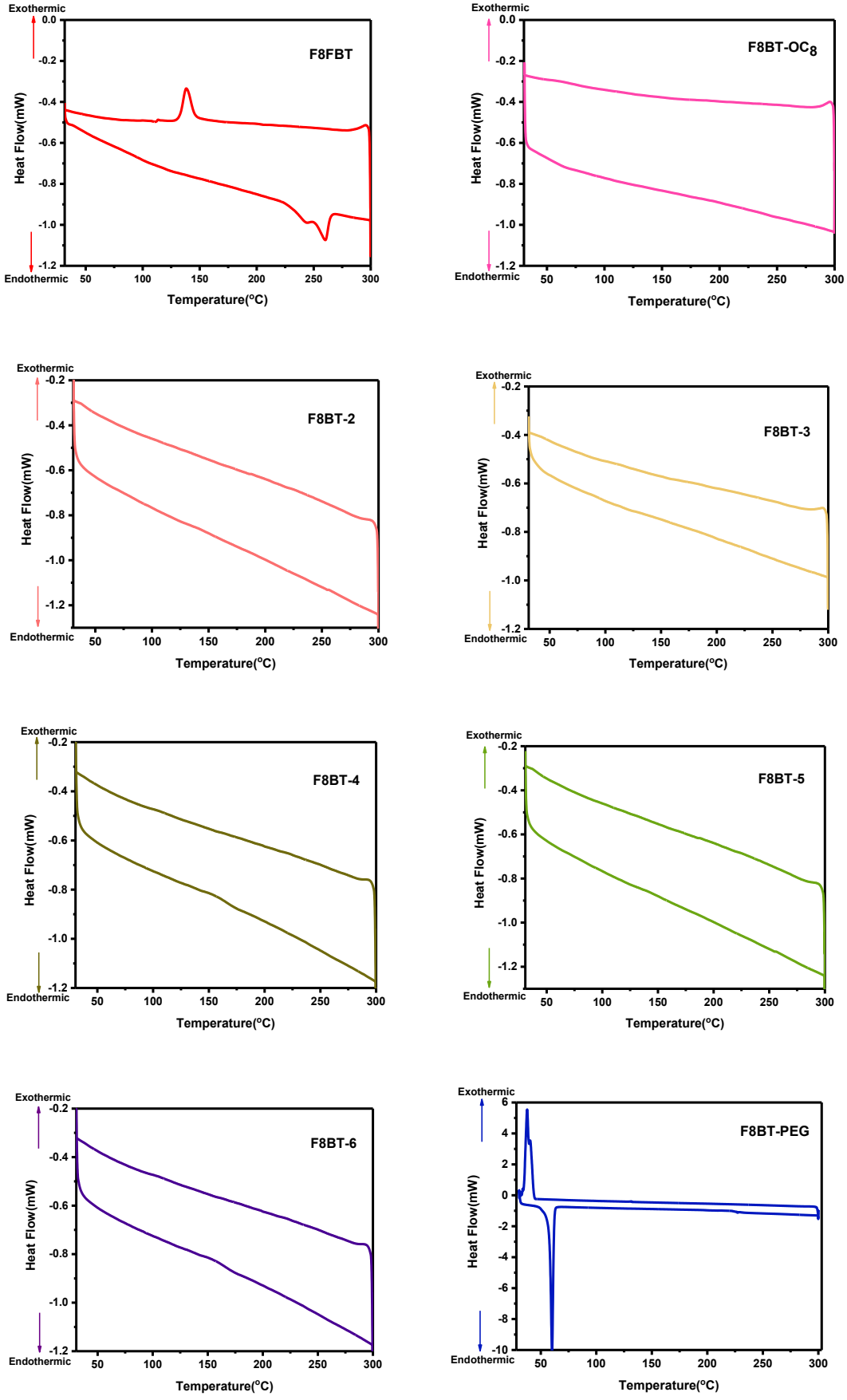


Figure 29: DSC heating and cooling curves of polymers between 30 °C and 300 °C at 20 °C/min.

The two peaks at 262°C and 138 °C are **F8FBT**'s melting point and crystal point respectively, which are very similar to the literature.[106] After the fluoride on conjugated backbone substituted, the thermal properties of substituted polymers become very different from **F8FBT**. In the heating cycles between 30 °C and 300 °C, there is clearly no endothermic or exothermic transition for **F8BT-OC$_8$** and **F8BT-m** (m= 2, 3, 4, 5, 6). However, for **F8BT-PEG**, in the heating cycles between 30 °C and 300 °C, there is one strong endothermic transition measured, which onsets at around 53 °C and peaks at 60 °C. Upon cooling these side chains solidify, giving one exothermic transition, which onsets at 43 °C and peaks at 38 °C. Also, we know the melting point and crystal point for only PEG are 66 °C and 40 °C respectively[107]. Clearly, the side chain PEG plays a dominant role in the crystallinity and thermal behaviors of **F8BT-PEG**.

2.7 Hydrophilicity

The alkoxy substituted **F8BT-OC$_8$** and **F8BT-m** (m= 2, 3, 4, 5, 6) all have the same solubility as **F8FBT**. They are all soluble in organic solvents, like chloroform, THF and chlorobenzene, but insoluble in polar solvents, like methanol and acetonitrile. However, when grafting the PEG (M_n= 10,000 g/mol) to the conjugated backbone of **F8FBT**, then the **F8BT-PEG** becomes not only soluble in chloroform and THF, but also soluble in polar solvents, such as methanol, DMSO or water. The change of solubility is due to the very hydrophilic grafted long chain PEG. Figure 30 shows the solubility of **F8BT-PEG** in polar solvents.

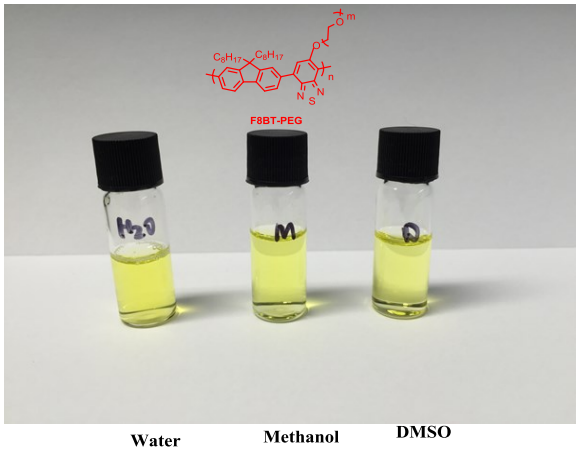


Figure 30 F8BT-PEG soluble in polar solvents (1 mg/ml)

In order to investigate the hydrophilicity of substituted polymers more quantitatively, one experiment was performed to sequentially add water into the THF solution of substituted polymers (2.5 mg/ml) until a set transmittance was reached. The THF solution will become cloudy when H_2O added because **F8FBT**, **F8BT-OC$_8$** and **F8BT-m** (m= 2, 3, 4, 5, 6) were not soluble in H_2O. The side chain of **F8BT-6**, hexaethylene glycol (m= 6), is very hydrophilic. No matter how much water added, the transmittance of THF/water solution of **F8BT-6** is still around 63% of the original transmittance of THF solution (without H_2O). Therefore we investigated the hydrophilicity of substituted polymers by adding H_2O until 65% of the original THF solution transmittance was reached. For example, the transmittance of **F8FBT** at 550 nm (only THF solution) was 83%. When 80 µL water was added to 3 ml THF solution (2.5 mg/ml), the transmittance at 550 nm decreased to 54%, which was around 65% of the original transmittance. The water fraction in the THF/water mixtures for **F8FBT** was then 2.6% (0.08/ 3.08 × 100% = 2.6%) (Figure 31). The other polymers were also measured the transmittance at 550 nm by adding H_2O to the original THF solution until the set transmittance was reached. For substituted polymers, the hydrophilicity increases from 2-ethyl-1-hexanol to hexaethylene glycol (m= 6), indicating more water needed to cause precipitation. The data is collected and summarized in **Table 4**.

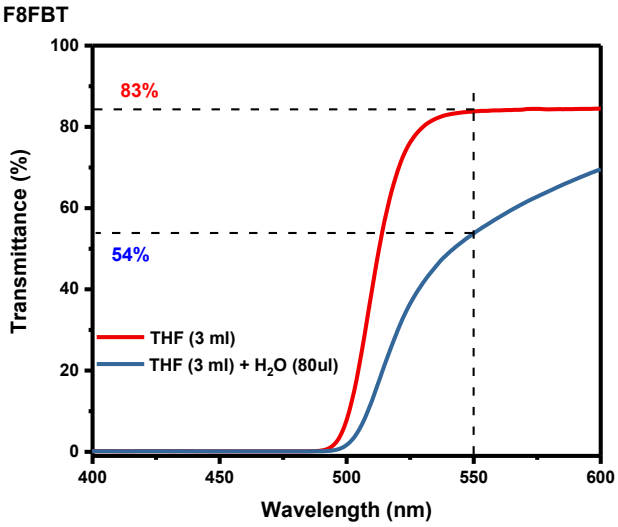


Figure 31 THF solution of **F8FBT** with H_2O

Table 4 Water needed for a set transmittance

Polymers	**F8FBT**	**F8BT-OC_8**	**F8BT-2**	**F8BT-3**	**F8BT-4**	**F8BT-5**	**F8BT-6**	**F8BT-PEG**
H_2O/(THF+H_2O)% (V:V)	2.6%	4.6%	12.9%	15.3%	28.6%	41.9%	45.3%	-

As **F8BT-PEG** is both water and THF soluble, the transmittance of solution did not change when water added. From the data in **Table 4**, clearly as the length of the ethylene glycol increases, the solubility in polar mixtures increases. According to the data in **Table 4**, the hydrophilicity of conjugated polymer can be modulated by the side chain.

2.8 Contact angle measurement

Contact angle measurement is a convenient and viable method to determine surface hydrophilicities.[108] A hydrophilic surface allows a drop of water to spread more than a hydrophobic surface as there is less resistance (tension) at the surface. Therefore, the contact angle between the water drop and the surface is smaller than that detected for a hydrophobic surface. Here, we use the contact angle measurement to investigate the hydrophilicity of substituted polymers. Thin films (5 mg/ml) were formed by spin-coating onto quartz substrates. Figure 32 demonstrates the water contact angle images of the polymer films and the contact angle data was summarized in **Table 5**. The contact angle of the **F8FBT** is 101.4°, while the contact angle of **F8BT-OC_8** and **F8BT-m** (m= 2, 3, 4, 5, 6) decrease gradually after grafting increasingly hydrophilic side chains. The contact angle data decrease gradually from 100.8° (**F8BT-OC_8**) to 85.6° (**F8BT-6**). Clearly, the more hydrophilic the side chains become, the smaller the contact angle will be. When the side chain is PEG, the **F8BT-PEG** becomes soluble in polar solvents, such as DMSO and water. The contact angle data of **F8BT-PEG** drop dramatically to 31.0°. The contact angle of pure PEG film is reported to be around 25°.[109] Clearly, the dramatic decrease of contact angle was due to the hydrophilic PEG chain.

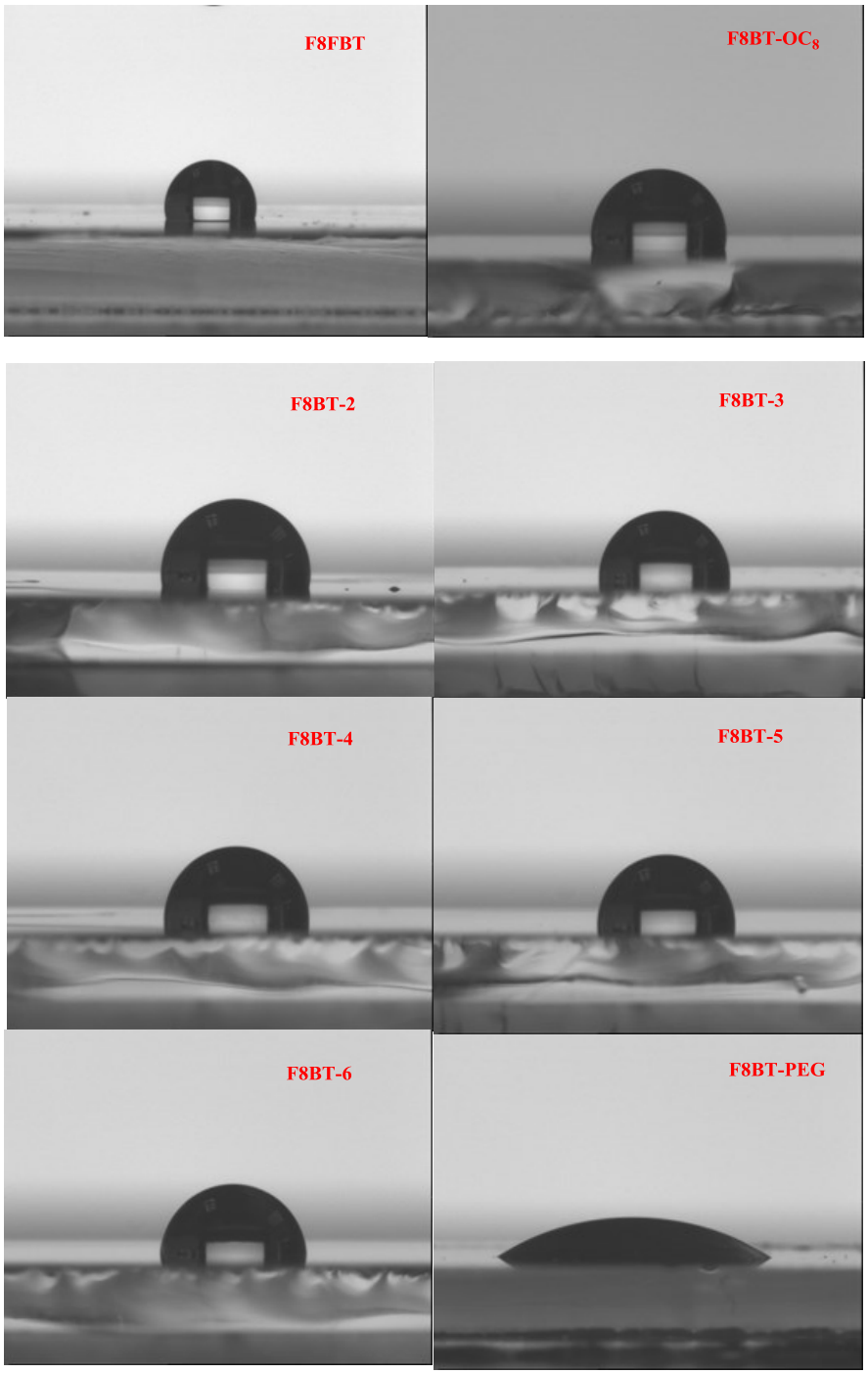


Figure 32. Water contact angle pictures of **F8FBT** and substituted polymers

The data of contact angles demonstrates the same trend as solution hydrophilicity measurement discussed in **2.7**. The data of contact angle measurement demonstrate that the hydrophilicity of polymers can be modulated by nucleophilic aromatic substitution quantitatively. Figure 33 shows the contact angle changes with increasingly hydrophilic side chains.

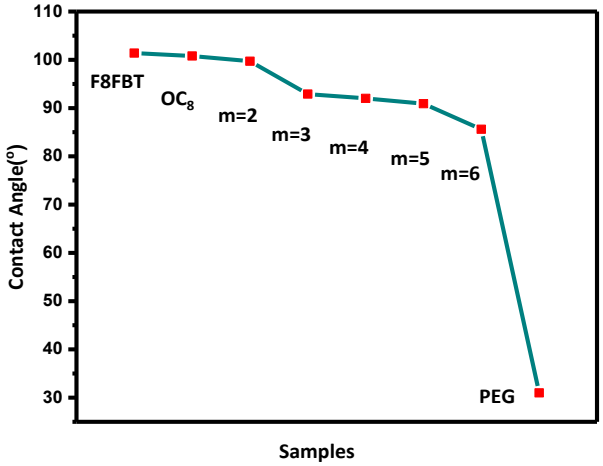


Figure 33 Contact Angle of **F8FBT** and the substituted polymers

Table 5 Contact Angle measurement

Polymers	[a]F8FBT	[a]F8BT-OC_8	[a]F8BT-2	[a]F8BT-3	[a]F8BT-4	[a]F8BT-5	[a]F8BT-6	[a]F8BT-PEG
Contact Angle	101.4°± 1.3°	100.8°± 1.1°	99.7°± 1.3°	92.9°± 1.6°	92.0°± 1.6°	90.9°± 1.4°	85.6°± 1.0°	31.0°± 1.2°

[a]Average of five measurements

2.9 Conclusions

The conjugated polymers with increasingly hydrophilic side chains have been synthesized by nucleophilic aromatic substitution via post-polymerization. The optical, electrical and thermal properties of substituted polymers have been investigated in this chapter. The results demonstrate that by increasing the length of the ethylene glycol side chain, the hydrophilicity of the polymer can be carefully tuned. However, the energetics and band gap of the polymers remain essentially constant. This method therefore allows a variety of side chains to be readily introduced into the polymer backbone.

2.10 Experimental methods

2.10.1 CV measurement

CV was carried out with a standard three-electrode cell in a 0.1 M tetrabutylammonium hexafluorophosphate ((TBA)PF_6) solution in acetonitrile at room temperature with a scanning rate of 0.1 V s^{-1}. A Pt rod working electrode (1.6 mm diameter), a Pt wire counter electrode, and an Ag/AgCl reference electrode were used. The oxidation potentials were calibrated with a standard ferrocene/ferrocenium (FOC) redox system as the standard (assuming the energy level of FOC is 4.8 e V below vacuum) for estimating the HOMO energy level of polymers. Samples were prepared by drop-casting solution on the Pt rod surface.

2.10.2 APS measurement

Measurement of APS was made using the KP technology APS-04 instrument. For APS measurements, the sample was illuminated with UV light from a monochromatic deuterium lamp source (4–7 eV). The raw photoemission data were corrected for offset and the cube root was taken, with the ionisation potential value found from the extrapolated intersection of the straight-line fit of the cube root of the photoemission with the baseline.

2.10.3 Contact angle measurement

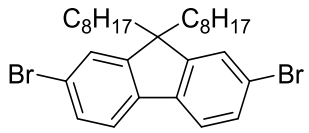
A Krüss DSA100E goniometer was used to carry out contact angle measurements using the static sessile drop method. All measurements took place at 25° C at a humidity of 65%. Thin films were spin coated onto quartz substrates at 2000 rpm from 5 mg/mL polymer solutions. Prior to spin-coating, quartz substrates were washed sequentially by soap water, acetone and isopropanol. Quartz substrates were then dried by flushing with nitrogen. For each measurement, a 5 µL drop of deionised water was suspended at the end of a needle and slowly brought into contact with the sample. Contact angles were measured 30 seconds after the withdrawal of the needle tip from the droplet to allow the drop time to equilibrate on the sample surface. Drop shapes were then fitted using the polynomial method. Each quoted contact angle was calculated from an average of five measurements made on the same sample.

2.10.4 Materials

2, 7-Dibromofluorene (97%, Sigma Aldrich), 1-bromooctane (98%, TCI Chemicals), tetra-n-butylammonium bromide (98%, Sigma Aldrich), 2-isopropoxy, 4, 4, 5, 5-tetramethyl-1, 3, 2-dioxaborolane(98%, Sigma Aldrich), 4, 7-dibromo-5-fluoro-2, 1, 3 benzothiadiazole(96%, Sigma Aldrich), *n*-Butyllithium solution (1.6 M in hexanes, Sigma Aldrich), tetrakis(triphenylphosphine)palladium(0)(99.9%, Strem Chemicals UK), 2-ethyl-1-hexanol (99.6%, Sigma Aldrich), diethylene glycol monomethyl ether (99%, Sigma Aldrich), triethylene glycol monomethyl ether (95%, Sigma Aldrich), 2, 5, 8 ,11, 14 pentaoxahexadecan-16-ol (98%, fluoroChem), hexaethylene glycol (97%, Sigma Aldrich)tetraethyleneglycol monomethyl ether (Technical Grade, Sigma Aldrich), hexaethylene glycol (97%, Sigma Aldrich), poly(ethylene glycol) methyl ether (average M_n= 10,000 g/mol, PDI ≤ 1.2, Sigma Aldrich) and Slide-A-Lyzer Dialysis Cassettes (20K MWCO, 3ml) (ThermoFisher SCIENTIFIC) were used as received. Other chemical reagents were analytical grade and used as received. Deionized water from our lab was used in this experiment.

2.10.5 Synthesis

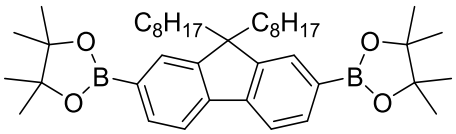
2, 7-Dibromo-9, 9-dioctylfluorene.[110]



2, 7-Dibromofluorene (2.00 g, 6.17 mmol), 1-bromooctane (2.63 g, 13.6 mmol), toluene (20 mL), 2ml NaOH (50 wt%) and tetrabutylammonium bromide (0.2 g, 0.6 mmol) were heated at 90 °C for 24 h. After cooling, mixture was diluted with ethyl acetate (50 ml) and the organic layer was washed with water (3 times, 3× 20 ml). The combined organics were dried over $MgSO_4$, and the solvent was removed under reduced pressure. The crude product was purified over silica gel column using hexane to give 2.57 g of white solid. (Yield 75%)

^{1}H-NMR (400 MHz, $CDCl_3$) δ 7.56 – 7.52 (m, 2H), 7.50 – 7.45 (m, 4H), 2.00 – 1.87 (m, 4H), 1.30 – 0.99 (m, 20H), 0.85 (t, *J* = 8.0 Hz, 6H), 0.59 (m, 4H).

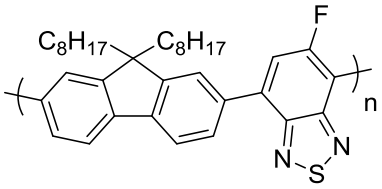
9, 9-Dioctyl-9*H*-fluorene-2, 7-diboronic acid bis (pinacol) ester [110]



To a solution of 2, 7-dibromo-9,9-dioctylfluorene (2.67 g, 4.87 mmol) in anhydrous THF (50 mL) at -78 °C was added, 7.3 mL (11.7 mmol) of *n*-butyllithium (1.6 M in hexane). The mixture was stirred at -78°C for 60 minutes. 2-Isopropoxy-4, 4, 5, 5-tetramethyl-1, 3, 2 dioxaborolane (2.18 g, 11.7 mmol) was added rapidly to the solution, and the resulting mixture was allowed to warm to room temperature and stirred for 24 h under argon. The mixture was poured into water and extracted with diethyl ether (3 times, 3× 50 ml). The organic extracts were combined and dried over $MgSO_4$. The solvent was removed under reduced pressure, and the residue was recrystallized from acetone to give 1.73 g white solid. (Yield 55%)

^{1}H-NMR (400 MHz, $CDCl_3$) δ 7.83 (m, 2H), 7.79 – 7.72 (m, 4H), 2.07 – 1.95 (m, 4H), 1.42 (s, 24H), 1.28 – 0.94 (m, 20H), 0.83 (t, *J* = 6.2 Hz, 6H), 0.56 (m, 4H).

F8FBT[111]



A mixture of 9, 9-dioctyl-9*H*-fluorene-2, 7-diboronic acid bis(pinacol) ester **5**, (975.47 mg, 1.518 mmol), 4, 7-dibromo-5-fluoro-2, 1, 3-benzothiadiazole **6** (473.42 mg, 1.518 mmol), tetrabutylammonium iodide (46 mg, 0.13 mmol) and $Pd(PPh_3)_4$ (35.1 mg, 0.0304 mmol) were added to a high-pressure microwave vial. The vial was sealed with a septum and degassed with argon before toluene (10 mL) and K_2CO_3 (2 M, 4 mL) solution were added. The mixture was heated at 120°C for 72 h. The reaction was cooled to room temperature and precipitated into methanol, stirred for 30 min and filtered through a Soxhlet thimble. The precipitates were further purified by washing with methanol, acetone and hexane

under argon for 24 respectively. The polymer remaining in the thimble was then dissolved in hot chloroform and precipitated into methanol to give 591 mg **F8FBT** (Yield 72%)

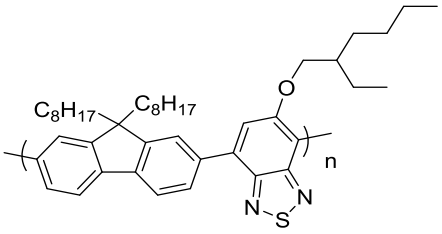
M_n: 38.5 kDa, M_w: 65.1 kDa, M_w/M_n (Đ): 1.69

^{1}H-NMR (400 MHz, $CDCl_3$) δ 8.15 – 7.79 (m, 7H), 2.16 (m, 4H), 1.33 – 1.08 (m, 20H), 0.99 (m, 4H), 0.84 (m, 6H).

^{19}F-NMR (400 MHz, $CDCl_3$) δ -114.5 ppm

The ^{1}H-NMR is in Appendix Figure 4.

F8BT-OC_8



A mixture of **F8FBT** (54 mg, 0.1 mmol) and KOH (112 mg, 2.0 mmol) were added to high pressure microwave vial. The vial was sealed with a septum and degassed with argon before anhydrous chlorobenzene and DMSO (3:1, v:v, 8 ml total) and 2-ethylhexanol (26 mg, 0.2 mmol) were added. The solution was heated at 120°C for 2 days. After reaction, the solution was precipitated into methanol dropwise, stirred for 30 min and filtered through a Soxhlet thimble. The precipitates were further purified by washing with acetone under argon for 24 h and the polymer was extracted with chloroform. Dry chloroform solution to yield **F8BT- OC_8** (52 mg, 82% yield).

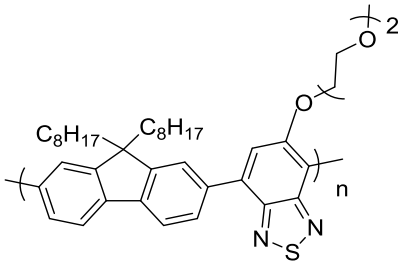
M_n: 37.5 kDa, M_w: 74.2 kDa, M_w/M_n (Đ): 1.98

^{1}H-NMR (400 MHz, $CDCl_3$) δ 8.17 – 7.74 (m, 7H), 4.22 (m, 2H), 2.17 (m, 4H), 1.81 (m, 2H), 1.44 (m, 2H), 1.32 (m, 8H), 1.19 (m, 20H), 1.01 (m, 4H), 0.92 (t, *J* = 6.0 Hz, 3H), 0.83 (t, *J* = 6.0 Hz, 6H).

^{19}F-NMR (400 MHz, $CDCl_3$) shows no fluorine signal

The ^{1}H-NMR is in Appendix Figure 5.

F8BT-2



A mixture of **F8FBT** (82 mg, 0.152 mmol) and KOH (170.5 mg, 3.04 mmol) were added to high pressure microwave vial. The vial was sealed with a septum and degassed with argon before anhydrous chlorobenzene and DMSO (3:1, v:v, 8 ml total) and 2-(2-methoxyethoxy)ethanol (36.5 mg, 0.304 mmol) were added. The solution was heated at 120°C for 2 days. After reaction, the solution was precipitated into methanol dropwise, stirred for 30 min and filtered through a Soxhlet thimble. The precipitates were further purified by washing with acetone under argon for 24 h and the polymer was extracted with chloroform. Dry chloroform solution to yield **F8BT-2** (75 mg, 77% yield).

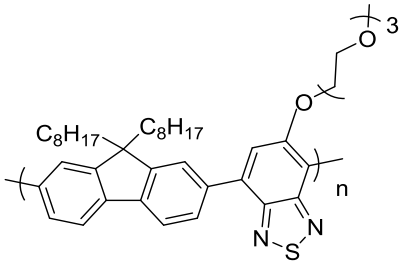
M_n: 45.4 kDa, M_w: 78.3 kDa, M_w/M_n (Đ): 1.72

^{1}H-NMR (400 MHz, $CDCl_3$) δ 8.23 – 7.72 (m, 7H), 4.39 (m, 2H), 3.85 (m, 2H), 3.68 (t, *J* = 4.8 Hz, 2H), 3.57 (t, *J* = 4.4 Hz , 2H), 3.39 (s, 3H), 2.14 (m, 4H), 1.19 (m, 20H), 1.09 – 0.91 (m, 4H), 0.83 (t, *J* = 6.0 Hz, 6H).

^{19}F-NMR (400 MHz, $CDCl_3$) shows no fluorine signal.

The ^{1}H-NMR is in Appendix Figure 6.

F8BT-3



A mixture of **F8FBT** (72 mg, 0.133 mmol) and KOH (150 mg, 2.66 mmol) were added to high pressure microwave vial. The vial was sealed with a septum and degassed with argon before anhydrous chlorobenzene and DMSO (3:1, v:v, 8 ml total) and triethylene glycol

monomethyl ether (43.7 mg, 0.266 mmol) were added. The solution was heated at 120°C for 2 days. After reaction, the solution was precipitated into methanol dropwise, stirred for 30 min and filtered through a Soxhlet thimble. The precipitates were further purified by washing with acetone under argon for 24 h and the polymer was extracted with chloroform. Dry chloroform solution to yield **F8BT-3** (57.5 mg, 63% yield).

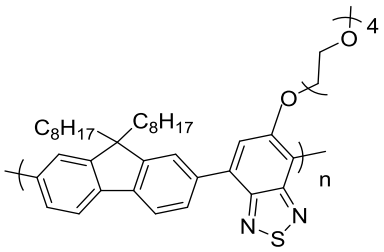
M_n: 54.1 kDa, M_w: 89.3 kDa, M_w/M_n (Đ): 1.65

^{1}H-NMR (400 MHz, $CDCl_3$) δ 8.33 – 7.68 (m, 7H), 4.38 (m, 2H), 3.86 (m, 2H), 3.67 (m, 6H), 3.54 (t, *J* = 4.4 Hz, 2H), 3.38 (s, 3H), 2.18 (m, 4H), 1.19 (m, 20H), 0.99 (m, 4H), 0.84 (t, *J* = 6.2 Hz, 6H).

^{19}F-NMR (400 MHz, $CDCl_3$) shows no fluorine signal.

The ^{1}H-NMR is in Appendix Figure 7.

F8BT-4



A mixture of **F8FBT** (75 mg, 0.139 mmol) and KOH (156 mg, 2.78 mmol) were added to high pressure microwave vial. The vial was sealed with a septum and degassed with argon before anhydrous chlorobenzene and DMSO (3:1, v:v, 8 ml total) and tetraethyleneglycol monomethyl ether (58 mg, 0.278 mmol) were added. The solution was heated at 120°C for 2 days. After reaction, the solution was precipitated into methanol dropwise, stirred for 30 min and filtered through a Soxhlet thimble. The precipitates were further purified by washing with acetone under argon for 24 h and the polymer was extracted with chloroform. Dry chloroform solution to yield **F8BT-4** (69 mg, 68% yield).

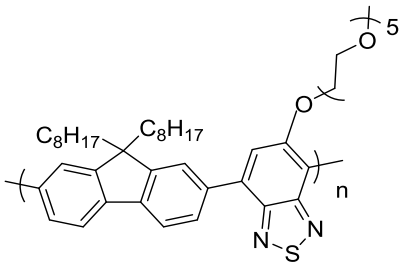
M_n: 55.2 kDa, M_w: 88.1 kDa, M_w/M_n (Đ): 1.60

^{1}H-NMR (400 MHz, $CDCl_3$) δ 8.26 – 7.73 (m, 7H), 4.38 (m, 2H), 3.84 (m, 2H), 3.76 – 3.59 (m, 10H), 3.55 (t, *J* = 4.2 Hz, 2H), 3.38 (s, 3H), 2.31 – 1.97 (m, 4H), 1.19 (m, 20H), 0.99 (m, 4H), 0.83 (t, *J* = 6.2 Hz, 6H).

^{19}F-NMR (400 MHz, $CDCl_3$) shows no fluorine signal.

The ^{1}H-NMR is in Appendix Figure 8.

F8BT-5



A mixture of **F8FBT** (65 mg, 0.120 mmol) and KOH (135 mg, 2.4 mmol) were added to high pressure microwave vial. The vial was sealed with a septum and degassed with argon before anhydrous chlorobenzene and DMSO (3:1, v:v, 8 ml total) and 2, 5, 8, 11, 14 pentaoxahexadecan-16-ol (60.7 mg, 0.240 mmol) were added. The solution was heated at 120°C for 2 days. After reaction, the solution was precipitated into methanol dropwise, stirred for 30 min and filtered through a Soxhlet thimble. The precipitates were further purified by washing with acetone under argon for 24 h and the polymer was extracted with chloroform. Dry chloroform solution to yield **F8BT-5** (66 mg, 71% yield).

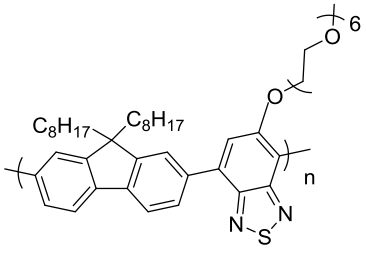
M_n: 50.8 kDa, M_w: 83.9 kDa, M_w/M_n (Đ): 1.65

^{1}H-NMR (400 MHz, $CDCl_3$) δ 8.16 – 7.83 (m, 7H), 4.38 (m, 2H), 3.83 (m, 2H), 3.74 – 3.60 (m, 14H), 3.55 (m, 2H), 3.38 (s, 3H), 2.15 (m, 4H), 1.19 (m, 20H), 0.99 (m, 4H), 0.82 (t, *J* = 6.2 Hz, 6H).

^{19}F-NMR (400 MHz, $CDCl_3$) shows no fluorine signal.

The ^{1}H-NMR picture is in Appendix Figure 9

F8BT-6



A mixture of **F8FBT** (58 mg, 0.107 mmol) and KOH (120 mg, 2.14 mmol) were added to high pressure microwave vial. The vial was sealed with a septum and degassed with argon before anhydrous chlorobenzene and DMSO (3:1, v:v, 8 ml total) and hexaethylene glycol (60.4 mg, 0.214 mmol) were added. The solution was heated at 120°C for 2 days. After reaction, the solution was precipitated into methanol dropwise, stirred for 30 min and filtered through a Soxhlet thimble. The precipitates were further purified by washing with acetone under argon for 24 h and the polymer was extracted with chloroform. Dry chloroform solution to yield **F8BT-6** (70.6 mg, 82% yield).

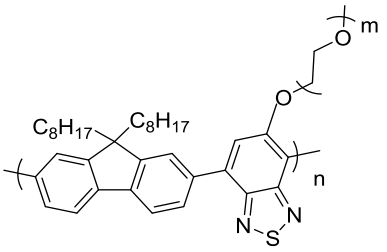
M_n: 49.9 kDa, M_w: 85.4 kDa, M_w/M_n (Đ): 1.71

^{1}H-NMR (400 MHz, $CDCl_3$) δ 8.21 – 7.76 (m, 7H), 4.39 (m, 2H), 3.85 (m, 2H), 3.67 (m, 18H), 3.56 (m, 2H), 3.39 (s, 3H), 2.14 (m, 4H), 1.19 (m, 20H), 0.99 (m, 4H), 0.83 (t, *J* = 6.2 Hz, 6H).

^{19}F-NMR (400 MHz, $CDCl_3$) shows no fluorine signal.

The ^{1}H-NMR is in Appendix Figure 10.

F8BT-PEG



A mixture of **F8FBT** (10.8 mg, 0.02 mmol), PEG (400 mg, 0.04 mmol, M_n= 10,000 g/mol, PDI ≤1.2) and KOH (22.4 mg, 0.4 mmol) were added to high pressure microwave vial. The vial was sealed with a septum and degassed with argon before anhydrous chlorobenzene and DMSO (3:1, v:v, 10 ml total) were added. The solution was heated at 120°C for 2 days. After reaction, the solvent was removed by distillation and the residue was dissolved in deionized water. Then the aqueous solution was injected into the dialysis cassettes by syringe (3ml maximum for one cassette). The cassettes were incubated in deionized water for 2 days with deionized water changed every 12 hours. The resulting aqueous solution was dried to afford **F8BT-PEG** as a bright yellow powder (167 mg, 79% yield).

^{19}F-NMR (400 MHz, $CDCl_3$) shows no fluorine signal.

^{1}H-NMR (400 MHz, $CDCl_3$) δ 3.62 (m, 4H)

There was very weak proton signal from conjugated backbone of F8BT in ^{1}H-NMR (see Appendix Figure 11) and the accurate integrations were difficult. As the PEG has very high molecular weight (M_n= 10,000 g/mol, PDI≤1.2), which means the proton signal is tremendously more intensive than F8BT's proton signal. That is the reason that the ^{1}H-NMR shows dominant PEG signal.

High purity was confirmed by DOSY NMR (Appendix Figure 12, 13).

3 Conjugated polyelectrolytes with modulated density of ionic groups as an interfacial layer in OPVs and OLEDs

3.1 Introduction

Conjugated polyelectrolytes (CPEs) have attracted considerable attention due to their promising potential application in organic optoelectronic devices , chemo-/bio-sensors and cell imaging.[112–115] CPEs are polymers which consist of backbones with π-delocalized electronic structures and pendant substituents with ionic groups (such as phosphate, carboxyl, quaternary ammonium, anionic carboxyl and sulfonic groups).[114,116,117] Because of the ionic nature of the side chains, CPEs can be soluble in polar solvents (methanol, DMSO and water).[114,118] The solubility in polar solvents of CPEs makes them promising as interfacial layer materials in organic electronic devices.[119,120] In particular, CPEs have been investigated widely as an interfacial layer in organic light emitting diodes (OLED)[121–123] and organic photovoltaic cells (OPV)[124–126]. Balanced charge injection and transport are important for highly efficient optoelectronic devices. By placing the CPEs between the active layer and electrodes (both cathode and anode), the work function (WF) of the adjacent metal electrode can be modified;[127,128] therefore, the energy levels at the metal/semiconductor interface can be tuned. (Figure 34)[129,130] The WF modification by CPEs results in their widespread applications in organic electronic devices using the typical thin-film device structure of a metal/semiconductor/metal configuration, in which energy level matching between the metal electrode and active layer is quite important for achieving a high-performance device.[131,132]

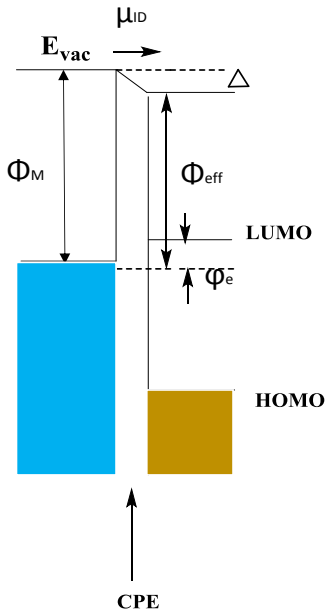


Figure 34 Energy levels of the metal/CPE/active layers in organic electronic devices. The introduction of a thin CPE layer results in a vacuum level (E_{vac}) shift at the metal/active interface by forming interfacial dipoles (μ_{ID}) and decreases the effective WF (Φ_{eff}), which is proportional to the magnitude (Δ) of the generated interfacial dipoles. This process leads to a decreased electron injection barrier (φ_e).[129]

It is well-known that a typical OPV device is usually composed of two materials which are used as electron donor and acceptor to form a bulk heterojunction(BHJ). The power conversion efficiency (PCE) cab be calculated in the following equation[133]:

$$PCE = \frac{V_{oc} \times J_{sc} \times \mathrm{FF}}{P_{in}}$$

Clearly, the fundamental parameters that determine the PCE include four main factors: the open-circuit voltage (V_{oc}), the short-circuit current density (J_{sc}), the fill factor (FF) and the power of the incident light $P_{in.}$ Significant improvements in PCE are due to the combined improvements in materials design, interface control, self-assembly of donor and acceptor phases, and device fabrications. CPEs have been widely utilized as the distinguished organic interfacial layers. This is because the chemical structure can be tailored and the interfacial compatibility can be greatly improved to achieve excellent optoelectronic properties. For example, the Lie Chen group synthesized n-type CPEs as electron transport layers (ETLs) and the solar cell performance was significantly improved from 6.8% (without CPE) to 8.3% for the fullerene system and improved from 9.0% (without CPE) to 10.57% for the non-fullerene

system[134]. Novel CPE interlayer material, PFS-FTEG (Figure 35), was synthesized via Suzuki polycondensation in water by the Jones group. The inverted OPV and perovskite devices, with maximum PCE of 15.1% (perovskite), were fabricated through incorporation of ZnO/PFS-FTEG as an interlayer.[135]

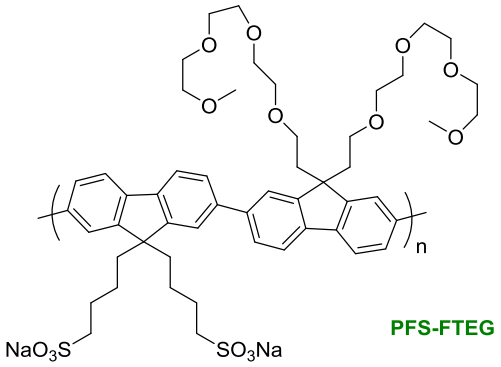


Figure 35 Structure of PFS-FTEG[135]

Generally, OLEDs are thin-film multilayer structures composed of a hole-transporting, an emitting, and an electron-transporting layer sandwiched between two electrodes.[136,137] The CPEs interfacial layers can facilitate holes and electrons entering into the emissive layer from their corresponding electrodes, leading to an increase in device performance by maintaining more balanced charge injection and transport. Much research has focused on the exploration of CPEs interfacial layers and on maximizing their brightness and power efficiency, while lowering their turn-on voltage. The Kim group reported a high performance green-emitting F8BT OLED with CPE electron injection layer (EIL) comprising different π-conjugated backbone structures (F8imBT-Br and F8im-Br) (Figure 36). The F8imBT-Br/Al device demonstrated 10.8 cd A^{-1} and 14.3 lm W^{-1} at 100 cd m^{-2} and 15.5 cd A^{-1} and 16.5 lm W^{-1} at 1000 cd m^{-2}.[138] The Friend group demonstrated improvement in OLED by employing a series of CPEs as an hole transport layer (HTL). In particular, the optimized OLEDs with PCPDT-K exhibit a maximum luminous efficiency (LE) of 25.97 cd A^{-1} and external quantum efficiency (EQE) of 5.66%.[139]

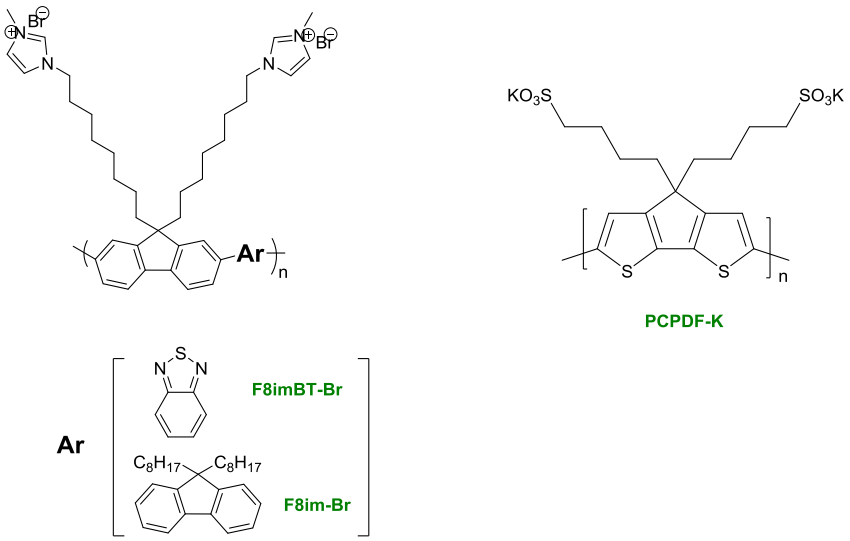


Figure 36 Structures of F8imBT-Br, F8im-Br and PCPDT-K[138,139]

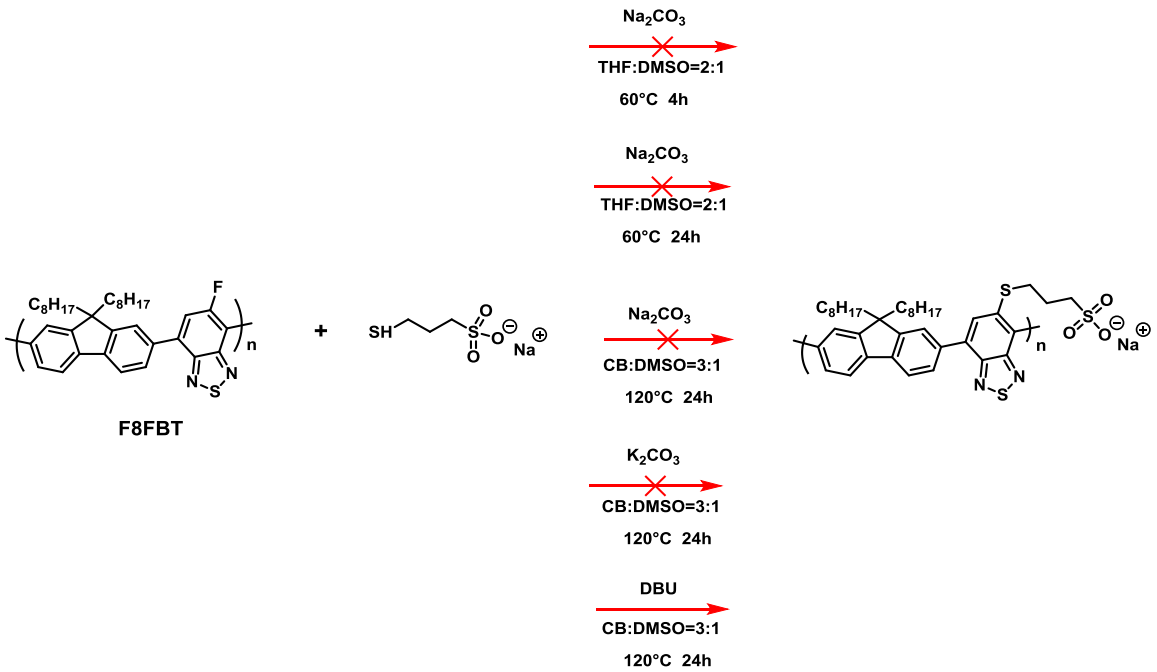
Much effort has been paid to the development of new CPEs interlayer materials to fulfil versatile applications in optoelectronic devices. For examples, many types of highly polar pendant groups (such as cationic,[140,141] anionic,[142,143] zwitterionic[144–146] and neutral pendant groups[147,148]) and conjugated main chain building blocks (such as fluorene,[149–151] carbazole,[152,153] triphenylamine,[154,155] thiophene[156,157]) have been used to design CPEs as interfacial layers.[158] The density of the ionic group is an important parameter which will influence the electrical properties of CPEs. However, to my knowledge, the research about the density of ionic groups on conjugated backbone is limited in previous papers.[159] A quantitative analysis about ionic densities in the CPEs is necessarily to aid in the understanding of CPEs as interfacial layers in organic optoelectronic devices. In this chapter, three CPEs with same conjugated backbone but different densities of ionic groups have been synthesized by post-polymerization. The effects of ionic densities on the energy level tuning process at the CPE/metal interface in the OPVs and OLEDs have been investigated.

3.2 Synthesis

3.2.1 Synthesis routes

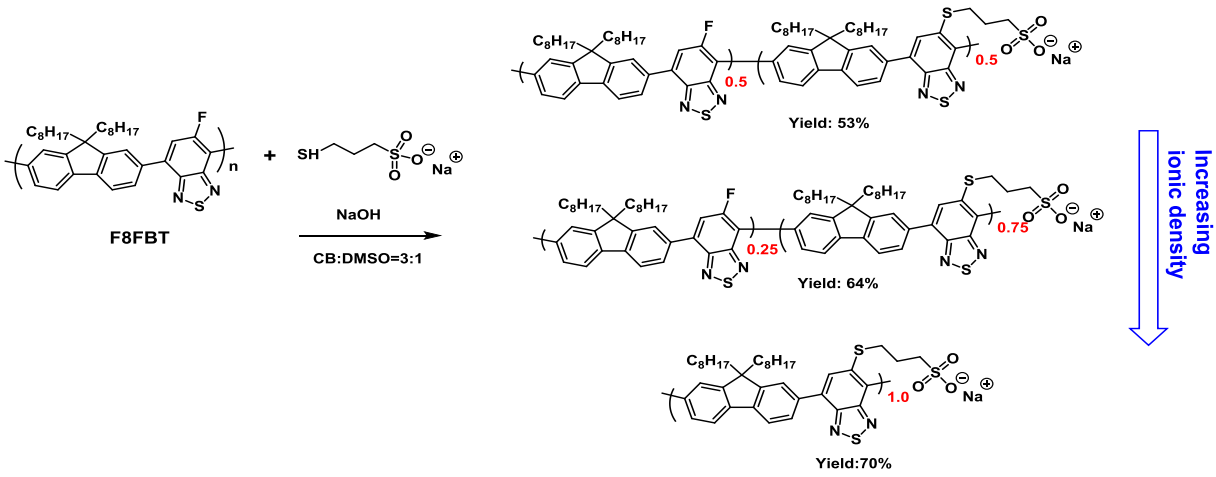
F8FBT was synthesized as discussed in Chapter 2 but with a different molecular weight (M_n= 26,000 g/mol, M_w= 67,500 g/mol, PDI= 2.60). **F8FBT** was then reacted with

3-mercapto-1-propanesulfonic acid sodium salt in solvent mixture of chlorobenzene and DMSO (3:1, volume) to give conjugated polyelectrolytes with different densities of ionic groups, **CPE 50%**, **CPE 75%** and **CPE 100%**. At first, we chose Na_2CO_3 as base to deprotonate the thiol group of 3-mercapto-1-propanesulfonic acid sodium salt (**Scheme 3**). The solvent was mixture of THF and DMSO (2:1, volume) and heated at 60 °C for 4 hours under argon. The ^{19}F-NMR demonstrated that the substitution reaction was not complete for **CPE 100%**. Even after prolonging the reaction time to 24 hours, the ^{19}F-NMR demonstrated that there was still obvious fluorine signal. Therefore we tried higher reaction temperature and the reaction was heated at 120 °C (CB: DMSO=3:1) for 24 hours. There was still fluorine signal from ^{19}F-NMR spectra remaining. K_2CO_3 was also used as base at 120 °C in the solvent mixture of chlorobenzene and DMSO (3:1, volume) for 24 hours. However, the ^{19}F-NMR demonstrated that the reaction was not complete. 1, 8-Diazabicyclo [5.4.0] undec-7-ene (**DBU**) was also investigated. After 24 hours at 120 °C in solvent mixture (CB: DMSO= 3:1), there was no fluorine signal remaining. However, there were many impurities in the products and the yield was also very low.



Scheme 3 Reaction conditions optimized to synthesize CPEs

Then, we used the NaOH as base for this reaction. After 24 hours reaction at 120°C in solvent mixture (CB: DMSO= 3:1), the ^{19}F-NMR demonstrated there was no fluorine signal in the product which means the fluoride has been all substituted. Also, the high temperature ^{1}H-NMR (373 K) demonstrated **CPE 100%** was obtained in high purity. For **CPE 50%** and **CPE 75%**, the reaction conditions were the same as **CPE 100%**, except a lower equivalence of 3-mercapto-1-propanesulfonic acid sodium salt was used. 0.5 eq. and 0.75 eq. of 3-mercapto-1-propanesulfonic acid sodium salt were used to replace the 50% and 75% of the fluorine groups to give **CPE 50%** and **CPE 75%** respectively (**Scheme 4**).



Scheme 4 Synthesis of **CPE 50%**, **CPE 75%** and **CPE 100%**

3.2.2 NMR analysis

While all of the CPEs have an identical π-conjugated backbone, each sample exhibits a different number of anionic charged sulfonic functionalities (SO_3^-), with cationic counter ions (Na^+). The enhanced ionic densities of synthesized CPEs was directly confirmed by integrating the signal intensity for $–S\text{-}CH_2\text{-}CH_2\text{-}CH_2\text{-}SO_3^-Na^+$ in the ^{1}H-NMR at high temperature (373 K). For **CPE 50%**, as only 50% of the fluoride was substituted by ionic thiol group, therefore the proton integration of each methylene from $–S\text{-}CH_2\text{-}CH_2\text{-}CH_2\text{-}SO_3^-Na^+$ should be just 1 (50% × 2 = 1) in comparison to the methylene signals from the dioctyl groups. From the high temperature ^{1}H-NMR (Appendix Figure 14), clearly each the methylene integration was around 1. The **CPE 75%** was confirmed by the each methylene

integration of 1.5 (75% × 2 = 1.5) in ^{1}H-NMR (Appendix Figure 15). The **CPE 100%** was confirmed by proton integration from each methylene was 2 in ^{1}H-NMR (100% × 2 = 2) (Appendix Figure 16) and ^{19}F-NMR (no fluorine signal) (Appendix Figure 17)

In addition, the CPEs were also confirmed by the aromatic comparison in ^{1}H-NMR (Figure 37). The BT acceptor becomes less electron deficient when the fluoride was substituted by 3-mercapto-1-propanesulfonic, indicating the protons on aromatic rings will show upfield shifts. Clearly, with fluoride substituted increasingly, the protons on aromatic rings from 7.9 ppm to 7.5 ppm show increasing upfield shifts.

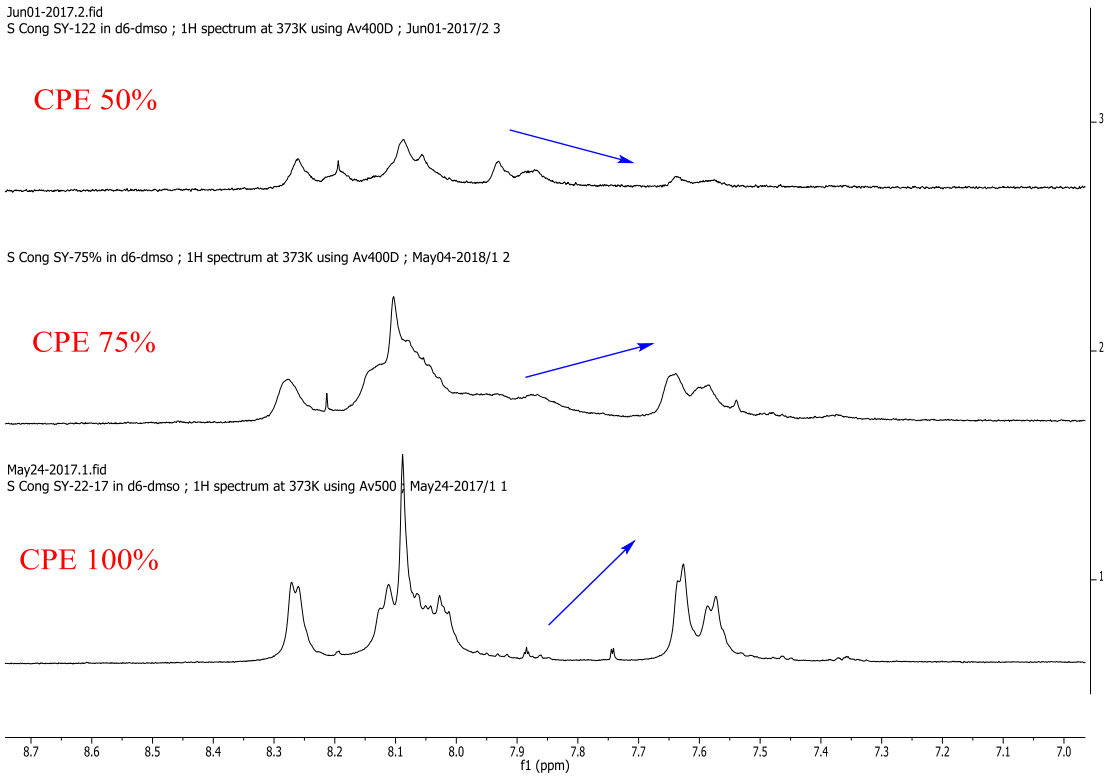


Figure 37: Aromatic comparison of CPEs in ^{1}H-NMR

3.2.3 Fourier-transform infrared spectroscopy

The CPEs were investigated by Fourier-transform infrared spectroscopy (FTIR) (Figure 38). The functional group regions for C=C (aromatic ring) and S=O (sulfonate) are 1650-1600 cm^{-1} and 1195-1168 cm^{-1} respectively. Clearly, the S=O functional group peak was only found in CPEs instead of **F8FBT**. As **CPE 50%** changes to **CPE 100%**, the ionic density increases in the repeat unit of $–S\text{-}CH_2\text{-}CH_2\text{-}CH_2\text{-}SO_3^-Na^+$. The enhanced ionic density of CPE

samples was directly confirmed by comparing the intensity of the S=O stretching peak relative to the aromatic (C=C) stretching peak in the FTIR spectra. The IR of 3-mercapto-1 propanesulfonic acid sodium salt alone was in Appendix Figure 18.

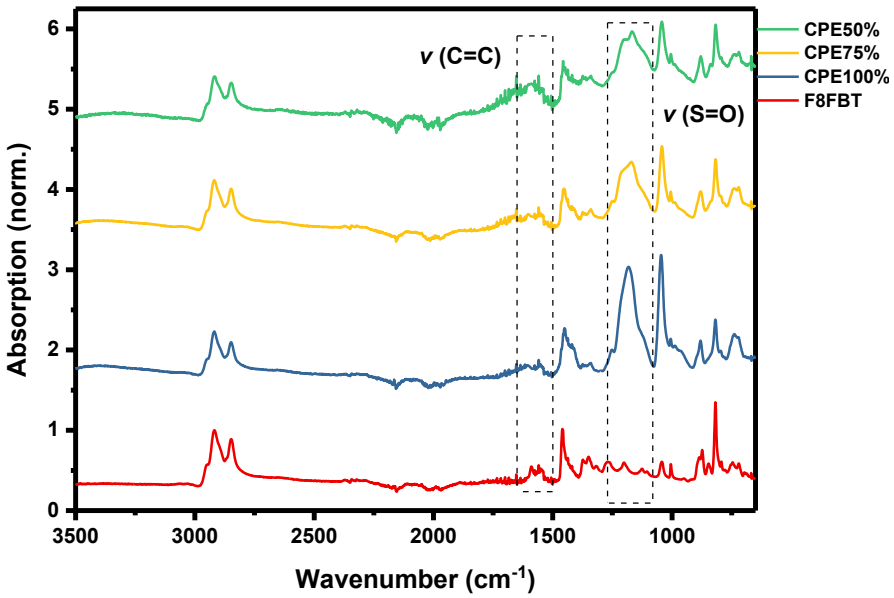


Figure 38 FTIR spectra of **F8FBT** and CPEs

3.2.4 X-ray photoelectron spectroscopy

The synthesized CPEs were investigated by X-ray photoelectron spectroscopy (XPS). XPS can provide quantitative information about the elemental composition and chemical specificity (e.g., oxidation state) of the surface.[159,160] Take **CPE 50%** for example. The XPS survey spectra shows the peaks with binding energy of 1071.2 eV, 688.3 eV, 532.0 eV, 401.0 eV, 285.6 eV and 166.3 eV. According to the binding energy, the **CPE 50%** shows the presence of C, N, O, F, S and Na. The atomic percentage of **CPE 50%** calculated from chemical structure was $C_{36.5}$ $N_{2.0}$ $Na_{0.5}$ $O_{1.5}$ $F_{0.5}$ $S_{2.0}$ while the atomic percentage from XPS was $C_{35.4}$ $N_{1.9}$ $Na_{0.6}$ $O_{2.8}$ $F_{0.4}$ $S_{1.9}$. The atomic percentage (number) calculated from CPE chemical structure was consistent with the XPS data. We note that the differences in the oxygen percentage are probably due to absorbed water. Clearly, the **CPE 50%** was confirmed by XPS in high purity. The atomic percentage data was summarized in **Table 6**. The XPS survey spectra for CPEs are in Appendix Figure 19-21.

Table 6 Atomic percentage (number) measured by XPS

Polymer	Chemical Structures	XPS
CPE 50%	$C_{36.5}N_{2.0}Na_{0.5}O_{1.5}F_{0.5}S_{2.0}$	$C_{35.4}N_{1.9}Na_{0.6}O_{2.8}F_{0.4}S_{1.9}$
CPE 75%	$C_{37.25}N_{2.0}Na_{0.75}O_{2.25}F_{0.25}S_{2.5}$	$C_{36.9}N_{1.9}Na_{0.7}O_{2.9}F_{0.2}S_{2.4}$
CPE 100%	$C_{38.0}N_{2.0}Na_{1.0}O_{3.0}S_{3.0}$	$C_{36.8}N_{2.0}Na_{0.9}O_{4.1}S_{3.2}$

3.3 CPEs in polar solvents

The solubility of CPEs is very different from the starting **F8FBT** in polar solvents. Before the reaction, the starting neutral **F8FBT** is soluble in chloroform, THF and chlorobenzene. After different densities of ionic functionalities grafted to the **F8FBT**, the synthesized CPEs were not soluble in chloroform, THF or chlorobenzene any more, but soluble in polar solvents, like DMSO and methanol, which is due to the hydrophilic ionic groups. The solubility in polar solvent allows the synthesized CPEs to be used as interfacial layers in organic optoelectronic devices. Figure 39 shows the solubility of **F8FBT** and CPEs in chloroform and DMSO respectively (2 mg/ml).

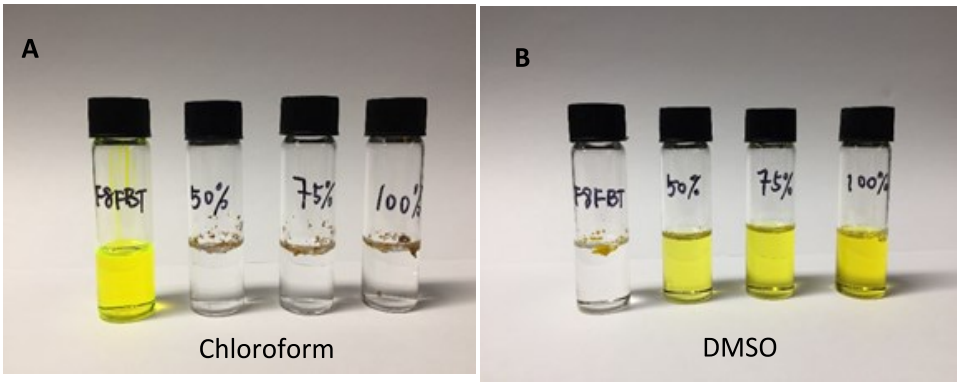


Figure 39 F8FBT and CPEs in (A) chloroform and (B) DMSO

3.4 Optical properties

3.4.1 Absorption spectra

UV-Vis absorption and photoluminescence (PL) spectra of the three CPEs are shown in Figure 40, and relevant data are summarized in **Table 7**. Clearly, the absorption spectra of three CPE is different from **F8FBT**. For **F8FBT**, a high energy band with a peak at 319 nm and a low energy band with a peak at 440 nm in chloroform solution. The three CPEs exhibit two main broad absorption bands in DMSO, with a peak around 320 nm in the high-energy band and a peak around 430 nm in the low-energy band.

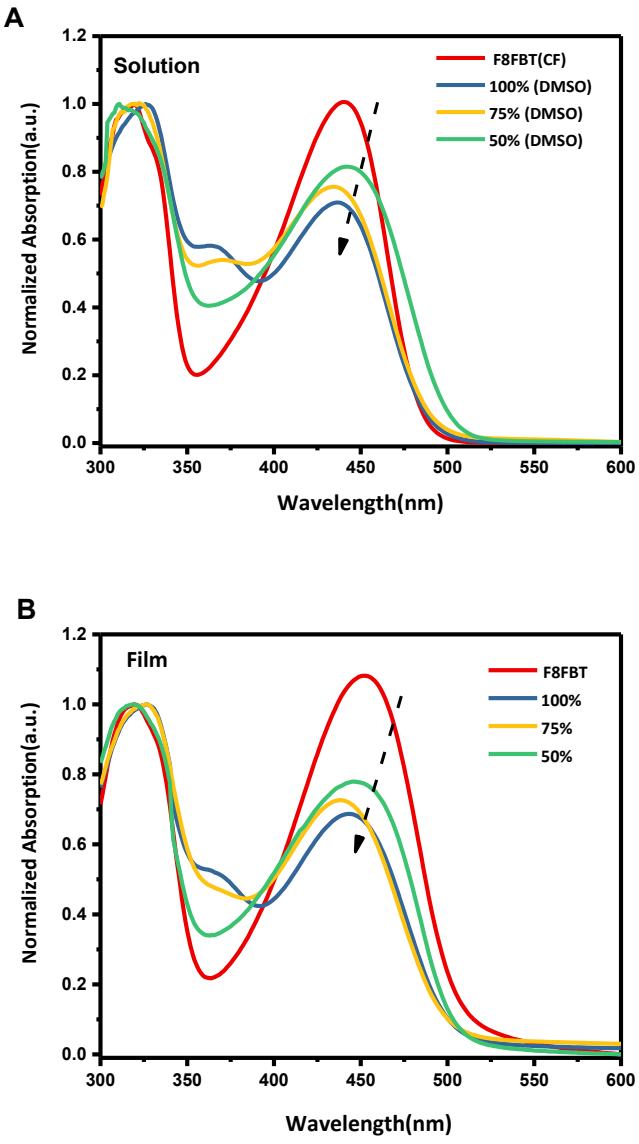


Figure 40 UV-Vis absorption spectra of three **CPEs** in solution (A) and film (B).

However, the low energy band of three CPEs have a lower absorption intensity than the high energy band. This is due to fluoride atom which is more electron deficient than sulfur atom from 3-mercapto-1-propanesulfonic. When the fluoride has been substituted by 3-mercapto-1-propanesulfonic, the 2, 1, 3-benzothiadiazole (BT) acceptor becomes less electron deficient. Noticeably, a new absorption peak is observed between 360 to 370 nm, increasing in intensity as function of thioalkyl substitution. The intensity of the small shoulder increases when more fluoride on conjugated backbone are substituted. The additional intense absorption is due to $N_{sulfur} \rightarrow \pi^*$ transitions.[161] Dr. Creamer from our group made some similar polymers which also shows the additional absorption when fluoride was substituted by thioalkyl group.[50]

In the solid state, the three CPEs demonstrate similar change trends as in DMSO solution. First, the intensity of low energy is also lower than high energy band, which has been discussed in DMSO solution. Second, a new absorption peak is observed between 360 to 370 nm, which is as function of thioalkyl substitution. Besides, the three CPEs all demonstrate slight red shift both in high energy band and low energy band compared with DMSO solution. The onsets of the absorption spectra of **CPE 100%**, **CPE 75%**, **CPE 50%** in thin films are at 502, 501 and 504 nm, respectively. The optical band gaps (E_g) of **CPE 50%**, **CPE 75%**, **CPE 100%**, were thus calculated to be 2.47, 2.47 and 2.46 eV, according to their onsets of the absorption spectra in the solid state.

3.4.2 Emission spectra

As demonstrated in Figure 41, the emission maxima of **F8FBT** is 532 nm in chloroform solution. **CPE 100%**, **CPE 75%**, **CPE 50%** exhibit a same emission maxima at 555 nm in DMSO solution resulting in a solution Stokes shift ($\Delta \lambda_{(sol)}$) of 119 nm, 120 nm, 113 nm respectively. In the solid state, **F8FBT** and **CPE 100%**, **CPE 75%** and **CPE 50%** have almost same emission peak at 546 nm. The thin film emission maximum of CPEs (546 nm) is slightly blue shifted in comparison to solution (555 nm). The solid state Stokes shift ($\Delta\lambda_{(film)}$) of **CPE 100%**, **CPE 75%** and **CPE 50%** is 102 nm, 101 nm and 100 nm respectively.

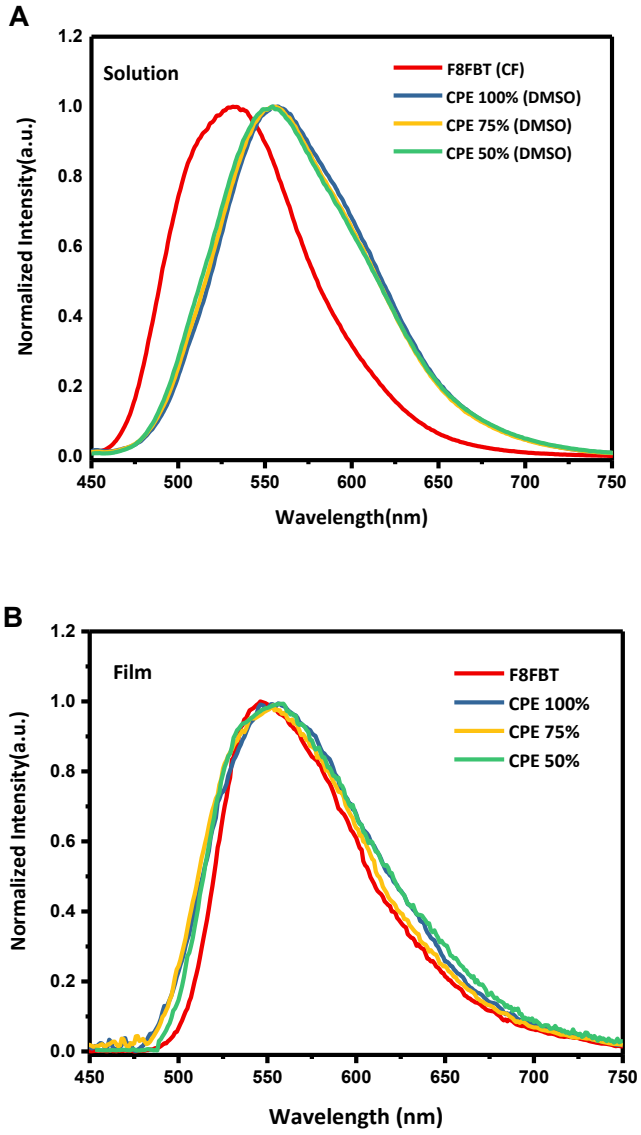


Figure 41 PL spectra of three CPEs in solutions (A) and film (B)

Table 7 Optical properties of three CPEs in solution and thin film states

Polymer	$\lambda_{abs,\ max}$ (sol) nm	$\lambda_{abs,\ max}$ (film) nm	$E_{g(opt)}$ eV	$\lambda_{em,\ max}$ (sol) nm	Δ λ (sol) nm	$\lambda_{em,\ max}$ (film) nm	Δ λ (film) nm
CPE100%	326[a], 436[b]	335[a],454[b]	2.47	555	119	546	102
CPE75%	318[a], 435[b]	335[a],455[b]	2.47	555	120	546	101
CPE50%	311[a], 442[b]	336[a],455[b]	2.46	555	113	546	100

[a] λ_{max} of high energy band.
[b] λ_{max} of low energy band.
$\lambda_{abs,\ max}$(sol) nm, $\lambda_{em,\ max}$ (sol) nm and Δλ (sol) nm were all investigated in DMSO solution.

3.5 Electronic properties

The solid state electronic properties of **F8FBT**, **CPE100%, CPE75%** and **CPE50%** were investigated using cyclic voltammetry (CV). Samples were all prepared by drop-casting the solution on the Pt rod surface. **F8FBT** and CPE samples were not soluble in acetonitrile and measured in anhydrous, degassed solutions of acetonitrile with tetrabutylammonium hexafluorophosphate (0.1M) electrolyte using an Ag/Ag^{+} as reference electrode. The cyclic voltammograms of all polymers are shown in Figure 42 and the electronic properties are summarized in **Table 8**. The HOMO levels of the polymers were estimated from the first onset of oxidation, assuming that the ferrocene/ferrocenium reference redox system is 4.8 eV below the vacuum level. [101,102]

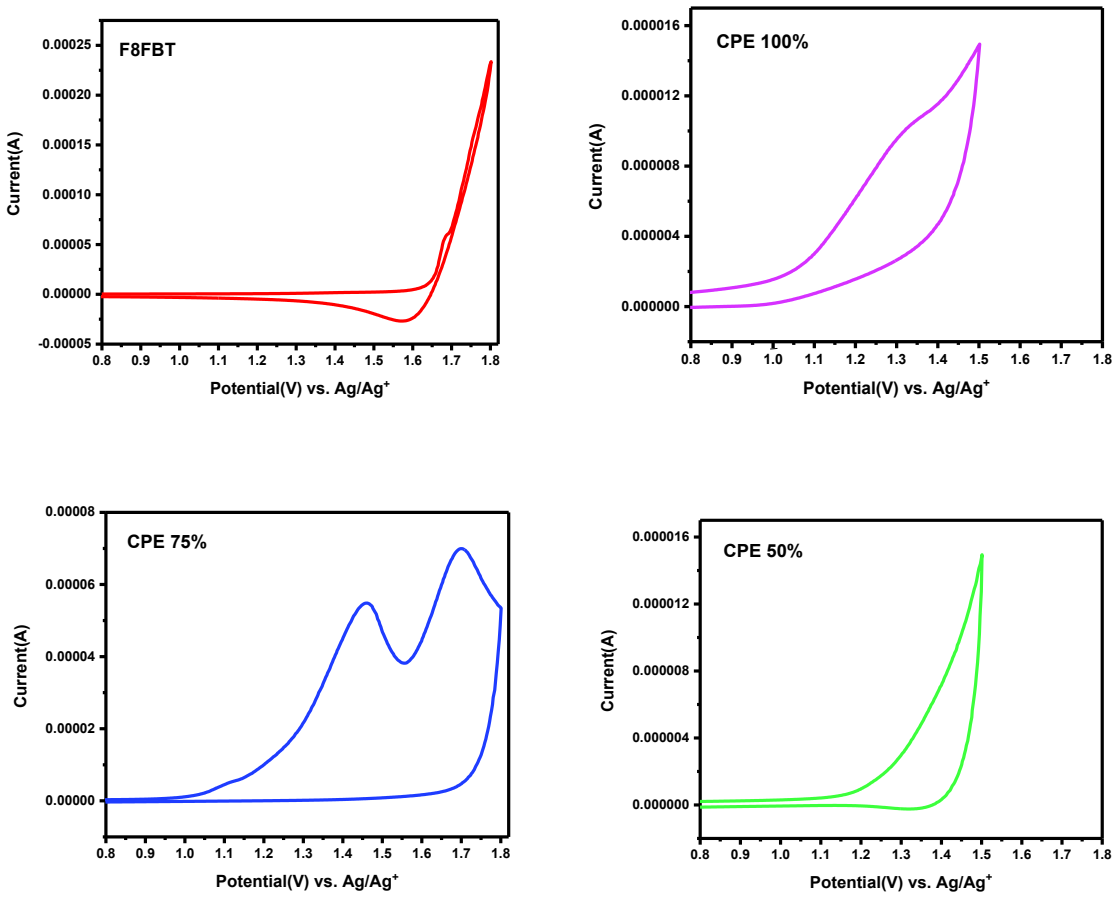


Figure 42: Cyclic voltammograms of thin films of **F8FBT** and CPEs in acetonitrile/ $[n–Bu_4N]PF_6$ solutions (0.1M) at a scan rate of 0.1 V/s.

The HOMO energy level of CPEs can be calculated from the onset oxidation potential $E_{ox(onset)}$, based on the reference energy level of ferrocene:

$$\boldsymbol{E_{HOMO} = -(E_{ox(onset)} + 4.8 - E_{FOC})}$$

$$\boldsymbol{E_{LUMO} = E_{HOMO} + E_{op}}$$

The onset voltages of oxidation process is 1.66 eV, 1.06 eV, 1.23 eV, 1.29 eV for **F8FBT**, **CPE100%**, **CPE75%** and **CPE50%** respectively. From Figure 42, the HOMO level of **F8FBT** was -6.08 eV, which was very similar as literature.[103] As fluoride was more electron deficient than substituted thioalkyl groups, the HOMO level of **F8FBT** is deeper than the CPEs. The more fluoride substituted by thioalkyl groups, the higher HOMO level of CPEs will be. The HOMO level of **CPE100%**, **CPE75%** and **CPE50%** is -5.48 eV, -5.65 eV, -5.71 eV by CV. Also, the LUMO level of **CPE100%**, **CPE75%** and **CPE50%** is calculated -3.01 eV, -3.18 eV, -3.25 eV by their HOMO energy levels and $E_{g(opt)}$. Although the CPEs have almost same band gap, but the HOMO and LUMO levels are influenced by fluoride substitution ratios.

Table 8: Electronic properties of **F8FBT** and CPEs

Polymer	[a]**$E_{g(opt)}$** (eV)	[b]**E_{ox}** (eV)	[b]**HOMO** (eV)	[c]**LUMO** (eV)
F8FBT	2.45	1.66	-6.08	-3.63
CPE100%	2.47	1.06	-5.48	-3.01
CPE75%	2.47	1.23	-5.65	-3.18
CPE50%	2.46	1.29	-5.71	-3.25

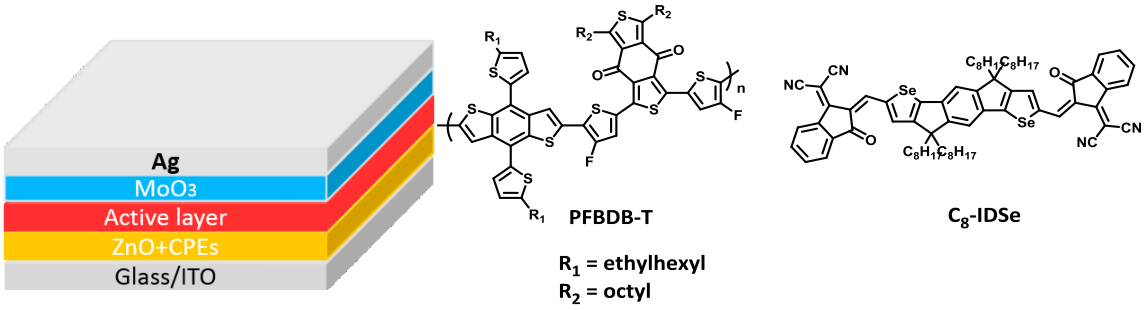
[a]Determined from $E_{g(opt)}$
[b]Determined from CV measurement, error ± 0.05 eV[104]
[c]Calculated from HOMO level and optical band gap

3.6 OPV performance

To investigate the electron transporting properties of CPEs with different ionic densities, the photovoltaic device performance containing CPEs were investigated in a device configuration with the following structure: Glass/ITO/ZnO+CPE / PFBDB-T: C_8-IDSe

/MoO_3/Ag. The photoactive layer materials, **PFBDB-T** and **C_8-IDSe** were synthesized by our group member, Dr Fei. The molecular structure of **PFBDB-T** and **C_8-IDSe** as well as the device structure are demonstrated in Figure 43. The **CPE 75%** and **CPE 100%** were then used in the fabrication of inverted OPV devices with a ZnO/CPE bilayer as the electron transport layer (ETL). The CPEs layer was spin-coated on top of ITO layer from methanol solution to form an interlayer. For comparison, a control device with the following structure: Glass/ITO/ZnO / PFBDB-T: C_8-IDSe /MoO_3/Ag was also fabricated and investigated. The corresponding photovoltaic parameters including short circuit current density (J_{sc}), open circuit voltage (V_{oc}), fill factor (FF) and PCE are summarized in **Table 9.** The J–V curves of the solar cells measured under AM 1.5G irradiation (100 mW cm^{-2}) are illustrated in Figure 44. The external quantum efficiency (EQE) spectrum using CPE as ETL are demonstrated in Figure 45.

(a)



(b)

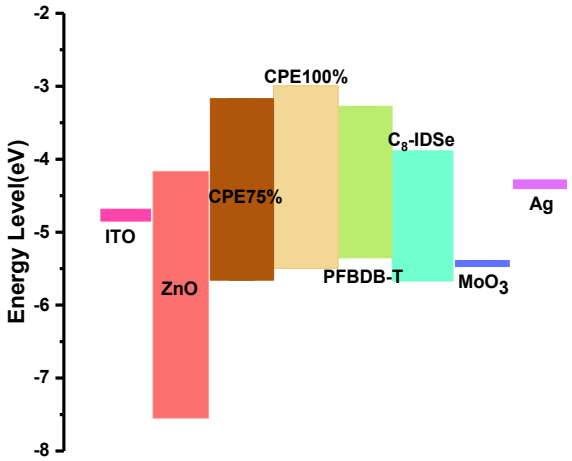


Figure 43 (a) Molecular structure of active layer blend of **PFBDB-T** and **C8-IDSe** (b) Energy levels of polymers

A typical control device without CPE interlayer exhibited a high PCE of 12.1 %, with a V_{oc} of 0.88 V, a J_{sc} of 20.5 mA cm^{-2} and an FF of 0.67. After using **CPE75%** and **CPE100%** as ETL respectively, the resulting devices both exhibited enhanced performances, which were mainly from the improvements of J_{sc} and FF simultaneously. The PCE values were increased to 12.6 % and 13.4 % for PSCs with **CPE75%** and **CPE100%** respectively. The V_{oc} of PSCs for **CPE 75%** and **CPE100%** was both 0.89 V which was slightly higher than a bare ZnO device. The FF of PSCs was increased from 0.67 for a bare ZnO electrode device to 0.69 for **CPE75%** device, 0.70 for **CPE 100%** device. Compared with the data increase in FF, the changes of J_{sc} with the incorporation of CPEs as interlayer are more important. The J_{sc} is increased from 20.5 mA cm^{-2} for a bare ZnO device to 20.6 mA cm^{-2} for **CPE75%** and 21.6 mA cm^{-2} for **CPE100%**. The statistical data (average values and standard deviations) of photovoltaic performances calculated from ten devices for each kind of PSCs (**Table 9**), which prove that the enhancements of device performances using CPEs as ETL are effective and reproducible.

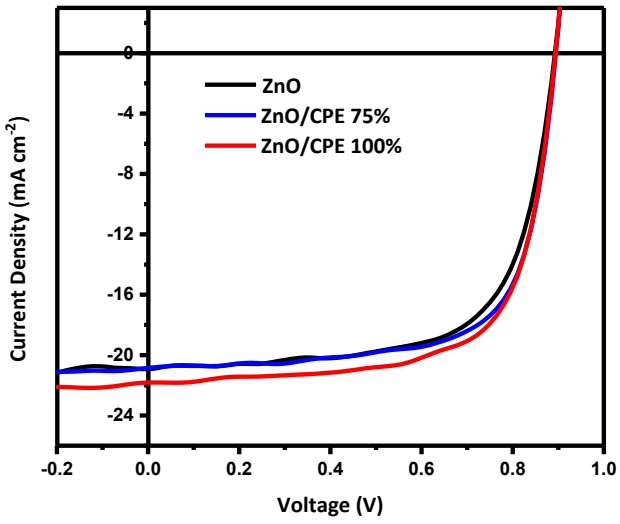


Figure 44: J-V curves for CPE as electron transport layers

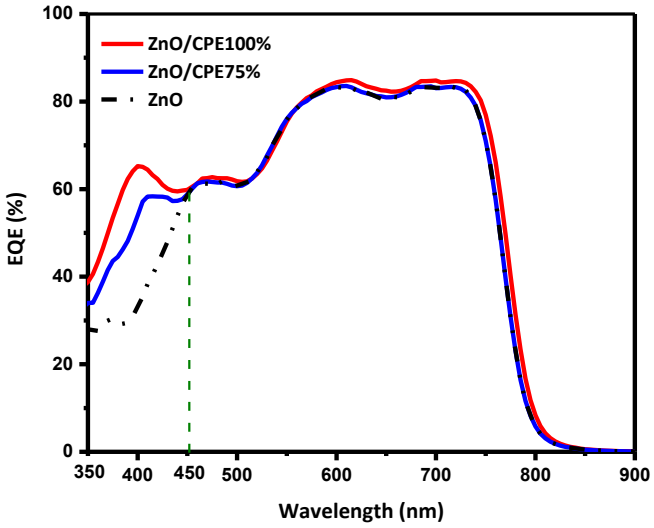


Figure 45: EQE of device using CPEs as the electron transport layer.

Table 9. Device Parameters of the PSC Devices with Different ETLs

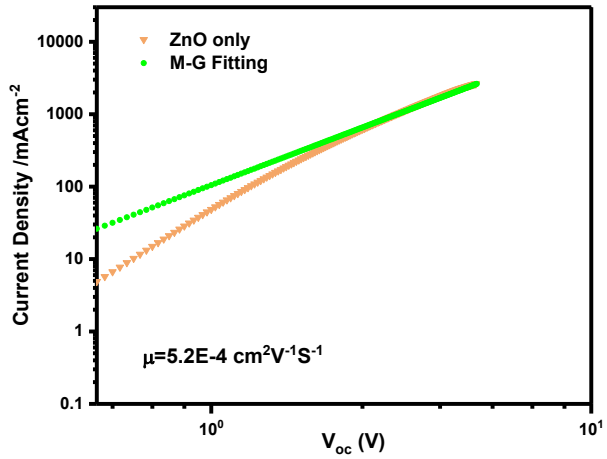
ETL	J_{sc} (mA/cm^2)	V_{oc} (V)	FF	PCE (%)
ZnO	**20.8**(20.5)[a]	**0.89**(0.88)[a]	**0.68**(0.67)[a]	**12.6**(12.1)[a]
ZnO/CPE75%	**21.0**(20.6)[a]	**0.89**(0.89)[a]	**0.70**(0.69)[a]	**13.1**(12.6)[a]
ZnO/CPE100%	**21.8**(21.6)[a]	**0.89**(0.89)[a]	**0.70**(0.70)[a]	**13.4**(13.4)[a]

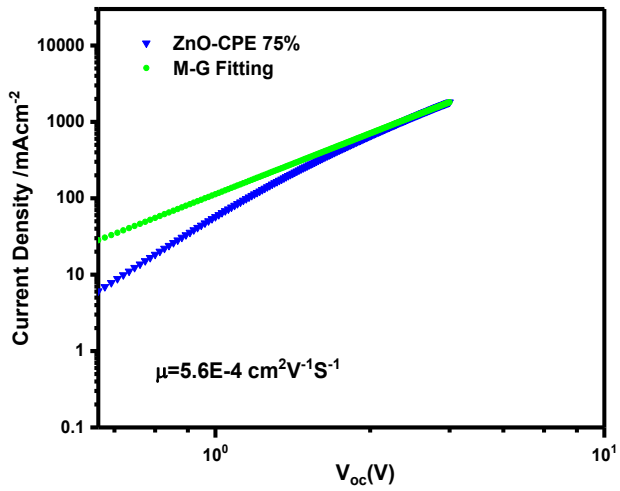
()[a] average values from over 10 devices

The **CPE75%** and **CPE100%** both demonstrated excellent interface modification capacities, while **CPE100%** exhibited better PCE than **CPE75%**. Notably, the difference between **CPE75%** and **CPE100%** is mainly due to J_{sc} improvement. The device with **CPE75%** demonstrated a J_{sc} of 20.6 mA cm^{-2}, which is lower than the device with the **CPE100%** (21.6 mA cm^{-2}). Besides, the difference of J_{sc} improvement was confirmed by EQE. Noticeably, the EQE between 350 nm to 450 nm for **CPE100%** was higher than **CPE75%**. The differences between **CPE 75%** and **CPE 100%** are energy levels and ionic group densities. Although **CPE 75%** has a deeper HOMO and LUMO level than **CPE 100%**, presumably the more ionic group

contribute more to increase interface dipole formation between CPE and the electrode which will decrease the work function effectively.

To get a more insightful understanding on the enhancements of device performances upon the incorporation of CPEs, a space-charge-limited current (SCLC) model using device with an ITO/ ZnO+CPE/active Layer/Ca/Al structure was shown in Figure 46. Current-voltage sweeps were carried out in the region of -5 to 5V in steps of 0.05 V. The thickness of the BHJ blend for SCLC measurement is about 120 nm. The electron mobility can be calculated from the slope of the $J^{1/2}$ V curves.





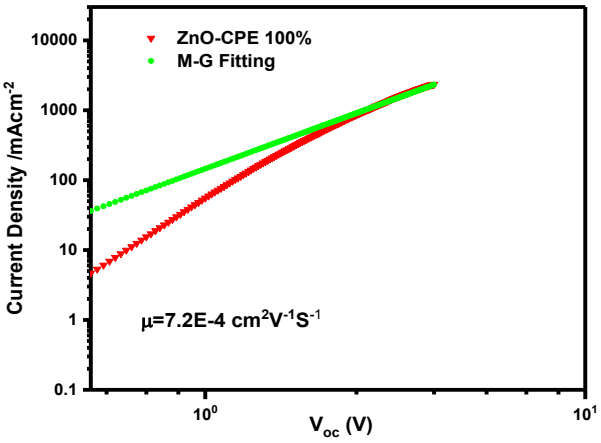


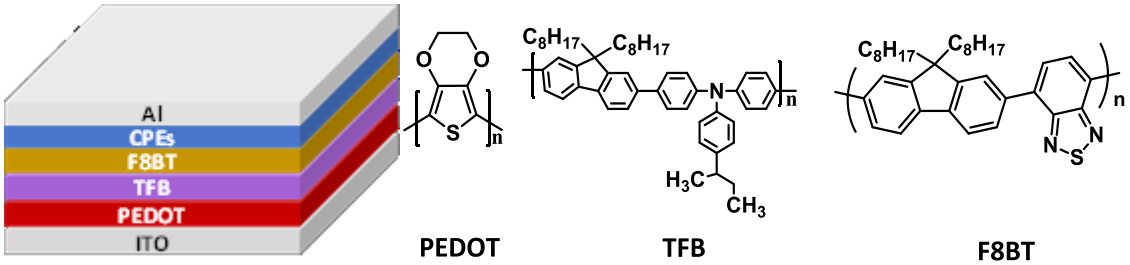
Figure 46 $J^{1/2}$ *V* of hole-only devices with the structures ITO/ ZnO+CPE/active Layer/Ca/Al (120nm)

An apparent electron mobility of 5.2×10^{-4} cm^2 V^{-1} S^{-1}, 5.6×10^{-4} cm^2 V^{-1} S^{-1}, 7.2×10^{-4} cm^2 V^{-1} S^{-1} was determined for the devices with ZnO only, ZnO/**CPE 75%** and ZnO/**CPE 100%** interlayer, respectively. Apparently, ZnO/CPEs increased the electron extraction better than bare ZnO structure. Besides, **CPE 100%** demonstrated higher electron mobility than **CPE 75%**, which means the more ionic groups benefit the electron movement.

3.7 OLED performance

To investigate the electron injecting/transporting properties of the synthesized CPEs with different ionic densities in OLEDs devices with the configuration ITO|PEDOT|TFB |F8BT|CPE|Al were fabricated and tested. OLEDs with a 100 nm Al cathode without CPE were also prepared as a reference device. The device structure and molecular structures of the emitting material F8BT, PEDOT and TFB are demonstrated in Figure 47.

(a)



(b)

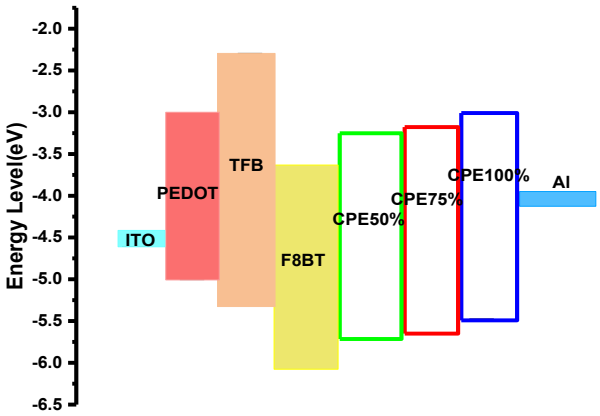
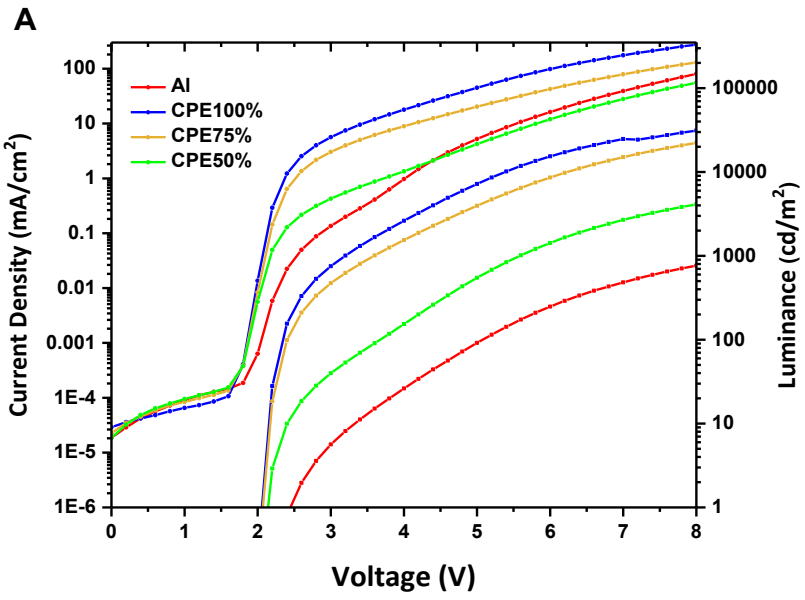


Figure 47. (a) Device configuration of OLED and chemical structures of F8BT. (b) Energy level of F8BT EIL OLED diagram (in eV).

The emitter F8BT was purchased from Cambridge Display Technology Ltd. **CPE50%**, **CPE75%** and **CPE100%** were all dissolved in DMSO, which did not dissolve other polymers used in this OLED device. CPEs were deposited as electron injection layer (EIL) (2 mg/ml) on top of the F8BT active layer prior to Al cathode evaporation. The corresponding energy level diagram is also displayed in Figure 47.



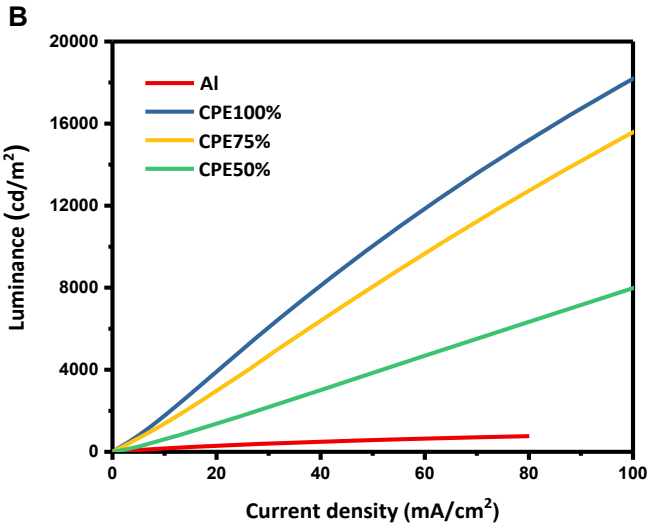


Figure 48 (A) J–V–L characteristics of F8BT OLEDs with CPEs EILs; filled symbols are J, open symbols are L. Data for Ca/Al devices is also shown for comparison. (B) L–J curves for all devices

Figure 48 demonstrated the current density–voltage–luminance (J– V–L) characteristics of the OLED devices with different CPEs as interfacial layers. The thickness of interfacial layers was 10 nm for all three CPEs materials. In the L-V characteristics, the **CPE50%/Al**, **CPE75%/Al** and **CPE100%/Al** demonstrated the same turn-on voltage (the voltage at which the brightness reaching 1 cd/m^2)[144] at 2.1 V whilst the Al device had a higher turn-on voltage at 2.5 V. Clearly, CPEs/Al devices all had a lower driving voltage than Al device, suggesting that the ionic groups were modifying the injection barrier. With increasing voltage, the CPEs/Al devices also demonstrated much higher luminance than Al device. For example, at voltage 3 V, the luminance is 752 cd/m^2, 472 cd/m^2, 40 cd/m^2, and 5.6 cd/m^2 for the **CPE100%/Al**, **CPE75%/Al**, **CPE50%/Al** and Al device respectively. At the voltage range from 2 V to 8 V, CPEs/Al all demonstrated much higher luminance than Al device. Among the CPEs/Al devices, the **CPE100%/Al** device has the highest luminance and the **CPE75%/Al** has higher luminance than **CPE50%/Al** from 2 V to 8 V.

From the J-V figure, the CPEs/Al all showed higher current density at the same voltage than Al device from 2 V to 8 V and **CPE100%/Al** device demonstrated the highest current density among CPEs/Al devices. Besides, the enhanced device performance by using CPE was also confirmed by the L-J figure: the CPEs/Al device displayed much higher luminance than Al alone device at the same current density. The enhanced performances of all three CPEs compare to Al alone may be related to the fact that the excitons quenching at Al layer is

separated from the emissive material. The difference within the three CPE is clearly related to their structures. The CPE100% has highest ionic densities among CPE materials which indicated more interfacial dipoles formation between CPE100% and Al than other CPE materials, resulting more shift in the vacuum level at Al and CPE100% interface.[162,163] This vacuum level shift will result in a change in the effective work function of the CPE covered metal electrode, which leading to a decrease in the electron injection barrier.[164] The enhanced device performances were obtained from the device by using a CPE EIL with a higher ID (CPE100%>CPE75%>CPE50%) due to the enhanced electron injection from the CPE/Al cathode.

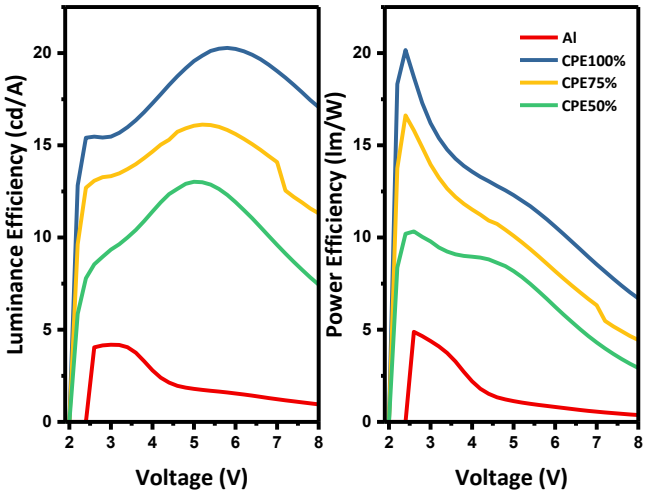


Figure 49 Luminous (cd A^{-1}) and luminous power (lm W^{-1}) efficiencies as a function of voltage for the F8BT OLEDs.

The luminous and luminous power efficiencies as a function of voltage for the CPEs/Al and Al devices are demonstrated in Figure 49. The performance of the four devices is summarized in **Table 10**. Clearly, the the **CPE50%/Al**, **CPE75%/Al** and **CPE100%/Al** devices all demonstrate much higher luminance and power efficiencies than the only Al device at the voltage range from 2 V to 8 V. The significantly higher efficiencies for the CPE/Al devices compared to the Al device suggest that the electron and hole densities within their F8BT EMLs are better balanced.

Table 10. Performances of OLEDs with CPEs/Al EILs with results for equivalent Al cathode devices for comparison

Cathode	luminous efficiency, η_L (cd/A)			luminous power efficiency, η_P (lm/W)		
	Peak	@ 100 cd/m^2	@1000 cd/m^2	Peak	@100cd/m^2	@ 1000 cd/m^2
Al	4.2@3.0 V	1.7	--	4.9@2.6 V	0.9	--
CPE100%/Al	20.3@5.8 V	13.6	15.7	20.2@2.4V	19.4	15.4
CPE75%/Al	16.1@5.2 V	12.7	14.0	16.6@2.4 V	16.6	12.2
CPE50%/Al	13.1@5.0 V	10.6	12.6	10.3@2.6 V	9.1	7.1

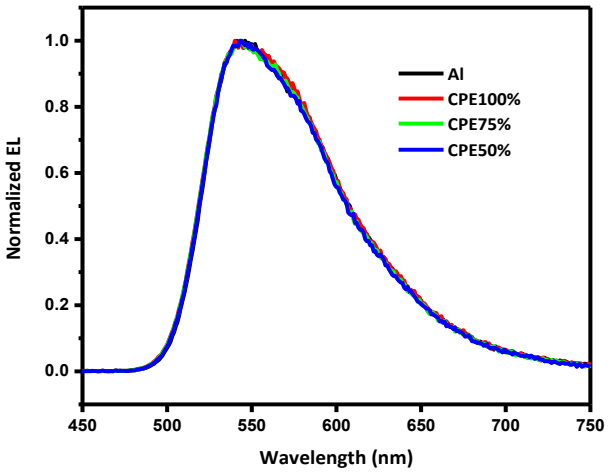


Figure 50. Normalized EL spectra of the F8BT OLEDs at 6 V.

CPEs/Al and Al devices demonstrate the same normalized electroluminescence spectra (EL)(Figure 50) which indicates the recombination zones are all in the F8BT layer and there is no energy transfer between the EML and CPEs/Al interlayers. Also, the normalized EL spectra of the CPEs/Al and Al devices that suggest that the emission predominantly originates from the F8BT EML rather than in the CPE. The fact that the EL spectra of the

CPE50%, **CPE75%** and **CPE100%** devices are identical further confirms that the CPE layers do not contribute to the EL emission.

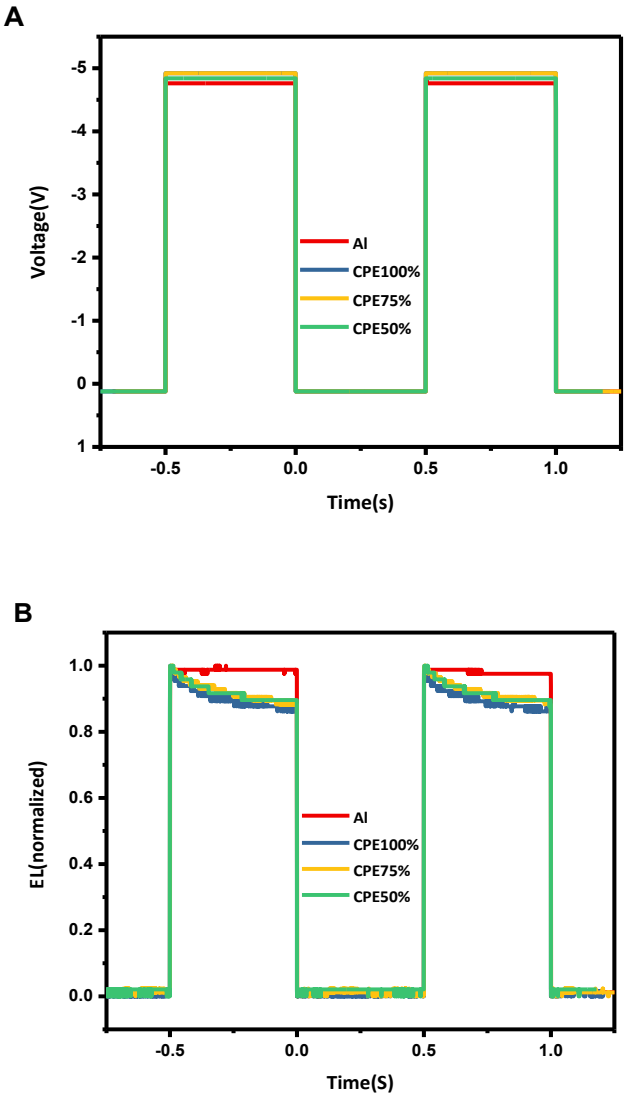


Figure 51. Transient response for the (A) Voltage and (B) EL intensity of F8BT OLEDs with **CPE50%**, **CPE75%** and **CPE100%** ETLs. Data for Al devices is also shown for comparison.

The transient response curves for voltage and electroluminescence intensity for the CPEs/Al and Al devices are demonstrated in Figure 51. These were measured with 5 V amplitude, 1 Hz repetition rate, and square wave pulses. Clearly, the voltage and EL signals for only Al device closely follow the square wave pulses. The voltage signal for **CPE50%/Al**, **CPE75%/Al** and **CPE100%/Al** also follow the square wave pulses very well and there is no voltage signal delay found in CPEs/Al devices. The CPEs/Al device demonstrate the same transient response as Al device for voltage. However, for **CPE50%/Al**, **CPE75%/Al** and

CPE100%/Al devices, the normalized EL intensity drops to 90% of initial intensity with time constant ~0.5 s. This slightly reduced intensity may be due to the exciton quenching by ion migration. There is, however, no accumulated decay in EL intensity from one pulse to the next, indicating that the CPEs devices do not undergo irreversible degradation.

3.8 Conclusions

In summary, a series of new CPEs comprising identical conjugated backbones but different densities of ionic groups were designed and developed as electrode interfacial materials to improve the device performance in OPV and OLEDs, respectively. Three CPE interlayer materials, **CPE50%**, **CPE75%** and **CPE100%**, were all synthesized via post-polymerization modification. The chemical structures, optical properties and energy levels of the CPEs were investigated. The synthesized CPEs possess excellent solubility in polar solvents which are desirable for fabricating efficient and stable organic optoelectronic devices by an orthogonal solution processing method. The relationships between the ionic densities on the polymer backbone and interface modification functions were systematically investigated in OPV and OLEDs. Inverted OPV devices with maximum PCE of 13.1% and 13.4% respectively were fabricated through incorporation of a solution processed **CPE75%** and **CPE100%** interlayer. The maximum PCE without CPE interlayer was 12.6 %. The improvement of OPV device is due to the electron mobility increase with CPE interlayer incorporation, which was confirmed by SCLC measurement. **CPE100%** demonstrated a better interface modification than **CPE75%**. The device performance improvement was also observed when CPE was employed as cathode interlayer in OLED. The **CPE50%**, **CPE75%** and **CPE100%** all demonstrated much better device performance than Al only device in OLED. The CPEs/Al show lower driving voltage, higher luminance, luminance efficiency and luminance power efficiency than Al device at same voltage. The **CPE75%** has a better performance than **CPE50%** while **CPE100%** demonstrated the best device performance. Our study suggested CPE as interfacial layer could improve the OPV and OLED device performance. Besides, the ionic densities of conjugated polyelectrolytes effect their interfacial modification abilities in OPV and OLED. When the difference of HOMO and LUMO level among **CPE50%**, **CPE75%** and **CPE100%** is limited, the ionic densities make a more contribution to interfacial

modification. More balanced charge injection and transport are obtained by **CPE100%** as interfacial layers in organic electronic devices.

3.9 Experimental methods

3.9.1 OPV device fabrication

OPVs were fabricated using PFBDB-T and C_8-IDSe as the donor and acceptor materials. Devices were fabricated onto pre-patterned ITO glass substrates with the device architecture ITO/ZnO+CPE/ PFBDB-T: C_8-IDSe /MoO_3/Ag. After sequential cleaning of the ITO with the detergent (Decon 90), acetone and isopropyl alcohol, a zinc acetate dihydrate precursor solution (219.5 mg in the mixture of 2 mL 2-methoxyethanol and 60 µL monoethanolamine) was spin coated on top of the ITO substrates, and annealed at 190 °C for 45 minutes. After a methanol solution (2 mg/ml) of the **CPE 75%** and **CPE 100%** was separately spin-coated on ZnO layer, which was then heated at 80 °C for 10 min. PFBDB-T/C_8-IDSe blend solution were dissolved in chlorobenzene (CB) at a ratio of 1:1, and a concentration of 20 mg/ml, and were stirred overnight at 50 °C. The blend solution was spin-coated onto the ZnO/CPE coated ITO substrate (2000 rpm, 1 min). The thicknesses of the active layers were ~80-100 nm. The active layers were used as-spun or annealed at 140 °C or 160°C for 15 min. To complete the devices, MoO_3 (10 nm) and Ag (100 nm) were evaporated sequentially under high vacuum under shadow masks to fabricate devices with an area of 5 mm^2. Current-voltage characteristics were measured with a Keithley 236 source/measure unit under AM 1.5 solar illumination (Oriel 300 W solar simulator) at an intensity of 100 mW/cm^2. All electrical measurements of OPVs were executed in the inert Nitrogen purged devices chamber.

3.9.2 OLED device fabrication

ITO-patterned glass substrates (size 12 mm × 8 mm) were cleaned in an ultrasonic bath using methanol, acetone, and isopropyl alcohol for 15 min. After a 5-min UV-zone treatment, a 40 nm-thickness PEDOT layer was spin-coated onto ITO substrates, which were then heated at 145 °C for 15 min. Then, a 15-nm-thickness hole transporting and electron-blocking TFB interlayer was spin-coated on top of PEDOT layer, and the assembly was baked

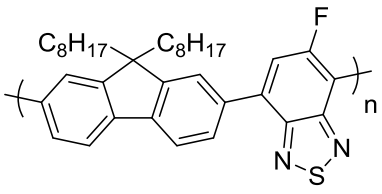
under nitrogen at 180 °C for 1 h. Subsequently, an emissive layer F8BT (Cambridge Display Technology Ltd) was spin-coated from a toluene solution. The thickness of the emissive layers were controlled by using different concentrations (12 mg/ml, 14.7 mg/ml, 16.2 mg/ml, 18 mg/ml and 20.2 mg/ml under 2000 rpm to from layers ranging from 60 nm to 112 nm; the error bar is 3 nm). After a DMSO solution (2 mg/ml) of the **CPE 50%**, **CPE 75%** and **CPE 100%** was separately spin-coated on emissive layer, which was then heated at 60 °C for 30 min. Finally, aluminum (100 nm) cathodes was deposited via thermal evaporation under vacuum conditions (1×10^{-7} Torr).

3.9.3 Materials

2, 7-Dibromofluorene (97%, Sigma Aldrich), 1-bromooctane (98%, TCI Chemicals), tetra-n-butylammonium bromide (98%, Sigma Aldrich), 2-isopropoxy, 4, 4, 5, 5-tetramethyl 1, 3, 2-dioxaborolane(98%, Sigma Aldrich), 4, 7-dibromo-5-fluoro-2, 1, 3-benzothiadiazole (96%, Sigma Aldrich), *n*-Butyllithium solution(1.6 M in hexanes), 3-mercapto-1-propanesulfonic acid sodium salt (95%, fluorochem), tetrakis (triphenylphosphine)palladium(0) (99.9%, Strem Chemicals UK Ltd). Other chemical reagents were of analytical grade and were used as received. Deionized water was used in the present experiment.

3.9.4 Synthesis

F8FBT (Refer to Chapter 2)[111]

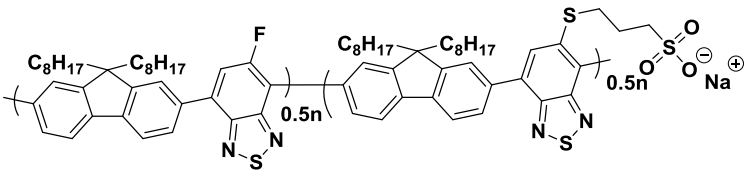


M_n: 26.0 kDa, M_w: 67.51 kDa, M_w/M_n (Đ): 2.60

^{1}H-NMR (400 MHz, $CDCl_3$) δ 8.15 – 7.79 (m, 7H), 2.16 (m, 4H), 1.33 – 1.08 (m, 20H), 0.99 (m, 4H), 0.84 (m, 6H).

^{19}F-NMR (400 MHz, $CDCl_3$) δ -114.5 ppm

CPE 50%

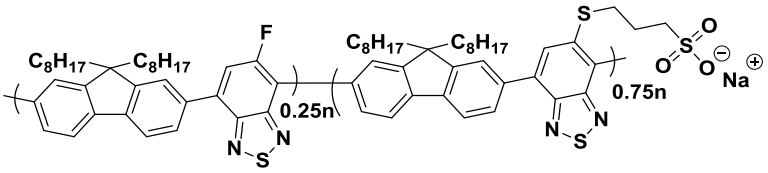


A mixture of **F8FBT** (172.53 mg, 0.319 mmol), sodium 3-mercapto-1-propanesulfonate (28.45 mg, 0.1595 mmol) and NaOH (128 mg, 3.19 mmol) were added to high pressure microwave vial. The vial was sealed with a septum and degassed with argon before anhydrous chlorobenzene and DMSO (3:1, v:v, 8 ml total) was added. The solution was heated at 120°C for 24 hours. After the solution was cooled to room temperature, it was precipitated into water. The resulting polymer was collected by filtration, washed with acetone and chloroform for 24 hours by Soxhlet respectively. Finally, dried overnight in vacuum to obtain **CPE50%** (105 mg, Yield 53%).

^{1}H-NMR (500 MHz, d-DMSO, 373K) δ 8.27 – 7.61 (m, 7H), 3.33 – 3.24 (m, 1 H), 2.58 (m, 1H), 2.14 (m, 4H), 2.08 (m, 1H), 1.14 (m, 20H), 0.92 (m, 4H), 0.77 (m, 6H).

^{19}F-NMR (400 MHz, $CDCl_3$) δ -114.1 ppm

CPE 75%

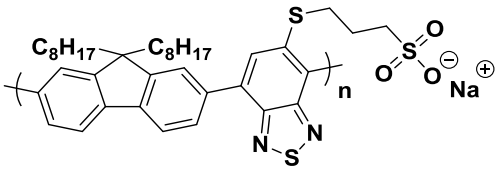


A mixture of **F8FBT** (145.1 mg, 0.269 mmol), sodium 3-mercapto-1-propanesulfonate (35.96 mg, 0.202 mmol) and NaOH (107.6 mg, 2.69 mmol) were added to high pressure microwave vial. The vial was sealed with a septum and degassed with argon before anhydrous chlorobenzene and DMSO (3:1, v:v, 10 ml total) was added. The solution was heated at 120°C for 24 hours. After the solution was cooled to room temperature, it was precipitated into water. The resulting polymer was collected by filtration, washed with acetone and chloroform for 24 hours by Soxhlet respectively. Finally, dried overnight in vacuum to obtain **CPE75%** (114 mg, Yield 64%).

^{1}H-NMR (500 MHz, d-DMSO, 373K) δ 8.27 (m, 1H), 8.19 – 7.61 (m, 7H), 3.33 – 3.24 (m, 1.5 H), 2.62 – 2.55 (m, 1.5H), 2.14 (m, 4H), 2.06 – 1.96 (m, 1.5H), 1.28 – 1.05 (m, 20H), 0.96 (m, 4H), 0.84 – 0.71 (m, 6H).

^{19}F-NMR (400 MHz, $CDCl_3$) δ -114.0 ppm

CPE 100%



A mixture of **F8FBT** (91.3 mg, 0.169 mmol), sodium 3-mercapto-1-propanesulfonate (30.11 mg, 0.169 mmol) and NaOH (67.6 mg, 1.69 mmol) were added to high pressure microwave vial. The vial was sealed with a septum and degassed with argon before anhydrous chlorobenzene and DMSO (3:1, v:v, 8 ml total) was added. The solution was heated at 120°C for 24 hours. After the solution was cooled to room temperature, it was precipitated into water. The resulting polymer was collected by filtration, washed with acetone and chloroform for 24 hours by Soxhlet respectively. Finally, dried overnight in vacuum to obtain **CPE100%** (133 mg, Yield 70%).

^{1}H-NMR (500 MHz, d-DMSO, 373K) δ 8.27 – 7.51 (m, 7H), 3.33 – 3.24 (m, 2 H), 2.58 (m, 2H), 2.14 (m, 4H), 2.01 (m, 2H), 1.25 – 1.05 (m, 20H), 0.94 (m, 4H), 0.78 (m, 6H).

^{19}F-NMR demonstrates no fluorine signal.

4 A new thermo-, pH and CO_2-responsive fluorescent graft copolymer

4.1. Introduction

Smart materials have received increasing interest as they are able to shrink or expand to change their optical properties or electrical properties when surrounding environment changes.[165,166] With the development of materials research, the new materials are designed to respond to external changes and adjust to our demands. Stimuli-responsive polymers, a class of smart materials, are playing a very important role in a wide range of fundamental fields, such as nanotechnology, sensors, catalysis, coatings, and drug delivery.[167–172] Stimuli responsive polymers are able to make physical and/or chemical changes when receiving an external signal. Smart polymers are characterized by their stimuli-responsive factors, which are dictated by the functional groups on a polymer chain. Different functionalities respond to different stimuli factors and the most commonly utilized stimuli factors are temperature[173,174], pH[175,176], light[177,178], ionic strength[179,180], electron transfer[181,182]. Among all the stimuli factors, temperature has gained the most attention and many novel thermo-responsive polymers have been synthesized.[183–185] For example, some polymers can exhibit a lower critical solution temperature (LCST), which is the lowest temperature at which temperature induced demixing occurs. When the temperature is below the LCST, the polymer chains and solvent molecules are in one homogeneous mixed phase. But when the temperature is above the LCST, phase separation occurs through an entropically driven process.[186] The potential advantages of using thermo-responsive polymers are mainly in the field of biomedical science which includes targeted drug delivery and bio-separation.[187,188] Among the thermo-responsive polymers reported, poly(*N*-isopropylacrylamide) (PNIPAM)[189,190], polyethylene glycol (PEG)[191–193], poly(2-ethyl-2-oxazolines)(PEO)[194,195] and poly(2-propyl-2-oxazoline) (PPO)[196,197] have gained much attention. The structures of PNIPAM, PEG, PEO and PPO are shown in Figure 52. These polymers will undergo phase transition in aqueous solution above a specific temperature. For example, PEO exhibits a phase transition behavior in aqueous solution at approximately 94 °C.[198] On the other hand, PPO and PNIPAM demonstrate their phase transition temperatures at approximately 36 °C,

which is very close to human body temperature.[199]

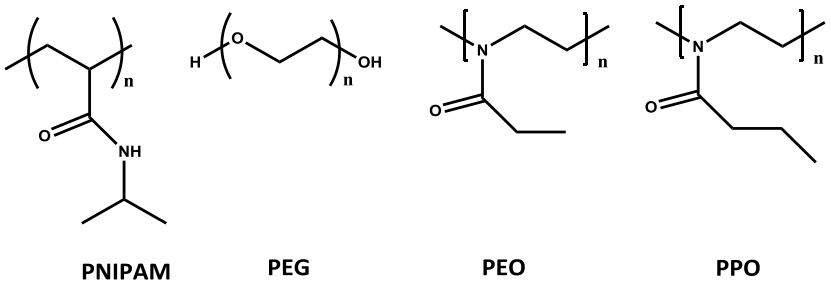


Figure 52 Structures of typical thermo-responsive polymers

To fulfil the diverse requirements of environmental systems, multi-stimuli-responsive polymers have received a great deal of attention in functional polymer research.[200–202] They allow efficient manipulation of hydrophilic/hydrophobic transitions in aqueous solution, as they are able to respond to changes of multiple external environment factors, such as temperature, pH, light, gas and electric fields.[203,204] An example of a multi-stimuli-responsive polymer is shown in Figure 53.[205] Single-stimuli-responsive polymers are a class of polymers which are only responsive to one stimuli factor. Compared to single-stimuli-responsive polymers, multi-stimuli-responsive polymers can undergo more physical property changes and the designed functions can be achieved by tuning numerous environmental factors.[206,207]

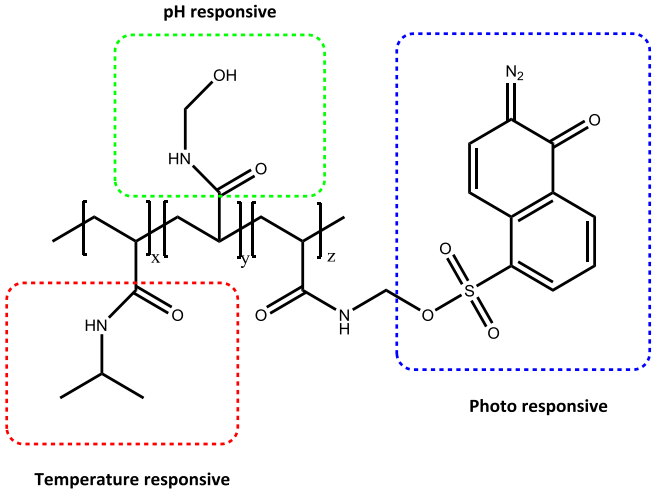


Figure 53 An example of multi-stimuli-responsive polymer, bearing thermo-, pH- and photosensitive moieties[205]

The usual way to prepare multi-stimuli-responsive polymers consists on the copolymerization of different monomers.[208,209] For example, temperature and pH responsive polymers are usually prepared through the copolymerization of a monomer containing a pH-responsive moiety and a monomer containing a thermo-responsive moiety. However, time-consuming multiple steps are generally involved in the synthesis of copolymers containing different responsive monomers. Besides, the way to synthesize multi-stimuli-responsive homopolymers has been reported.[210,211] For example, the Song group synthesized a temperature and pH/CO_2-responsive homopolymer, poly(N-(2-(diethylamino)ethyl)-N-(3- (isopropylamino)-3-oxopropyl)acrylamide). The pH/CO_2-responsive and thermo-responsive moieties of amide and amine were combined in one polymer backbone.[212] However, the synthesis of the monomer containing several different responsive moieties for multi-stimuli-responsive homopolymers was difficult and involved several steps. Therefore, alternative routes to multi-stimuli-responsive polymers with concise functional composition are needed.

Post-polymerization modification enables the synthesis of many functional polymers, which are difficult or impossible to prepare via direct polymerization.[35,213,214] Post-polymerization allowed systematic variations in structures based on the same reactive scaffold, without variables usually created from the polymerization of individual monomers (e.g., molecular weight and dispersity).[50] Inspired by these advantages, a new thermo- and pH/CO_2 responsive graft copolymer was designed and synthesized by post-polymerization in this chapter. As the conjugated backbone contains a diethylamino group, it was expected that the conjugated polymers would be responsive to pH and CO_2.[215] Besides, if a thermos responsive polymer could be grafted on the conjugated backbone by post-polymerization, the synthesized graft copolymer should be responsive to three factors: pH, CO_2 and temperature.

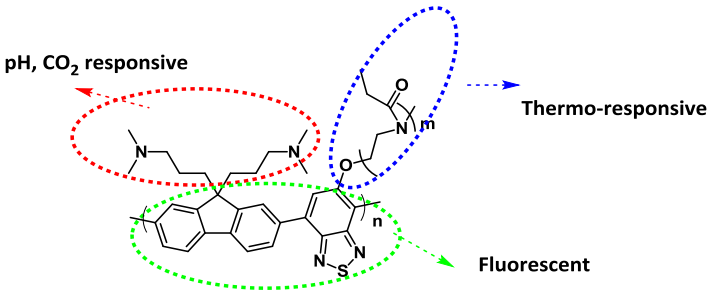


Figure 54 Structure of target thermo- and pH/CO_2-responsive graft copolymer

In this chapter, we present a new and facile method to prepare multi-stimuli-responsive polymer using a conjugated polymer as the main backbone and thermo-responsive PEO and PPO as the "side chain" (Figure 54). More importantly, this facile synthesis method gave us an effective strategy to design and synthesize multi-stimuli-responsive polymers. If you want to synthesize multi-stimuli-responsive polymers which are responsive to three different stimuli factors, like A, B and C. Normally we need to prepare three different monomers containing A, B and C moieties first, then combine these monomers through copolymerization. Alternatively, prepare a monomer containing the three stimuli responsive moieties A, B and C to make a homopolymer. The disadvantages about synthesis of multi-stimuli-responsive copolymers and homopolymers have been discussed above. However, with the post-polymerization method proposed in this chapter, we can graft different stimuli factors to the precursory conjugated backbone to synthesize graft copolymer. The basic post-polymerization strategy to synthesize multi-responsive polymers was demonstrated in Figure 55.

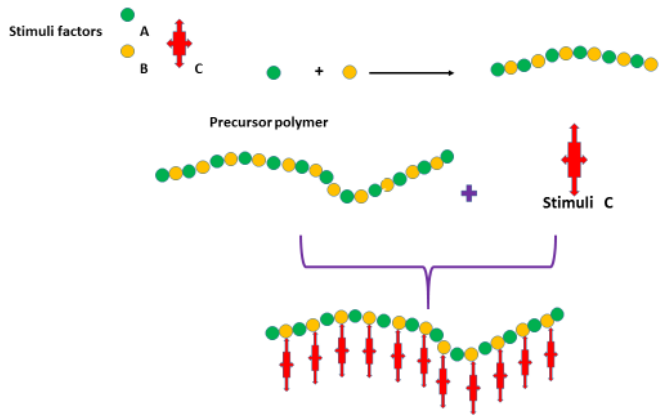


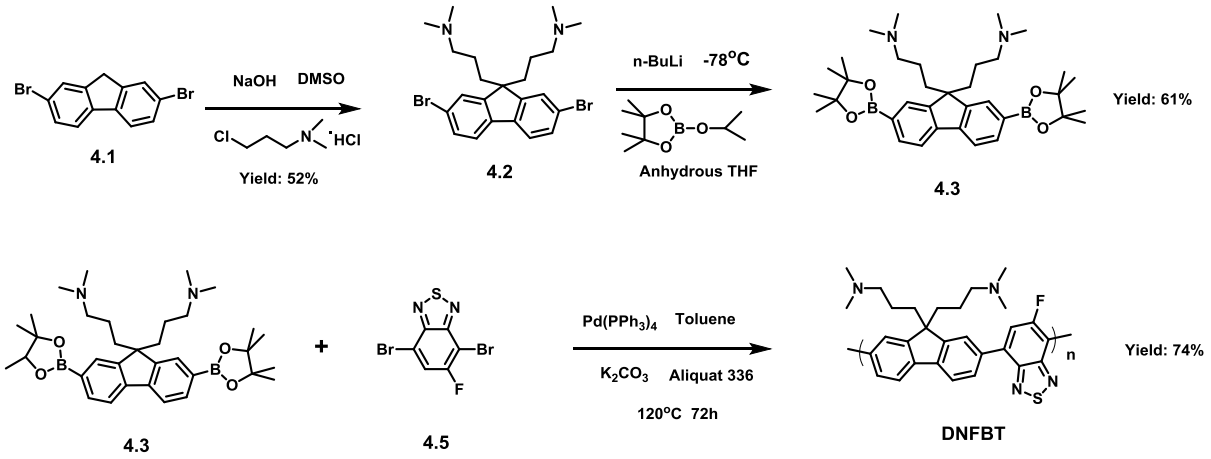
Figure 55 Strategy to synthesize multi-stimuli-responsive polymers by post-polymerization

4.2. Synthesis of monomers and graft copolymers

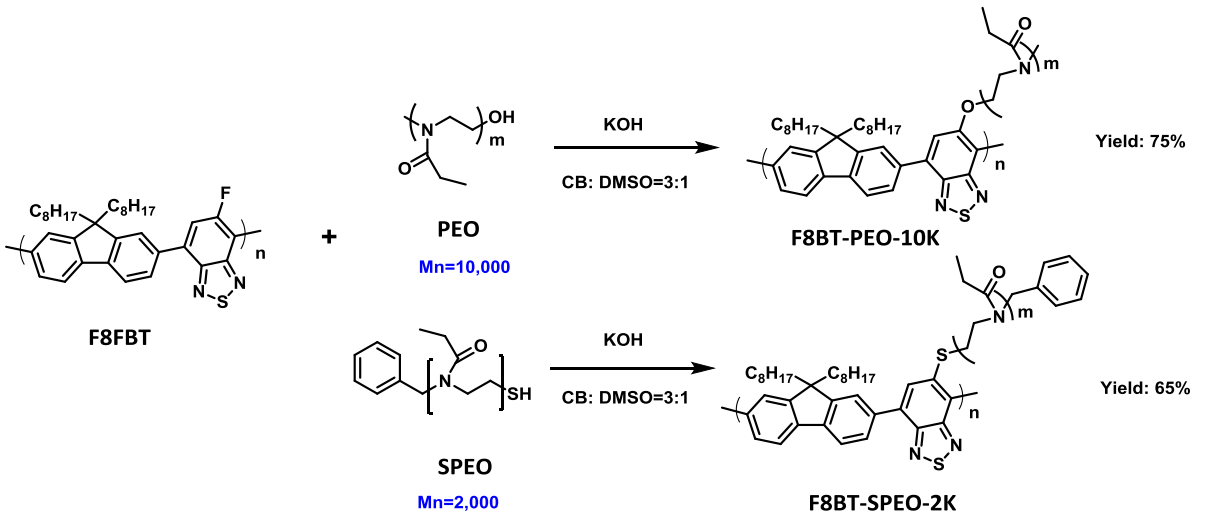
4.2.1 Synthesis routes

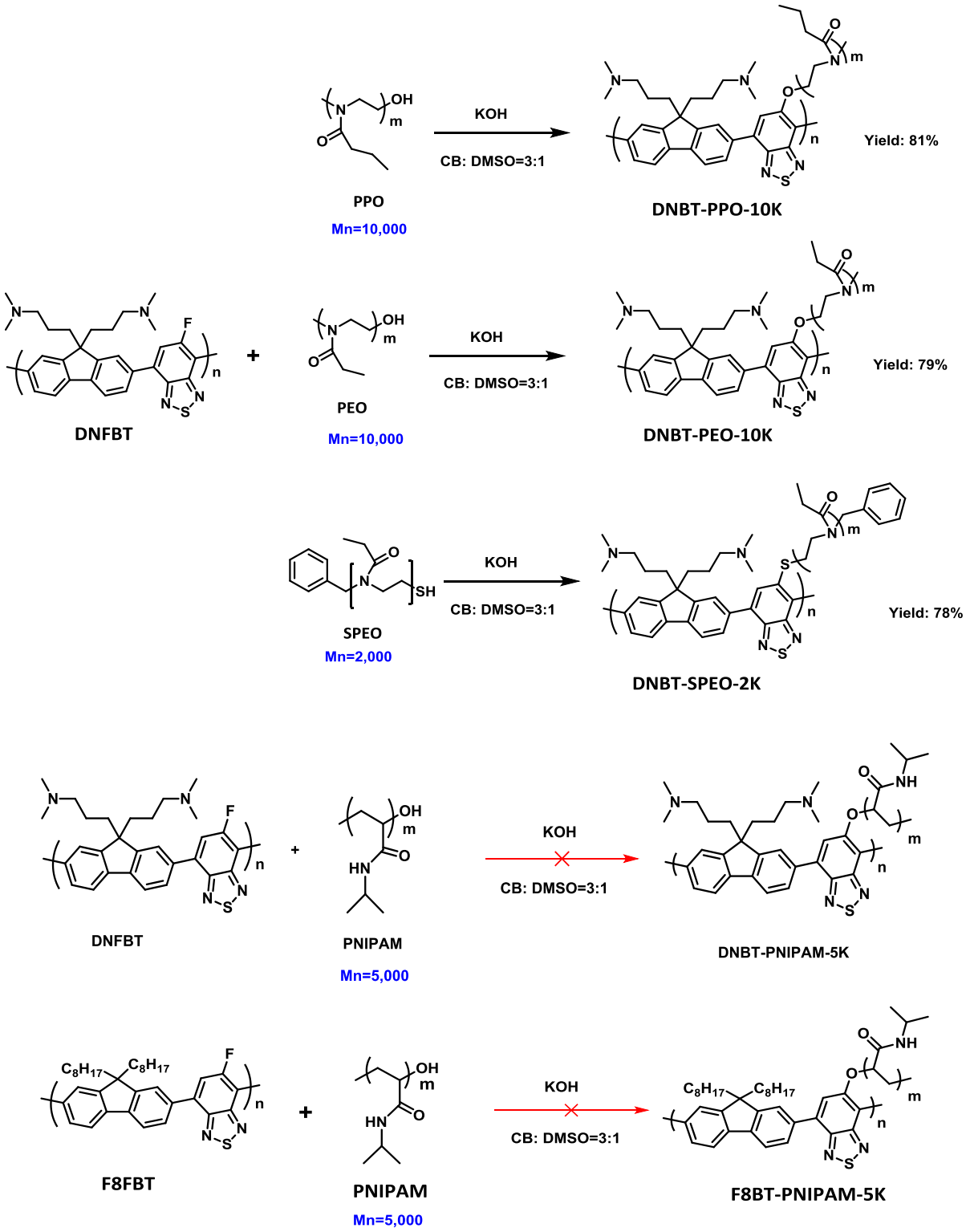
A series of graft copolymers have been synthesized by post-polymerization modification through fluoride substitution on aromatic backbone according to **Scheme 5**, **6**. A mixture of

monomer **4.1**, tetrabutylammoium bromide and 3-dimethylaminopropylchloride hydrochloride was reacted with a 50 wt % aqueous solution of NaOH. After reaction, the crude product was purified by column chromatography using methanol to give pure monomer **4.2** (Yield 52%). Then monomer **4.2** was then converted to the boronic ester by treatment with n-BuLi, followed by quenching of the resulting dianion with 2-isopropoxy-4, 4, 5, 5 tetramethyl-1, 3, 2-dioxaborolane. The crude product was recrystallized from acetone to give pure monomer **4.3** (Yield 61%). For the conjugated polymers, **DNFBT** (M_n= 38,500 g/mol, M_w= 65,100 g/mol, PDI= 1.69) and **F8FBT** (M_n= 26,000 g/mol, M_w= 67,500 g/mol, PDI= 2.60) were synthesized under typical Suzuki polymerization condition.[110] After 3 days of heating at 120 °C in toluene, the solution was then precipitated into methanol and filtered. Then Soxhlet extraction washes the polymer with methanol, acetone, hexane and chloroform for 24 hours respectively.



Scheme 5 Synthesis of **DNFBT**





Scheme 6 Synthesis of graft copolymers

The graft copolymer **DNBT-PPO**, **DNBT-PEO**, **DNBT-SPEO**, **F8BT-PEO** and **F8BT-SPEO** were all synthesized by S_NAr substituted reactions. At first, we used K_2CO_3 as a base in a mixture of chlorobenzene and DMSO to synthesize graft copolymers **DNBT-SPEO** and **F8BT-SPEO**.

However, when the same reaction condition was used for the other graft copolymers' synthesis, the ^{19}F-NMR demonstrated that there was always fluorine signal even after prolonged heating. The use microwave heating did not help. ^{19}F-NMR demonstrated that the fluoride substitution was not complete in all cases. Clearly changing the end group on the graft from a thiol to an alcohol required a stronger base in agreement with their respective acidities. In addition, a thiol group is a stronger nucleophile than an alcohol helping to promote the substitution reaction. Based on this consideration, KOH was used in this reaction. The graft copolymers **DNBT-PPO**, **DNBT-PEO** and **F8BT-PEO** were successfully synthesized using KOH as a base. As the graft copolymers **DNFBT-PPO**, **DNBT-SPEO** and **F8BT-SPEO** were not soluble in water, the crude product was precipitated into water to remove the excess polymer PPO or SPEO. However, the graft copolymer **DNBT-PEO** and **F8BT-PEO** were both soluble in water. Therefore after reaction, the reaction solvents (mixture of chlorobenzene and DMSO) was removed by heating and the crude products were dissolved in distilled water. The excess polymer PEO were removed by dialysis for 2 days. However, attempts to graft PNIPAM to conjugated backbone went unsuccessful which was maybe due to poor stability at high temperature and strongly basic reaction environment.

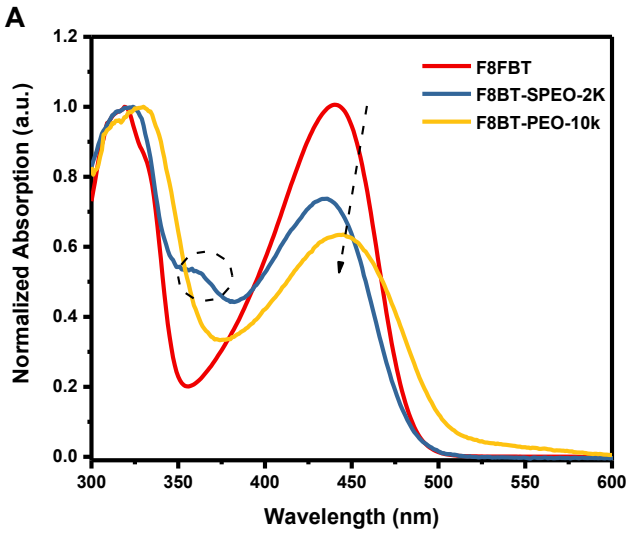
4.2.2 NMR analysis

All the graft copolymers were confirmed by DOSY-NMR, ^{1}H-NMR and ^{19}F-NMR. Take polymer **DNBT-PEO** for example. The ^{19}F-NMR shows no fluorine signal which indicated the fluoride was fully substituted by side chain PEO. Besides, the protons from the side chain PEO were dominant in ^{1}H-NMR and the proton signal from conjugated backbone DNBT was very weak (Appendix Figure 35). As the side chain PEO has a very high molecular weight (M_n= 10,000 g/mol, PDI≤1.3), which means the proton signal is tremendously more intensive than DNBT's (molecular weight of repeating unit was 487) proton signal. That is the reason that the ^{1}H-NMR shows dominant PEO signal. The DOSY NMR of **DNFBT** and PEO mixtures was investigated (Appendix Figure 36). In DOSY NMR, each component in a mixture can be pseudo-separated, based on its own diffusion coefficient.[94] Clearly, the proton signal consisted of three parallel signal lines, and the first signal line belonged to the deuterated solvent ($CDCl_3$). The second and third signal lines belonged to PEO and **DNFBT** respectively.

Apparently, the proton signal of **DNFBT** and PEG was from two separated signal lines. Besides, the DOSY NMR of **DNBT-PEO** alone was investigated (Appendix Figure 37). As expected, there was only one signal line which meant all the protons were from **DNBT-PEO**, indicating the high purity of **DNBT-PEO**.

4.2.3 UV-Vis absorption

The graft copolymers were also confirmed by the absorption spectra (Figure 56). All polymers demonstrated two absorption bands, a high energy band corresponding to the π-π* transition and a low energy band corresponding to the ICT. Clearly, after the fluoride fully substituted by side chains, the intensity of low energy band was reduced. The intensity reduction in the low energy band is related to the change in electron accepting ability of the BT comonomers as the electron deficient fluoride is replaced by less electron deficient side chains, which was the same as discussed in Chapter 2 (see 2.3.1). Besides, a new absorption peak is observed between 360 to 370 nm for graft copolymers **F8BT-SPEO** and **DNBT-SPEO** containing thioalkyl group. The additional intense absorption is due to $N_{sulfur} \rightarrow \pi^*$ transitions, which was the same as discussed in Chapter 3 (see 3.4.1).



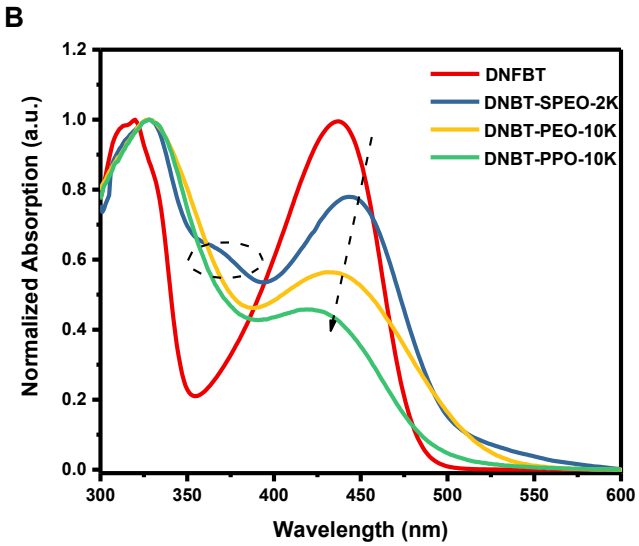


Figure 56 UV-Vis absorption of **F8FBT**, **DNFBT** and graft copolymers in chloroform

4.3 Solution behavior of graft copolymers

The temperature-responsive properties of the graft copolymers was investigated initially by heating the aqueous solutions at temperature above LCST and then cooling at temperature below LCST. The overall solution behaviors of graft copolymers which are dependent on the "side chain" PEO, PPO and SPEO are summarized in Figure 58. It was found that **F8BT-SPEO** containing poly(2-ethyl-2-oxazoline) (M_n= 2,000 g/mol) was not soluble in water. Besides, **F8BT-SPEO** was not responsive to pH or CO_2 as expected. But it demonstrated excellent solubility in polar solvents (methanol, DMSO) (Appendix Figure 38) as a result of the hydrophilic side chain, poly(2-alkyl-2-oxazoline) (M_n= 2,000 g/mol). Increasing the length of the graft, **F8BT-PEO** containing poly(2-alkyl-2-oxazoline) (M_n= 10,000 g/mol) was soluble in water but not pH or CO_2 responsive. Heating solution of **F8BT-PEO** did not result in any obvious LCST phenomenon. We believe this may be due to the low polymer concentration because of **F8BT-PEO**'s limited solubility in water (less than 1 mg/ml). **DNBT-SPEO** containing poly(2-ethyl-2-oxazoline) (M_n= 2,000 g/mol) was not soluble in water even at the boiling temperature similar to **F8BT-SPEO**, but was soluble in water after bubbling with CO_2 at room temperature (Figure 57). Neutralizing the resulting solution with the NaOH resulted in becoming cloudy. But after bubbling with CO_2 again, the solution then becomes transparent. However, when the CO_2 saturated solution was heated to boiling temperature

of water, no soluble-to-insoluble phase transition was found. It means that **DNBT-SPEO** is not thermo-responsive, but only CO_2 responsive.

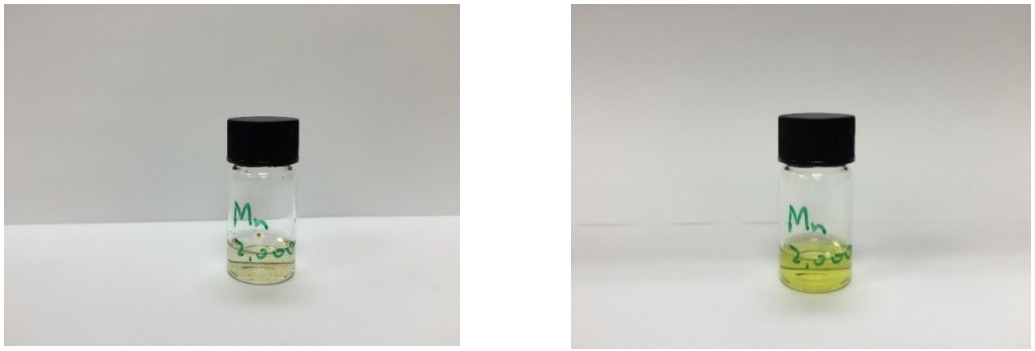


Figure 57: **DNBT-SPEO** before (left) and after (right) bubbling with CO_2

DNBT-PEO containing poly(2-ethyl-2-oxazoline) (M_n= 10,000 g/mol) was pH, CO_2, and thermo-responsive. The thermo-response of **DNBT-PEO** is summarized in Figure 59. **DNBT-PPO** containing poly(2-propyl-2-oxazoline) (M_n= 10,000 g/mol) was not water soluble. It is maybe due to the grafted side chain poly(2-propyl-2-oxazoline) being less hydrophilic than poly(2-ethyl-2-oxazoline). Nevertheless, **DNBT-PPO** demonstrated excellent solubility in polar solvents (methanol, DMSO) (Appendix Figure 39).

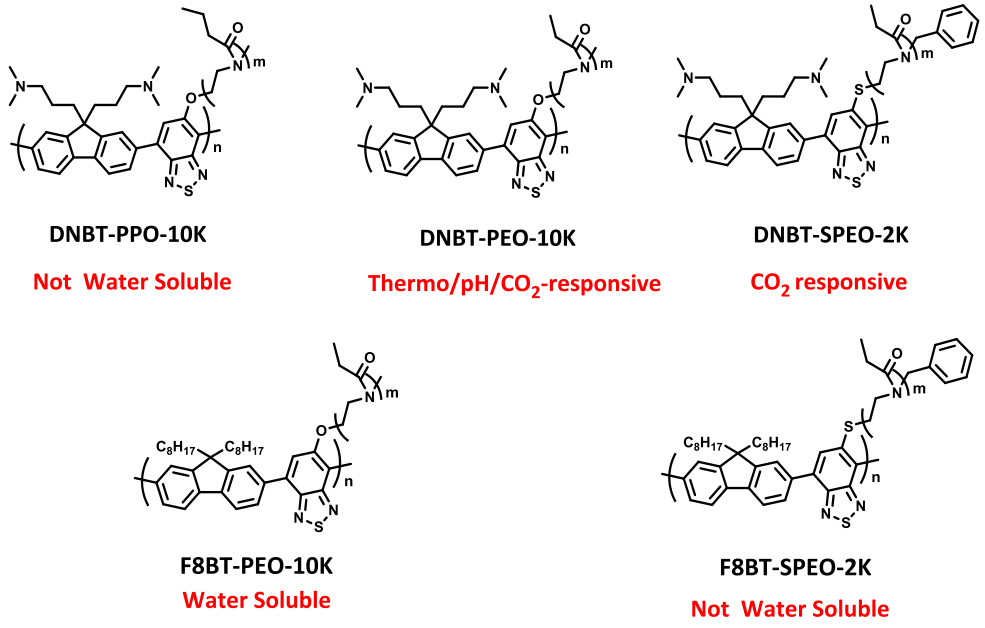


Figure 58 Summary of the solution behaviors of graft copolymers

4.3.1 Effect of polymer concentration.

It was found that the aqueous solution of **DNBT-PEO** was transparent at room temperature. Upon heating the solution above LCST, it becomes cloudy and further becomes transparent when cooling down to room temperature. This process confirms the reversible soluble to insoluble phase transition of **DNBT-PEO** at LCST. The LCST of the thermo-responsive polymers was determined by transmittance analysis at 550 nm on a Varian 100 UV–vis spectrophotometer equipped with a thermo-regulator (1 °C) with the heating/cooling rate at 1 °C/min, in which the LCST was determined at 50% transmittance of the maximal and minimal transmittance.[216–218] For example, the transmittance of **DNBT-PEO** (0.5 wt%) at 25°C was 76% and the transmittance decreased to 58% when the temperature was 70°C. The transmittance decreased further to only 2.4% when the temperature reached 80°C. The transmittance remained around 2.4 % even reaching 85°C. So the 50% transmittance of the maximal (76%) and minimal transmittance (2.4%) was 39.2% and the corresponding temperature was 72°C with a transmittance of 38.8%. Then 72 °C was the LCST of **DNBT-PEO** (0.5 wt%) (Figure 59).

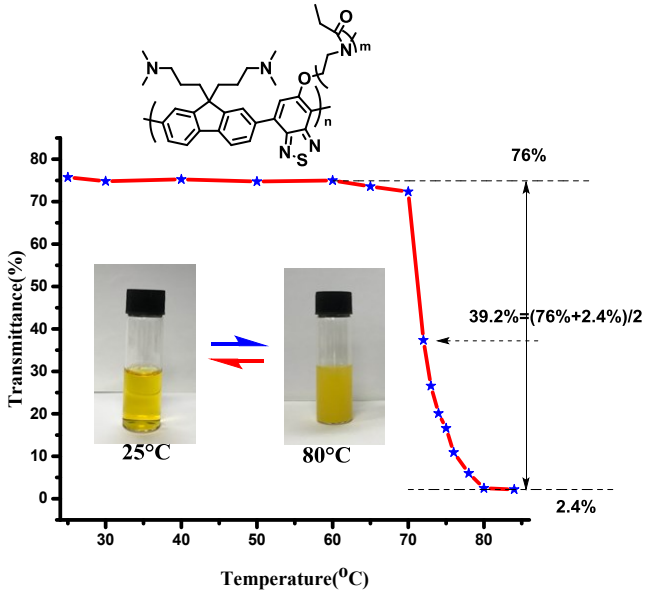


Figure 59: LCST of **DNBT-PEO** (0.5 wt%) measured by transmittance

Furthermore, as the polymer concentration can affect the LCST, the effect of concentration on LCST of **DNBT-PEO** was investigated. The temperature dependent transmittance for 0.25wt%, 0.5 wt % and 1.0 wt % aqueous **DNBT-PEO** solutions is shown in Figure 60.

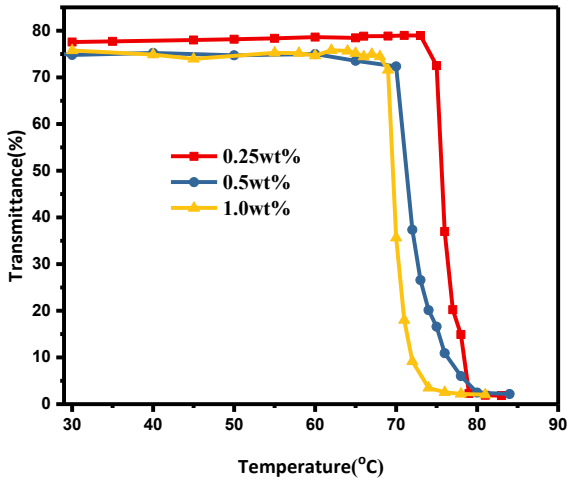


Figure 60 The effect of the polymer concentration on LCST of **DNBT-PEO**.

Figure 60 indicates the LCST of **DNBT-PEO** is directly correlated to polymer concentration. The LCST decreases from 76 to 70 °C when the concentration of polymer increases from 0.25 to 1.0 wt %. This is maybe because the polymer-polymer inter- and intramolecular hydrophobic interactions increase as concentration increases and extensive hydrogen bonding interactions are less pronounced between water molecules and polymer molecules. Less energy input is required to disrupt these interactions. Therefore, the transition temperature is lowered. The reversible soluble-to-insoluble phase change structure is demonstrated in Figure 61**.** Also, the soluble-to-insoluble phase change structure is confirmed by dynamic light scattering (DLS).

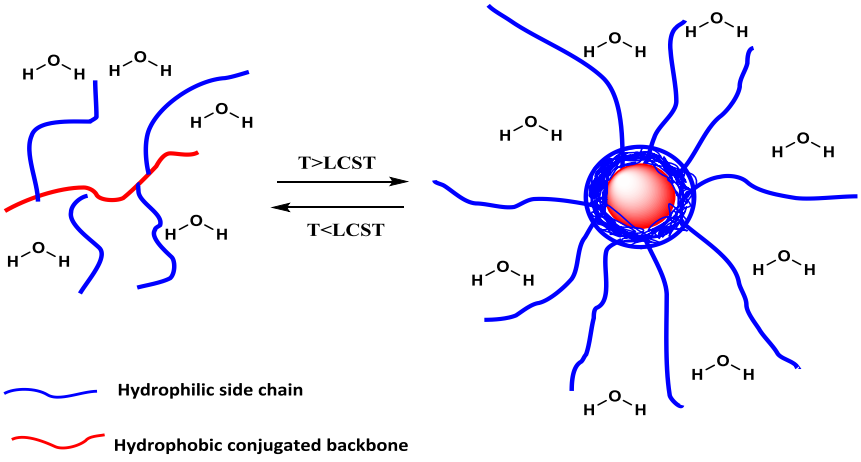


Figure 61. Reversible soluble-to-insoluble phase structure of **DNBT-PEO**.

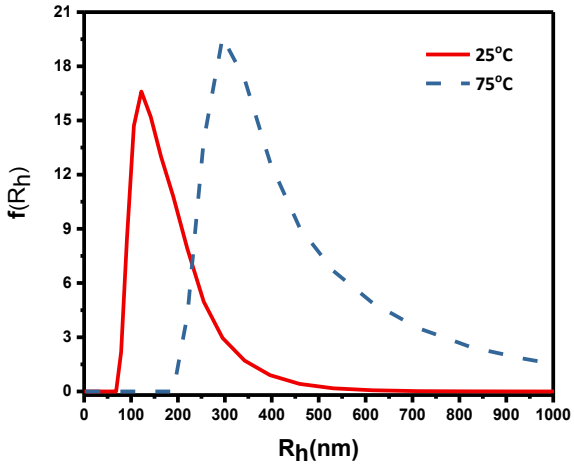


Figure 62. Hydrodynamic radius distributions, $f(R_h)$, obtained at 25 °C and 75 °C for the aqueous solutions of **DNBT-PEO** (0.5 wt%).

The hydrodynamic size distribution of **DNBT-PEO** in water (0.5 wt%) at 25 °C and 75 °C is demonstrated in Figure 62. **DNBT-PEO** demonstrates a number-average hydrodynamic radius, R_h, 122 nm for 25 °C and 295 nm for 75 °C. Clearly, when the temperature is above LCST (72 °C at 0.5 wt%), the size of **DNBT-PEO** increased dramatically from 122 nm to 295 nm. The conjugated backbone is water insoluble, but the 'side chain' PEO is water soluble. When the temperature of aqueous solution is above LCST, the **DNBT-PEO** aggregates into the structure, which is expected to have a hydrophobic core and a hydrophilic corona (Figure 61).

4.3.2 Effect of isotopic solvent

Isotopic solvents are useful to study intermolecular forces, especially hydrogen-bonding interactions.[219] For example, the LCST of PNIPAM in D_2O is 1 °C higher than in H_2O,[220] while the LCST of poly[N-(2-methacryloyloxyethyl)pyrrolidone] (PNMEP) in D_2O is 8.5 °C lower than in H_2O[221] (Figure 63). According to the category of thermo-responsive polymers summarized by Hudson, PNIPAM and PNMEP belong to two different types.[222] Below the LCST, PNIPAM is in coil conformation because of the hydrogen-bonding interactions between the polymer and water molecules. However, when the temperature is above the LCST, the hydrogen-bonding interactions are broken, and the polymer chains collapse into globule conformation.[223,224] For PNMEP, their LCST transitions are from intermolecular

interactions such as hydrogen bonding and hydrophobic interactions. During the LCST transition, PNMEP did not undergo intramolecular conformation collapse like the PNIPAM, but their hydrophilic-hydrophobic balance is broken, resulting in PNMEP's intermolecular aggregation.[225,226]

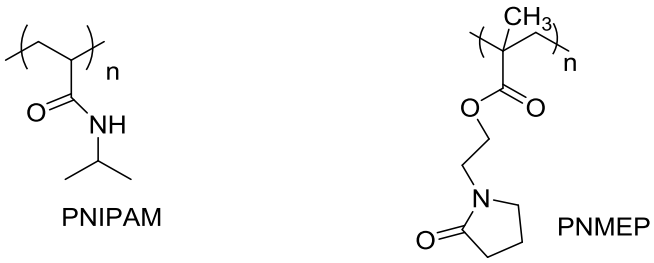


Figure 63 Structures of PNIPAM and PNMEP

As the hydrogen bonding of PNIPAM amides with the D_2O is 5% stronger than that with H_2O,[227] therefore more energy is needed to break these hydrogen bonds to collapse into globule conformation. This leads to a higher LCST of PNIPAM in D_2O than H_2O. As the hydrophobic interactions were slightly weaker in D_2O than in H_2O,[228] less energy is needed to break the hydrophilic-hydrophobic balance. This maybe lead to a lower LCST of PNMEP in D_2O than H_2O. Figure 64 indicates that the LCST of **DNBT-PEO** (0.5 wt%) in deuterated water (D_2O) is slightly lower than that in water (H_2O) (68 °C vs 72 °C), similar to PNMEP in deuterated water.[183]

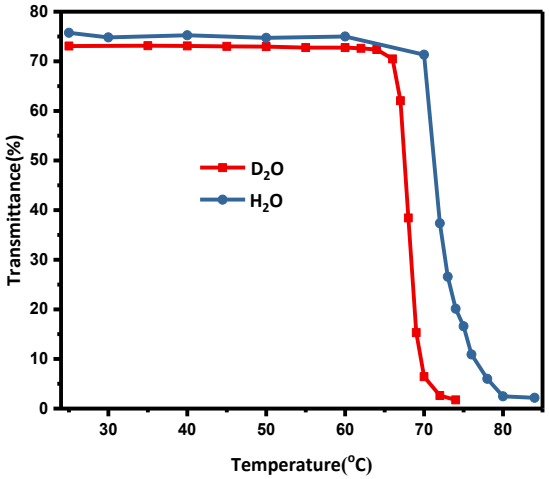


Figure 64. Temperature-dependent transmittance of the aqueous solution of **DNBT-PEO** in H_2O and D_2O, in which the polymer concentration is 0.5 wt %.

4.3.3 ^{1}H-NMR analysis at different temperatures

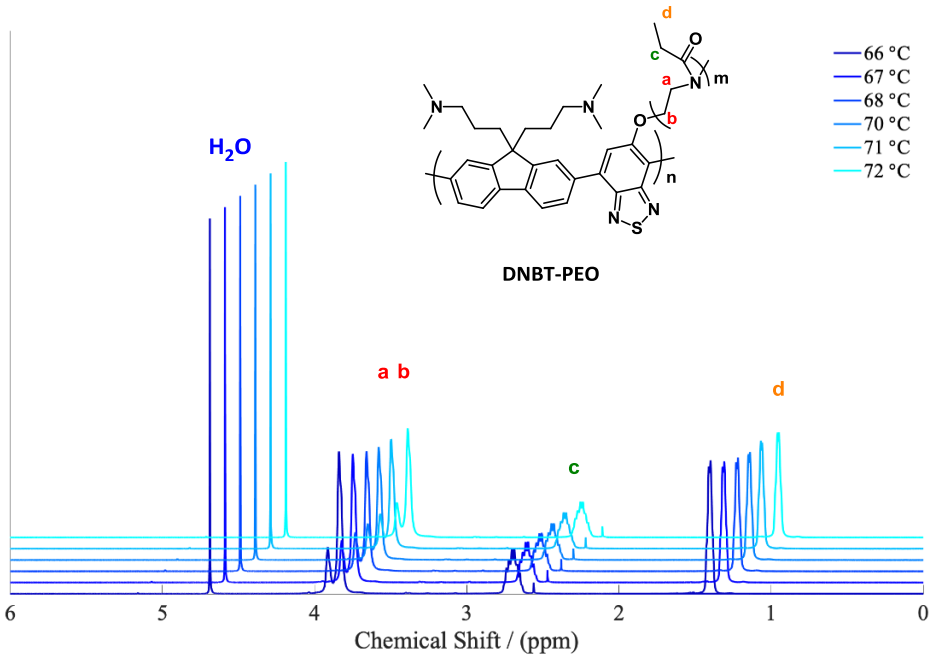


Figure 65. Stacked temperature variable ^{1}H-NMR spectra of **DNBT-PEO** in D_2O at different temperatures (0.5 wt%).

In order to understand this behavior above LCST for 0.5wt % **DNBT-PEO**, temperature variable ^{1}H-NMR analysis was performed in D_2O. The ^{1}H-NMR spectra of **DNBT-PEO** with change of temperature from 66 to 72 °C is demonstrated is Figure 65. The temperature range is decided as such is due to the LCST of 0.5wt % **DNBT-PEO** in D_2O being 68 °C. The noise of each measurement has been taken into account, data are normalized by the internal standard of water signal at δ = 4.70 ppm. Weakening of the signal amplitude for protons **a, b**, **c**, **d** upon heating from 66 to 72 °C is apparent. This observation is consistent with the observations of decreasing transmittance upon heating. This suggests the polymer chains are dehydrated upon heating. This is because the polymer chains exhibit weaker hydrogen bonding interactions with water upon heating.

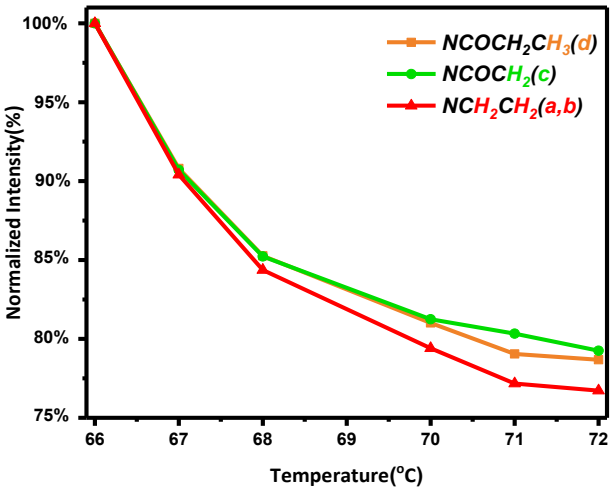


Figure 66. The temperature-dependent signals of the characteristic protons on the backbone and side chain of PEO (0.5 wt %).

To quantify and get a deeper insight for the change of signal amplitude, three characteristic signals, **a, b** (***NCH$_2$CH$_2$***) with δ = 3.92–3.82 ppm, **c** (***NCOCH$_2$***) with δ = 2.75-2.64 ppm and **d** (***NCOCH$_2$CH$_3$***) with δ = 1.43-1.38 ppm, which are normalized by the internal standard of H_2O at = 4.70 ppm, at different temperatures are demonstrated in Figure 66. These three protons signals are chosen, since the corresponding protons signals can be affected by hydrogen bonding and therefore can provide the information about the hydrogen bonding between the polymer chains and the D_2O solvent.[229] As demonstrated in Figure 66, the normalized integral of all three signals decreases at temperature from 66 to 72 °C. In comparison, the signals of **a** and **b** decreases slightly faster than **c** and **d** in this temperature range. Therefore, the decrease of solubility is due to the weakening/disrupted hydrogen bonding interactions between **a, b, c** and **d** moieties with D_2O in which **a** and **b** moieties make a slightly greater contribution.

4.3.4 Effect of addition NaCl

Some additions which could affect the LCST of polymer have been reported, such as NaCl.[230,231] It is because the addition of electrolytes provokes flocculation of the aqueous colloidal dispersions and this phenomenon is called the salting out effect.[232] The effect of NaCl on the LCST of **DNBT-PEO** was investigated as demonstrated in Figure 67. 0.5 wt%

DNBT-PEO solution were made first, then NaCl was added to make **DNBT-PEO** aqueous solution containing different NaCl concentrations. For some thermo-responsive polymers, such as polyacrylamides,[233] the LCST of the thermo-responsive polymers generally decreases with adding inorganic salts. When no NaCl is added in the solution, there are significant amount of hydrogen bonding interactions between water molecules and hydrophilic parts of the polymers. However, the hydrogen bonding interactions between polymer chains with water molecules are disrupted by charged ions when NaCl is added in aqueous solution. This is because charged ions interact stronger with water molecules. Therefore, the polymer-polymer inter- and intramolecular hydrophobic interactions is more pronounced and the solubility of polymer decreases.

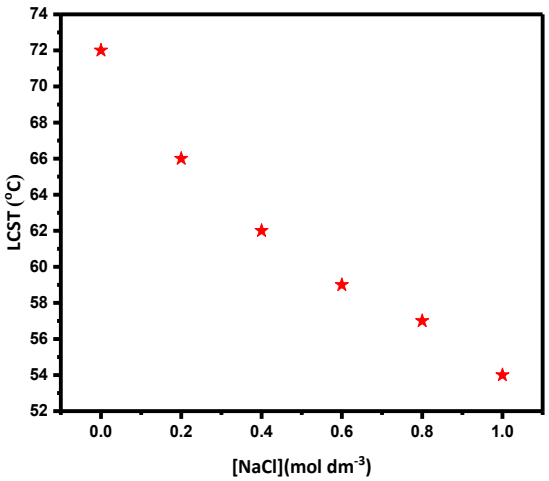


Figure 67. Effect of NaCl on the LCST of the 0.5wt % **DNBT-PEO** aqueous solution.

As seen in Figure 67, similarly with the LCST-type thermo-responsive polymer mentioned above, the LCST of the 0.5 wt % aqueous solution of **DNBT-PEO** decreases from 72 to 54 °C when the NaCl concentration increases from 0 to 1.0 mol·dm^{-3}. Clearly, the LCST of **DNBT-PEO** can be easily tuned by adding inorganic salts.

4.3.5 Effect of Urea.

The addition of urea is usually used to diagnose the hydrogen bonding between the polymer chains and the solvent to check the solution-to-insoluble phase transition of thermo-responsive polymers at LCST.[234,235] For some thermo-responsive polymers, like

PNIPAM, which are capable of undergoing hydrogen bonding with urea, the LCST usually decreases with the addition of urea.[236] However, for other thermo-responsive polymers, like poly(2-oxazoline)s and poly(vinyl ether)s which are incapable of forming hydrogen bonding with urea, the LCST usually increases with the addition of urea.[220] 0.5 wt% **DNBT-PEO** solution were made first, then urea was added to make **DNBT-PEO** aqueous solution containing different urea concentrations. Figure 68 indicates that the LCST of the 0.5 wt % aqueous solution of **DNBT-PEO** increases from 72 to 81 °C when the concentration of the urea increases from 0 to 0.5 mol· dm^{-3}. This suggests that the present thermo-responsive **DNBT-PEO** in the presence of urea undergoes the phase transition similarly with PEO but differently with PNIPAM.

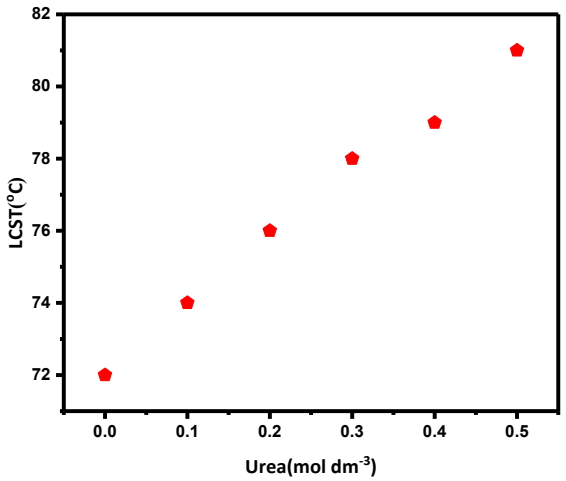


Figure 68. Effect of Urea on the LCST of the 0.5wt % **DNBT-PEO** aqueous solution.

4.3.6 pH response

It is expected that **DNBT-PEO** is pH and CO_2 responsive because of the existence of basic dimethylamino groups on the conjugated backbone. The LCST of **DNBT-PEO** at the pH range from 2.47 to 12.02 is shown in Figure 69. Furthermore, the effect of pH on the optical properties of **DNBT-PEO** was also investigated. Figure 69 indicates that **DNBT-PEO** in the aqueous solution with pH 2.47, and no soluble-to-insoluble phase transition is observed in the temperature window from 25°C to 85°C. Dissolving **DNBT-PEO** directly in neutral water leads to the 0.50 wt % aqueous solution with pH 7.2, and the varied pH aqueous solution of **DNBT-PEO** is prepared by adding suitable amount of pH 1.0 M HCl or 1.0 M NaOH aqueous

solution. At case of pH > 7.2, the soluble-to-insoluble phase transition of **DNBT-PEO** is observed. It is found that the LCST of **DNFBT-PEO** decreases from 70 to 68 °C due to the salting-out effect when pH increases from 8.26 to 10.12. When the pH of the **DNBT-PEO** aqueous solution increases to pH = 12.02, due to the salting-out effect caused by NaOH, the LCST decreases further to 63 °C. The lack of LCST at low pH is likely due to the positive charge on the side chains. This will prevent collapse of the main chain due to columbic repulsions.

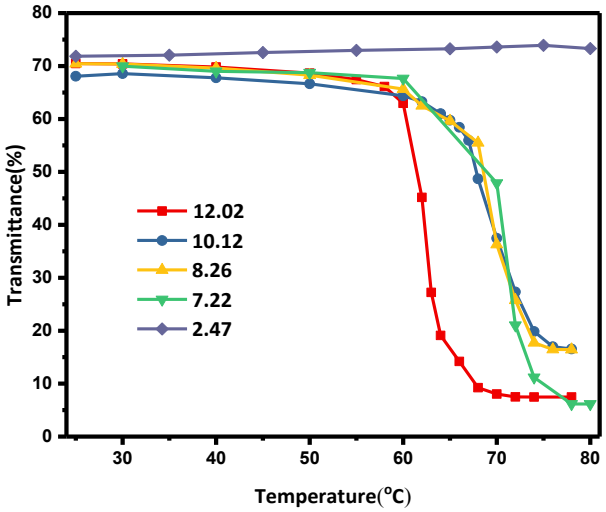


Figure 69 pH-dependent transmittance of the 0.50 wt % **DNBT-PEO** aqueous solution

Also, we studied the absorption properties of **DNBT-PEO** solutions with varied pH values to obtain the correlation for pH and absorption. Changes induced by the pH on the absorption spectra of **DNBT-PEO** are demonstrated in Figure 70A. When the pH is in the range of 8.8 to 12.7, the absorption spectra of **DNBT-PEO** are almost same and display two bands with peaks at 339 and 449 nm, which are assigned to the π−π* transitions of the conjugated main backbone and the ICT respectively.[50] However, when the pH was adjusted below 7.3, the two absorption bands both show slight blue-shift with two peaks around 330nm and 429nm respectively. Also, the normalized intensity of ICT becomes stronger when pH changes from 8.8 to 7.3. Generally, the neutral amino groups of **DNBT-PEO** will be protonated in the presence of an acid environment. Thus, the blue shift of the UV-vis absorption of **DNBT-PEO** in acidic environment compared to that in basic environment can be explained by the decreased conjugation length caused by electrostatic repulsions between positively charged

ammonium groups. Similar observations have been made in other conjugated polymers.[237] The UV-vis absorption of **DNBT-PEO** at pH 4.9 is almost same as those for pH < 4.9 suggests the formation of stable cationic species in the aqueous system in the presence of acid. When the pH value is increased to higher than 7.3, the positive charges could be partially neutralized by NaOH. Consequently, the decreased charge density on polymer leads to the conjugate backbone more planar, which results in the red shift of the UV-vis absorption in basic environment.[238]

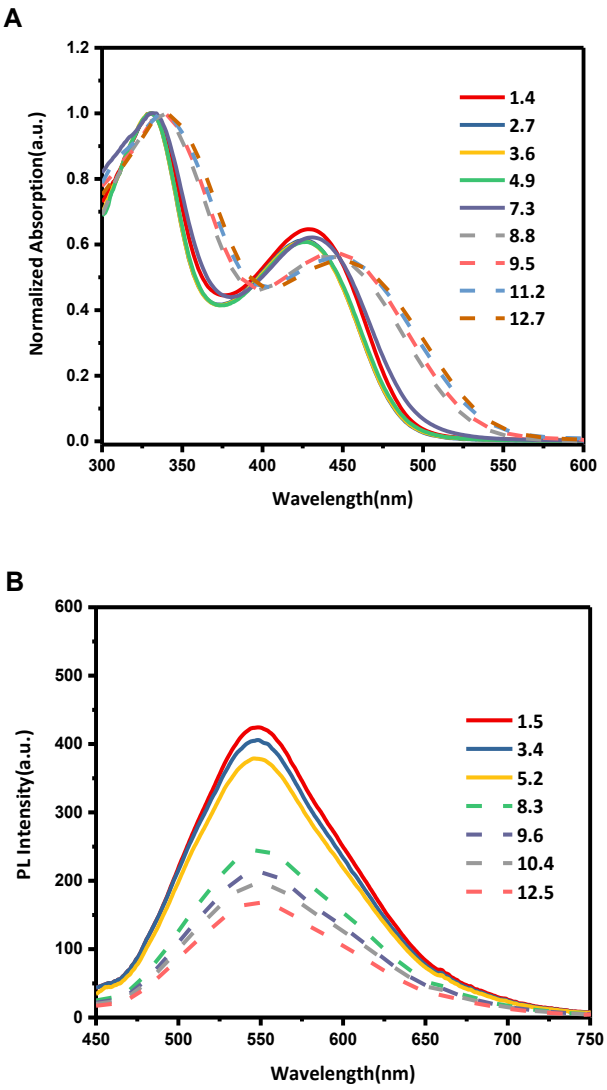


Figure 70 A) Aqueous solution of **DNBT-PEO** in different pH; B) Fluorescent spectra of **DNBT-PEO** in aqueous solution with varied pH

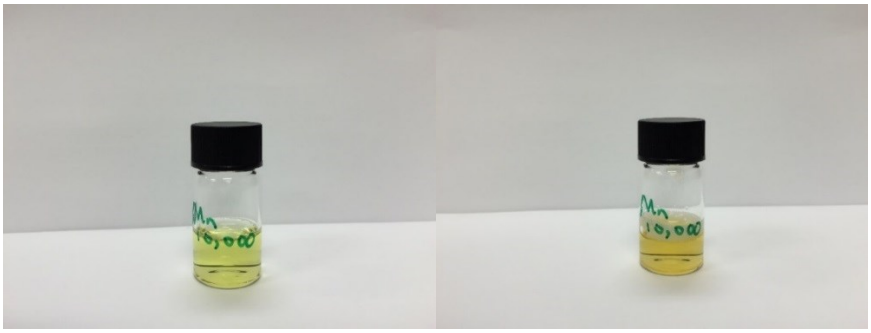


Figure 71 DNBT-PEO (0.5 wt%) in pH 1.4 (left) and 12.7 (right)

As expected from the UV, the color of **DNBT-PEO** at pH 1.4 and 12.7 are slightly different and the aqueous solution pictures are shown in Figure 71. As demonstrated in Figure 70B, the relative fluorescence intensity of **DNBT-PEO** changed in varied pH, but the emission wavelength did not. Clearly, the fluorescence intensity is strong when pH is in the acid range. The fluorescence intensity decreases sharply when the aqueous solution becomes basic. There is a little change in the intensity or shape of the emission band as the pH increases from 1.5 to 5.2. A reduction of 36% in the emission intensity is observed when the pH is changed from 5.2 to 8.3. The PL intensity then decrease gradually down to pH = 12.3. The similar emission wavelength is presumably due to structured rearrangement following photo excitation, such that fluorescence emits from a common, more planar segment. The decrease in intensity is likely because the polymers became more aggregated when the electrostatic repulsion is reduced at high pH.[238]

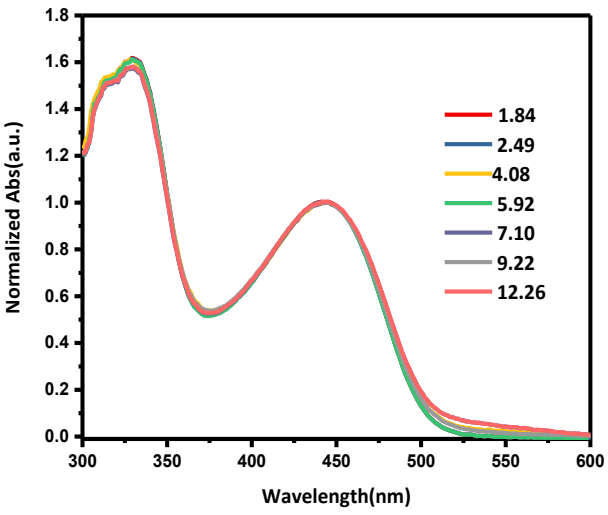


Figure 72 Aqueous solution of **F8BT-PEO** in different pH

As polymer **F8FBT-PEO** is water soluble, the UV of aqueous solution of **F8BT-PEO** at the pH range from 1.84 to 12.26 is summarized as Figure 72. The absorption of **F8BT-PEO** displays two bands at 324 and 445 nm, which are assigned to the π–π* transitions of the conjugated backbone and the ICT respectively. Clearly, there is little change of the absorption shape at varied pH, which indicates that **F8BT-PEO** is not pH responsive.

4.3.7 CO_2 response

CO_2 responsive polymer materials attracts considerable attention due to its low cost, nontoxicity, biocompatibility and good reversibility, and the use of CO_2 as a "green" trigger for responsive polymers is also promising for applications.[239–241] Responsive mechanisms of CO_2 responsive polymers can be divided into three categories according to their responsive behaviors.[242] The first group features responsive groups such as amidines, tertiary amines, bulky secondary amines and bulky primary amines.[215,243] They can switch from neutral to cationic when reacting with CO_2 in water.[244] In the second category, the responsive groups (carboxylic and phenols) change from a neutral moiety to a charged moiety with the addition of CO_2.[245] The third category consists of responsive groups, i.e., amines having N–H bonds and no bulky group adjacent to the nitrogen. Amines can react with CO_2 to form an "ammonium carbamate salt bridge," which results in a cross-link.[246] Amidines and guanidines that contain an N–H bond also belong to this category.

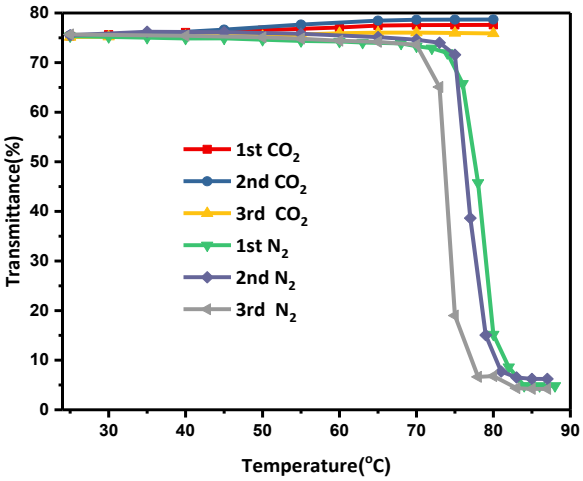


Figure 73 Temperature-dependent transmittance of the 0.50 wt % **DNBT-PEO** aqueous solution upon the N_2/CO_2 bubbling

The amine-based **DNBT-PEO** was investigated with CO_2 in water. The LCST of **DNBT-PEO** disappears after bubbling with CO_2 and then reversibly recovers upon removal of CO_2 by bubbling with N_2 (Figure 73). This is presumably due to protonation of the dimethylamine groups by carbonic acid. As seen no LCST is observed when the amine groups are protonated. Then **DNBT-PEO** becomes reversibly thermo-responsive with the LCST at 76 °C after bubbling with N_2, and **DNBT-PEO** further becomes soluble in water after bubbling CO_2.

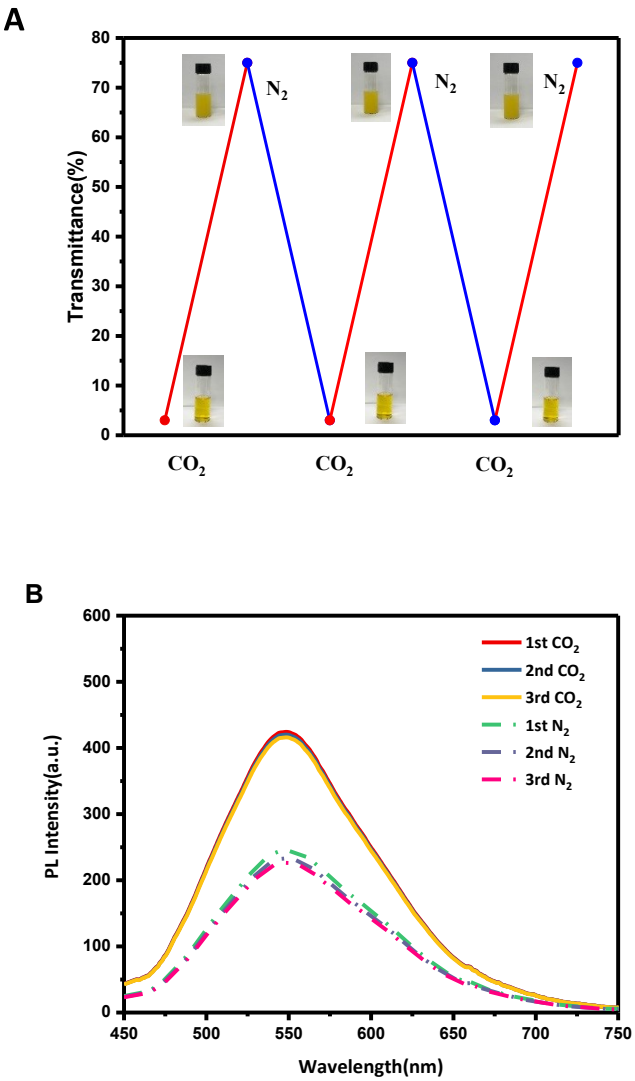


Figure 74. Fluorescence spectra of **DNBT-PEO** in solution upon CO_2/N_2 bubbling

As we can see, the transmittance quickly dropped from 75% to nearly 0% when **DNBT-PEO** solution was placed at a relatively higher temperature (76 °C), subsequently cooling the aqueous solution could reversibly increase the transparency to its original value again. Three heating–cooling cycles were repeated, indicating the excellent repeatability of **DNBT-PEO**.

As shown in Figure 74, the fluorescence intensity of **DNBT-PEO** increased after CO_2 exposure. The fluorescence intensity decreased after bubbling with N_2 which was agreement with Figure 70B that the intensity was stronger in protonation system. Clearly, the solution demonstrated good fluorescent reversibility upon three consecutive CO_2 and N_2 cycles, which indicated that **DNBT-PEO** can be used as a fluorescent sensor for CO_2. Interestingly, the **DNBT-SPEO** cannot dissolve in water, but it becomes water soluble after bubbling with CO_2. The polymeric tertiary amines are more hydrophobic in their neutral form and more hydrophilic when the tertiary amine group becomes protonated to make the bicarbonate salt. The bicarbonate salt after CO_2 bubble aid the solubility in water and that is the reason **DNBT-SPEO** can dissolve after CO_2 bubble.[215] This protonation and deprotonation can be performed reversibly by addition and removal of CO_2 (Figure 75).

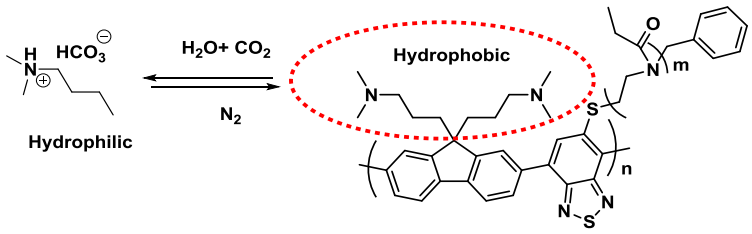


Figure 75 CO_2-switchability mechanism of **DNBT-SPEO** in water

Besides, the LCST of the CO_2 saturated aqueous solution was investigated and summarized in the Figure 76. Clearly, the CO_2 saturated aqueous solution did not demonstrate reversible soluble-to-insoluble phase transition at the temperature range from 25 to 85°C, which means the CO_2 saturated **DNBT-SPEO** aqueous solution is not thermo-responsive.

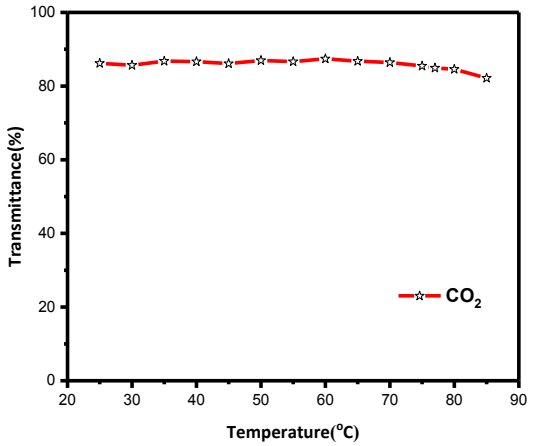


Figure 76 The transmittance of the CO_2 bubbling **DNBT-SPEO** aqueous solution

4.4 Conclusions

In this chapter, a series of graft copolymers have been synthesized through post-polymerization and characterized. Among these polymers, the graft copolymer **DNBT-PEO** is thermo- and pH/CO_2-responsive. Appending diethylamino groups on the conjugated backbones endows the graft copolymer **DNBT-PEO** to give response to pH and CO_2. Also, the graft copolymer **DNBT-PEO** is thermo-responsive because of the grafted polymer PEO. The LCST of **DNFBT-PEO** in aqueous solution decreased from 76 to 70 °C when the polymer concentration increases from 0.25 wt% to 1.0 wt%, which indicates that its thermal transitions can be tunable by only changing the solution concentration. It is found that the LCST of **DNBT-PEO** in deuterated water (D_2O) is slightly lower than those in water (H_2O), and the LCST decreases with the addition of NaCl, and increases with the addition of urea. The temperature-variable ^{1}H-NMR analysis suggests that the dehydration of **DNBT-PEO** at temperature above LCST is ascribed to the weakened or disrupted hydrogen bonding by (***NCH$_2$CH$_2$***), (***NCOCH$_2$***) and (***NCOCH$_2$CH$_3$***) moieties with water. The pH also affects the thermo-response of **DNBT-PEO**, as indicated by the decreasing LCST of **DNBT-PEO** with the pH increasing. Also, the fluorescence intensity in acid range is much stronger than the basic range. Besides, the thermo-response of **DNBT-PEO** can be reversibly tuned by N_2/CO_2 bubbling. The graft copolymer **DNBT-PEO** synthesized by post-polymerization helps to open a new strategy to design multi-stimuli-responsive polymeric materials.

4.5. Experimental methods

4.5.1 Characterization

The molecular weight and the $Đ_M$ of the synthesized polymers were determined by GPC equipped with a Waters 600E GPC system, where chlorobenzene was used as the eluent and the narrow-polydispersity polystyrene was used as the calibration standard. The ^{1}H-NMR, ^{19}F-NMR and DOSY-NMR analysis were performed on a Bruker Avance III 400 MHz NMR spectrometer, and for polymers dissolved in $CDCl_3$ and D_2O, the proton signals at δ = 7.26 ppm and δ= 4.79 ppm of the internal solvents were used as standard.

4.5.2 Dialysis process

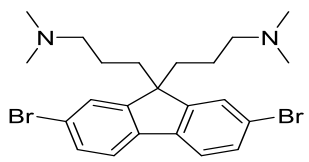
First, hydrated the 20K cassette for 5 minutes in deionized water. Then removed excess water and filled the syringe with the sample. With the bevel sideways, inserted the tip of the needle through one of the syringe ports located at a top corner of the cassette. Injected sample slowly. Kept the cassette in the deionized water for 2 days and changed the deionized water every 12 hours. With the bevel sideways, inserted the tip of the needle through another syringe port located at a corner of the cassette. Withdrew the sample into the syringe.

4.5.3 Materials.

2, 7-Dibromofluorene(97%, Sigma Aldrich), 3-dimethylamino-1-propyl chloride hydrochloride(96%, Sigma Aldrich), 2-isopropoxy, 4, 4, 5, 5-tetramethyl-1, 3, 2-dioxaborolane(98%, Sigma Aldrich), 4, 7-dibromo-5-fluoro-2, 1, 3-benzothiadiazole(96%, Sigma Aldrich), *n*-Butyllithium solution(1.6 M in hexanes, Sigma Aldrich), tetrakis(triphenylphosphine)palladium(0)(99.9%, Strem Chemicals), poly(2-ethyl-2-oxazoline) (M_n= 10,000 g/mol, PDI ≤1.3) (Sigma Aldrich), poly(2-ethyl-2-oxazoline)(α-benzyl, ω-thiol terminated, M_n= 2,000 g/mol, PDI <1.3) (Sigma Aldrich), poly(2-propyl-2-oxazoline) (M_n= 10,000 g/mol, PDI ≤1.2) (Sigma Aldrich) and Slide-A-Lyzer Dialysis Cassettes (20K MWCO, 3ml) (ThermoFisher SCIENTIFIC)were used as received. Other chemical reagents were of analytical grade and were also used as received. Deionized water was used in the present experiment.

4.5.4 Synthesis

2,7-dibromo-N,N,N',N'-tetramethyl-9H-fluorene-9,9-dipropanamine.[117]

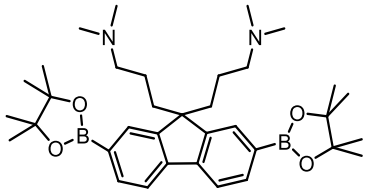


To a stirred mixture of 2, 7-dibromofluorene (6.04 g, 18.64 mmol) and DMSO (50 ml) under nitrogen were added tetrabutylammoium bromide (80 mg) and 50 wt % aqueous solution of

NaOH (8 ml). A DMSO solution (10 ml) of 3-dimethylaminopropylchloride hydrochloride (8.25 g, 52.2 mmol) was added drop-wise to the mixture. The reaction mixture was stirred at 90 ^{o}C for 24 h and then was diluted with 50 mL of water. The product was extracted with ether (3 × 100 mL) and the combined organic layer was washed with 10% NaOH (aq) (2 × 100 mL), water (3 × 100 mL). The solution was dried over $MgSO_4$, filtered, and removed by vacuum evaporation to yield a crude solid. The crude product was purified by column chromatography using methanol as the eluent to give pure monomer **4.2** (Yield 52%).

^{1}H-NMR (400 MHz, $CDCl_3$) δ 7.53-7.44 (m, 2H), 7.50 – 7.44 (m, 4H), 2.09 – 1.92 (m, 20H), 0.77 (m, 4H).

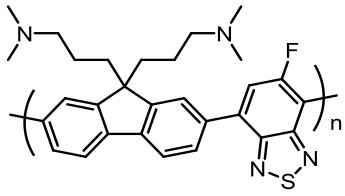
2,7-bis(4,4,5,5-tetramethyl-1,3,2-dioxaborolane-2-yl)-9,9-bis(6-(N,N-dimethylamino)-propyl)fluorine. [247]



To a solution of 2, 7-dibromo-N, N, N', N'-tetramethyl-9H-fluorene-9, 9-dipropanamine (1 g, 2.02 mmol) in anhydrous THF (15 mL) at -78 ^{o}C, 2.8 mL (4.45 mmol) of n-butyllithium (1.6M in hexane) was added by syringe. The mixture was stirred at -78 ^{o}C for 60 min. 2-isopropoxy-4, 4, 5, 5-tetramethyl-1, 3, 2-dioxaborolane (1.7 mL, 8.1 mmol) was added rapidly to the solution, and the resulting mixture was warmed to room temperature and stirred for 24 h under argon. The mixture was poured into water and extracted with ether. The combined organic layer was washed with brine and dried over $MgSO_4$. The solvent was removed by rotary evaporation, and the residue was purified by recrystallization from acetone to provide 0.72 g product (Yield 61%).

^{1}H-NMR (400 MHz, $CDCl_3$) δ 7.83 – 7.72 (m, 6H), 2.10 – 2.03 (m, 4H), 2.03 – 1.94 (m, 20H), 1.39 (s, 24H), 0.75 (m, 4H).

DNFBT



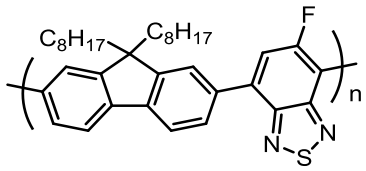
A mixture of 2, 7-bis(4, 4, 5, 5-tetramethyl-1,3,2-dioxaborolane-2-yl)-9, 9-bis(6-(N,N dimethylamino)-propyl)fluoride (484.01 mg, 0.823 mmol), 4, 7-dibromo-5-fluoro-2, 1, 3 benzothiadiazole (256.58 mg, 0.823 mmol), $Pd(PPh_3)_4$ (19.1 mg, 0.0165 mmol), toluene (6ml), Aliquet 336 (0.2 ml) and 3ml of K_2CO_3 (50 wt%) aqueous solution were degassed with nitrogen and stirred at 120°C for 3 days. After cooling to room temperature, the solution was precipitated into methanol and water mixture (1:1, v:v). Then the product was washed with acetone for 24 hours, and the polymer was dissolved in chloroform. The dissolved polymer was precipitated into acetone again, filtered and dried to give pure **DNFBT**. (296 mg, 74% yield).

M_n: 26.0 kDa, M_w: 87.51 kDa, M_w/M_n (Đ): 3.37

^{1}H-NMR (400 MHz, $CDCl_3$) δ 8.31 – 7.80 (m, 7H), 2.41 – 2.07 (m, 20H), 1.36 – 1.04 (m, 4H).

^{19}F-NMR (400 MHz, $CDCl_3$) δ -114.4 ppm

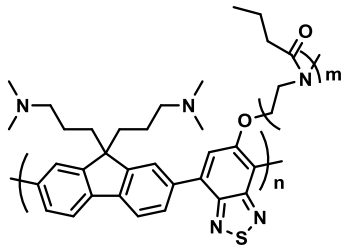
F8FBT (Refer to Chapter 2)



^{1}H-NMR (400 MHz, $CDCl_3$) δ 8.15 – 7.79 (m, 7H), 2.16 (m, 4H), 1.33 – 1.08 (m, 20H), 0.99 (m, 4H), 0.84 (m, 6H).

^{19}F-NMR (400 MHz, $CDCl_3$) δ -114.5 ppm

DNBT-PPO



A mixture of **DNFBT** (7.5 mg, 0.015 mmol), poly(2-propyl-2-oxazoline) (M_n= 10,000 g/mol, PDI≤1.2) (300 mg, 0.03 mmol) and KOH (16.8 mg, 0.3 mmol) were added to high pressure vial. The vial was sealed with a septum and degassed with nitrogen, before anhydrous chlorobenzene and DMSO (3:1= v:v, 10 ml in total) were added. The solution was heated at 120°C for 2 days. After reaction, the resulting solution was precipitated into water. Collect the precipitation and dried overnight to yield **DNBT-PPO** (132 mg, 81% yield) as yellow solid.

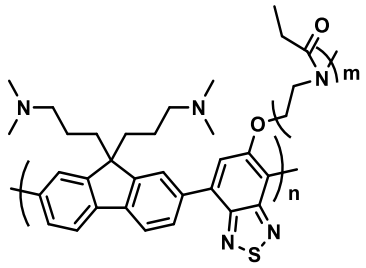
^{1}H-NMR (400 MHz, d-DMSO) shows dominant PPO signal.

δ 2.97 (m, 4H), 2.27 (t, *J* = 6.0 Hz, 2H), 1.54 (m, 2H), 0.89 (t, *J* = 6.0 Hz, 3H).

^{19}F-NMR (400 MHz, $CDCl_3$) demonstrates no fluorine signal.

High purity was confirmed by DOSY-NMR (Appendix Figure 33, 34).

DNBT-PEO



A mixture of **DNFBT** (4.3 mg, 0.0084 mmol), poly(2-ethyl-2-oxazoline) (M_n= 10,000 g/mol, PDI≤ 1.3) (168 mg, 0.0168 mmol) and KOH (9.4 mg, 0.168 mmol) were added to high pressure vial. The vial was sealed with a septum and degassed with nitrogen, before anhydrous chlorobenzene and DMSO (3:1= v:v, 8 ml in total) were added. The solution was heated at 120°C for 2 days. After reaction, remove the solvent and dissolve the product with deionized water. The product was purified by dialysis in deionized water for 2 days (change the deionized water every 12 hours). Then dry the aqueous solution by heating and the product was bright yellow (73 mg, 79% yield)

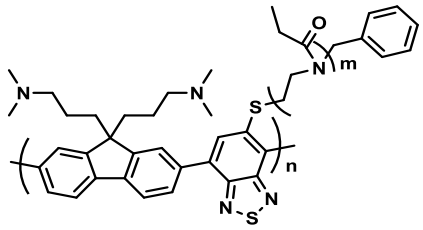
^{1}H-NMR (400 MHz, $CDCl_3$) shows dominant PEO signal

δ 3.59 (m, 4H), 2.44 (m, 2H), 1.13 (m, 3H).

^{19}F-NMR (400 MHz, $CDCl_3$) demonstrates no fluorine signal.

High purity was confirmed by DOSY-NMR (Appendix Figure 36, 37).

DNBT-SPEO



A mixture of **DNFBT** (13 mg, 0.027 mmol), poly(2-ethyl-2-oxazoline) (α-benzyl, ω-thiol terminated, average M_n 2,000 g/mol, PDI <1.3) (108 mg, 0.054 mmol) and K_2CO_3 (74.6 mg, 0.54 mmol) were added to high pressure vial. The vial was sealed with a septum and degassed with nitrogen, before anhydrous chlorobenzene and DMSO (3:1= v:v, 10 ml in total) were added. The solution was heated at 120°C for 24 hours. After reaction, the resulting solution was precipitated into water. Collect the precipitation and dry the precipitation to give pure **DNBT-SPEO** (52 mg, 78% yield).

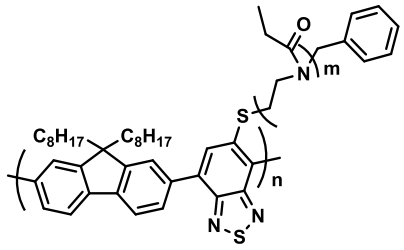
^{1}H-NMR (400 MHz, $CDCl_3$) shows dominant SPEO signal.

δ 3.57 (m, 4H), 2.42 (m, 2H), 1.13 (m, 3H).

^{19}F-NMR (400 MHz, $CDCl_3$) demonstrates no fluorine signal.

High purity was confirmed by DOSY-NMR (Appendix Figure 30, 31).

F8BT-SPEO



A mixture of **F8FBT** (6.2 mg, 0.011 mmol), poly(2-ethyl-2-oxazoline)(α-benzyl, ω-thiol terminated, average M_n= 2,000 g/mol, PDI <1.3) (44 mg, 0.022 mmol) and K_2CO_3 (30.4 mg, 0.22 mmol) were added to high pressure vial. The vial was sealed with a septum and degassed with nitrogen, before anhydrous chlorobenzene and DMSO (3:1= v:v, 8 ml in total) were added. The solution was heated at 120°C for 24 hours. After reaction, the resulting solution was precipitated into water. Collect the precipitation and dry the precipitation to give pure **F8BT-SPEO** (19 mg, 65% yield).

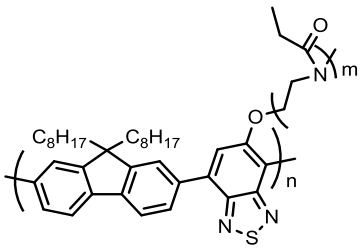
^{1}H-NMR (400 MHz, $CDCl_3$) shows dominant SPEO signal

δ 3.56 (m, 4H), 2.44 (m, 2H), 1.16 (m, 3H).

^{19}F-NMR (400 MHz, $CDCl_3$) demonstrates no fluorine signal.

High purity was confirmed by DOSY-NMR (Appendix Figure 24, 25).

F8BT-PEO



A mixture of **F8FBT** (7 mg, 0.013 mmol), poly(2-ethyl-2-oxazoline) (M_n= 10,000 g/mol, PDI≤1.3) (260 mg, 0.026 mmol) and KOH (14.6 mg, 0.26 mmol) were added to high pressure vial. The vial was sealed with a septum and degassed with nitrogen, before anhydrous chlorobenzene and DMSO (3:1=v:v, 10 ml in total) were added. The solution was heated at 120°C for 2 days. After reaction, remove the solvent and dissolve the products with deionized water. The product was purified by dialysis in deionized water for 2 days (change the deionized water every 12 hours) to remove excess PEO. Then dry the aqueous solution by heating and the product was yellow (103 mg, 75% yield).

^{1}H-NMR (400 MHz, $CDCl_3$) shows dominant PEO signal.

δ 3.52 (m, 4H), 2.38 (m, 2H), 1.08 (m, 3H).

^{19}F-NMR (400 MHz, $CDCl_3$) demonstrates no fluorine signal.

High purity was confirmed by DOSY-NMR (Appendix Figure 27, 28).

5. pH-responsive optical properties of water soluble conjugated polyelectrolytes

5.1. Introduction

Conjugated polyelectrolytes (CPEs) have been studied widely for applications in optoelectronic devices, chemo-/biosensors and biological imaging, *etc*. The chemical and physical properties of CPEs are based on the conjugated main backbone and ionic pendant groups. In Chapter 3, the applications of CPEs as interfacial layers in OPV and OLED have been investigated. Conjugated polyampholyte (CPA), another type of ionic conjugated polymer, has also been used for a variety of applications. CPA is a zwitterionic structure, i.e. containing cationic and anionic groups on a polymeric backbone simultaneously.[248,249] Figure 77 displays the structures of two CPA synthesized by post-polymerization in this chapter. CPA has been used as adsorptive materials for the removal of heavy metals [250,251] or applied as a stabilizer for catalysts.[252,253] More importantly, CPA can make a contribution to the understanding the solution behaviour of biological materials, such as proteins and can be used for applications in biotechnology and medicine.[254–256] The excellent water solubility with the useful optical and electrical properties (from the conjugated backbone) makes CPA as a sensor platform in aqueous media.

As CPA contains cationic and anionic groups, they can be mainly categorized into four classes based on their the pH response:[257] (1) polyampholytes have strong cationic (i.e., quaternary alkyl ammonium groups) and strong anionic groups (i.e., sulfonate groups). The strong anionic and cationic remain unchanged over the whole range of pH; (2) polyampholytes have weak anionic groups (e.g., carboxylate groups) which can be neutralized at low pH, combined with strong cationic groups which remain unchanged over the whole range of pH ; (3) polyampholytes have weak cationic groups (e.g., amine hydrohalides) and strong anionic groups and the weak cationic groups can be neutralized at high pH; (4) polyampholytes have both weak anionic and weak cationic groups and the two ionic groups are both responsive to pH. Clearly, the two CPA synthesized in this chapter with weak cationic groups and strong anionic groups at low pH belong to type 3. The amine

group can be protonated in acidic environment and neutralized when the pH increases to basic range.

Two CPA containing same conjugated backbone but with different densities of ionic groups have been synthesized. Poly(ethylene glycol) (PEG) is very hydrophilic and it has been widely integrated into biomaterials to suppress nonspecific adsorption of biological substances.[258,259] PEG and ionic groups were grafted to the hydrophobic conjugated backbone to improve the water solubility of CPA via post-polymerization. The synthesized conjugated polyampholytes consist of three parts, a hydrophobic conjugated backbone, a hydrophilic PEG (M_n= 10,000 g/mol) and an ionic sulfonic group. The intermolecular interactions of two CPA at different pH will be investigated in this chapter.

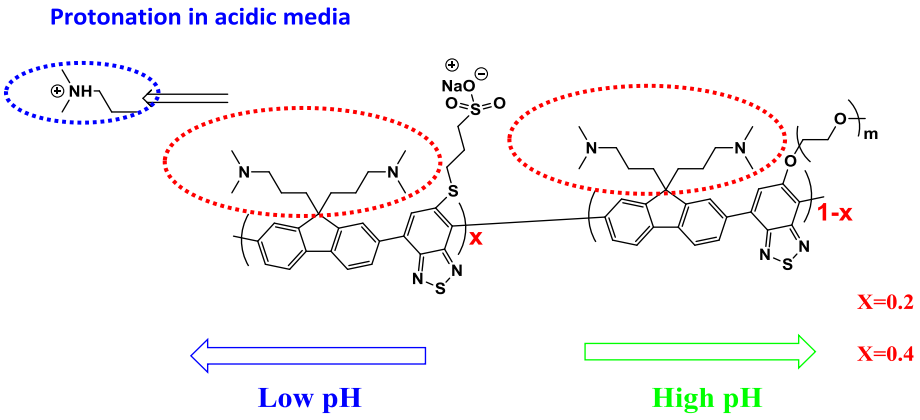


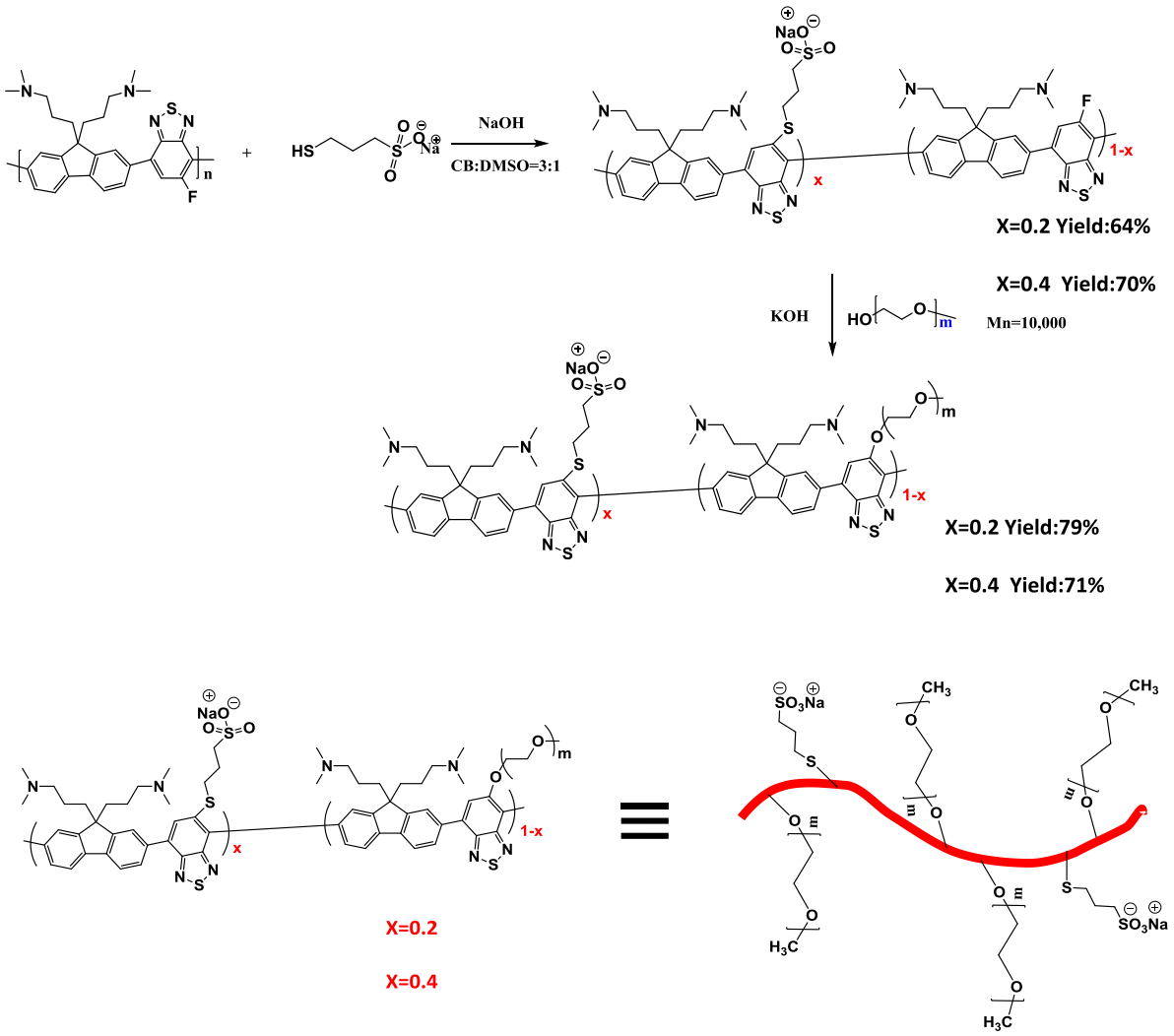
Figure 77. Molecular structure of conjugated polyampholytes.

5.2. Synthesis of polyampholytes

5.2.1 Synthesis routes

The synthetic route toward the **DNBT-20%-80%** and **DNBT-40%-60%** are shown in **Scheme 7**. First, **DNFBT** (M_n= 38,500 g/mol, M_w= 65,100 g/mol, PDI= 1.69) was reacted with 0.2 eq. and 0.4 eq. of sodium 3-mercapto-1-propanesulfonate under strong base NaOH in chlorobenzene and DMSO mixture to give **DNFBT-20%** and **DNFBT-40%** respectively. The reaction condition was same as fluoride substitution in Chapter 3. Then **DNFBT-20%** and **DNFBT-40**% were reacted with PEG (M_n= 10,000 g/mol) to give water soluble **DNBT-20%-80%** and **DNBT-40%-60%** respectively. The ^{19}F-NMR was used to monitor this reaction. When ^{19}F-NMR demonstrated no fluorine signal, indicating the reaction was complete and

then the reaction solvent was removed by heating. The remaining **DNBT-20%-80%** and **DNBT-40%-60%** were dissolved in deionized water and purified by dialysis to remove excess PEG. All polymers were characterized by ^{1}H-NMR and ^{19}F-NMR.



Scheme 7: Synthetic route of two conjugated polyampholytes

5.2.2 X-ray photoelectron spectroscopy

The synthesized **DNFBT-20%** and **DNFBT-40%** were investigated by XPS. For **DNFBT-20%**, the XPS survey spectra shows the peaks with binding energy of 1071.2 eV, 688.2 eV, 532.0 eV, 400.2 eV, 285.6 eV and 166.3 eV. According to the binding energy, the **DNFBT-20%** shows the presence of C, N, O, F, S and Na. For **DNFBT-40%**, the XPS survey spectra shows the peaks with binding energy of 1071.2 eV, 688.3 eV, 532.0 eV, 400.3 eV, 285.6 eV and 166.3 eV. According to the binding energy, the **DNFBT-40%** shows the presence of C, N, O, F, S and

Na. Besides, the atomic percentage (number) calculated from chemical structure was consistent well with the XPS data. The atomic percentage of **DNFBT-20%** calculated from chemical structure was $C_{29.6}N_{4.0}Na_{0.2}O_{0.6}F_{0.8}S_{1.4}$ while the atomic percentage from XPS was $C_{29.8}N_{3.1}Na_{0.2}O_{1.7}F_{0.7}S_{1.1}$. And the atomic percentage of **DNFBT-40%** calculated from chemical structure was $C_{30.2}N_{4.0}Na_{0.4}O_{1.2}F_{0.6}S_{1.8}$ and the atomic percentage from XPS was $C_{29.9}N_{3.1}Na_{0.5}O_{2.7}F_{0.6}S_{1.4}$. Clearly, the **DNFBT-20%** and **DNFBT-40%** were confirmed by XPS in high purity. The atomic percentage data was summarized in **Table 11**. The XPS survey spectra for **DNFBT-20%** and **DNFBT-40%** are in Appendix Figure 40, 41. The high oxygen content is likely related to water contamination.

Table 11 Atomic percentage (number) measured by XPS

CPA	Chemical structures	XPS
DNFBT-20%	$C_{29.6}N_{4.0}Na_{0.2}O_{0.6}F_{0.8}S_{1.4}$	$C_{29.8}N_{3.1}Na_{0.2}O_{1.7}F_{0.7}S_{1.1}$
DNFBT-40%	$C_{30.2}N_{4.0}Na_{0.4}O_{1.2}F_{0.6}S_{1.8}$	$C_{29.9}N_{3.1}Na_{0.5}O_{2.7}F_{0.6}S_{1.4}$

5.2.3 Fourier-transform infrared spectroscopy

Apart from high temperature (373 K) ^{1}H-NMR and XPS, the **DNFBT-20%** and **DNFBT-40%** were investigated by FTIR (Figure 78). The functional group region for C=C (aromatic ring) and S=O (sulfonate) are 1650-1600 cm^{-1} and 1195-1168 cm^{-1} respectively. As **DNFBT-20%** changes to **DNFBT-40%**, the ionic density increases in the repeat unit of $–S\text{-}CH_2\text{-}CH_2\text{-}CH_2\text{-}SO_3^-Na^+$. The enhanced ionic density was directly confirmed by comparing the intensity of the S=O stretching peak relative to the aromatic (C=C) stretching peak in the IR spectra.

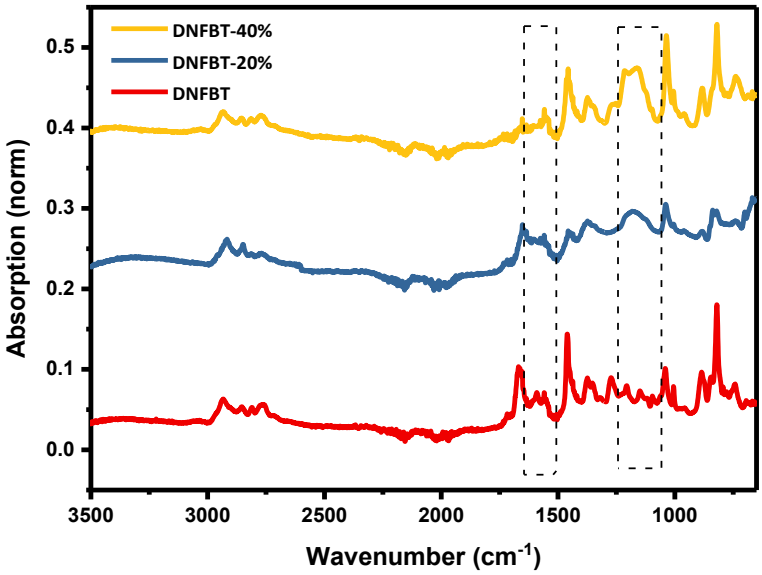


Figure 78 FTIR spectra of polymer **DNFBT**, **DNFBT-20%** and **DNFBT-40%**

5.2.4 UV-Vis absorption analysis

Also, the **DNFBT-20%** and **DNFBT-40%** were investigated by the absorption spectra (Figure 79). Both polymers demonstrated two absorption bands, a high energy band corresponding to the π-π* transition and a low energy band corresponding to ICT. After the fluoride partly substituted by side chains, the intensity of low energy band was reduced. The intensity reduction in the ICT was the same as discussed in Chapter 2 (see 2.3.1). Noticeably, the more fluoride substituted, the more intensity reduction in ICT. Compared with **DNFBT-20%**, a more intensity reduction was found in **DNFBT-40%**, indicating more fluoride substituted.

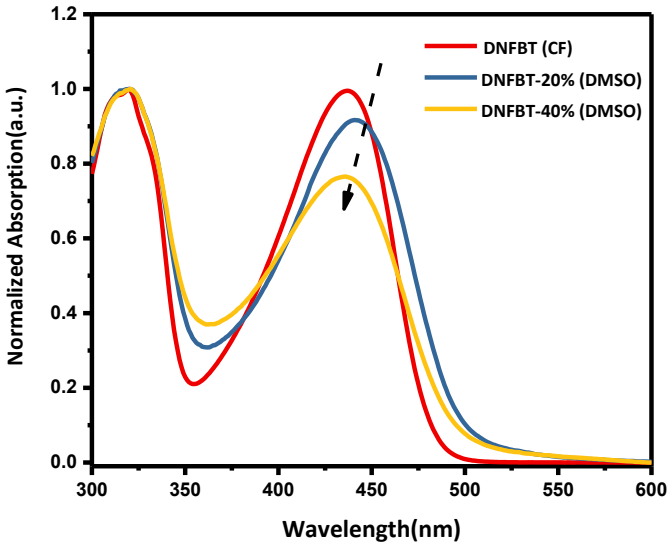


Figure 79 UV-Vis absorption spectra of **DNFBT**, **DNFBT-20%** and **DNFBT-40%**

5.2.5 NMR analysis

DNFBT-20% and **DNFBT-40%** have an identical π-conjugated backbone, but a different number of ionic densities. The enhanced ionic density was directly confirmed by integrating the signal intensity for $–S\text{-}CH_2\text{-}CH_2\text{-}CH_2\text{-}SO_3^-Na^+$ in the ^{1}H-NMR at high temperature (373 K). For **DNFBT-20%**, as only 20% of the fluoride was substituted by ionic thiol group, therefore the proton integration of each methylene from $–S\text{-}CH_2\text{-}CH_2\text{-}CH_2\text{-}SO_3^-Na^+$ should be just 0.4 (20% × 2 = 0.4). From the high temperature ^{1}H-NMR (Appendix Figure 42), each the methylene integration was around 0.4. The **DNFBT-40%** was confirmed by the each methylene integration of 0.8 (40% × 2 = 0.8) in ^{1}H-NMR (Appendix Figure 43).

In addition, the two CPAs were confirmed by DOSY-NMR, ^{1}H-NMR and ^{19}F-NMR. Take **DNBT-40%-60%** for example. The ^{19}F-NMR shows no fluorine signal which indicated the fluoride was fully substituted. Besides, the protons from the side chain PEG were dominant in ^{1}H-NMR and the signal of the protons from conjugated backbone and ionic thioalkyl group were very weak (Appendix Figure 49). As the PEG has very high molecular weight (M_n= 10,000 g/mol, PDI≤1.2), indicating the proton signal is tremendously more intensive than DNBT's proton signal. That is the reason that the ^{1}H-NMR shows dominant PEG signal. The DOSY NMR of **DNFBT-40%** and PEO mixtures was investigated. There were three parallel signal lines from Appendix Figure 47, and the first signal line was deuterated solvent

(d-DMSO). The second and third signal lines belonged to PEG and **DNFBT-40%** respectively. Besides, the **DNBT-40%-60%** alone was investigated in DOSY-NMR (Appendix Figure 48). Clearly, there was only one signal line which demonstrated the high purity of **DNBT-40% -60%**.

5.3 Solubility

After the ionic sulfonic groups and hydrophilic PEG were grafted to the hydrophobic conjugated backbone, the solubility of **DNBT-20%-80%** and **DNBT-40%-60%** (both 2 mg/ml) was changed as expected. They were both able to dissolve in water and Figure 80 demonstrated the excellent solubility in water. Besides, the two conjugated polyampholytes are also soluble in other polar solvents, like methanol and DMSO. As CPAs are synthetic analogues for proteins, the excellent solubility in aqueous solution can make a contribution to understand the aqueous solution behavior of biological molecules.

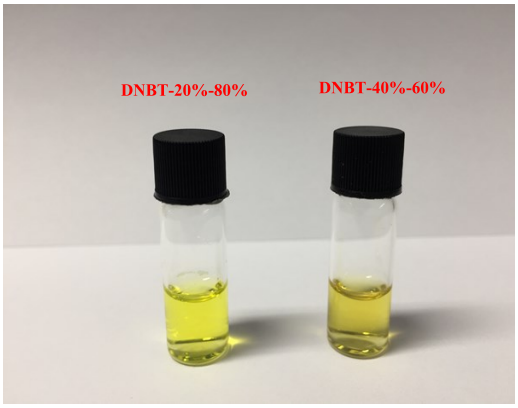


Figure 80 Solubility of two CPAs in aqueous solution

5.4. Optical properties of CPAs

5.4.1 UV-Vis absorption and photoluminescence spectra

Figure 81 presents the UV-Vis absorption and photoluminescence (PL) spectra (0.1 mg/ml) of two CPAs in water and dichloromethane (DCM). The data of optical properties are summarized in **Table 12**. It is clear from the absorption spectra that the two CPAs

demonstrated different absorption shapes which was due to different PEG and ionic sulfonic groups composition ratios. As demonstrated in Figure 81, the two CPAs both have two main absorption bands, a high energy band corresponding to the π-π* transition and a low energy band corresponding to ICT.

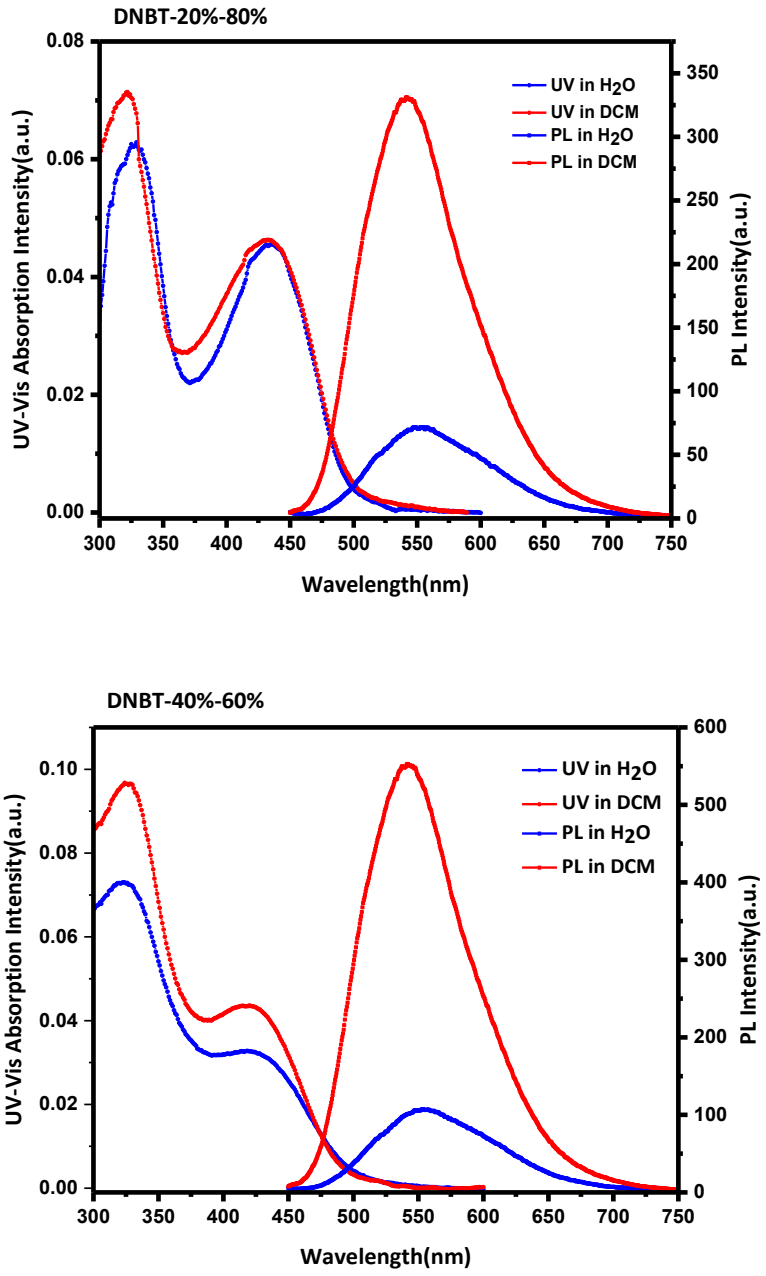


Figure 81: UV-Vis absorption and PL spectra of two CPAs in H_2O and DCM solution (0.1 mg/ml)

For **DNBT-20%-80%**, it has a high energy absorption band peak at 329 nm and a low energy absorption band peak at 435 nm in water. The **DNBT-40%-60%** has two absorption peaks at

323 and 418 nm in water. Clearly, the two absorption peaks of **DNBT-40%-60%** are both slight blue shift compared with **DNBT-20%-80%** in water. The same blue shift was also found in DCM solution. The difference in the absorption between the two polymers can be related to the different percentages of thioalkyl and alkoxy group on the BT unit. Higher percentage of thiol group leads to a blue shift and a reduction in intensity of the ICT band. The blue shift corresponds to a widening in the optical band gap. As sulfur is a larger atom than oxygen, which will cause a more twisted backbone conformation, resulting in a reduced conjugation length and widening band gap[98]. It is the reason that higher percentage of thioalkyl groups leads to a blue shift. Since thioalkyl group are less donating than alkoxy group,[260,261] we believe the reduced ICT intensity is not the result of increased donation into the BT unit but instead due to a reduced conjugation length because of backbone twisting. It appears steric effects are the dominant factor in the reduced ICT intensity.

On the other hand, the PL maxima in water was 555 nm and 553 nm for **DNBT-20%-80%** and **DNBT-40%-60%** respectively**.** In DCM solution, the PL maxima was both slight blue-shift. The PL maxima in DCM was 541 nm and 542 nm for **DNBT-20%-80%** and **DNBT-40%-60%.** Noticeably, the concentration of two CPAs in DCM and water were both 0.1 mg/ml, but the PL intensity in DCM was much higher than the data in water. The difference is likely caused by the nature of the excited state which was more stabilized in polar solvent. As H_2O has higher polarity than DCM, the excited state is more stabilized in H_2O and more likely to be lower in energy[262] which was responsive for the longer wavelength emission in H_2O. The reduced emission intensity is most likely due to CPAs aggregation in H_2O. Because of the inherent amphiphilic structures of the CPA (hydrophobic backbones and hydrophilic side chains), they tend to self-assemble into supramolecular aggregates in aqueous solutions through π-π stacking between adjacent polymer chains.[263] Similar observations have been made in other CPAs.[264,265] For **DNBT-20%-80%**, there was a larger Stokes shift in H_2O (120 nm) than DCM (109 nm). The same trend was found in **DNBT-40%-60%**, a larger Stokes shift in H_2O (135 nm) than DCM (127 nm).

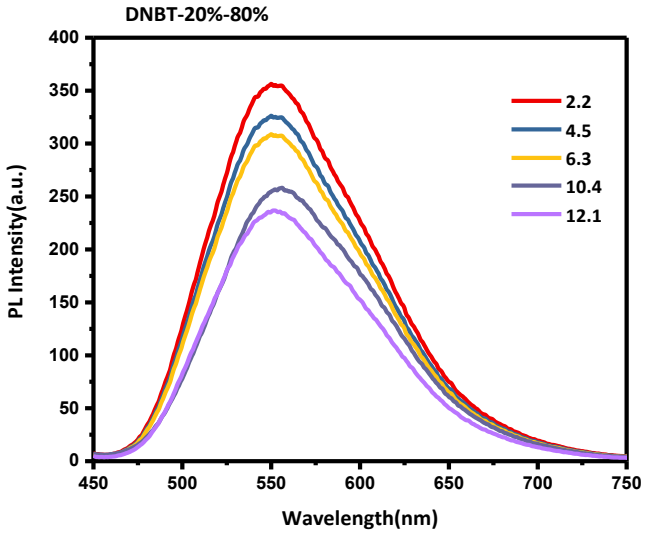
Table 12 Optical Properties of two CPAs in H_2O and DCM

CPA	$\lambda_{abs,\ max(H2O)}$	$\lambda_{em,\ max(H2O)}$	Δ λ (sol) nm	$\lambda_{abs,\ max(DCM)}$	$\lambda_{em,\ max(DCM)}$	Δ λ (sol) nm
DNBT-20%-80%	329[a],435[b]	555	120	322[a],432[b]	541	109
DNBT-40%-60%	323[a],418[b]	553	135	321[a],415[b]	542	127

[a] λ_{max} of high energy band.
[b] λ_{max} of low energy band.

5.4.2 Photoluminescence as function of pH

Figure 82 presents the photoluminescence of two CPAs in water as a function of pH. For the PL measurements, 10 mL of an aqueous solution of two CPAs (both 1 mg/ml) was prepared respectively and their pH was adjusted with the addition of HCl or NaOH solution (both 1 mol·dm^{-3}). We note that the overall amount of HCl or NaOH added was very small compared to the 10 mL, in the region of 0.1 ml, such that the changes in PL observed are not related in changes in concentration. Once a stable reading was obtained by pH meter, a 3 mL solution was transferred to a quartz cuvette for the PL measurement.



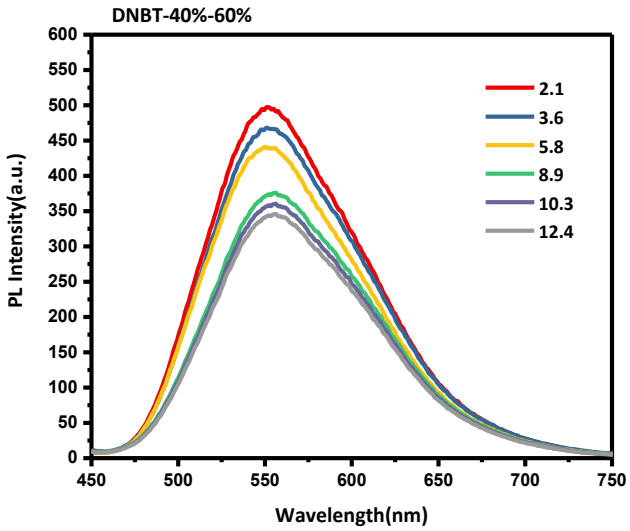


Figure 82 PL measurement of the CPAs in water (both 1 mg/ml) with changing the solution pH.

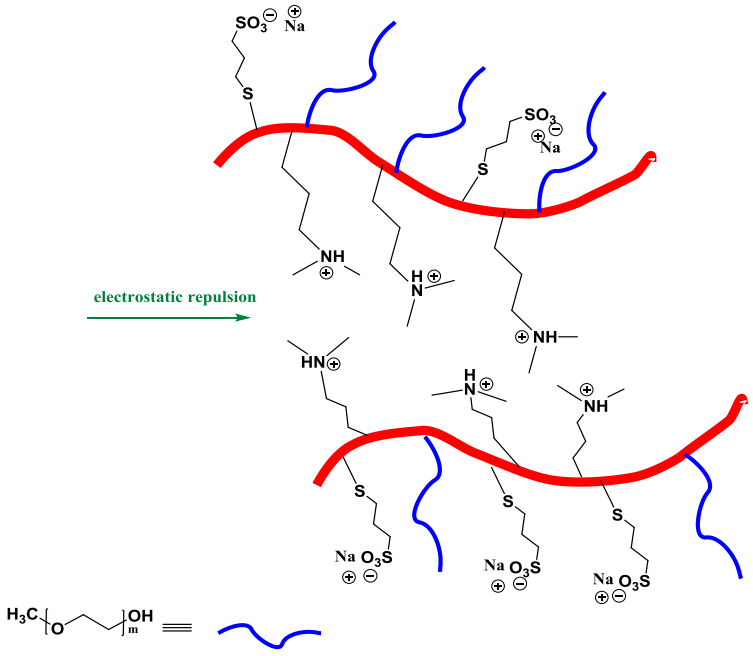


Figure 83 Electrostatic repulsion in acidic environment

Clearly, with increasing from pH 2 to pH 12, the two CPAs both demonstrated decreasing PL intensity gradually. The weak amine groups are supposed to form cations when the pH is in the acidic range, and the strong electrostatic repulsion between cationic amine groups effectively reduces CPE aggregation in water (Figure 83). Therefore it is believed the

modification to the pH conditions can change the optical properties. Clearly, this electrostatic repulsion becomes weaker gradually with increasing pH. As the cationic amines are weak cationic groups and they can be neutralized at high pH, thus the charge neutralization process leads to reduction of the electrostatic repulsion. Therefore, the polymer chains becomes more 'aggregated' in the basic environment, resulting in the emission intensity reduction.[266] Dynamic lighting scattering (DLS) measurements also support the aggregation in basic environment. (see 5.5)

5.4.3 Photoluminescence changes with concentrations

Figure 84 compares the PL spectra of **DNBT-20%-80%** and **DNBT-40%-60%** with increasing concentration (0.1, 0.3, 0.5, 0.7 and 1.0 mg/ml) at pH=2 and 12 respectively. Clearly, the PL intensity both increased at pH=2 and pH=12 gradually with concentration, indicating no significant aggregation with increasing polymer concentration. Also, the PL intensity at pH=2 is always higher than pH=12 when the aqueous solution is in same concentration.

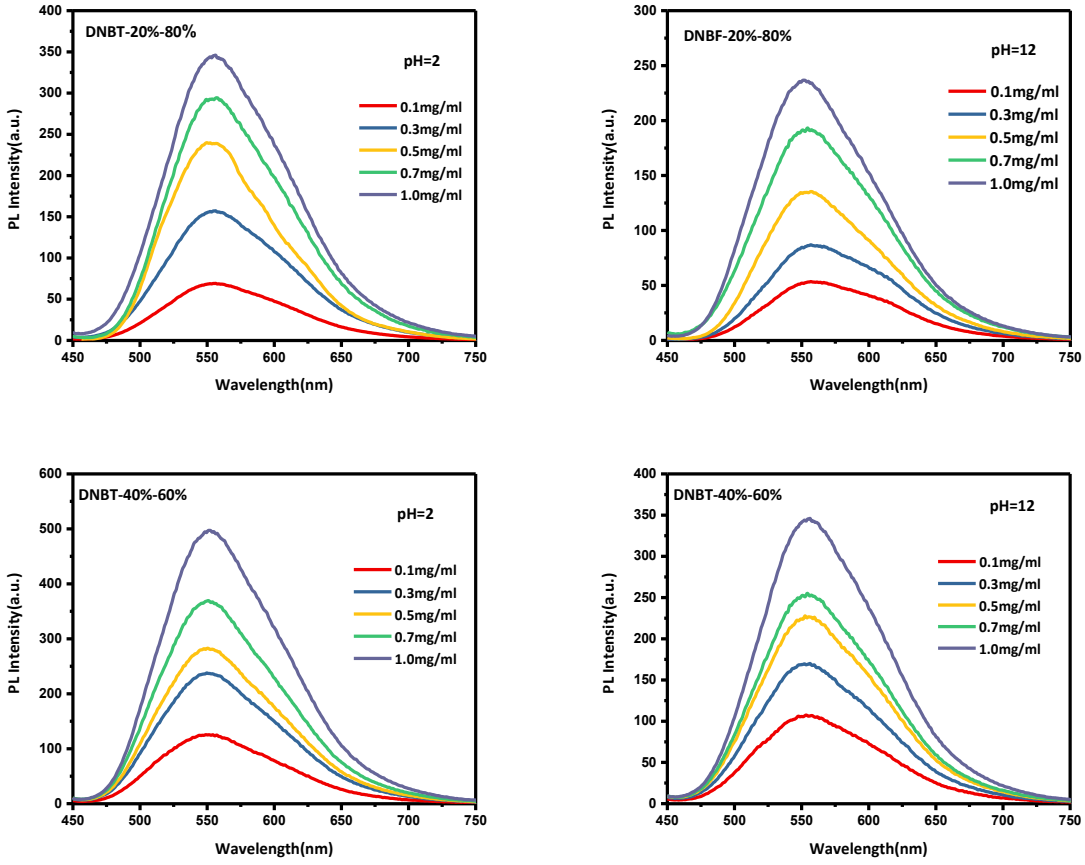


Figure 84 PL spectra of two CPAs at pH=2 and pH=12 with changing concentration in water.

5.5 Dynamic light scattering

Benefiting from the introduction of a hydrophilic PEG and ionic sulfonic groups, the obtained **DNBT-20%-80%** and **DNBT-40%-60%** both demonstrated excellent water solubility at room temperature. Since the hydrophobic conjugated backbone is insoluble in water, while the side chains are highly hydrophilic, the CPA should self-assemble in aqueous solution.[263] The assembly behaviors in water were investigated by DLS. Figure 85 demonstrated the hydrodynamic size distribution of **DNBT-20%-80%** and **DNBT-40%-60%** assemblies in water at with concentration of 1 mg/ml at pH 2 and pH 12 respectively.

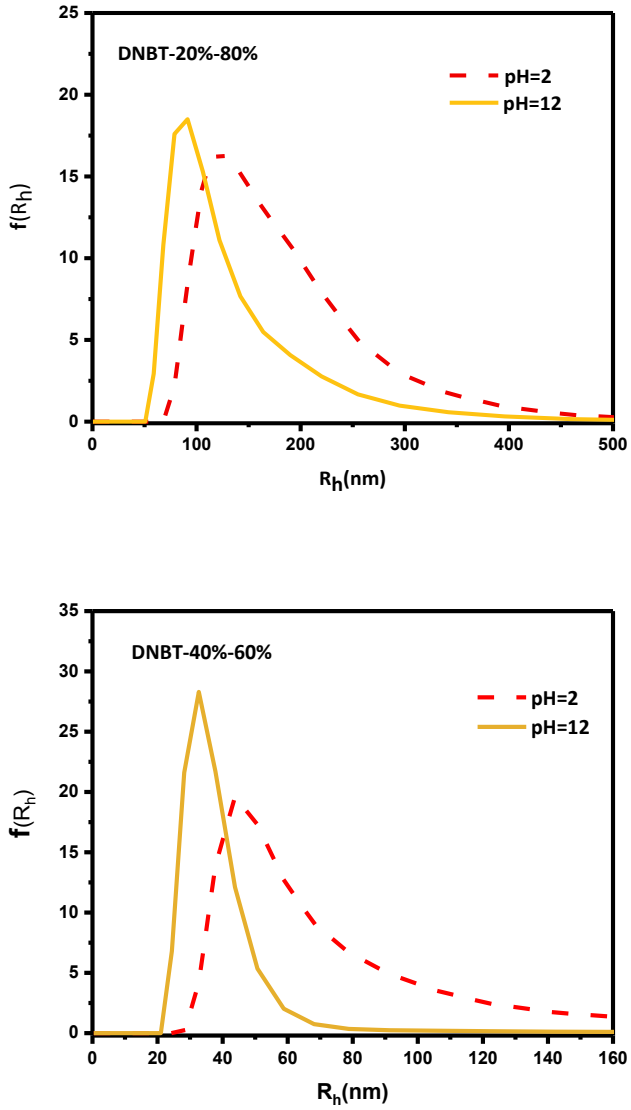


Figure 85 Typical hydrodynamic radius distributions, $f(R_h)$, obtained at various pH obtained for the aqueous solutions of two CPAs at 25 ^{o}C (concentration was 1 mg/ml).

Clearly, the **DNBT-20%-80%** demonstrated a number-average hydrodynamic radius, R_h, of approximately 122 nm and 91 nm for pH=2 and pH=12, respectively. The **DNBT-40%-60%** demonstrated a number-average hydrodynamic radius, R_h, of approximately 44 nm and 33 nm for pH2 and pH 12, respectively. The hydrodynamic radius of **DNBT-20%-80%** is larger than **DNBT-40%-60%.** This is due to **DNBT-20%-80%** contains more long side chain PEG than **DNBT-40%-60%**. Noticeably, hydrodynamic radius at pH=2 is larger than pH=12 for both **DNBT-20%-80%** and **DNBT-40%-60%.** This is likely due to the electrostatic repulsion between cationic amine groups at pH 2, which has been discussed in 5.4.2. This electrostatic repulsion decreases gradually when amine groups deprotonated at pH 12.

5.6. Conclusions

Water-soluble **DNBT-20%-80%** and **DNBT-40%-60%** were synthesized via post-polymerization with both cationic amine groups and negative sulfonic groups at acidic environment. The photoluminescence intensity in water were influenced by pH. The photoluminescence intensity increases with acidity of aqueous solution increases. Under acidic condition, there was strong electrostatic repulsion between cationic amine groups. Also, the process was reversible when cationic amine groups were deprotonated at high pH. This study provides insight into how the electrostatic interaction and resulting charge-mediated aggregation can be controlled using CPA structures. Also, the electrostatic interaction at different pH can be extended further to the design of new optical platforms for bio-imaging.

5.7 Experimental methods

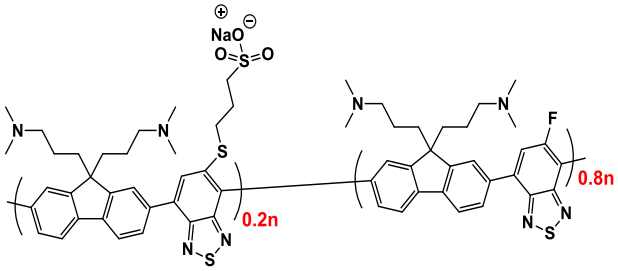
5.7.1 Laser light scattering

Dynamic light scattering (DLS) were performed using a ZetaSizer Nano ZS (Malvern). Nanoparticles tracking analysis (NTA) was acquired on a Malvern Instruments NS3000. Solutions were diluted 100× with water before injection. The capture settings of the NTA were kept consistent for all samples at a screen gain of 1 and a camera level of 11 and the

process settings were kept consistent at a screen gain of 11 and a detection threshold of 5. All data were averaged over three measurements.

5.7.2 Synthesis

DNFBT-20%

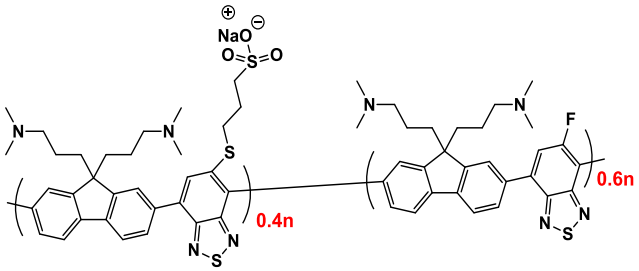


A mixture of **DNFBT** (110 mg, 0.226 mmol), sodium 3-mercapto-1-propanesulfonate (8.06 mg, 0.0452 mmol) and NaOH (120 mg, 3 mmol) were added to high pressure microwave vial. The vial was sealed with a septum and degassed with argon before anhydrous chlorobenzene and DMSO (3:1, v:v, 8 ml total) was added. The solution was heated at 120°C for 24 hours. After the solution was cooled to room temperature, it was precipitated into water and collect the polymer. The resulting polymer was recovered by filtration, washed with acetone for 24 hours by Soxhlet. Finally, dried overnight in vacuum to give **DNFBT-20%** (75 mg, Yield 64%).

^{1}H-NMR (400 MHz, d-DMSO, 373K) δ 8.25-7.90 (m, 7H), 3.55 – 3.53 (m, 0.4 H), 2.73 – 2.69 (m, 0.4 H), 2.09 – 2.05 (m, 0.4 H), 2.03 – 1.96 (m, 8 H), 1.32 – 1.24 (m, 12 H), 0.88 – 0.85 (m, 4 H)

^{19}F-NMR (400 MHz, $CDCl_3$) δ -114.3 ppm

DNFBT-40%

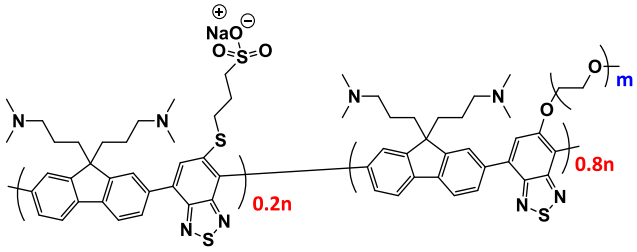


A mixture of **DNFBT** (122.3 mg, 0.251 mmol), sodium 3-mercapto-1-propanesulfonate (17.91 mg, 0.1005 mmol) and NaOH (101 mg, 2.51 mmol) were added to high pressure microwave vial. The vial was sealed with a septum and degassed with argon before anhydrous chlorobenzene and DMSO (3:1, v:v, 10 ml total) was added. The solution was heated at 120°C for 24 hours. After the solution was cooled to room temperature, it was precipitated into water and collect the polymer. The resulting polymer was recovered by filtration, washed with acetone for 24 hours by Soxhlet extraction. Finally, dried overnight in vacuum to give **DNFBT-40%** (96.6 mg, Yield 70%).

^{1}H-NMR (400 MHz, d-DMSO, 373K) δ 8.24-7.92 (m, 7H), 3.55 – 3.53 (m, 0.8 H), 2.74 – 2.69 (m, 0.8 H), 2.07 – 2.04 (m, 0.8 H), 2.05 – 1.96 (m, 8 H), 1.35 – 1.25 (m, 12 H), 0.88 – 0.85 (m, 4 H)

^{19}F-NMR (400 MHz, $CDCl_3$) δ -114.4 ppm

DNBT-20%-80%



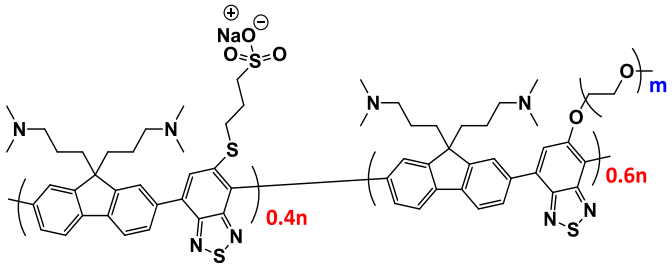
A mixture of **DNFBT-20%** (10.8 mg, 0.021 mmol), PEG (340 mg, 0.034 mmol) (M_n= 10,000 g/mol, PDI ≤1.1) and KOH (13.6 mg, 0.34 mmol) were added to high pressure microwave vial. The vial was sealed with a septum and degassed with argon before anhydrous chlorobenzene and DMSO (3:1, v:v, 12ml total) were added. The solution was heated at 120°C for 2 days. After reaction, removed the solvent and dissolved the polymer with deionized water. The polymer was purified by dialysis in deionized water for 2 days (change the deionized water every 12 hours). Then dry the aqueous solution to give **DNBT-20%-80%** (141 mg, 79% yield).

^{1}H-MMR (400 MHz, $CDCl_3$) shows dominant PEG signal δ 3.63 (m, 4H).

^{19}F-NMR (400 MHz, $CDCl_3$) demonstrates no fluorine signal.

High purity was confirmed by DOSY-NMR (Appendix Figure 44, 45).

DNBT-40%-60%



A mixture of **DNFBT-40%** (11.0 mg, 0.02 mmol), PEG (240 mg, 0.024 mmol) (M_n= 10,000 g/mol, PDI ≤1.1) and KOH (9.6 mg, 0.24 mmol) were added to high pressure microwave vial. The vial was sealed with a septum and degassed with argon before anhydrous chlorobenzene and DMSO (3:1, v:v, 10 ml total) were added. The solution was heated at 120°C for 2 days. After reaction, removed the solvent and dissolved the polymer with deionized water. The polymer was purified by dialysis in deionized water for 2 days (change the deionized water every 12 hours). Then dry the aqueous solution to give **DNBT-40%-60%** (93 mg, 71% yield).

^{1}H-MMR (400 MHz, $CDCl_3$) shows dominant PEG signal δ 3.64 (m, 4H).

^{19}F-NMR (400 MHz, $CDCl_3$) demonstrates no fluorine signal.

High purity was confirmed by DOSY-NMR (Appendix Figure 47, 48).

6. Conclusion

From Chapter 2 to Chapter 5, a series of functional polymers have been synthesized via post-polymerization and their physical and chemical properties were investigated in this thesis. Some of the polymers synthesized in this thesis are shown in Figure 86. Post-polymerization modification is an attractive approach for the synthesis of functional polymers that overcomes problems related to the limited functional-group tolerance of a number of polymerization strategies. The approach of grafting functional groups on the fluorinated conjugated backbone via post-polymerization in this thesis was successful. This approach gives us an effective and powerful technique to design and synthesize functional polymers. As the demand increases for functional polymers with precise properties and chemical functionalities, we believe post-polymerization modification will continue to grow in both breadth and scope.

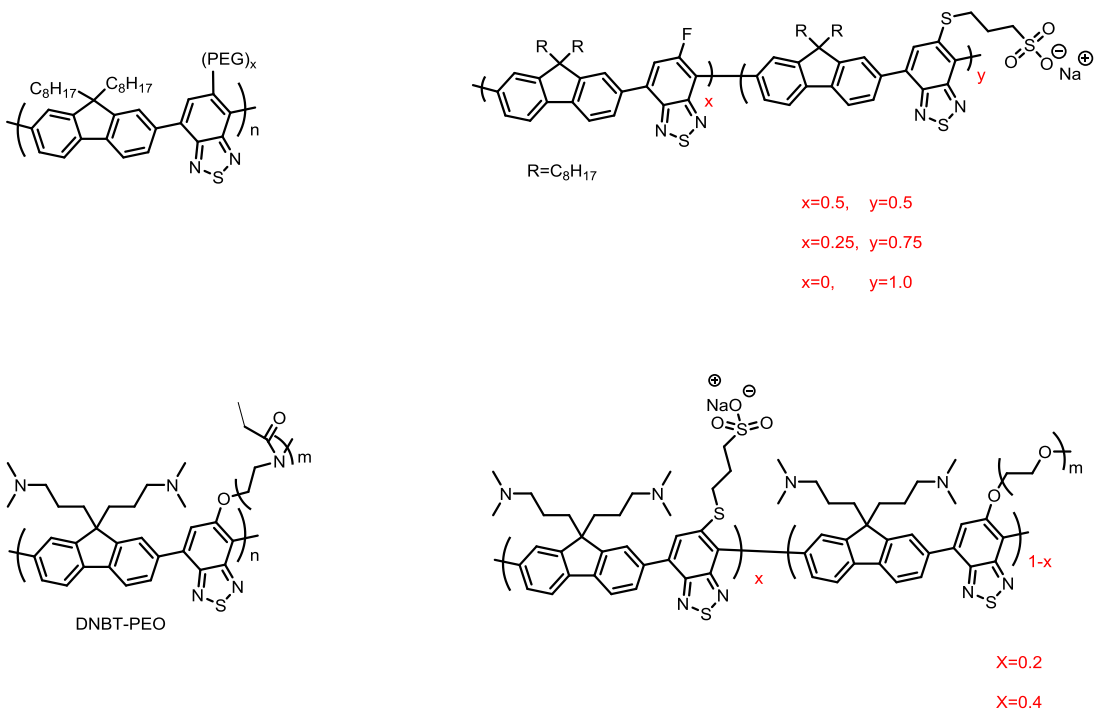


Figure 86 Main polymers synthesized via post-polymerization in this thesis

While advances have been made in designing functional polymers with post-polymerization modification, some challenges still exist in this thesis. For CPEs in Chapter 3, graft copolymers in Chapter 4 and CPAs in Chapter 5, we did not have the molecular weights by

GPC in our lab. The solvent used in the CPC was chlorobenzene which could not dissolve the CPEs. However, the GPC gave a very low molecular weight of the graft copolymers. For example, the apparent M_n was only 12,300 g/mol for **DNBT-PEO-10K** by GPC, despite the M_n of starting **DNFBT** was 38,700 g/mol. This may be due to the adsorption of **DNBT-PEO-10K** onto the surface of GPC stationary phase, which limits the reproducibility and separation efficiency. However, when the GPC solvent changed to THF, the apparent molecular weight was still low (M_n= 14,700 g/mol) for **DNBT-PEO-10K**. For the CPEs, graft copolymers and CPAs, DMF and H_2O are good solvents according to the literature.[267–269] The next step will be to use these solvents in GPC to detect the molecular weight.

The principles of post-polymerization modification include reaction efficiency, selectivity and amenability to ambient conditions. These are many of the same principles of ‘‘green’’ chemistry, and therefore post-polymerization modification take an important role in the field focused on cleaner and more efficient process design. I believe post-polymerization modification can be utilized to further develop sophisticated materials while minimizing the cost and environmental impact of production.

7. References

1 C. Zhu, L. Liu, Q. Yang, F. Lv and S. Wang, *Chem. Rev.*, 2012, **112**, 4687–4735.

2 L. Dou, Y. Liu, Z. Hong, G. Li and Y. Yang, *Chem. Rev.*, 2015, **115**, 12633–12665.

3 J. R. Pouliot, F. Grenier, J. T. Blaskovits, S. Beaupré and M. Leclerc, *Chem. Rev.*, 2016, **116**, 14225–14274.

4 U. H. F. Bunz, *Chem. Rev.*, 2000, **100**, 1605–1644.

5 S. W. Thomas, G. D. Joly and T. M. Swager, *Chem. Rev.*, 2007, **107**, 1339–1386.

6 X. Feng, L. Liu, S. Wang and D. Zhu, *Chem. Soc. Rev.*, 2010, **39**, 2411–2419.

7 A. Reale, L. LaNotte, L. Salamandra, G. Polino, G. Susanna, T. M. Brown, F. Brunetti and A. DiCarlo, *Energy Technol.*, 2015, **3**, 385–406.

8 Y.-J. Cheng, S.-H. Yang and C.-S. Hsu, *Chem. Rev.*, 2009, **109**, 5868–5923.

9 K. L. Chan, R. E. Martin, A. B. Holmes, A. C. Grimsdale and P. G. Jokisz, *ChemInform*, 2009, **40**, 897–1091.

10 D. Tyler McQuade, A. E. Pullen and T. M. Swager, *Chem. Rev.*, 2000, **100**, 2537–2574.

11 H. S. Majumdar, A. Bandyopadhyay, A. Bolognesi and A. J. Pal, *J. Appl. Phys.*, 2002, **91**, 2433–2437.

12 H. J. Yen, C. Shan, L. Wang, P. Xu, M. Zhou and H. L. Wang, *Polymers (Basel).*, 2017, **9**.

13 J. Roncali, *Macromol. Rapid Commun.*, 2007, **28**, 1761–1775.

14 A. Facchetti, *Chem. Mater.*, 2011, **23**, 733–758.

15 H. Zhou, L. Yang and W. You, *Macromolecules*, 2012, **45**, 607–632.

16 T. Lei, J. Y. Wang and J. Pei, *Chem. Mater.*, 2014, **26**, 594–603.

17 J. Mei and Z. Bao, *Chem. Mater.*, 2014, **26**, 604–615.

18 J. Mei, D. H. Kim, A. L. Ayzner, M. F. Toney and Z. Bao, *J. Am. Chem. Soc.*, 2011, **133**, 20130–20133.

19 J. D. Ferry, *J. Am. Chem. Soc.*, 1950, **72**, 3746–3752.

20 L. J. Fetters, D. J. Lohse, D. Richter, T. A. Witten and A. Zirkel, *Macromolecules*, 1994, **27**, 4639–4647.

21 W. E. Mahmoud, *Polym. Adv. Technol.*, 2011, **22**, 2550–2555.

22 M. P. Aplan and E. D. Gomez, *Ind. Eng. Chem. Res.*, 2017, **56**, 7888–7901.

23 T. Yokozawa and A. Yokoyama, *Chem. Rev.*, 2009, **109**, 5595–5619.

24 W. Ma, J. Y. Kim, K. Lee and A. J. Heeger, *Macromol. Rapid Commun.*, 2007, **28**, 1776–1780.

25 Y. Huang, W. Wen, S. Mukherjee, H. Ade, E. J. Kramer and G. C. Bazan, *Adv. Mater.*, 2014, **26**, 4168–4172.

26 T. Yokozawa and Y. Ohta, *Chem. Rev.*, 2016, **116**, 1950–1958.

27 P. Devendar, R. Y. Qu, W. M. Kang, B. He and G. F. Yang, *J. Agric. Food Chem.*, 2018, **66**, 8914–8934.

28 C. J. Mathews, P. J. Smith and T. Welton, *Chem. Commun.*, 2000, 1249–1250.

29 P. Espinet and A. M. Echavarren, *Angew. Chemie - Int. Ed.*, 2004, **43**, 4704–4734.

30 Staudinger, H. Rubber Chem. *Technol*. 1939, 12, 117–118.

31 G. E. Serniuk, F. W. Banes and M. W. Swaney, *J. Am. Chem. Soc.*, 1948, **70**, 1804–1808.

32 J. S. Siegel, Y. Tobe, P. Merino, S. J. Collier, S. K. Singh, E. Zysman-Colman, D. A. Alonso, C. Nájera, K. Abou-Hadeed, H.-J. Hansen, T. Nishinaga, S. Ito, N. Morita, H. Sano, J. Nishimura, M. Iyoda, D. A. Black, K. Fagnou, M. Abe, T. Yamamoto, L. Pu, T. Itoh, F. Aldabbagh, O. Gibbons, S. Toyota, T. Iwanaga, I. G. Stará, I. Starý, C.-S. Chang, Y.-T. Wu, W.-C. Lin, S. R. Waldvogel, N. Welschoff, T. Haino, H. Iwamoto, T. Shinmyozu, M. Shibahara, T. Takeda, S. Koo, T. Masuda, M. Shiotsuki, F. Sanda, F.

Aldabbagh and O. Gibbons, *Monocyclic Arenes, Quasiarenes, Annu.*, 2013, 1.

33 S. Perrier, P. Takolpuckdee and C. A. Mars, *Macromolecules*, 2005, **38**, 2033–2036.

34 Z. Zhang, W. Wang, H. Xia, J. Zhu, W. Zhang and X. Zhu, *Macromolecules*, 2009, **42**, 7360–7366.

35 K. A. Günay, P. Theato and H. A. Klok, *J. Polym. Sci. Part A Polym. Chem.*, 2013, **51**, 1–28.

36 S. Matsumura, A. R. Hlil, C. Lepiller, J. Gaudet, D. Guay, Z. Shi, S. Holdcroft and A. S. Hay, *J. Polym. Sci. Part A Polym. Chem.*, 2008, **46**, 7207–7224.

37 B. Wei, L. Ouyang, J. Liu and D. C. Martin, *J. Mater. Chem. B*, 2015, **3**, 5028–5034.

38 F. Biedermann, E. A. Appel, J. Del Barrio, T. Gruendling, C. Barner-Kowollik and O. A. Scherman, *Macromolecules*, 2011, **44**, 4828–4835.

39 P. Ferruti, A. Bettelli and A. Feré, *Polymer (Guildf).*, 1972, **13**, 462–464.

40 H. Gaballa, S. Lin, J. Shang, S. Meier and P. Theato, *Polym. Chem.*, 2018, **9**, 3355–3358.

41 Y. Chujo, K. Sada and T. Saegusa, *Macromolecules*, 1990, **23**, 2636–2641.

42 H. Ritter and R. Sperber, *Macromolecules*, 1994, **27**, 5919–5920.

43 I. Kosif, E. J. Park, R. Sanyal and A. Sanyal, *Macromolecules*, 2010, **43**, 4140–4148.

44 G. T. Zugates, D. G. Anderson, S. R. Little, I. E. B. Lawhorn and R. Langer, *J. Am. Chem. Soc.*, 2006, **128**, 12726–12734.

45 M. Friedman, J. F. Cavins and J. S. Wall, *J. Am. Chem. Soc.*, 1965, **87**, 3672–3682.

46 R. Wang, W. Chen, F. Meng, R. Cheng, C. Deng, J. Feijen and Z. Zhong, *Macromolecules*, 2011, **44**, 6009–6016.

47 W. H. Binder and R. Sachsenhofer, *Macromol. Rapid Commun.*, 2007, **28**, 15–54.

48 B. Parrish, R. B. Breitenkamp and T. Emrick, *J. Am. Chem. Soc.*, 2005, **127**, 7404–7410.

49 D. G. Barrett and M. N. Yousaf, *Biomacromolecules*, 2008, **9**, 2029–2035.

50 M. M. Stevens, Z. Fei, P. D. Howes, M. Heeney, J. Panidi, M. A. McLachlan, C. H. Burgess, C. S. Wood, A. V. Marsh, A. Creamer, R. Godin, T. D. Anthopoulos, I. Hamilton, S. Cong, T. Wu and A. Casey, *Nat. Commun.*, 2018, **9**.

51 P. L. Golas and K. Matyjaszewski, *Chem. Soc. Rev.*, 2010, **39**, 1338–1354.

52 P. Lundberg, C. J. Hawker, A. Hult and M. Malkoch, *Macromol. Rapid Commun.*, 2008, **29**, 998–1015.

53 C. Feng, Y. Li, D. Yang, J. Hu, X. Zhang and X. Huang, *Chem. Soc. Rev.*, 2011, **40**, 1282–1295.

54 M. K. Thakur, V. K. Thakur, R. K. Gupta and A. Pappu, *ACS Sustain. Chem. Eng.*, 2016, **4**, 1–17.

55 H. Kang, R. Liu and Y. Huang, *Polymer (Guildf).*, 2015, **70**, A1–A16.

56 C. Bhavsar, M. Momin, S. Gharat and A. Omri, *Expert Opin. Drug Deliv.*, 2017, **14**, 1189–1204.

57 H. Mittal, S. S. Ray and M. Okamoto, *Macromol. Mater. Eng.*, 2016, **301**, 496–522.

58 S. Cesana, A. Kurek, M. A. Baur, J. Auernheimer and O. Nuyken, *Macromol. Rapid Commun.*, 2007, **28**, 608–615.

59 C. Weber, C. Becer, R. Hoogenboom and U. Schubert, *Work*, 2009, 2965–2971.

60 Y. Zhang, Z. Shen, D. Yang, C. Feng, J. Hu, G. Lu and X. Huang, *Macromolecules*, 2010, **43**, 117–125.

61 G. Li, W. H. Chang and Y. Yang, *Nat. Rev. Mater.*, 2017, **2**, 1–13.

62 Y. Jiang and J. McNeill, *Chem. Rev.*, 2017, **117**, 838–859.

63 P. M. Beaujuge and J. R. Reynolds, *Chem. Rev.*, 2010, **110**, 268–320.

64 A. J. Hackett, J. Malmström and J. Travas-Sejdic, *Prog. Polym. Sci.*, 2017, **70**, 18–33.

65 C. Chiang, 2018.

66 S. Xiao, Q. Zhang and W. You, *Adv. Mater.*, 2017, **29**, 1–8.

67 J. Geng, C. Sun, J. Liu, L. De Liao, Y. Yuan, N. Thakor, J. Wang and B. Liu, *Small*, 2015, **11**, 1603–1610.

68 S. Savagatrup, A. S. Makaram, D. J. Burke and D. J. Lipomi, *Adv. Funct. Mater.*, 2014, **24**, 1169–1181.

69 J. Lai, B. Sunderland, J. Xue, S. Yan, W. Zhao, M. Folkard, B. D. Michael and Y. Wang, *Appl. Surf. Sci.*, 2006, **252**, 3375–3379.

70 M. Kobayashi, Y. Terayama, H. Yamaguchi, M. Terada, D. Murakami, K. Ishihara and A. Takahara, *Langmuir*, 2012, **28**, 7212–7222.

71 Y. Yu, C. K. Chen, W. C. Law, J. Mok, J. Zou, P. N. Prasad and C. Cheng, *Mol. Pharm.*, 2013, **10**, 867–874.

72 G. Gao, D. Lange, K. Hilpert, J. Kindrachuk, Y. Zou, J. T. J. Cheng, M. Kazemzadeh-Narbat, K. Yu, R. Wang, S. K. Straus, D. E. Brooks, B. H. Chew, R. E. W. Hancock and J. N. Kizhakkedathu, *Biomaterials*, 2011, **32**, 3899–3909.

73 Q. Zhao, X. Zhou, T. Cao, K. Y. Zhang, L. Yang, S. Liu, H. Liang, H. Yang, F. Li and W. Huang, *Chem. Sci.*, 2015, **6**, 1825–1831.

74 Y. H. Chan and P. J. Wu, *Part. Part. Syst. Charact.*, 2015, **32**, 11–28.

75 K. Faïd and M. Leclerc, *J. Am. Chem. Soc.*, 1998, **120**, 5274–5278.

76 J. Davis, A. Glidle, A. E. G. Cass, J. Zhang and J. M. Cooper, *J. Am. Chem. Soc.*, 1999, **121**, 4302–4303.

77 D. Wang, X. Gong, P. S. Heeger, F. Rininsland, G. C. Bazan and A. J. Heeger, *Proc. Natl. Acad. Sci.*, 2002, **99**, 49–53.

78 C. Fan, K. W. Plaxco and A. J. Heeger, *J. Am. Chem. Soc.*, 2002, **124**, 5642–5643.

79 P. Baek, L. Voorhaar, D. Barker and J. Travas-Sejdic, *Acc. Chem. Res.*, 2018, **51**, 1581–

1589.

80 M. Zuwei, C. Gao, J. Yuan, A. Ji, Y. Gong and J. Shen, *J. Appl. Polym. Sci.*, 2002, **85**, 2163–2171.

81 Y. H. Zhao, B. K. Zhu, L. Kong and Y. Y. Xu, *Langmuir*, 2007, **23**, 5779–5786.

82 F. Huang, H. Wu and Y. Cao, *Chem. Soc. Rev.*, 2010, **39**, 2500–2521.

83 H. Wu, F. Huang, Y. Mo, W. Yang, D. Wang, J. Peng and Y. Cao, *Adv. Mater.*, 2004, **16**, 1826–1830.

84 K. Zhang, C. Zhong, S. Liu, C. Mu, Z. Li, H. Yan, F. Huang and Y. Cao, *ACS Appl. Mater. Interfaces*, 2014, **6**, 10429–10435.

85 S. Sax, N. Rugen-Penkalla, A. Neuhold, S. Schuh, E. Zojer, E. J. W. List and K. Müllen, *Adv. Mater.*, 2010, **22**, 2087–2091.

86 R. Trattnig, L. Pevzner, M. Jäger, R. Schlesinger, M. V. Nardi, G. Ligorio, C. Christodoulou, N. Koch, M. Baumgarten, K. Müllen and E. J. W. List, *Adv. Funct. Mater.*, 2013, **23**, 4897–4905.

87 C. Ba, D. A. Ladner and J. Economy, *J. Memb. Sci.*, 2010, **347**, 250–259.

88 I. Banerjee, R. C. Pangule and R. S. Kane, *Adv. Mater.*, 2011, **23**, 690–718.

89 J. P. Bearinger, S. Terrettaz, R. Michel, N. Tirelli, H. Vogel, M. Textor and J. A. Hubbell, *Nat. Mater.*, 2003, **2**, 259–264.

90 V. A. Liu, W. E. Jastromb and S. N. Bhatia, *J. Biomed. Mater. Res.*, 2002, **60**, 126–134.

91 N. Xia, C. J. May, S. L. McArthur and D. G. Castner, *Langmuir*, 2002, **18**, 4090–4097.

92 K. L. Prime and G. M. Whitesides, *Science (80-.).*, 1991, **252**, 1164–1167.

93 Y. Bakkour, V. Darcos, S. Li and J. Coudane, *Polym. Chem.*, 2012, **3**, 2006–2010.

94 A. Jerschow and N. Müller, *Macromolecules*, 1998, **31**, 6573–6578.

95 R. Yang, R. Tian, Q. Hou, W. Yang and Y. Cao, 2003, 7453–7460.

96 H. Xing, M. Lu, L. Xian, J. Zhang, T. Yang, L. Yang and P. Ding, *Asian J. Pharm. Sci.*, 2017, **12**, 292–298.

97 K. Nakamura and R. Endo, *J. Appl. Polym. Sci.*, 1981, **26**, 2657–2664.

98 A. Casey, R. S. Ashraf, Z. Fei and M. Heeney, *Macromolecules*, 2014, **47**, 2279–2288.

99 Z. G. Zhang and Y. Li, *Sci. China Chem.*, 2015, **58**, 192–209.

100 H. Song, K. Wang, Z. Kuang, Y. S. Zhao, Q. Guo and A. Xia, *Phys. Chem. Chem. Phys.*, 2019, **21**, 3894–3902.

101 W. Zhang, C. Wang, G. Liu, J. Wang, Y. Chen and R. W. Li, *Chem. Commun.*, 2014, **50**, 11496–11499.

102 Q. D. Ling, F. C. Chang, Y. Song, C. X. Zhu, D. J. Liaw, D. S. H. Chan, E. T. Kang and K. G. Neoh, *J. Am. Chem. Soc.*, 2006, **128**, 8732–8733.

103 W. Zhong, J. Liang, S. Hu, X. F. Jiang, L. Ying, F. Huang, W. Yang and Y. Cao, *Macromolecules*, 2016, **49**, 5806–5816.

104 C. M. Cardona, W. Li, A. E. Kaifer, D. Stockdale and G. C. Bazan, *Adv. Mater.*, 2011, **23**, 2367–2371.

105 J. R. Harwell, T. K. Baikie, I. D. Baikie, J. L. Payne, C. Ni, J. T. S. Irvine, G. A. Turnbull and I. D. W. Samuel, *Phys. Chem. Chem. Phys.*, 2016, **18**, 19738–19745.

106 W. Zhong, J. Liang, S. Hu, X. F. Jiang, L. Ying, F. Huang, W. Yang and Y. Cao, *Macromolecules*, 2016, **49**, 5806–5816.

107 K. Pielichowski and K. Flejtuch, *Polym. Adv. Technol.*, 2002, **13**, 690–696.

108 G. Hurwitz, G. R. Guillen and E. M. V. Hoek, *J. Memb. Sci.*, 2010, **349**, 349–357.

109 P. Kim, D. H. Kim, B. Kim, S. K. Choi, S. H. Lee, A. Khademhosseini, R. Langer and K. Y. Suh, *Nanotechnology*, 2005, **16**, 2420–2426.

110 R. Yang, R. Tian, Q. Hou, W. Yang and Y. Cao, *Macromolecules*, 2003, **36**, 7453–7460.

111 W. Yang, F. Huang, Y. Cao, S. Hu, W. Zhong, J. Liang, X.-F. Jiang and L. Ying, *Macromolecules*, 2016, **49**, 5806–5816.

112 C. V. Hoven, A. Garcia, G. C. Bazan and T. Q. Nguyen, *Adv. Mater.*, 2008, **20**, 3793–3810.

113 H. Jiang, P. Taranekar, J. R. Reynolds and K. S. Schanze, *Angew. Chemie Int. Ed.*, 2009, **48**, 4300–4316.

114 A. Duarte, K. Y. Pu, B. Liu and G. C. Bazan, *Chem. Mater.*, 2011, **23**, 501–515.

115 J. W. Jo, J. W. Jung, S. Bae, M. J. Ko, H. Kim, W. H. Jo, A. K. Y. Jen and H. J. Son, *Adv. Mater. Interfaces*, 2016, **3**, 1–8.

116 Y. Shi, C. K. Mai, S. L. Fronk, Y. Chen and G. C. Bazan, *Macromolecules*, 2016, **49**, 6343–6349.

117 F. Huang, H. Wu, D. Wang, W. Yang and Y. Cao, *Chem. Mater.*, 2004, **16**, 708–716.

118 K. Landfester, S. Ghasimi, K. A. I. Zhang, Z. J. Wang, S. Prescher and J. Yuan, *Angew. Chemie Int. Ed.*, 2015, **54**, 14549–14553.

119 J. H. Seo, A. Gutacker, Y. Sun, H. Wu, F. Huang, Y. Cao, U. Scherf, A. J. Heeger and G. C. Bazan, *J. Am. Chem. Soc.*, 2011, **133**, 8416–8419.

120 A. J. Heeger, A. Garcia, T.-Q. Nguyen, G. C. Bazan, R. Yang and C. Hoven, *J. Am. Chem. Soc.*, 2007, **129**, 10976–10977.

121 A. Fallahi, M. Alahbakhshi, E. Mohajerani, F. Afshar Taromi, A. R. Mohebbi and M. Shahinpoor, *J. Phys. Chem. C*, 2015, **119**, 13144–13152.

122 S. Ohisa, T. Kato, T. Takahashi, M. Suzuki, Y. Hayashi, T. Koganezawa, C. R. McNeill, T. Chiba, Y. J. Pu and J. Kido, *ACS Appl. Mater. Interfaces*, 2018, **10**, 17318–17326.

123 S. Tekoglu, M. Petzoldt, S. Stolz, U. H. F. Bunz, U. Lemmer, M. Hamburger and G. Hernandez-Sosa, *ACS Appl. Mater. Interfaces*, 2016, **8**, 7320–7325.

124 H. Liu, X. Cheng, L. Huang, H. Xu, L. Chen, Y. Chen and A. Hu, *ACS Appl. Mater. Interfaces*, 2016, **9**, 1145–1153.

125 J. B. Park, M. Isik, H. J. Park, I. H. Jung, D. Mecerreyes and D. H. Hwang, *ACS Appl. Mater. Interfaces*, 2018, **10**, 4887–4894.

126 L. J. Richter, A. L. Briseno, E. Puodziukynaite, H. Lee, D. M. DeLongchamp, J. C. Stephenson, T. Emrick, D. A. Fischer and Y. Zhang, *J. Am. Chem. Soc.*, 2014, **137**, 540–549.

127 Y. Jin, G. C. Bazan, A. J. Heeger, J. Y. Kim and K. Lee, *Appl. Phys. Lett.*, 2008, **93**.

128 D. Vak, D.-Y. Kim, S.-H. Oh, S.-I. Na, B. Lim and J. Jo, *Adv. Funct. Mater.*, 2010, **20**, 1977–1983.

129 B. H. Lee, I. H. Jung, H. Y. Woo, H. K. Shim, G. Kim and K. Lee, *Adv. Funct. Mater.*, 2014, **24**, 1100–1108.

130 O. Inganäs, Q. Bao, Z. Ma, C. Musumeci, Z. Tang, F. N. Ajjan and W. Cai, *J. Mater. Chem. A*, 2016, **4**, 15670–15675.

131 S. Braun, W. R. Salaneck and M. Fahlman, *Adv. Mater.*, 2009, **21**, 1450–1472.

132 H. S. Ishii K Ito, E Seki, K, *Adv. Mater.*, 1999, **11**, +.

133 N. Zhou, A. Facchetti, R. P. Ortiz, J. W. Hennek, D. B. Tice, T. J. Marks, J. Smith, L. X. Chen, J. Strzalka, R. P. H. Chang, X. Guo, S. J. Lou, S. Li and J. T. L. Navarrete, *Nat. Photonics*, 2013, **7**, 825–833.

134 Y. Tan, Z. Liao, Y. Chen, L. Chen, Z. Yu, Y. Zhou, L. Hu, F. Wu and B. Huang, *Macromolecules*, 2018, **51**, 8197–8204.

135 J. Subbiah, V. D. Mitchell, N. K. C. Hui, D. J. Jones and W. W. H. Wong, 2017, 8551–8554.

136 Y. Seino, S. Inomata, H. Sasabe, Y. J. Pu and J. Kido, *Adv. Mater.*, 2016, **28**, 2638–2643.

137 J. Guo, X. L. Li, H. Nie, W. Luo, S. Gan, S. Hu, R. Hu, A. Qin, Z. Zhao, S. J. Su and B. Z. Tang, *Adv. Funct. Mater.*, 2017, **27**.

138 M. Suh, J. Bailey, S. W. Kim, K. Kim, D. J. Yun, Y. Jung, I. Hamilton, N. Chander, X. Wang, D. D. C. Bradley, D. Y. Jeon and J. S. Kim, *ACS Appl. Mater. Interfaces*, 2015, **7**, 26566–26571.

139 B. R. Lee, J. C. Yu, J. H. Park, S. Lee, C. K. Mai, B. Zhao, M. S. Wong, E. D. Jung, Y. S. Nam, S. Y. Park, D. Di Nuzzo, J. Y. Kim, S. D. Stranks, G. C. Bazan, H. Choi, M. H. Song and R. H. Friend, *ACS Nano*, 2018, **12**, 5826–5833.

140 F. Huang, L. Hou, H. Wu, X. Wang, H. Shen, W. Cao, W. Yang and Y. Cao, *J. Am. Chem. Soc.*, 2004, **126**, 9845–9853.

141 R. Yang, H. Wu, Y. Cao and G. C. Bazan, *J. Am. Chem. Soc.*, 2006, **128**, 14422–14423.

142 B. H. Lee, J. H. Lee, S. Y. Jeong, S. B. Park, S. H. Lee and K. Lee, *Adv. Energy Mater.*, 2015, **5**, 1–5.

143 X. Li, Y. C. Wang, L. Zhu, W. Zhang, H. Q. Wang and J. Fang, *ACS Appl. Mater. Interfaces*, 2017, **9**, 31357–31361.

144 G. Pace, R. H. Friend, J. Fang, F. Gao, G. Tu, B. H. Wallikewitz, C. Müller and W. T. S. Huck, *J. Am. Chem. Soc.*, 2010, **133**, 683–685.

145 A. Kumar, G. Pace, A. A. Bakulin, J. Fang, P. K. H. Ho, W. T. S. Huck, R. H. Friend and N. C. Greenham, *Energy Environ. Sci.*, 2013, **6**, 1589–1596.

146 C. Duan, L. Wang, K. Zhang, X. Guan and F. Huang, *Adv. Mater.*, 2011, **23**, 1665–1669.

147 X. Xu, B. Han, J. Chen, J. Peng, H. Wu and Y. Cao, *Macromolecules*, 2011, **44**, 4204–4212.

148 F. Huang, Y. Zhang, M. S. Liu and A. K. Y. Jen, *Adv. Funct. Mater.*, 2009, **19**, 2457–2466.

149 H. D. Burrows, M. J. Tapia, S. M. Fonseca, A. J. M. Valente, V. M. M. Lobo, L. L. G. Justino, S. Qiu, S. Pradhan, U. Scherf, N. Chattopadhyay, M. Knaapila and V. M. Garamus, *ACS Appl. Mater. Interfaces*, 2009, **1**, 864–874.

150 M. Redecker, D. D. C. Bradley, M. Inbasekaran, W. W. Wu and E. P. Woo, *Adv. Mater.*, 1999, **11**, 241–246.

151 H. D. Burrows, S. M. Fonseca, C. L. Silva, A. A. C. C. Pais, M. J. Tapia, S. Pradhan and U. Scherf, *Phys. Chem. Chem. Phys.*, 2008, **10**, 4420–4428.

152 R. A. Kee and M. Gauthier, *Polymer (Guildf).*, 2007, **49**, 2335–2346.

153 X. Liu, W. Wen and G. C. Bazan, *Adv. Mater.*, 2012, **24**, 4505–4510.

154 S. Fan, R. Liu, W. Shi, Y. Cao, W. Yang and F. Huang, *J. Mater. Chem.*, 2006, **16**, 2387.

155 W. Shi, X. Jiang, W. Zen, F. Huang, W. Yang, R. Liu and Y. Cao, *Macromol. Chem. Phys.*, 2009, **210**, 150–160.

156 M. B. Ramey, J. I. A. Hiller, M. F. Rubner, C. Tan, K. S. Schanze and J. R. Reynolds, *Macromolecules*, 2005, **38**, 234–243.

157 J. H. Seo, E. B. Namdas, A. Gutacker, A. J. Heeger and G. C. Bazan, *Adv. Funct. Mater.*, 2011, **21**, 3667–3672.

158 C. Duan, K. Zhang, X. Guan, C. Zhong, H. Xie, F. Huang, J. Chen, J. Peng and Y. Cao, *Chem. Sci.*, 2013, **4**, 1298–1307.

159 B. H. Lee, I. H. Jung, H. Y. Woo, H. K. Shim, G. Kim and K. Lee, *Adv. Funct. Mater.*, 2014, **24**, 1100–1108.

160 D. Regonini, A. Jaroenworaluck, R. Stevens and C. R. Bowen, 2010, 139–144.

161 S. Belviso, M. Amati, R. Rossano, A. Crispini and F. Lelj, *Dalt. Trans.*, 2015, **44**, 2191–2207.

162 C. Duan, L. Wang, K. Zhang, X. Guan and F. Huang, *Adv. Mater.*, 2011, **23**, 1665–1669.

163 A. Garcia, R. C. Bakus, P. Zalar, C. V. Hoven, J. Z. Brzezinski and T. Q. Nguyen, *J. Am. Chem. Soc.*, 2011, **133**, 2492–2498.

164 R. Yang, A. Garcia, D. Korystov, A. Mikhailovsky, G. C. Bazan and T. Q. Nguyen, *J. Am. Chem. Soc.*, 2006, **128**, 16532–16539.

165 X. Yu, H. Cheng, M. Zhang, Y. Zhao, L. Qu and G. Shi, *Nat. Rev. Mater.*, 2017, **2**, 1–14.

166 B. O. Okesola and D. K. Smith, *Chem. Soc. Rev.*, 2016, **45**, 4226–4251.

167 Y. Zhu, R. Batchelor, A. B. Lowe and P. J. Roth, *Macromolecules*, 2016, **49**, 672–680.

168 M. Urban, M. A. C. Stuart, W. T. S. Huck, F. Winnik, M. Müller, S. Zauscher, V. V. Tsukruk, G. B. Sukhorukov, I. Luzinov, C. Ober, J. Genzer, I. Szleifer, M. Stamm and S. Minko, *Nat. Mater.*, 2010, **9**, 101–113.

169 L. Lei, Q. Zhang, S. Shi and S. Zhu, *ACS Macro Lett.*, 2016, **5**, 828–832.

170 J. H. Kim, D. Yim and W. D. Jang, *Chem. Commun.*, 2016, **52**, 4152–4155.

171 M. Huang, K. Zhao, L. Wang, S. Lin, J. Li, J. Chen, C. Zhao and Z. Ge, *ACS Appl. Mater. Interfaces*, 2016, **8**, 11226–11236.

172 S. Ding, S. Cao, A. Zhu and G. Shi, *Anal. Chem.*, 2016, **88**, 12219–12226.

173 G. Wu, S. C. Chen, Q. Zhan and Y. Z. Wang, *Macromolecules*, 2011, **44**, 999–1008.

174 S. Qian, Y. Guo, Y. Hou, G. Han, W. Zhang and H. Khan, *Polymer (Guildf).*, 2019, **167**, 159–166.

175 S. Sanjuan, P. Perrin, N. Pantoustier and Y. Tran, *Langmuir*, 2007, **23**, 5769–5778.

176 G. W. De Groot, M. G. Santonicola, K. Sugihara, T. Zambelli, E. Reimhult, J. Vörös and G. J. Vancso, *ACS Appl. Mater. Interfaces*, 2013, **5**, 1400–1407.

177 S. Singh, K. Friedel, M. Himmerlich, Y. Lei, G. Schlingloff and A. Schober, *ACS Macro Lett.*, 2015, **4**, 1273–1277.

178 J. Anderski, L. Mahlert, J. Sun, W. Birnbaum, D. Mulac, S. Schreiber, F. Herrmann, D.

Kuckling and K. Langer, *Int. J. Pharm.*, 2019, **557**, 182–191.

179 L. Nucara, V. Piazza, F. Greco, V. Robbiano, V. Cappello, M. Gemmi, F. Cacialli and V. Mattoli, *ACS Appl. Mater. Interfaces*, 2017, **9**, 4818–4827.

180 X. Wang, S. Zhang, Y. Xu, X. Zhao and X. Guo, *Langmuir*, 2018, **34**, 8264–8273.

181 M. Mazurowski, M. Gallei, J. Li, H. Didzoleit, B. Stühn and M. Rehahn, *Macromolecules*, 2012, **45**, 8970–8981.

182 P. Wang, S. Chen, Z. Cao and G. Wang, *ACS Appl. Mater. Interfaces*, 2017, **9**, 29055–29062.

183 M. Dan, Y. Su, X. Xiao, S. Li and W. Zhang, *Macromolecules*, 2013, **46**, 3137–3146.

184 A. Gallardo, I. Quijada-Garrido, J. M. García-García, R. París and M. Liras, *Macromolecules*, 2011, **44**, 3739–3745.

185 M. T. Savoji, S. Strandman and X. X. Zhu, *Langmuir*, 2013, **29**, 6823–6832.

186 J. A. Barker and W. Fock, *Discuss. Faraday Soc.*, 1953, **15**, 188–195.

187 D. Schmaljohann, *Adv. Drug Deliv. Rev.*, 2006, **58**, 1655–1670.

188 J. E. Chung, M. Yokoyama and T. Okano, *J. Control. Release*, 2000, **65**, 93–103.

189 U. S. Schubert, S. Hoeppener, M. Sahn, C. Weber, T. Yildirim, P. Sungur and M. Dirauf, *Macromolecules*, 2016, **49**, 7257–7267.

190 S. K. Filippov, A. Bogomolova, L. Kaberov, N. Velychkivska, L. Starovoytova, Z. Cernochova, S. E. Rogers, W. M. Lau, V. V. Khutoryanskiy and M. T. Cook, *Langmuir*, 2016, **32**, 5314–5323.

191 X. Tan, X. Cao, X. Lu, K. Zhang, D. Wang, J. Zheng and F. Jia, *J. Am. Chem. Soc.*, 2016, **138**, 9097–9100.

192 A. K. S. Chandel, C. U. Kumar and S. K. Jewrajka, *ACS Appl. Mater. Interfaces*, 2016, **8**, 3182–3192.

193 K. Zhou, Y. Li, Y. Peng, X. Cui, J. Dai and M. Cui, *Anal. Chem.*, 2018, **90**, 8576–8582.

194 P. Tang, S. Di Cio, W. Wang and J. E. Gautrot, *Langmuir*, 2018, **34**, 10019–10027.

195 S. Jacobs, K. Kempe, U. S. Schubert, H. M. L. Lambermont-Thijs, R. Hoogenboom and M. M. W. M. Fijten, *Macromolecules*, 2010, **43**, 4098–4104.

196 O. Sedlacek, B. D. Monnery, S. K. Filippov, R. Hoogenboom and M. Hruby, *Macromol. Rapid Commun.*, 2012, **33**, 1648–1662.

197 C. Weber, R. Hoogenboom and U. S. Schubert, *Prog. Polym. Sci.*, 2012, **37**, 686–714.

198 M. M. Bloksma, R. M. Paulus, H. P. C. Van Kuringen, F. Van Der Woerdt, H. M. L. Lambermont-Thijs, U. S. Schubert and R. Hoogenboom, *Macromol. Rapid Commun.*, 2012, **33**, 92–96.

199 D. Roy, W. L. A. Brooks and B. S. Sumerlin, *Chem. Soc. Rev.*, 2013, **42**, 7214–7243.

200 Y. Yamauchi, V. Malgras, B. P. Bastakoti, S. Guragain and K. Nakashima, *Chem. - A Eur. J.*, 2015, **21**, 13164–13174.

201 Y.-T. Shieh, F.-Z. Hu and C.-C. Cheng, *ACS Appl. Nano Mater.*, 2017, **1**, 384–393.

202 S. Thayumanavan, X. Guo, J. Zhuang, X. Liu, D. Hu, Z. Jiang and Y. Xu, *Macromolecules*, 2016, **49**, 6186–6192.

203 X. Fu, L. Hosta-Rigau, R. Chandrawati and J. Cui, *Chem*, 2018, **4**, 2084–2107.

204 X.-X. Shi, H.-J. Li, Y.-R. Zhang, J. Wang, H. Huang, J.-Z. Du, Q.-Y. Huang, Q.-S. Tong and W. Xu, *Polym. Chem.*, 2018, **10**, 656–662.

205 P. Schattling, F. D. Jochum and P. Theato, *Polym. Chem.*, 2014, **5**, 25–36.

206 X. An, A. Zhu, H. Luo, H. Ke, H. Chen and Y. Zhao, *ACS Nano*, 2016, **10**, 5947–5958.

207 Z. Cao, X. Zhou and G. Wang, *ACS Appl. Mater. Interfaces*, 2016, **8**, 28888–28896.

208 C. M. Schilli, M. Zhang, E. Rizzardo, S. H. Thang, Y. K. Chong, K. Edwards, G. Karlsson and A. H. E. Müller, *Macromolecules*, 2004, **37**, 7861–7866.

209 A. Klaikherd, C. Nagamani and S. Thayumanavan, *J. Am. Chem. Soc.*, 2009, **131**, 4830–4838.

210 X. Jiang, C. Feng, G. Lu and X. Huang, *ACS Macro Lett.*, 2014, **3**, 1121–1125.

211 X. Cai, L. Zhong, Y. Su, S. Lin and X. He, *Polym. Chem.*, 2015, **6**, 3875–3884.

212 Z. Song, K. Wang, C. Gao, S. Wang and W. Zhang, *Macromolecules*, 2016, **49**, 162–171.

213 M. A. Gauthier, M. I. Gibson and H. A. Klok, *Angew. Chemie - Int. Ed.*, 2009, **48**, 48–58.

214 R. Barbey and H. A. Klok, *Langmuir*, 2010, **26**, 18219–18230.

215 A. Darabi, P. G. Jessop and M. F. Cunningham, *Chem. Soc. Rev.*, 2016, **45**, 4391–4436.

216 S. Li, Y. Su, M. Dan and W. Zhang, *Polym. Chem.*, 2014, **5**, 1219–1228.

217 G. Luo, Y. Guo, C. Liu, G. Han, X. Ma and W. Zhang, *RSC Adv.*, 2019, **9**, 12936–12943.

218 N. Poly, M. Copolymers, P. Yang and F. J. Stadler, 1–21.

219 G. Jancso and W. A. Van Hook, *Chem. Rev.*, 1974, **74**, 689–750.

220 P. Kujawa and F. M. Winnik, *Macromolecules*, 2001, **34**, 4130–4135.

221 J. Sun, Y. Peng, Y. Chen, Y. Liu, J. Deng, L. Lu and Y. Cai, *Macromolecules*, 2010, **43**, 4041–4049.

222 H. Cheng, S. Xie, Y. Zhou, W. Huang, D. Yan, J. Yang and B. Ji, *J. Phys. Chem. B*, 2010, **114**, 6291–6299.

223 J. Gao and C. Wu, *Macromolecules*, 2002, **30**, 6873–6876.

224 M. Rusu, S. Wohlrab, D. Kuckling, H. Möhwald and M. Schönhoff, *Macromolecules*, 2006, **39**, 7358–7363.

225 E. S. Gil and S. M. Hudson, *Prog. Polym. Sci.*, 2004, **29**, 1173–1222.

226 E. S. Ron and L. E. Bromberg, *Adv. Drug Deliv. Rev.*, 1998, **31**, 197–221.

227 G. Némethy and H. A. Scheraga, *J. Chem. Phys.*, 1964, **41**, 680–689.

228 Y. Marcus and A. Ben-Naim, *J. Chem. Phys.*, 1985, **83**, 4744–4759.

229 Z. Song, K. Wang, C. Gao, S. Wang and W. Zhang, *Macromolecules*, 2016, **49**, 162–171.

230 H. Du and X. Qian, *J. Polym. Sci. Part B Polym. Phys.*, 2011, **49**, 1112–1122.

231 M. Hahn, E. Görnitz and H. Dautzenberg, *Macromolecules*, 1998, **31**, 5616–5623.

232 J. F. Lutz, Ö. Akdemir and A. Hoth, *J. Am. Chem. Soc.*, 2006, **128**, 13046–13047.

233 D. Gravel, X. X. Zhu, D. Lessard, D. Avoce and I. Idziak, *Macromolecules*, 2002, **32**, 1260–1263.

234 Y. Lu, X. Ye, K. Zhou and W. Shi, *J. Phys. Chem. B*, 2013, **117**, 7481–7488.

235 J. Wang, B. Liu, G. Ru, J. Bai and J. Feng, *Macromolecules*, 2016, **49**, 234–243.

236 Y. Gao, J. Yang, Y. Ding and X. Ye, *J. Phys. Chem. B*, 2014, **118**, 9460–9466.

237 Q. L. Fan, Y. Zhou, X. M. Lu, X. Y. Hou and W. Huang, *Macromolecules*, 2005, **38**, 2927–2936.

238 Y. Gao, C. C. Wang, L. Wang and H. L. Wang, *Langmuir*, 2007, **23**, 7760–7767.

239 S. Lin and P. Theato, *Macromol. Rapid Commun.*, 2013, **34**, 1118–1133.

240 N. Nath and A. Chilkoti, *Adv. Mater.*, 2002, **14**, 1243–1247.

241 D. Han, X. Tong, O. Boissière and Y. Zhao, *ACS Macro Lett.*, 2012, **1**, 57–61.

242 S. Lin and P. Theato, *Macromol. Rapid Commun.*, 2013, **34**, 1118–1133.

243 A. Darabi, A. R. Shirin-Abadi, J. Pinaud, P. G. Jessop and M. F. Cunningham, *Polym. Chem.*, 2014, **5**, 6163–6170.

244 T. Endo, D. Nagai, T. Monma, H. Yamaguchi and B. Ochiai, *Macromolecules*, 2004, **37**, 2007–2009.

245 Z. Guo, Y. Feng, S. He, M. Qu, H. Chen, H. Liu, Y. Wu and Y. Wang, *Adv. Mater.*, 2013, **25**, 584–590.

246 M. George and R. G. Weiss, *Langmuir*, 2002, **18**, 7124–7135.

247 H. Xiao, J. Miao, J. Cao, W. Yang, H. Wu and Y. Cao, *Org. Electron. physics, Mater.*

Appl., 2014, **15**, 758–774.

248 E. Ji, D. G. Whitten and K. S. Schanze, *Langmuir*, 2011, **27**, 1565–1568.

249 M. Bernards and Y. He, *J. Biomater. Sci. Polym. Ed.*, 2014, **25**, 1479–1488.

250 G. J. Copello, L. E. Diaz and V. Campo Dall' Orto, *J. Hazard. Mater.*, 2012, **217**–**218**, 374–381.

251 S. Morisada, H. Suzuki, S. Emura, Y. Hirokawa and Y. Nakano, *Adsorption*, 2008, **14**, 621–628.

252 J. M. Lázaro Martínez, A. K. Chattah, G. A. Monti, M. F. Leal Denis, G. Y. Buldain and V. Campo Dall' Orto, *Polymer (Guildf).*, 2008, **49**, 5482–5489.

253 G. Raj, C. Swalus, A. Guillet, M. Devillers, B. Nysten and E. M. Gaigneaux, *Langmuir*, 2013, **29**, 4388–4395.

254 F. Wang and G. C. Bazan, *J. Am. Chem. Soc.*, 2006, **128**, 15786–15792.

255 O. K. Nag, J.-E. Jeong, T. L. Nguyen and H. Y. Woo, *Macromol. Res.*, 2015, **23**, 457–465.

256 C. Xing, L. Liu, Z. Shi, Y. Li and S. Wang, *Adv. Funct. Mater.*, 2010, **20**, 2175–2180.

257 A. B. Lowe and C. L. McCormick, *Chem. Rev.*, 2002, **102**, 4177–4190.

258 A. V. Salvekar, W. M. Huang, R. Xiao, Y. S. Wong, S. S. Venkatraman, K. H. Tay and Z. X. Shen, *Acc. Chem. Res.*, 2017, **50**, 141–150.

259 A. A. D'souza and R. Shegokar, *Expert Opin. Drug Deliv.*, 2016, **13**, 1257–1275.

260 K. Li, Z. Li, K. Feng, X. Xu, L. Wang and Q. Peng, *J. Am. Chem. Soc.*, 2013, **135**, 13549–13557.

261 D. Lee, S. W. Stone and J. P. Ferraris, *Chem. Commun.*, 2011, **47**, 10987–10989.

262 S. K. Panja, N. Dwivedi and S. Saha, *RSC Adv.*, 2016, **6**, 105786–105794.

263 C. Tan, M. R. Pinto and K. S. Schanze, *Chem. Commun.*, 2002, 446–447.

264 C. Tan, M. R. Pinto, M. E. Kose, I. Ghiviriga and K. S. Schanze, *Adv. Mater.*, 2004, **16**,

1208–1212.

265 Y. Q. Huang, Q. L. Fan, X. F. Liu, N. N. Fu and W. Huang, *Langmuir*, 2010, **26**, 19120–19128.

266 S. H. Lee, S. Kömürlü, X. Zhao, H. Jiang, G. Moriena, V. D. Kleiman and K. S. Schanze, *Macromolecules*, 2011, **44**, 4742–4751.

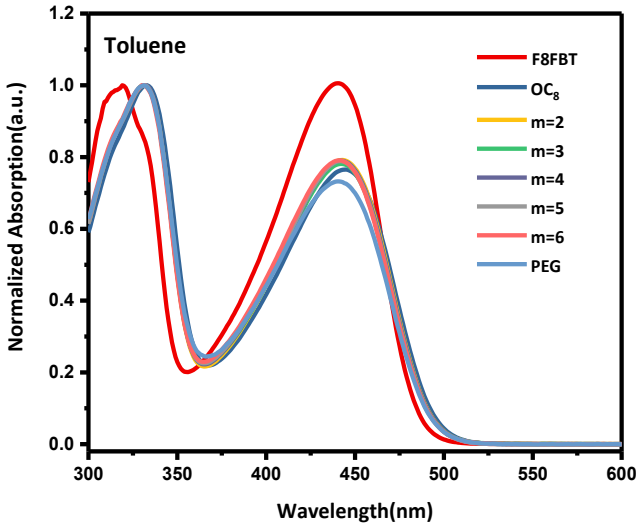
267 B. R. Lee, J. C. Yu, J. H. Park, S. Lee, C. K. Mai, B. Zhao, M. S. Wong, E. D. Jung, Y. S. Nam, S. Y. Park, D. Di Nuzzo, J. Y. Kim, S. D. Stranks, G. C. Bazan, H. Choi, M. H. Song and R. H. Friend, *ACS Nano*, 2018, **12**, 5826–5833.

268 A. Domard, M. Rinaudo and C. Rochas, *J. Polym. Sci. Polym. Phys. Ed.*, 1979, **17**, 673–681.

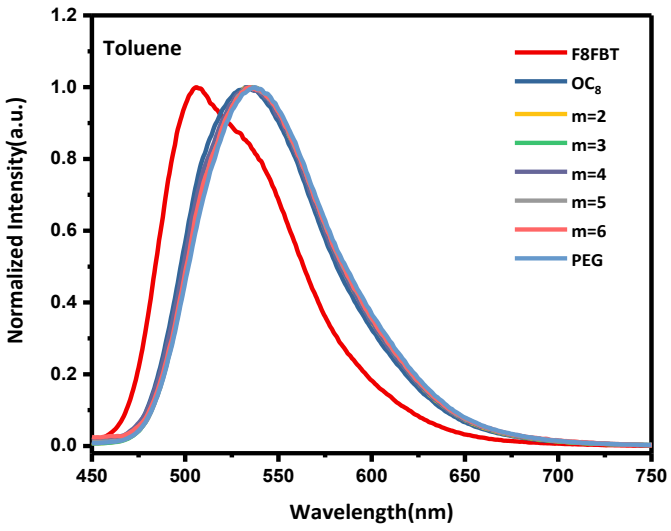
269 Z. Yang, H. Peng, W. Wang and T. Liu, *J. Appl. Polym. Sci.*, 2010, **116**, 2658–2667.

8. Appendix

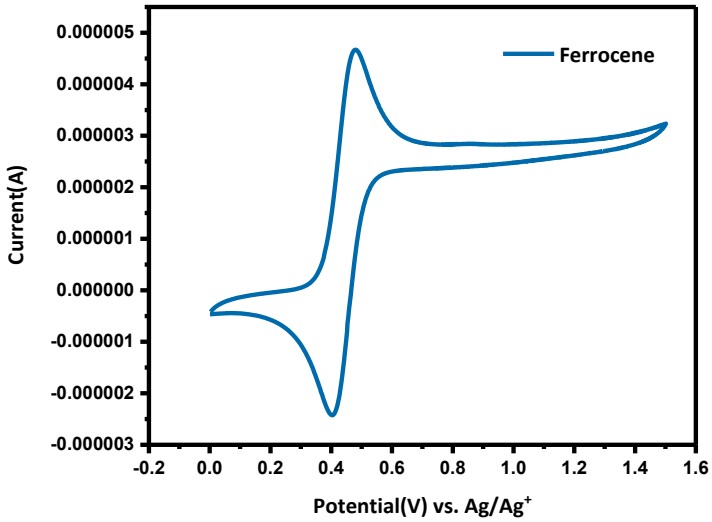
8.1 Chapter 2



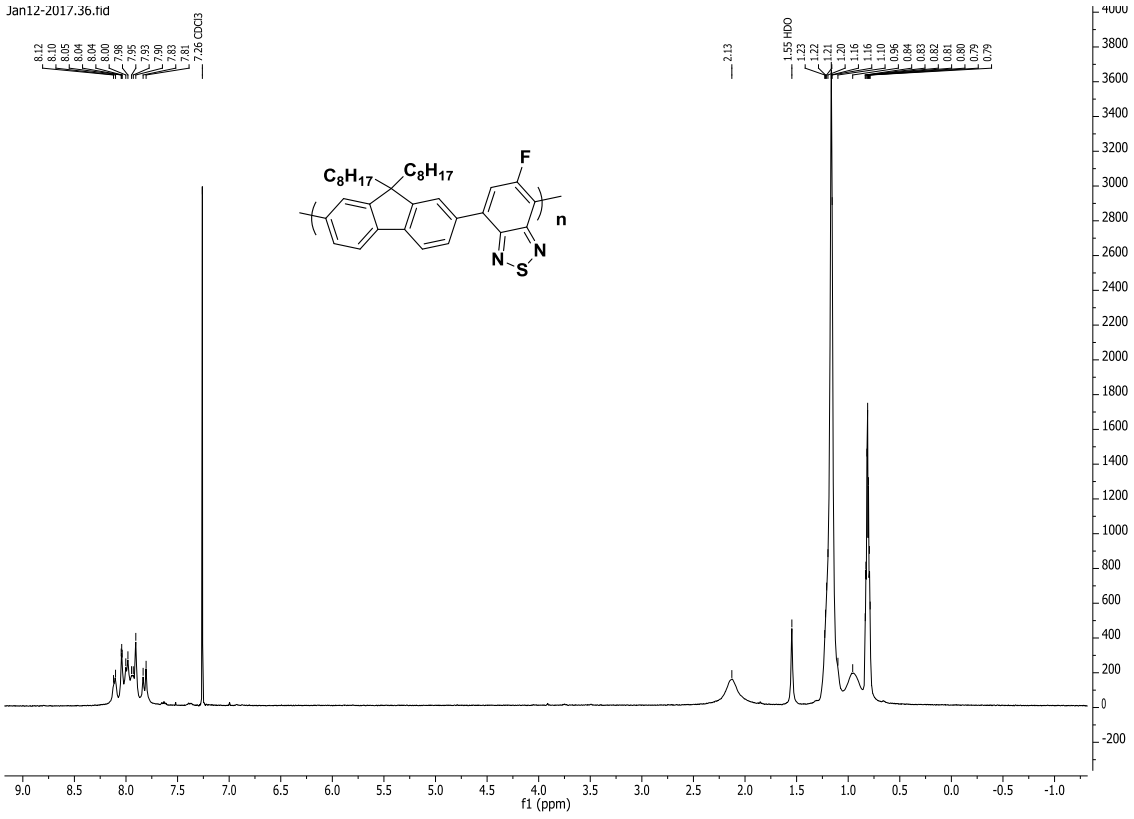
Appendix Figure 1: UV absorption of polymers in toluene solution



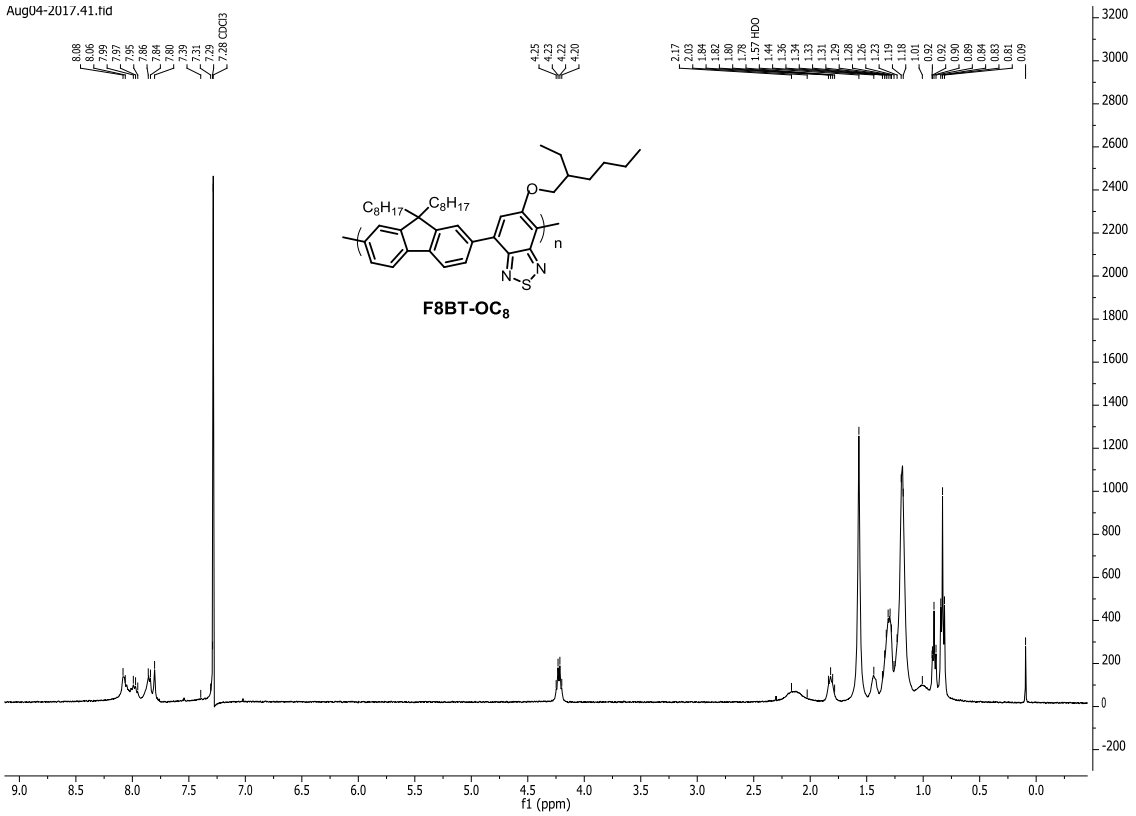
Appendix Figure 2: PL spectra of polymers in toluene solution



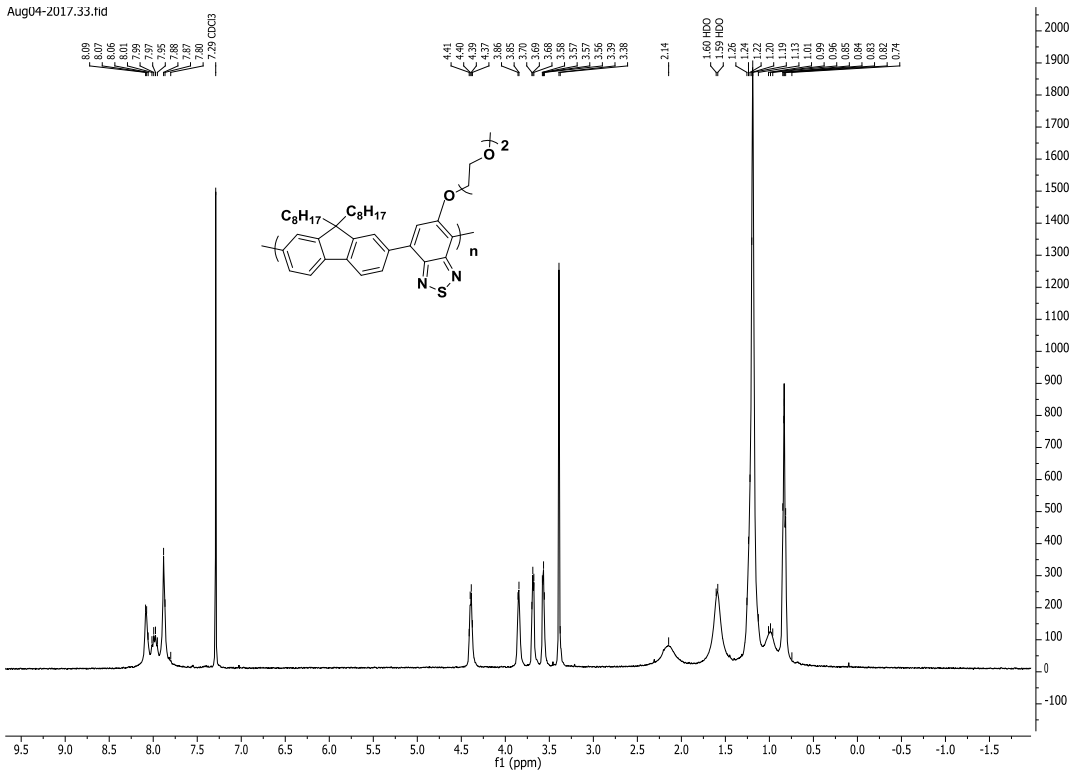
Appendix Figure 3: Cyclic voltammograms of ferrocene



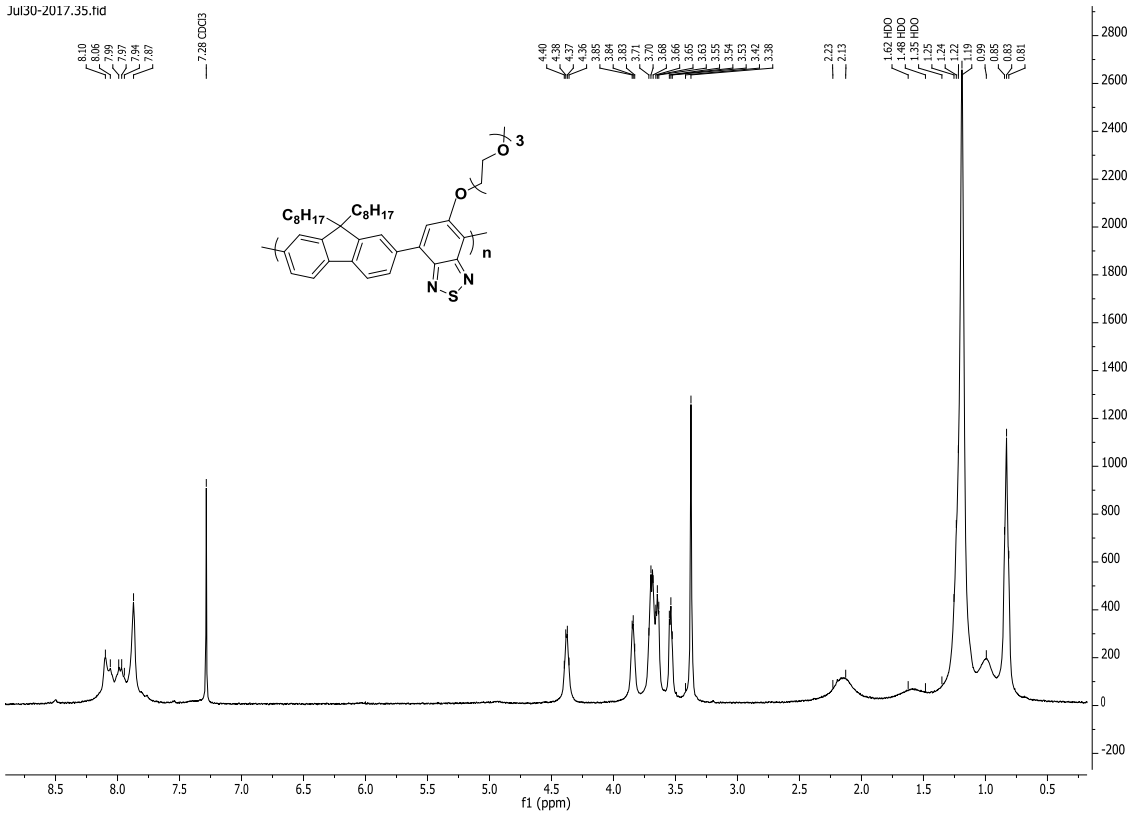
Appendix Figure 4: ^{1}H-NMR of **F8FBT** ($CDCl_3$)



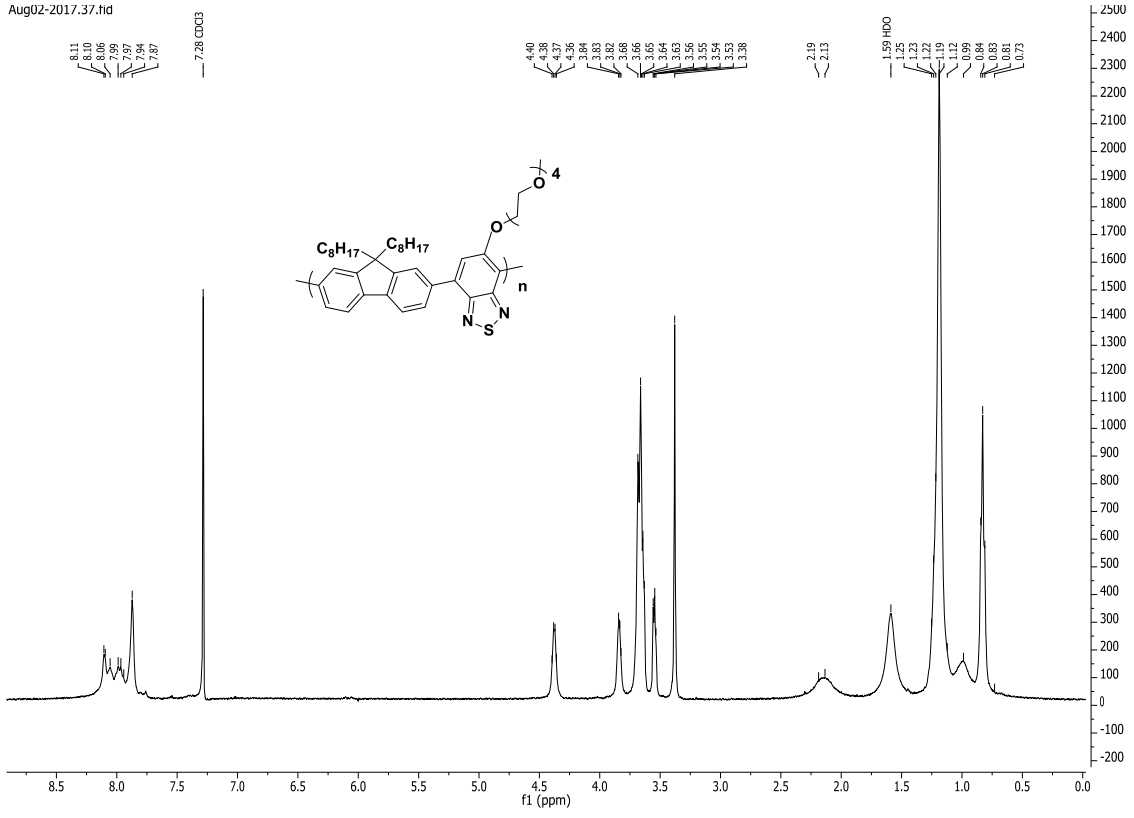
Appendix Figure 5: ^{1}H-NMR of **F8BT-OC$_8$** ($CDCl_3$)



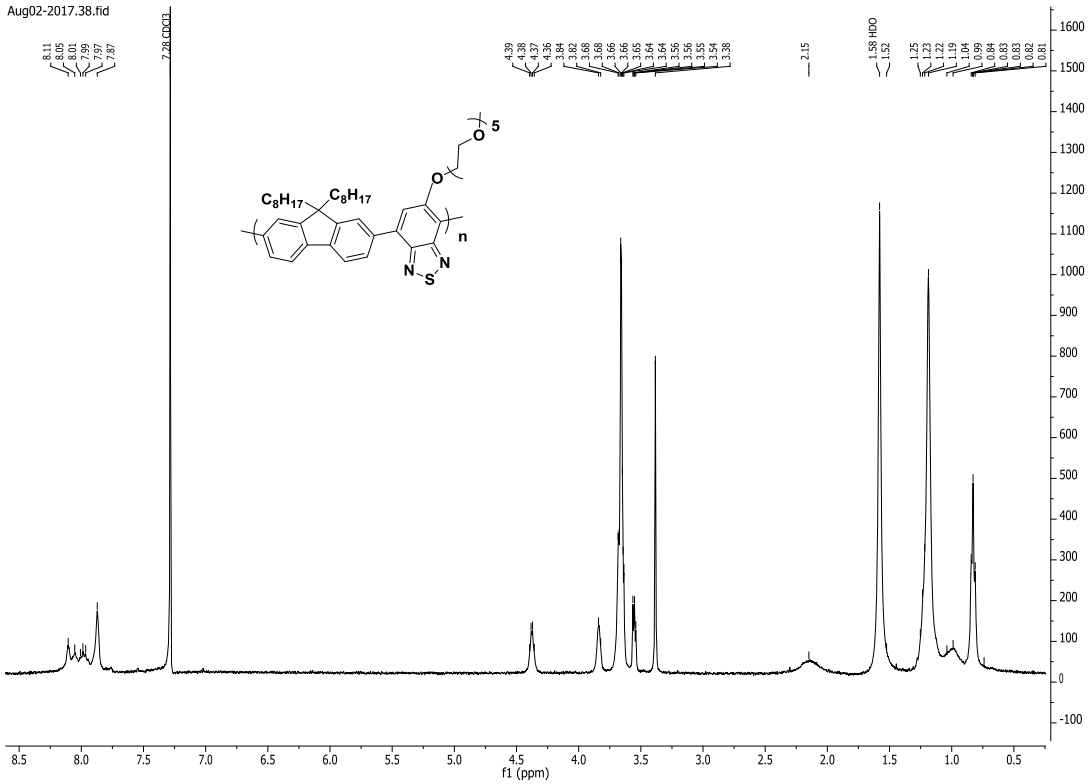
Appendix Figure 6: ^{1}H-NMR of **F8BT-2** ($CDCl_3$)



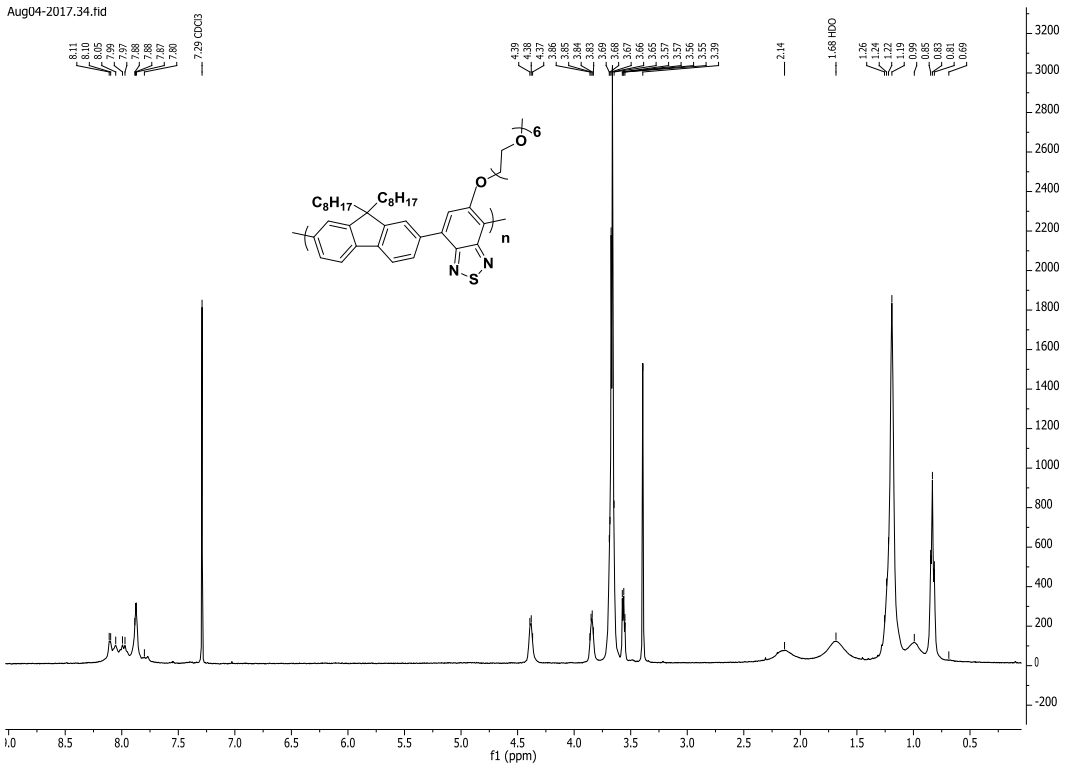
Appendix Figure 7: ^{1}H-NMR of **F8BT-3** ($CDCl_3$)



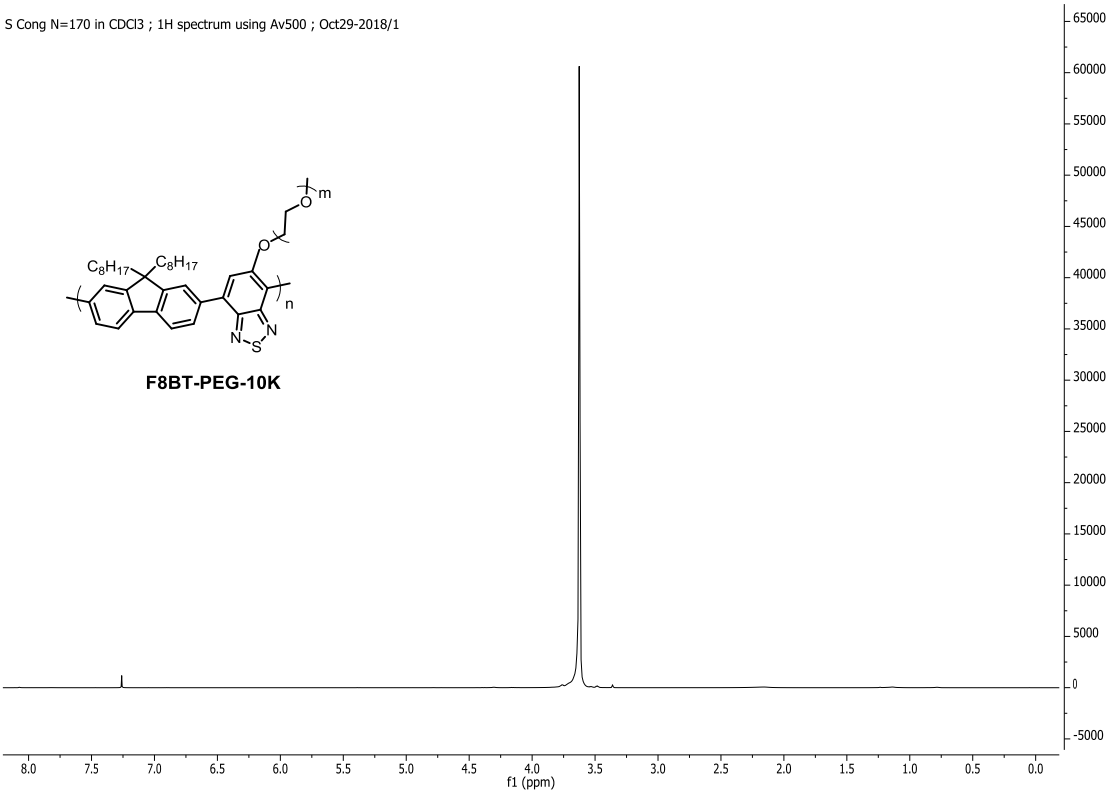
Appendix Figure 8: ^{1}H-NMR of **F8BT-4** ($CDCl_3$)



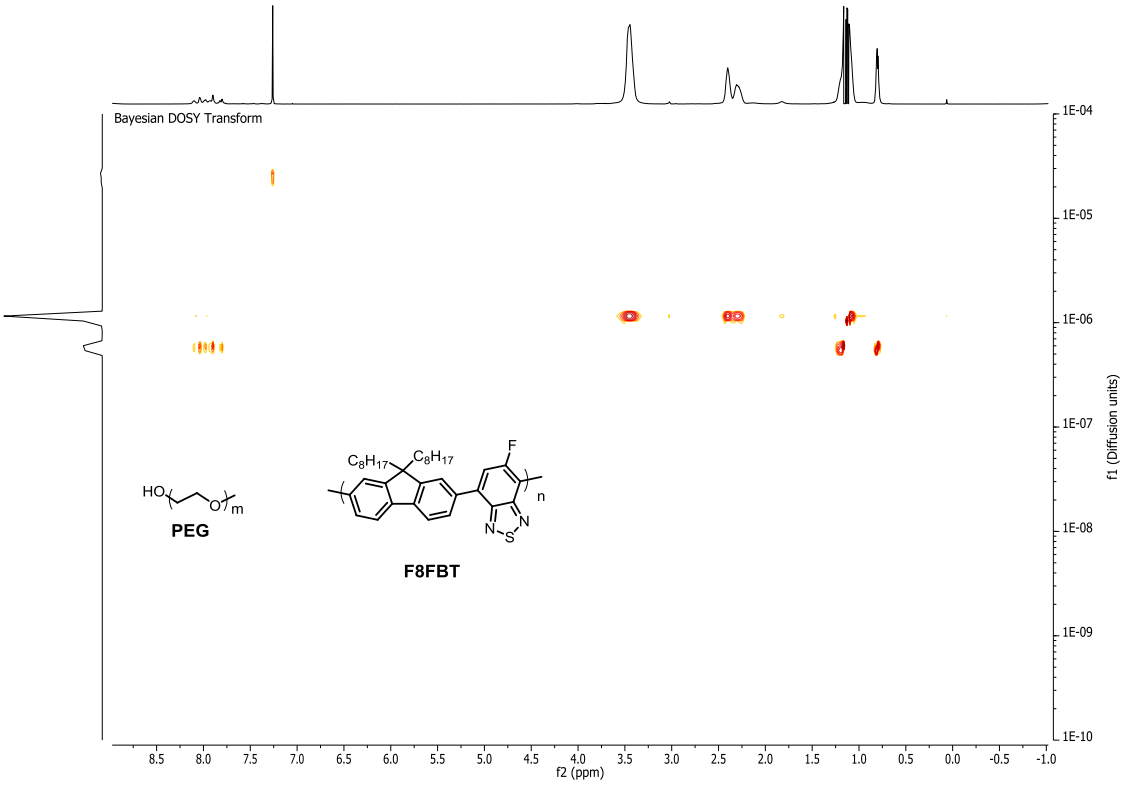
Appendix Figure 9: ^{1}H-NMR of **F8BT-5** ($CDCl_3$)



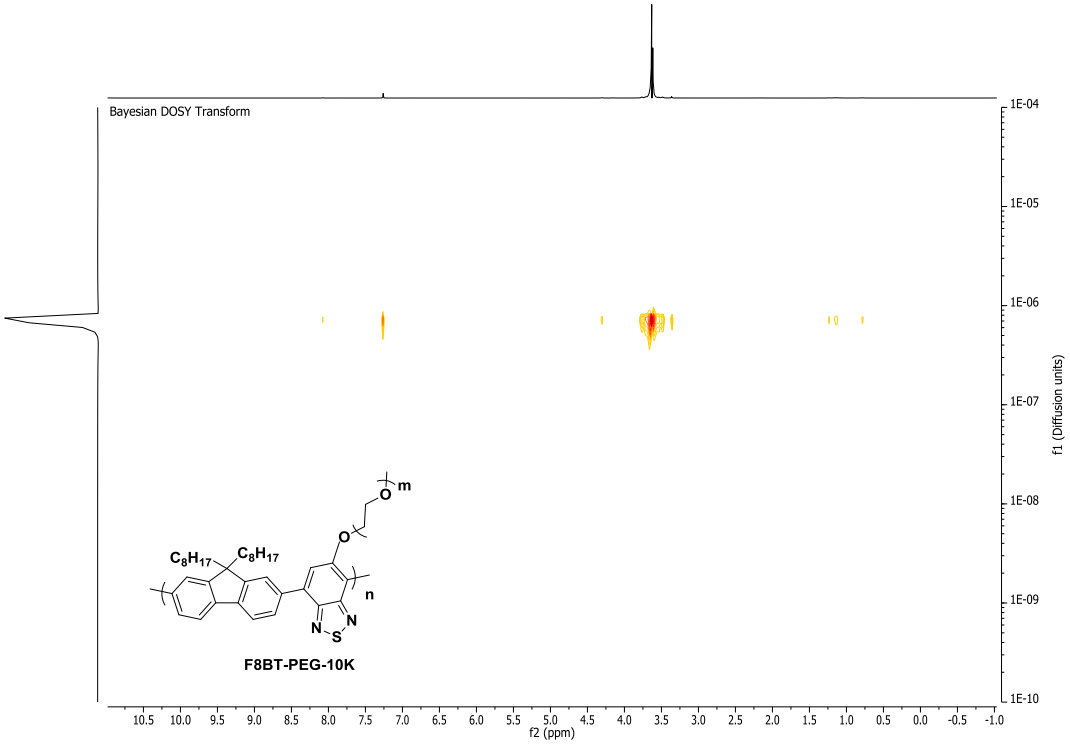
Appendix Figure 10: ^{1}H-NMR of **F8BT-6** ($CDCl_3$)



Appendix Figure 11: ^{1}H-NMR of **F8BT-PEG** ($CDCl_3$)

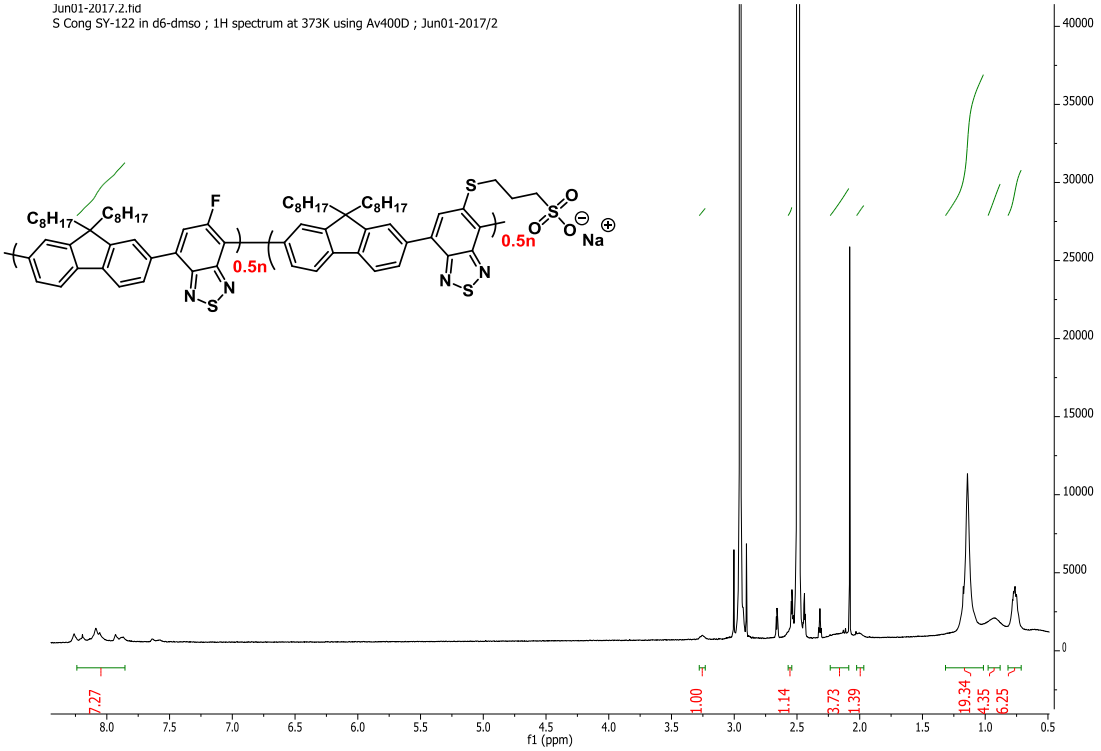


Appendix Figure 12: DOSY-NMR of **F8FBT** and **PEG** mixture ($CDCl_3$)

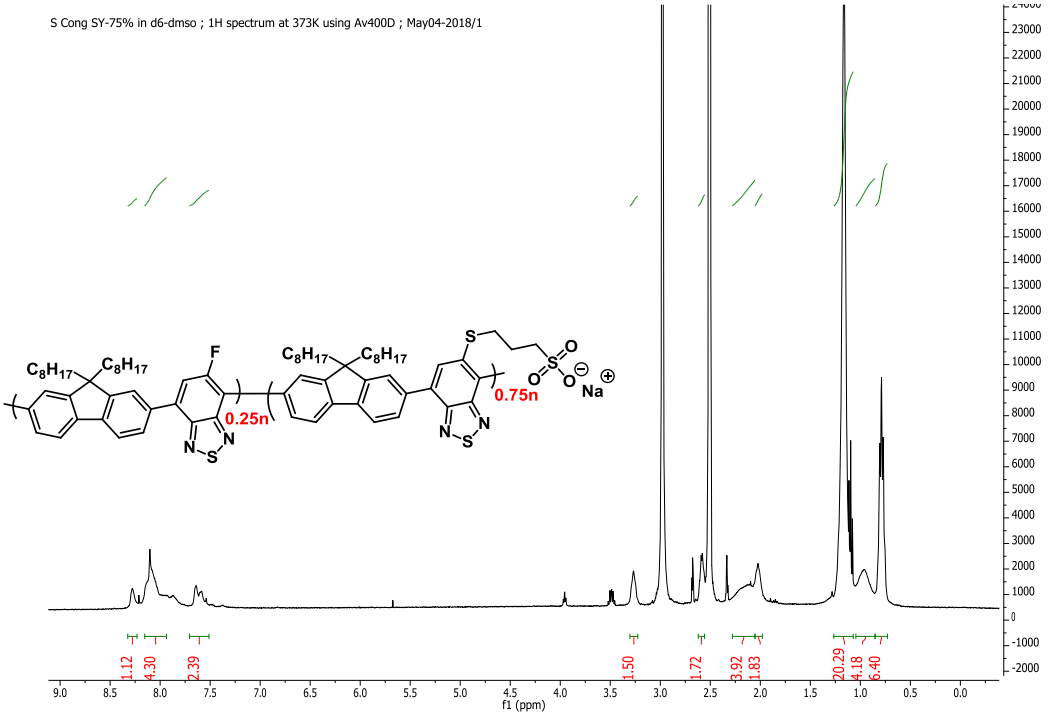


Appendix Figure 13: DOSY-NMR of **F8BT-PEG** ($CDCl_3$)

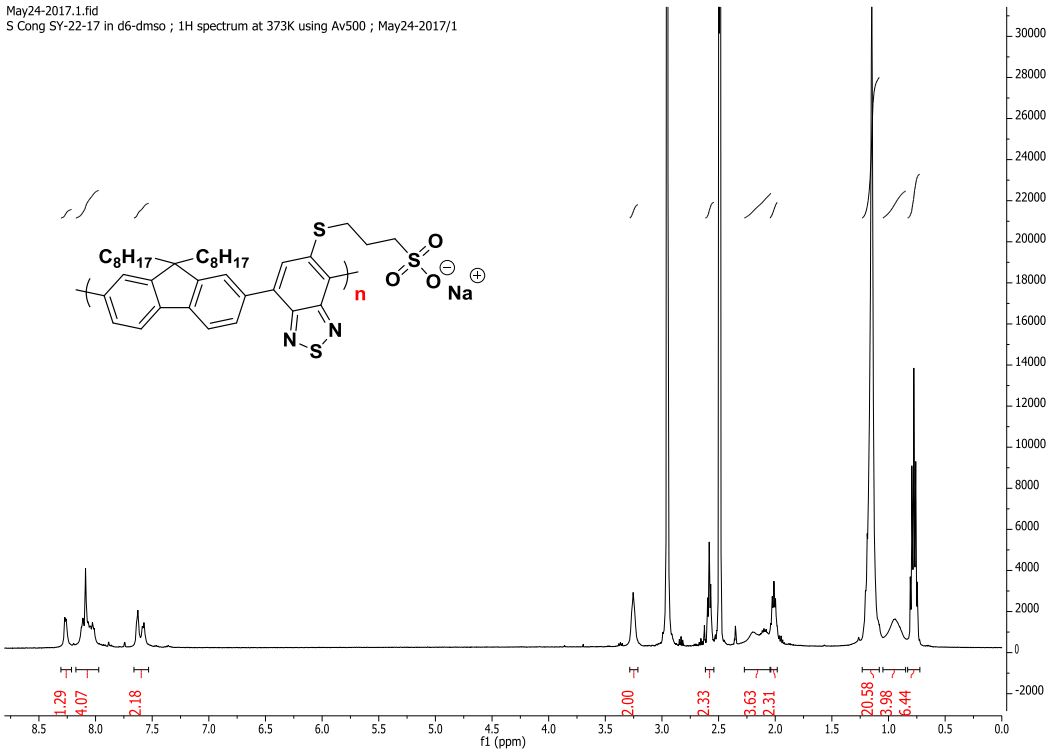
8.2 Chapter 3



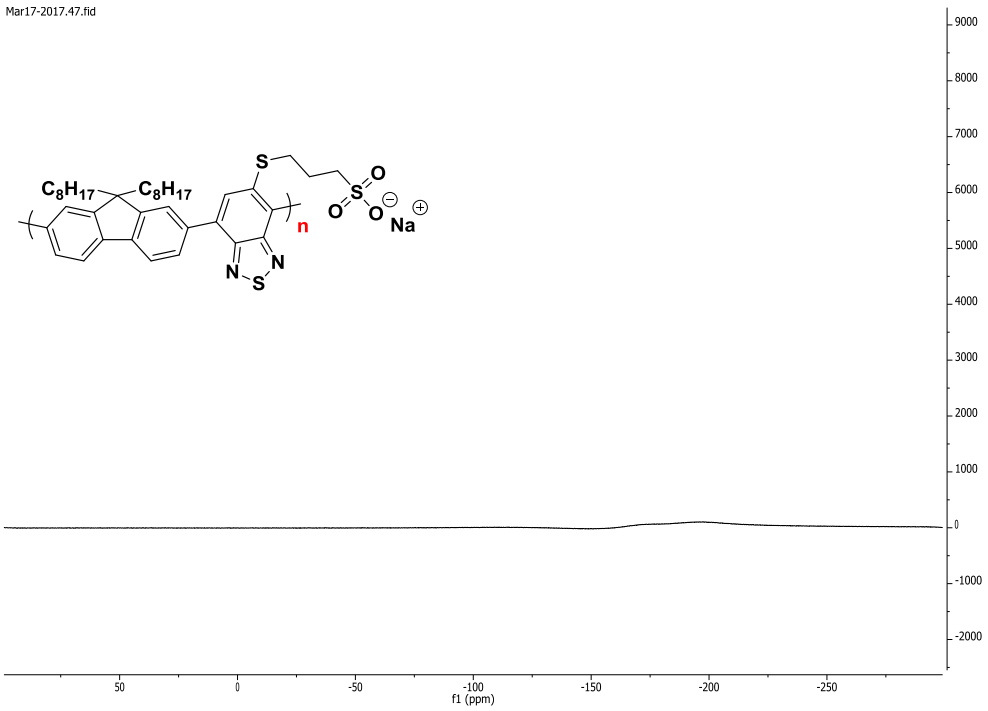
Appendix Figure 14: ^{1}H-NMR of **CPE 50%** (d-DMSO at 373K)



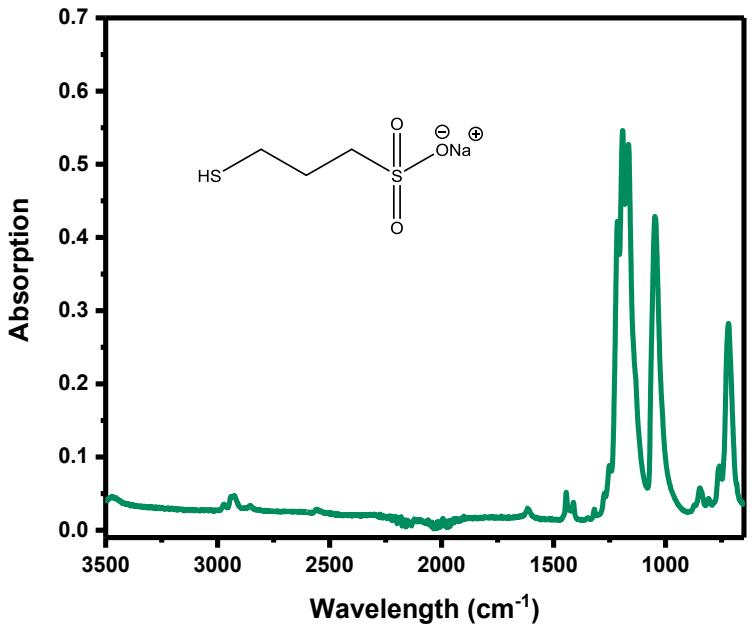
Appendix Figure 15: ^{1}H-NMR of **CPE 75%** (d-DMSO at 373K)



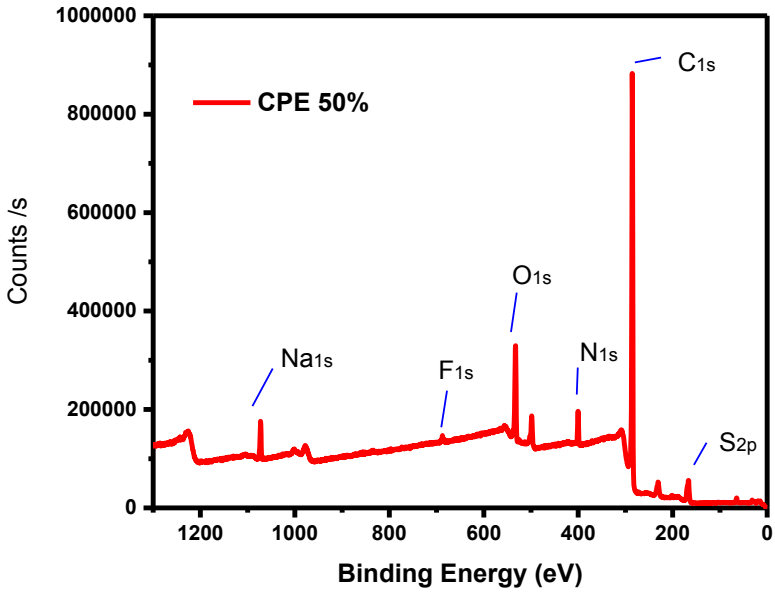
Appendix Figure 16: ^{1}H-NMR of **CPE 100%** (d-DMSO at 373K)



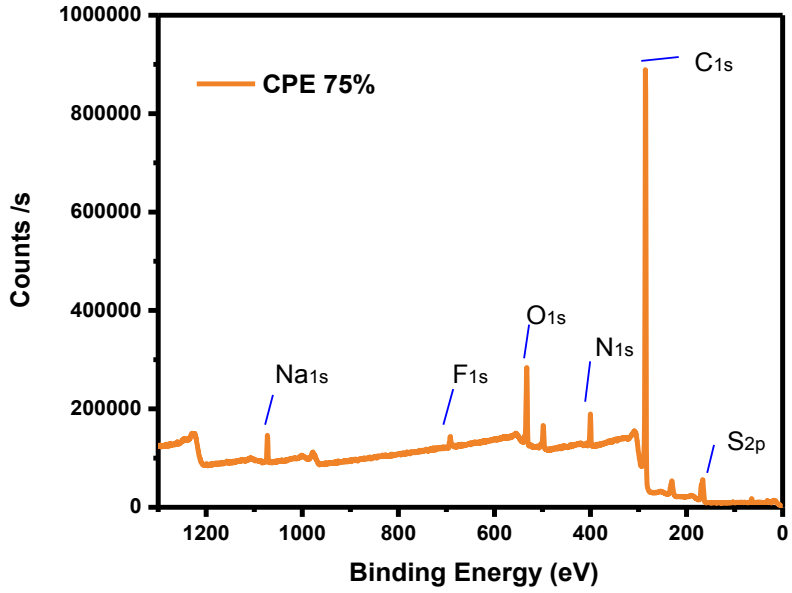
Appendix Figure 17: ^{19}F-NMR of **CPE 100%** (d-DMSO)



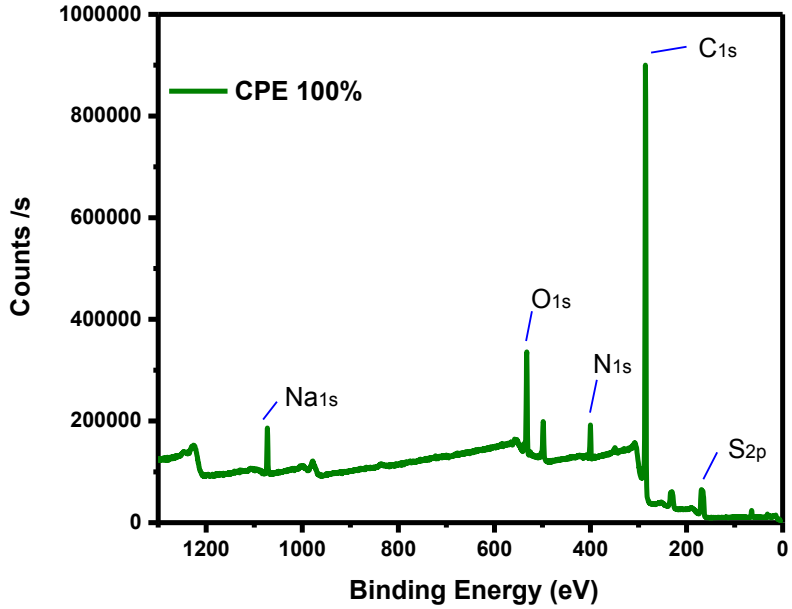
Appendix Figure 18 FTIR of 3-mercapto-1-propanesulfonic acid sodium salt



Appendix Figure 19 XPS spectra of **CPE50%**

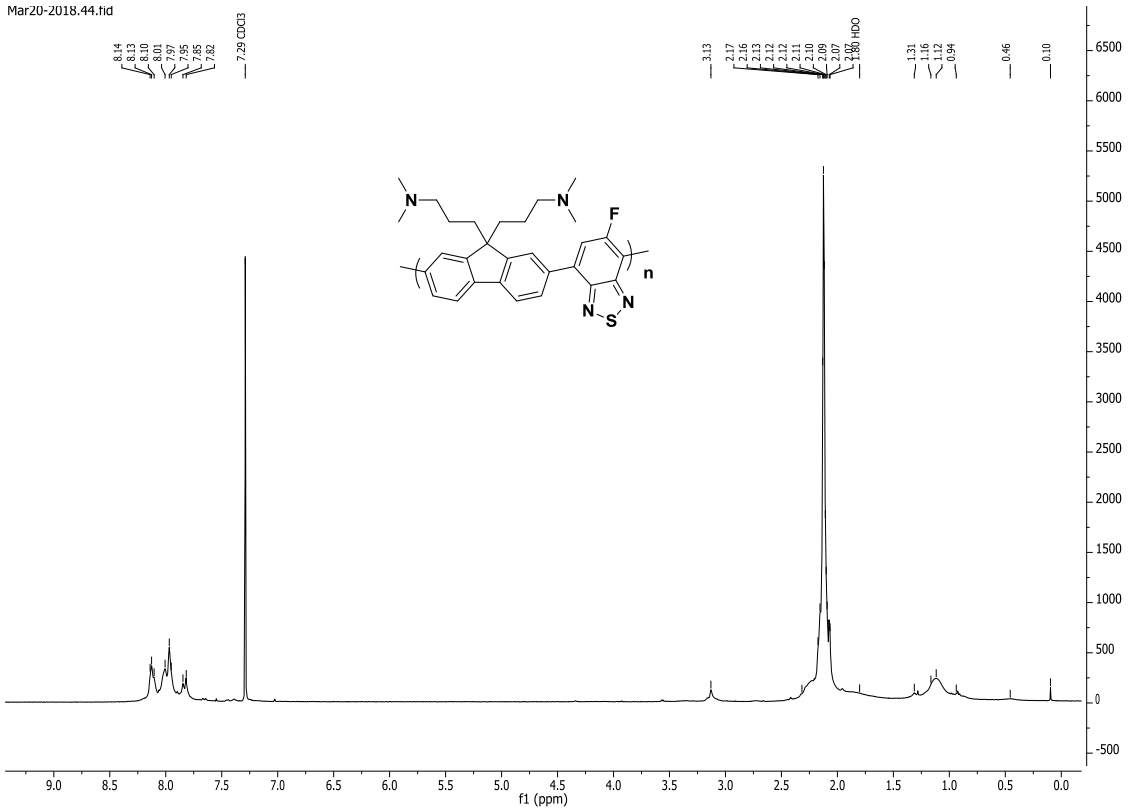


Appendix Figure 20 XPS spectra of **CPE75%**

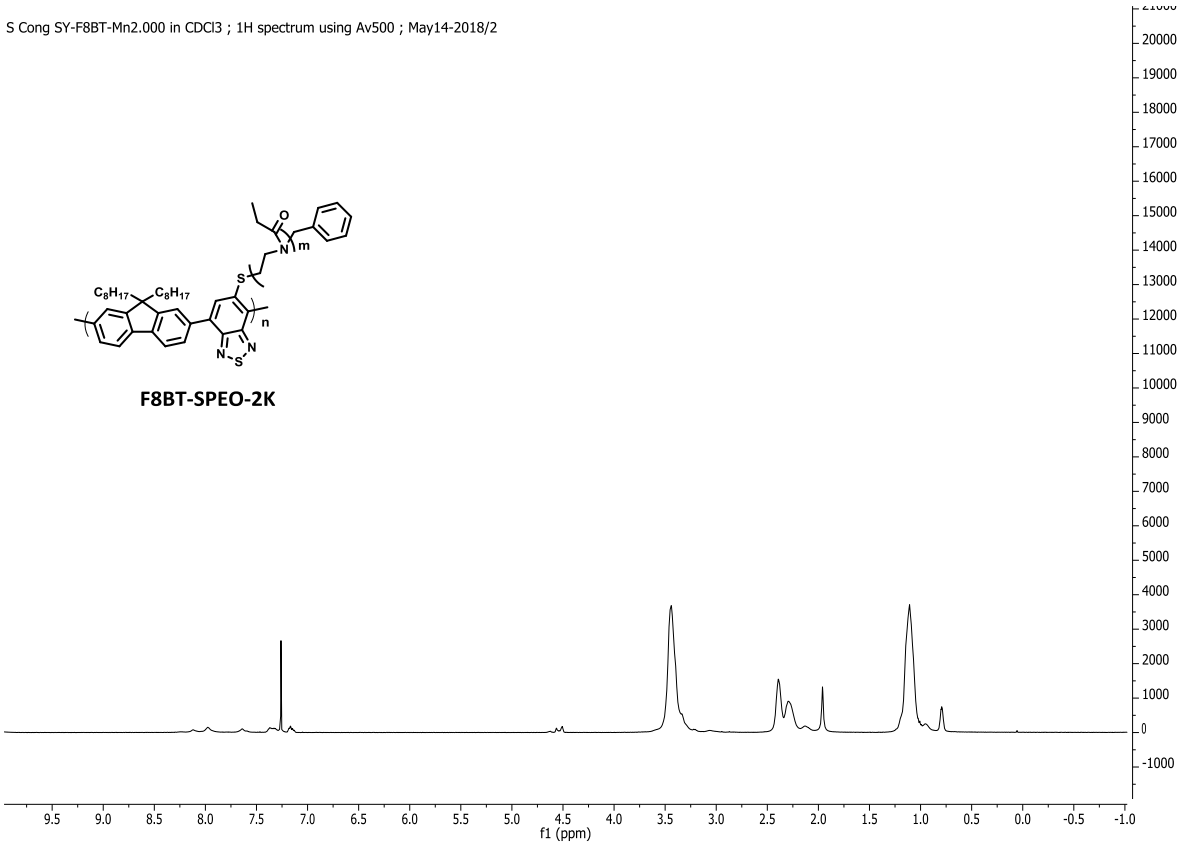


Appendix Figure 21 XPS spectra of **CPE100%**

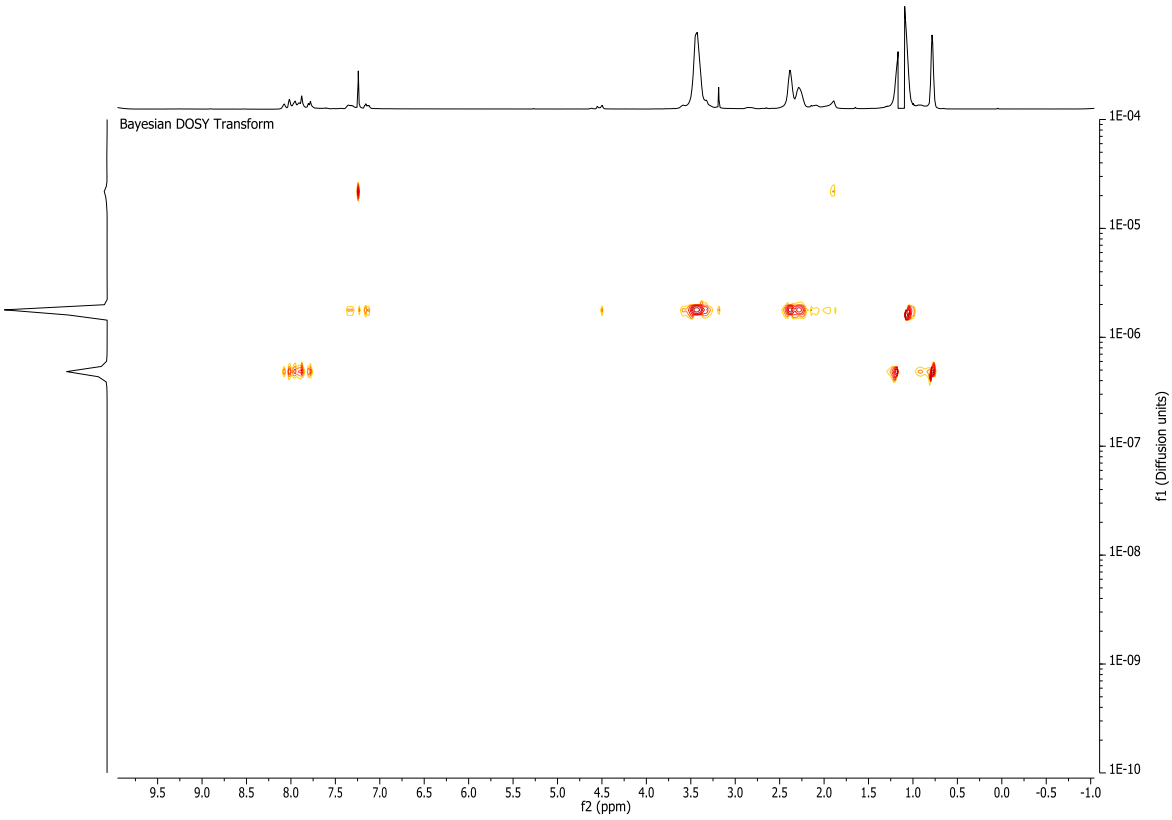
8.3 Chapter 4



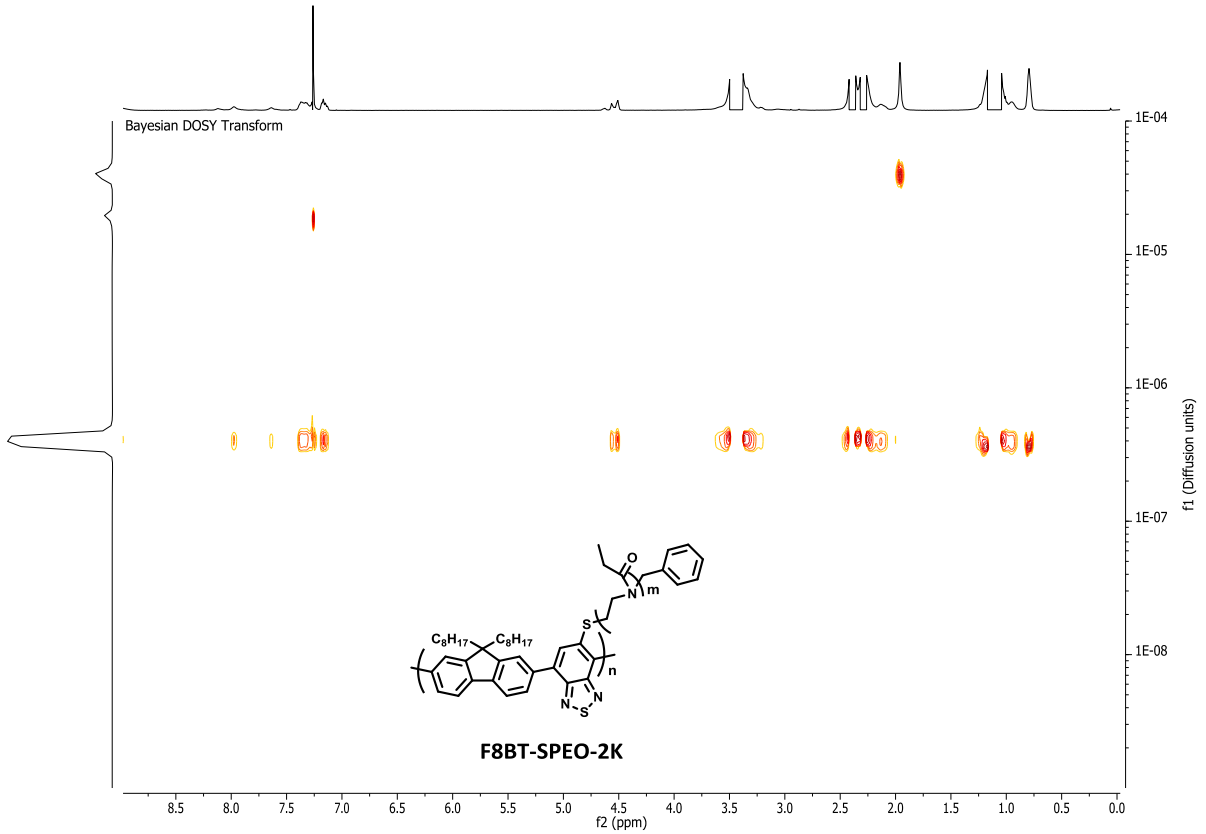
Appendix Figure 22: ^{1}H-NMR of **DNFBT** ($CDCl_3$)



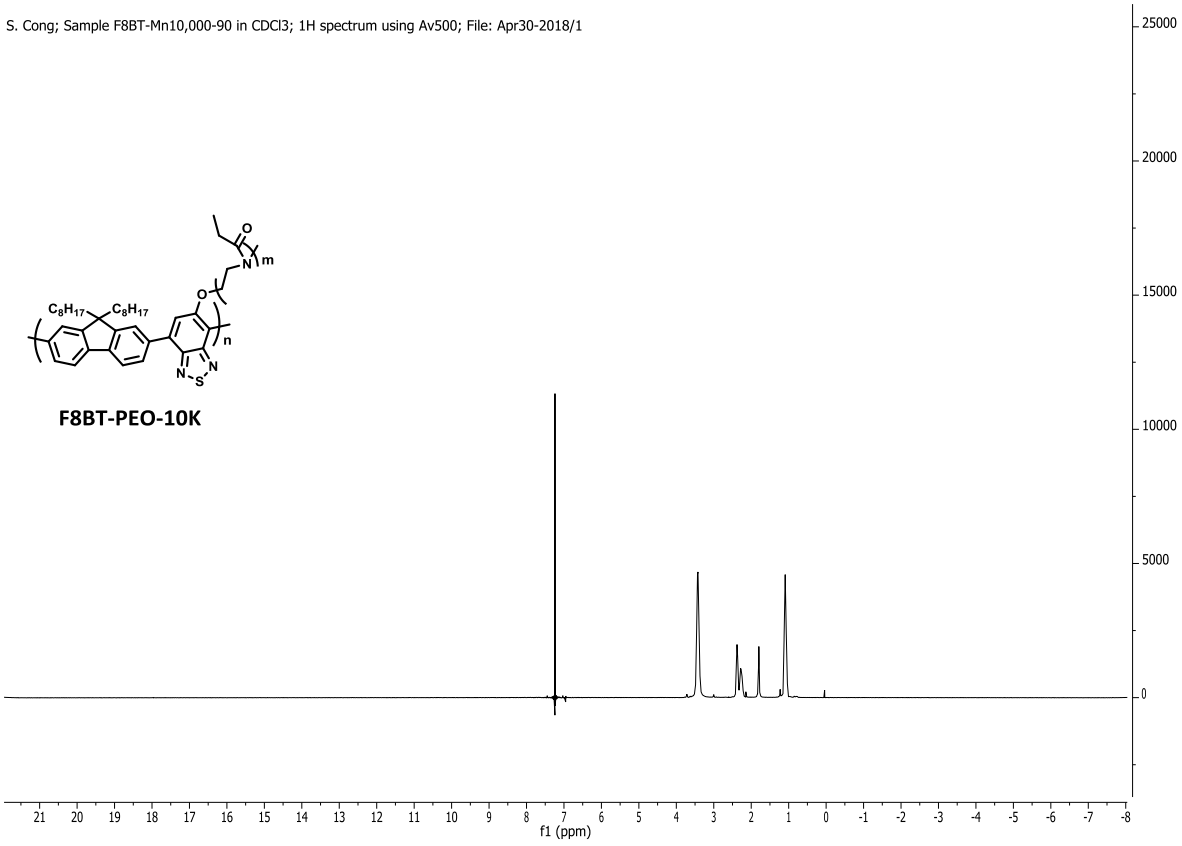
Appendix Figure 23: ^{1}H-NMR of **F8BT-SPEO-2K** ($CDCl_3$)



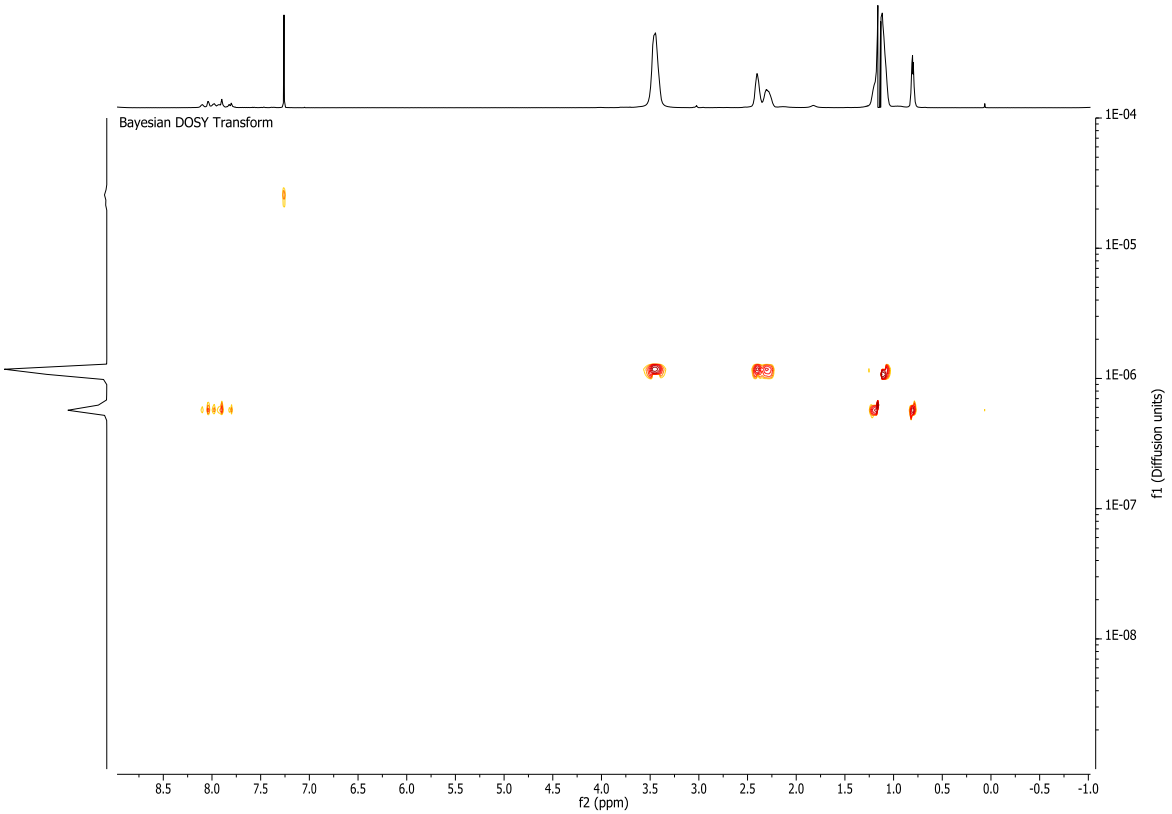
Appendix Figure 24: DOSY-NMR of **F8FBT** and **SPEO** mixture ($CDCl_3$)



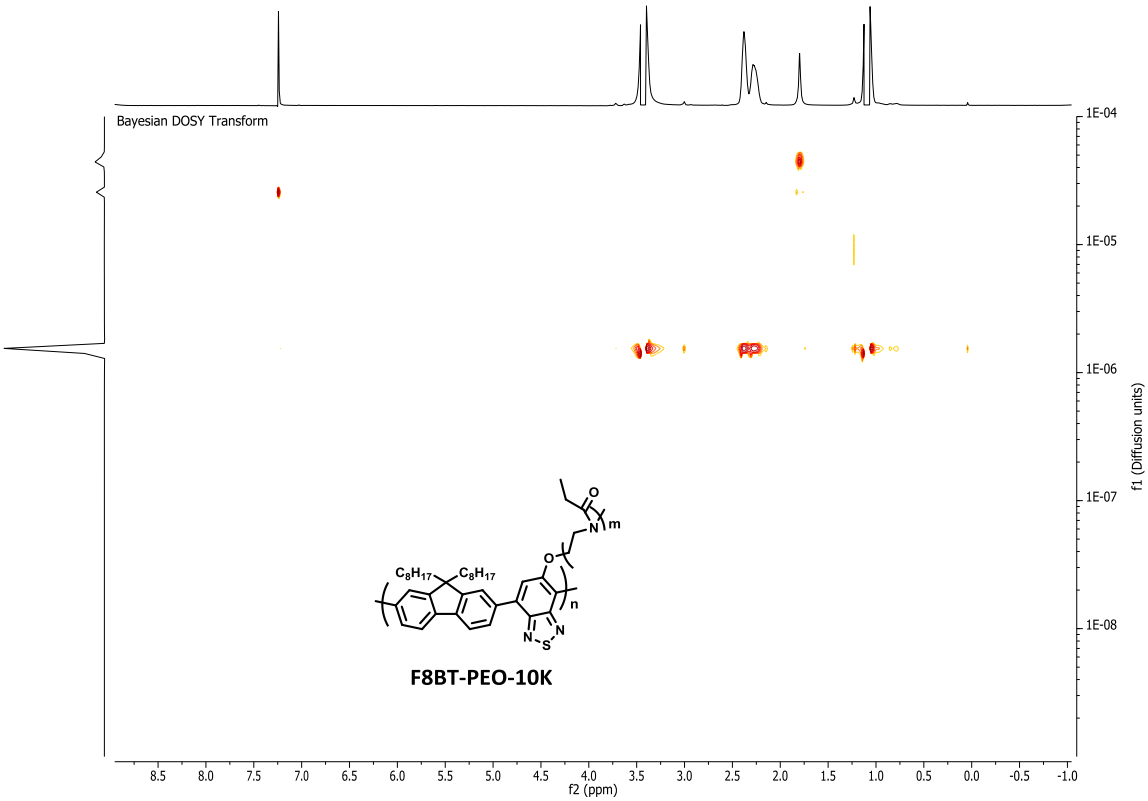
Appendix Figure 25: DOSY -NMR of **F8BT-SPEO-2K** ($CDCl_3$)



Appendix Figure 26: ^{1}H-NMR of **F8BT-PEO-10K** ($CDCl_3$)

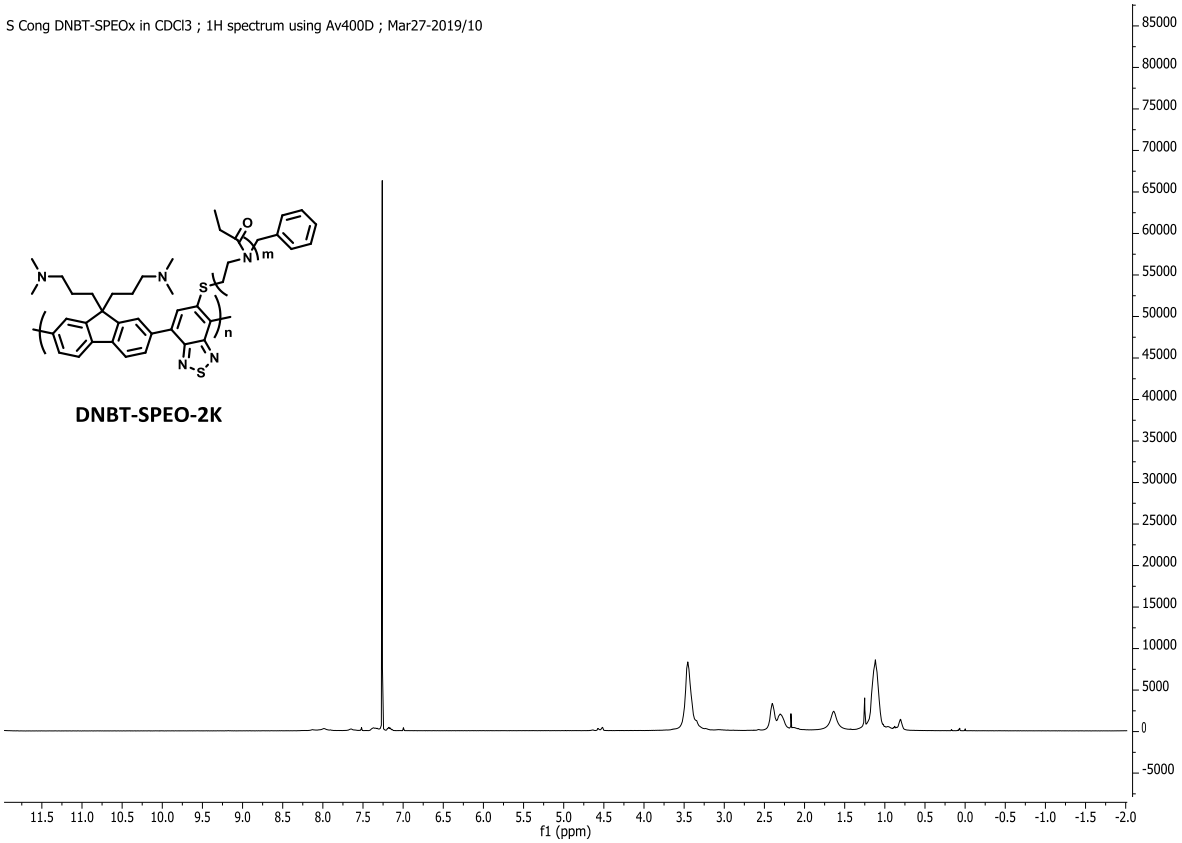


Appendix Figure 27: DOSY -NMR of **F8FBT** and **PEO** mixture ($CDCl_3$)

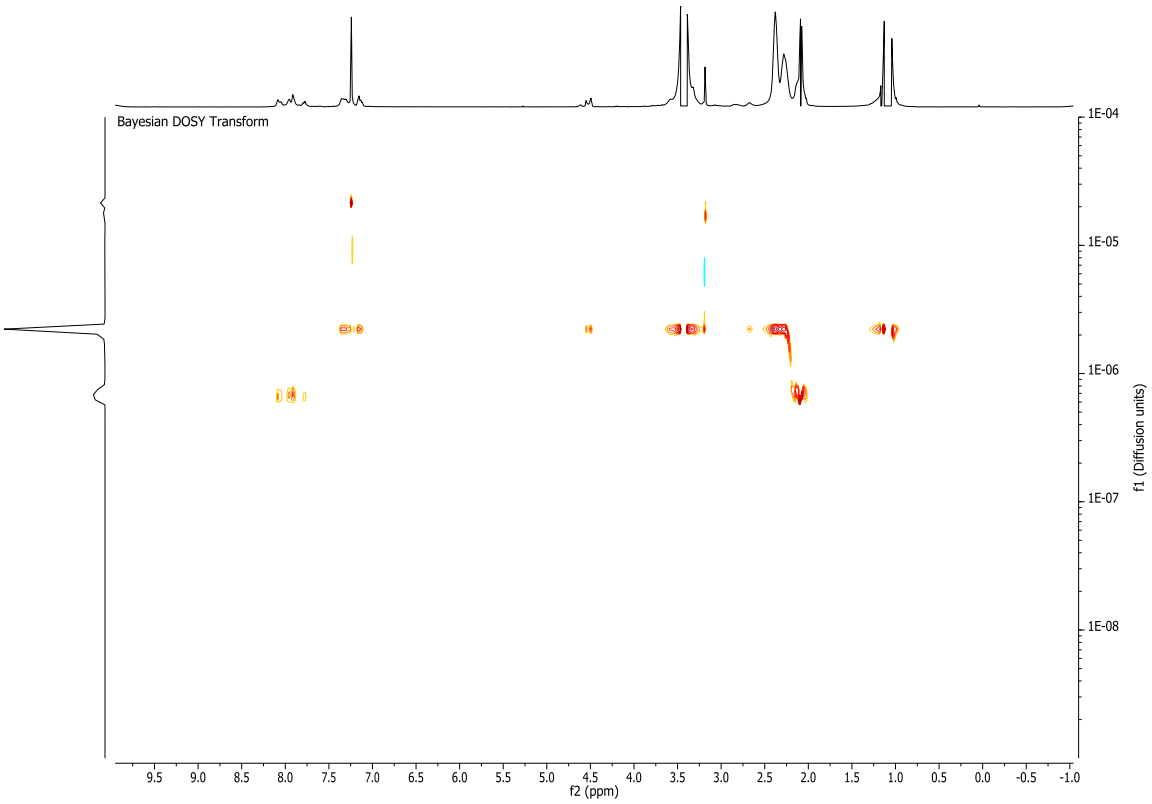


F8BT-PEO-10K

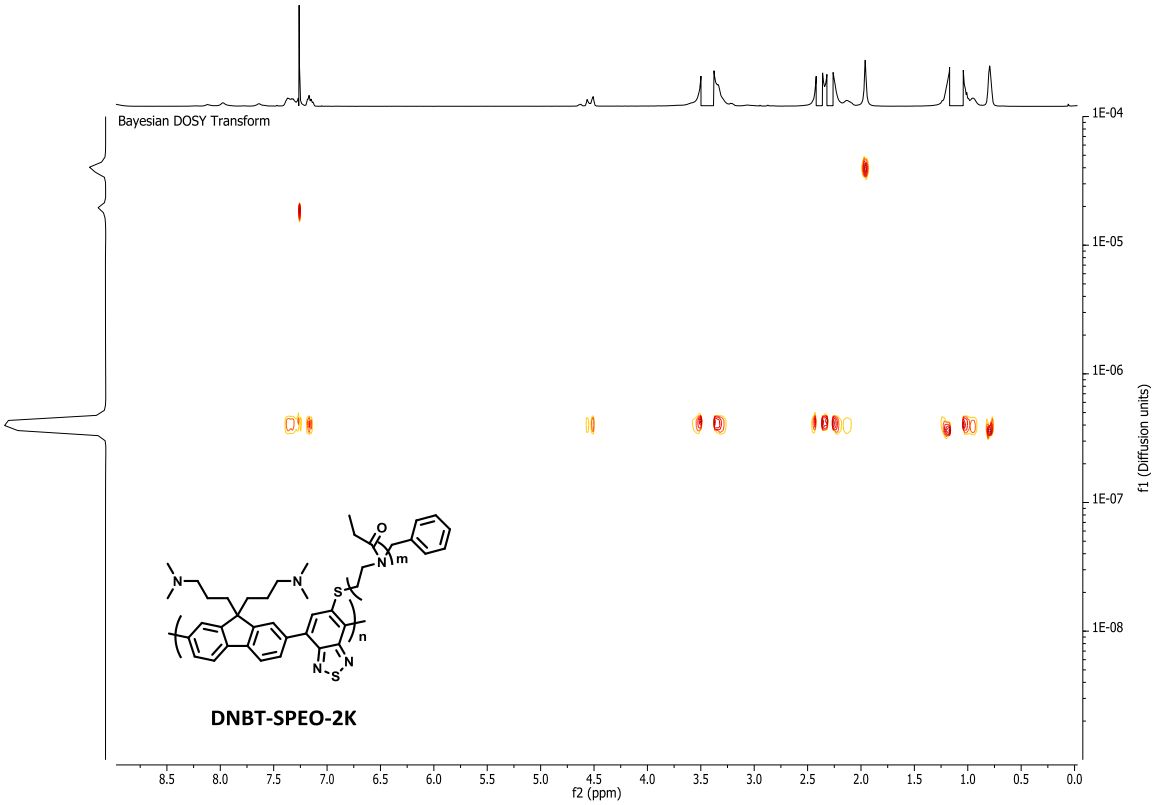
Appendix Figure 28: DOSY -NMR of **F8BT-PEO** ($CDCl_3$)



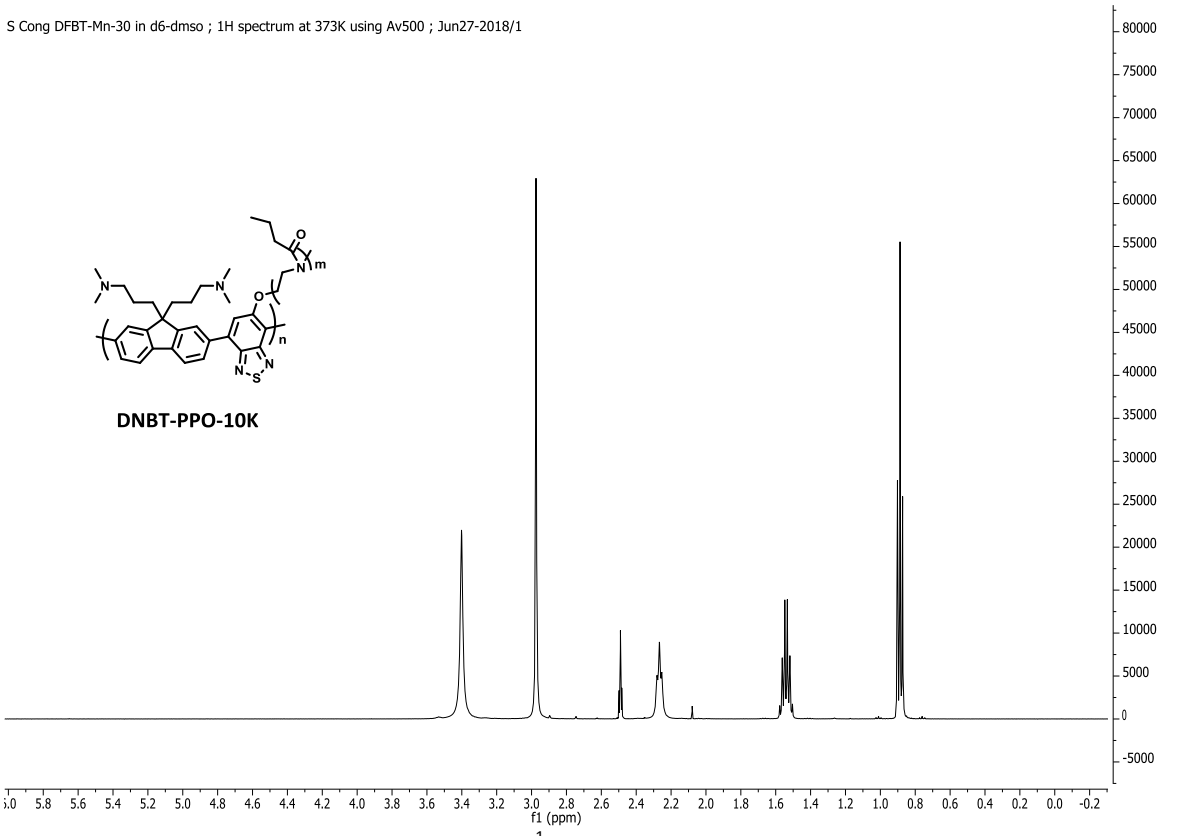
Appendix Figure 29: ^{1}H-NMR of **DNBT-SPEO** ($CDCl_3$)



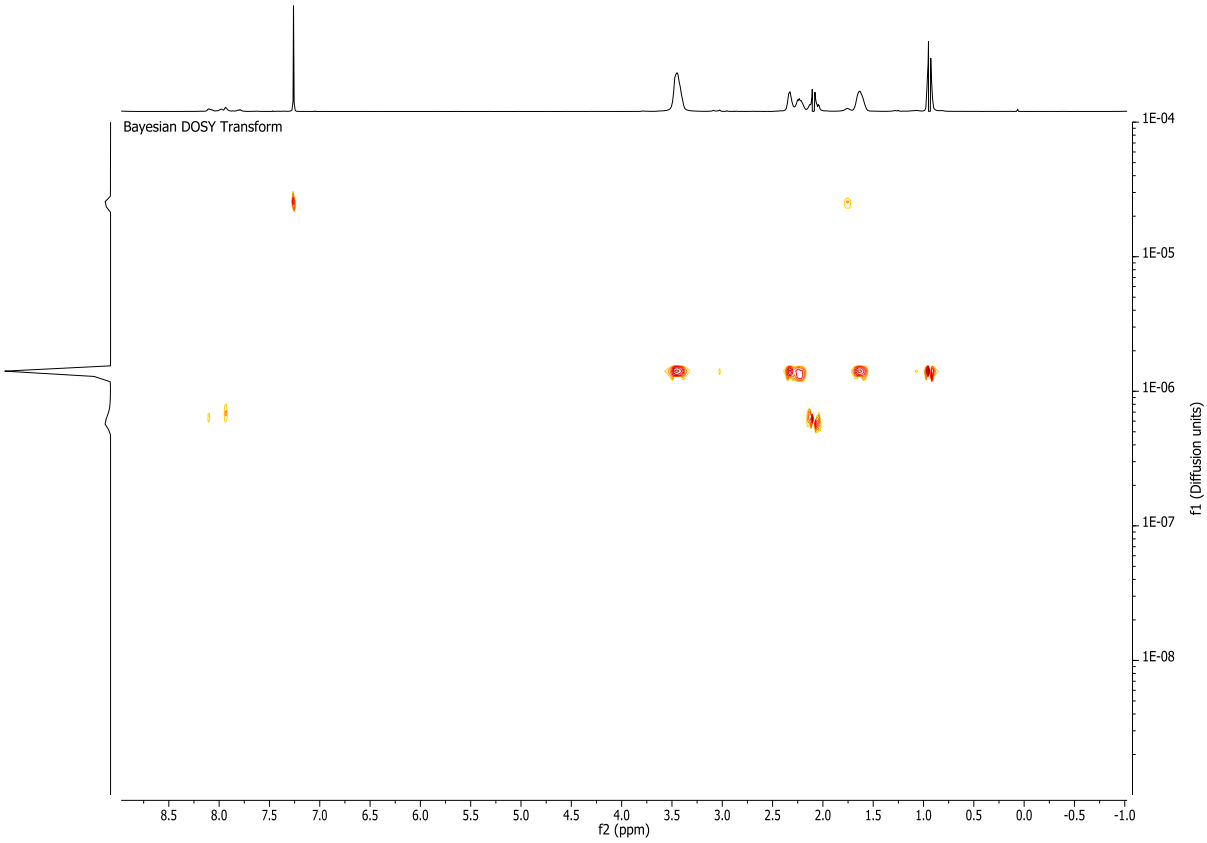
Appendix Figure 30: DOSY -NMR of **DNFBT** and **SPEO** mixture ($CDCl_3$)



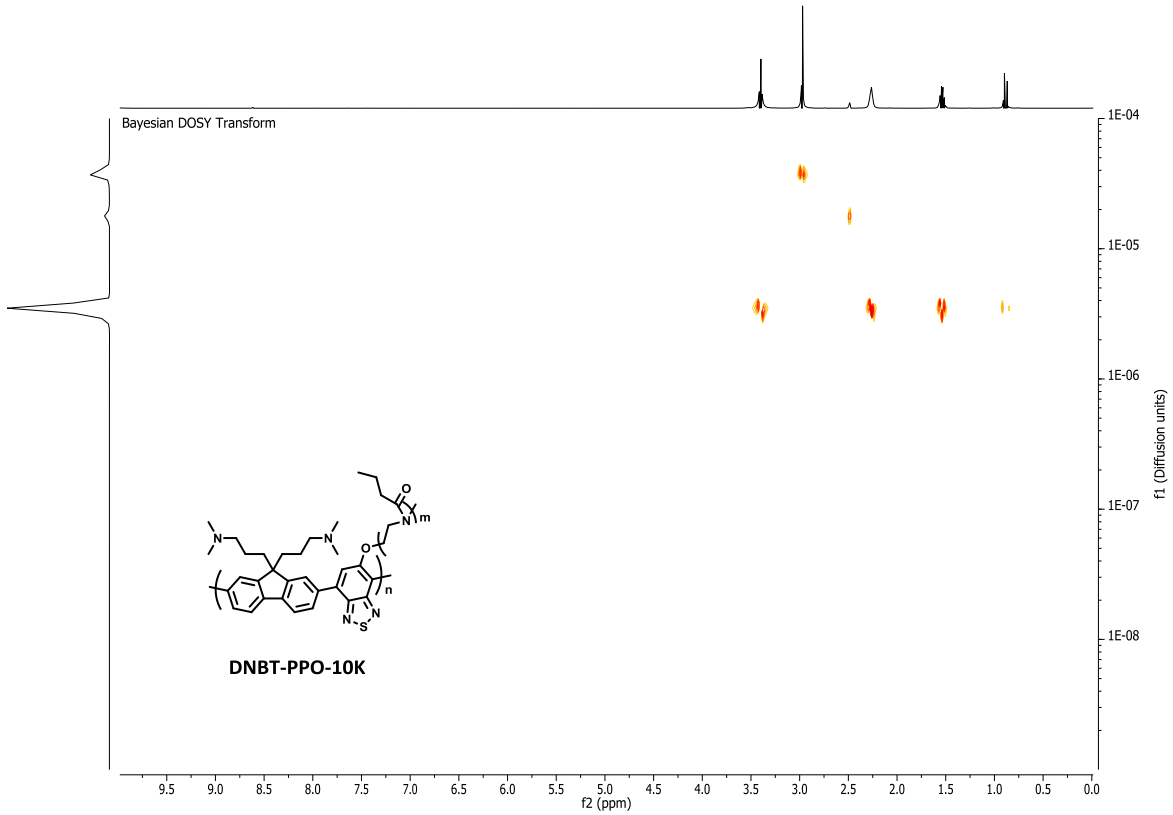
Appendix Figure 31: DOSY-NMR of **DNBT-SPEO** ($CDCl_3$)



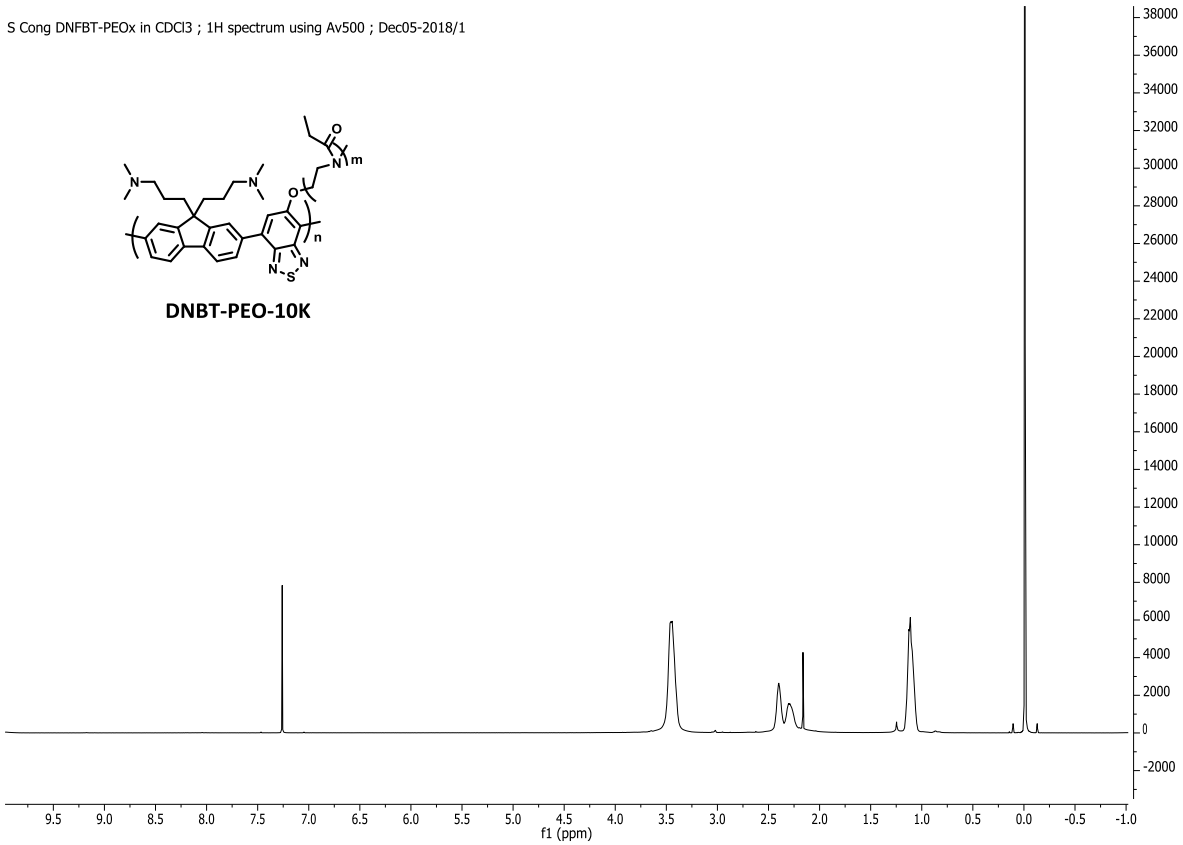
Appendix Figure 32: ^{1}H-NMR of **DNBT-PPO** (d-DMSO)



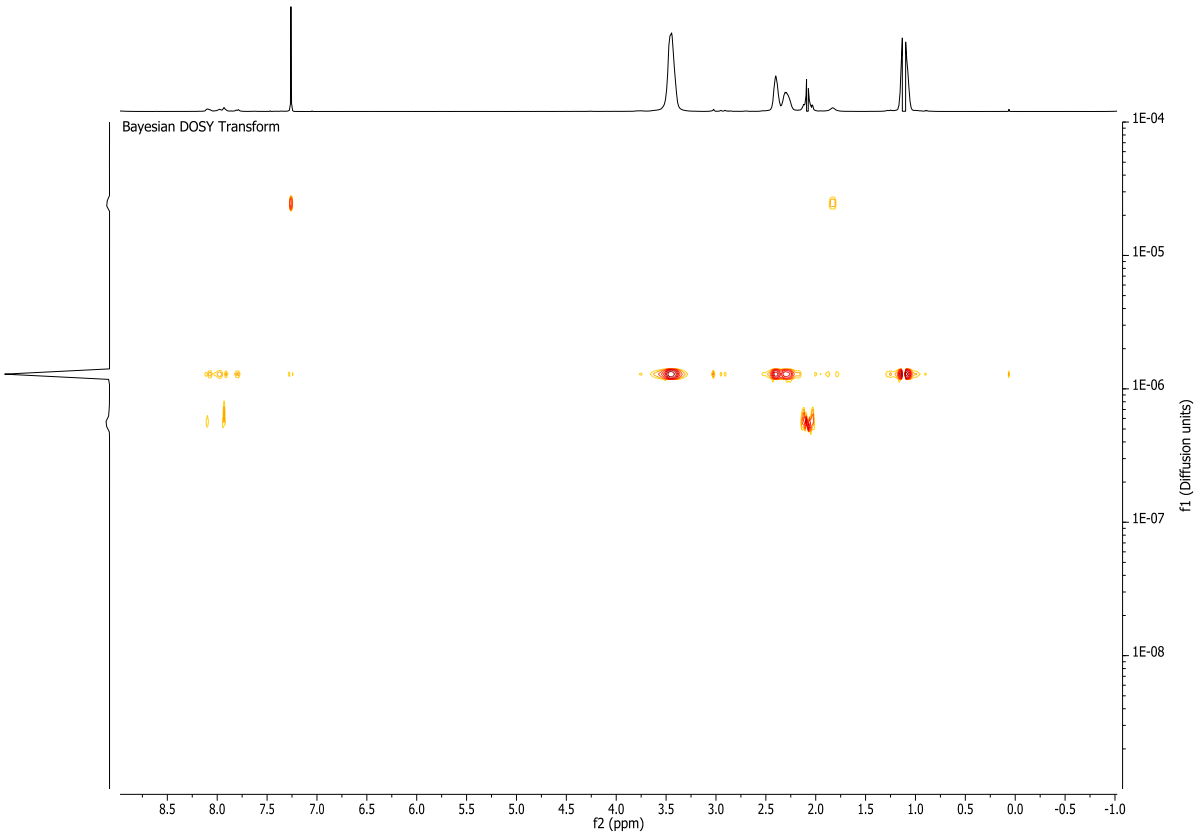
Appendix Figure 33: DOSY-NMR of **DNFBT** and **PPO** mixture ($CDCl_3$)



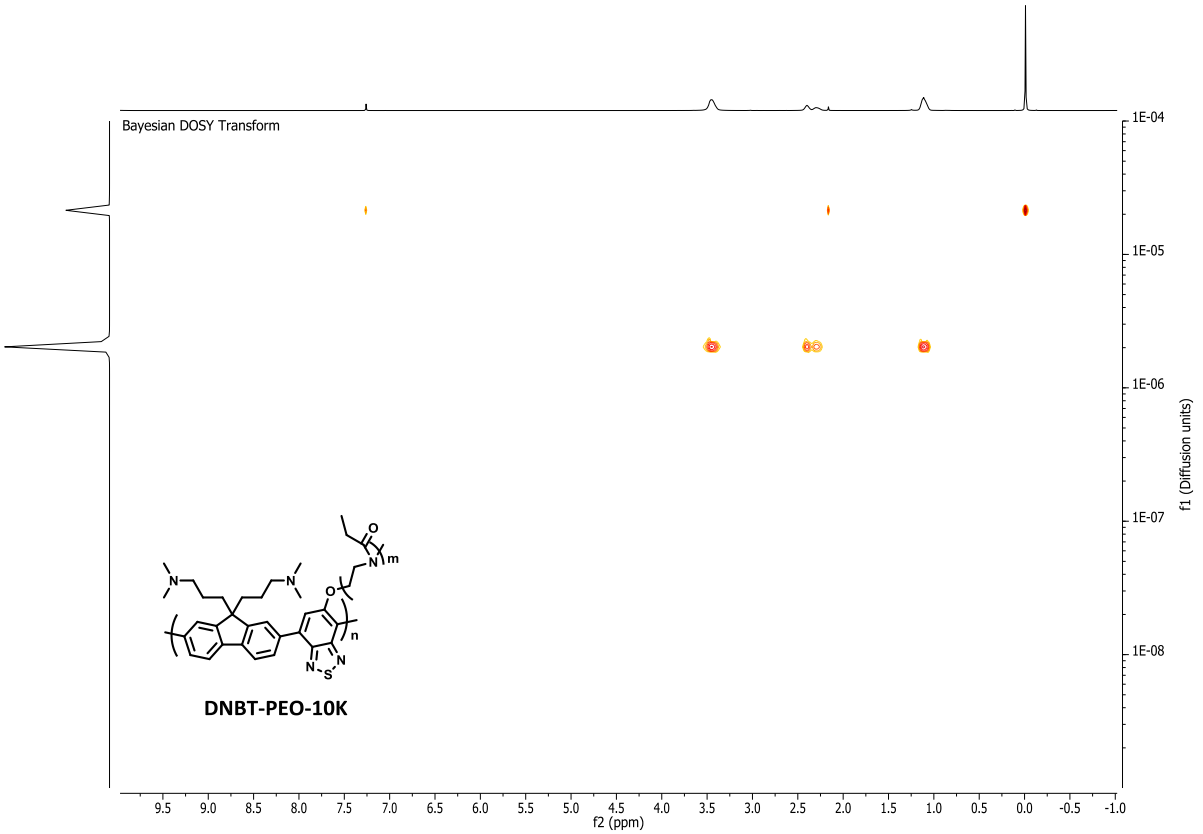
Appendix Figure 34: DOSY-NMR of **DNBT-PPO** (d-DMSO)



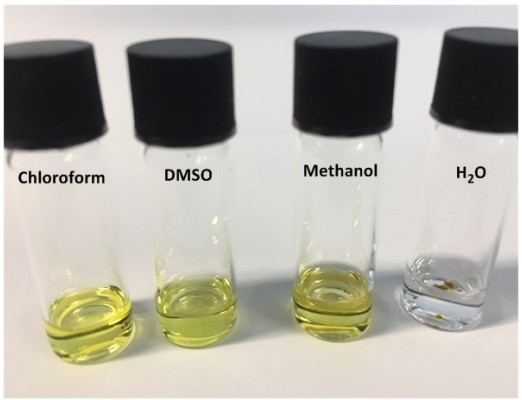
Appendix Figure 35: ^{1}H-NMR of **DNBT-PEO** ($CDCl_3$)



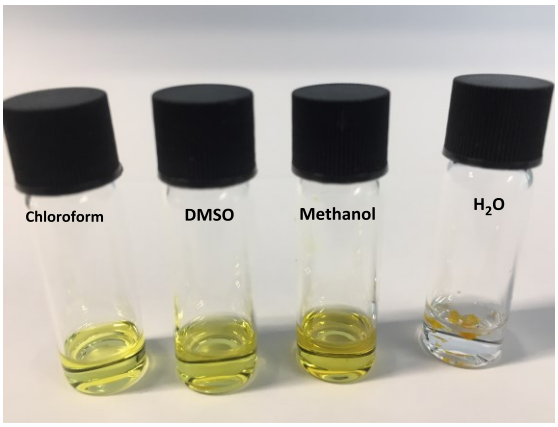
Appendix Figure 36: DOSY-NMR of **DNFBT** and **PEO** mixture ($CDCl_3$)



Appendix Figure 37: DOSY -NMR of **DNBT-PEO** ($CDCl_3$)

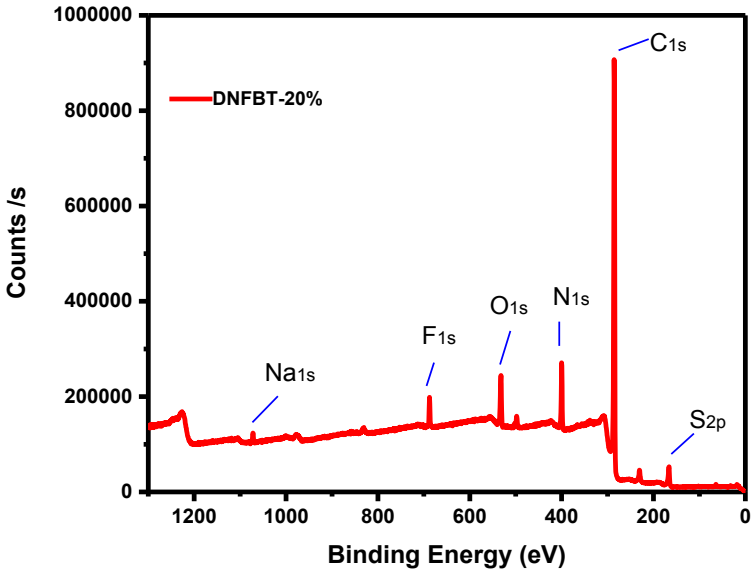


Appendix Figure 38: **F8BT-SPO** in polar solvents

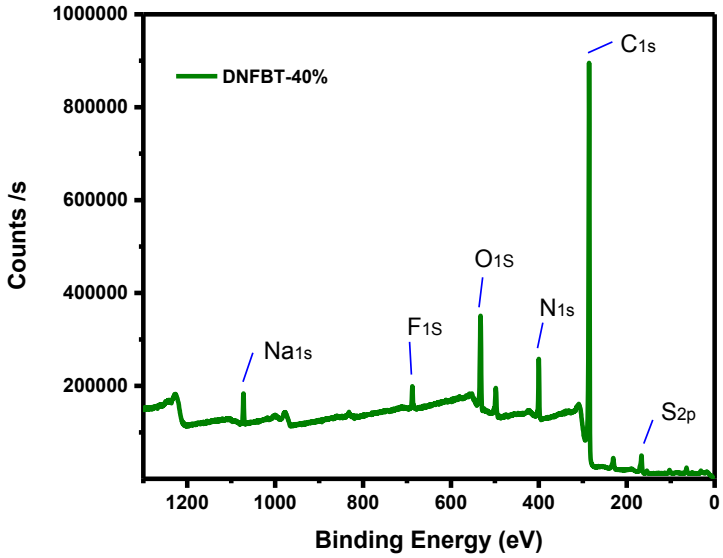


Appendix Figure 39: **DNBT-PPO** in polar solvents

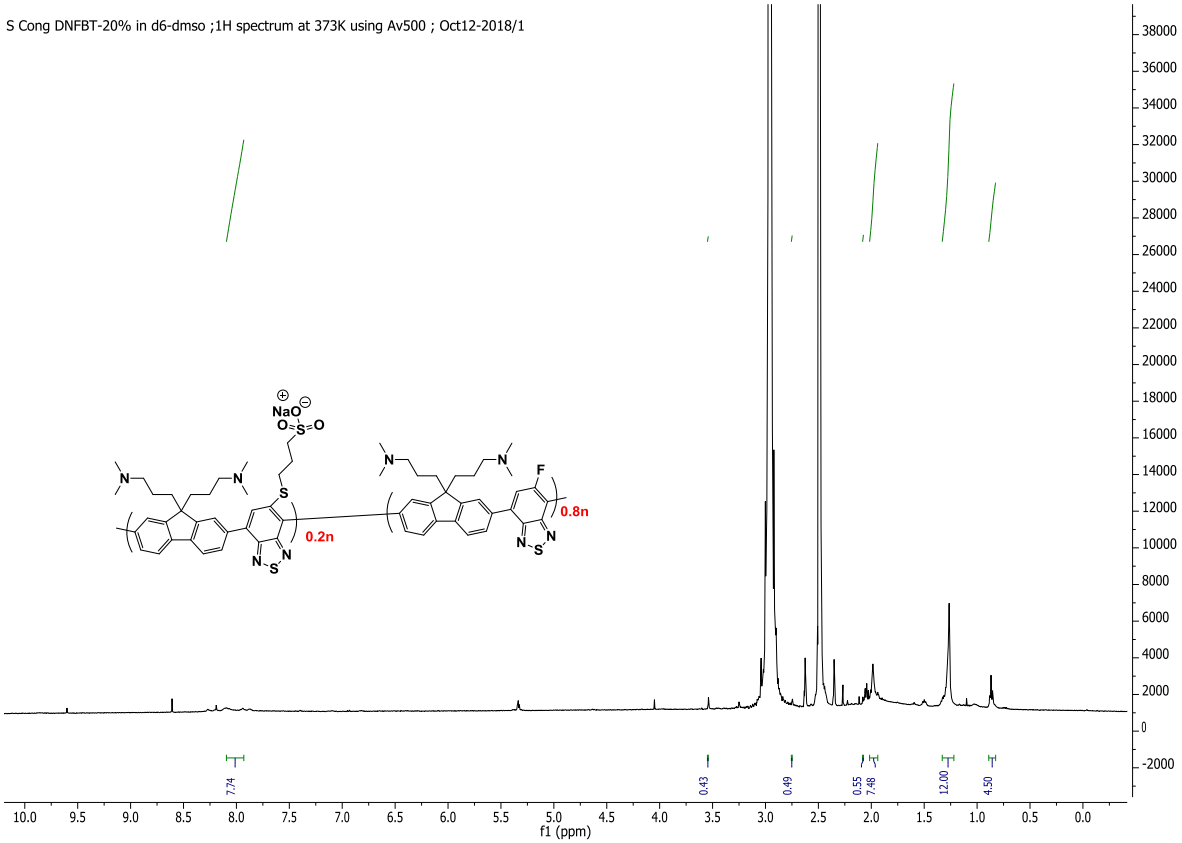
8.4 Chapter 5



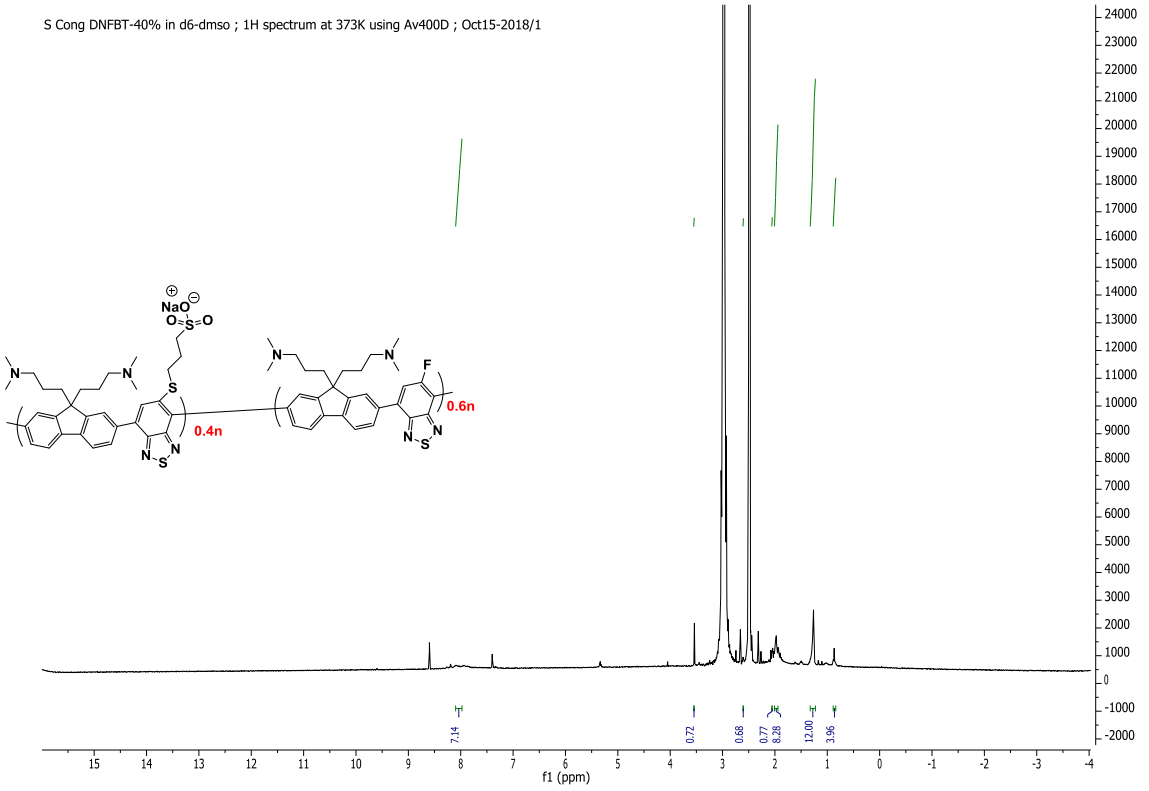
Appendix Figure 40 XPS spectra of **DNFBT-20%**



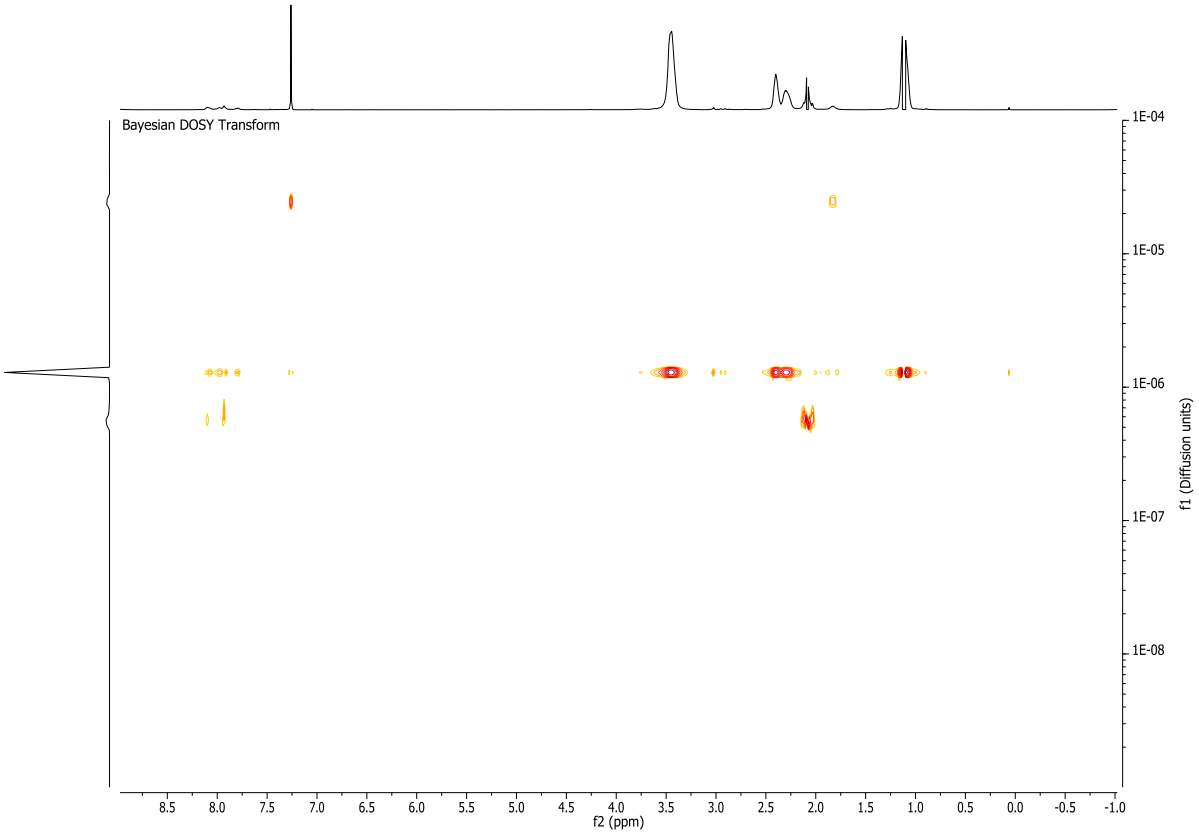
Appendix Figure 41 XPS spectra of **DNFBT-40%**



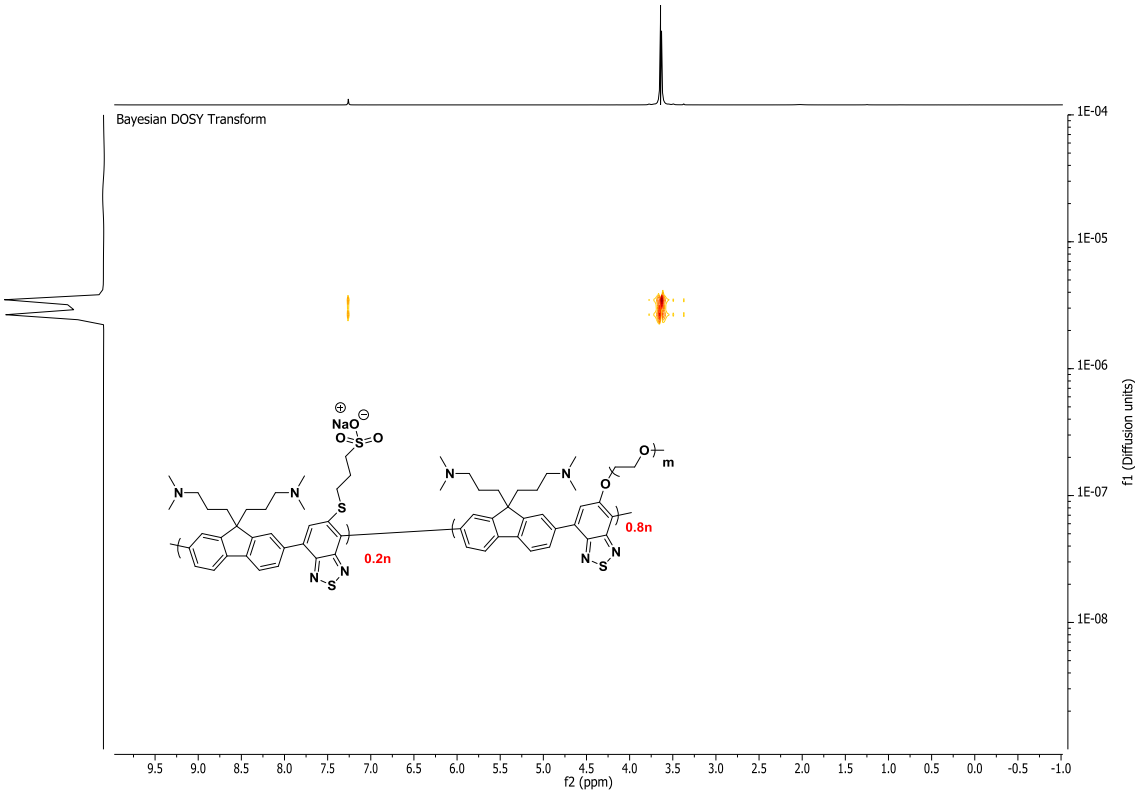
Appendix Figure 42: ^{1}H-NMR of **DNFBT-20%** (d-DMSO at 373K)



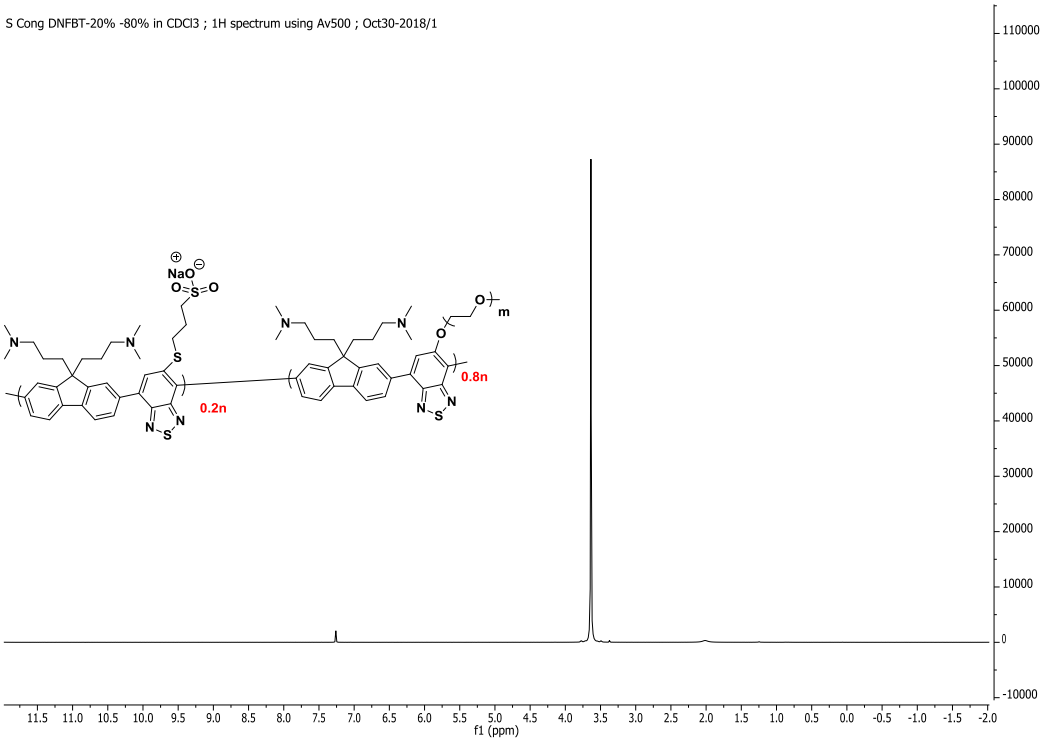
Appendix Figure 43: ^{1}H-NMR of **DNFBT-40%** (d-DMSO at 373K)



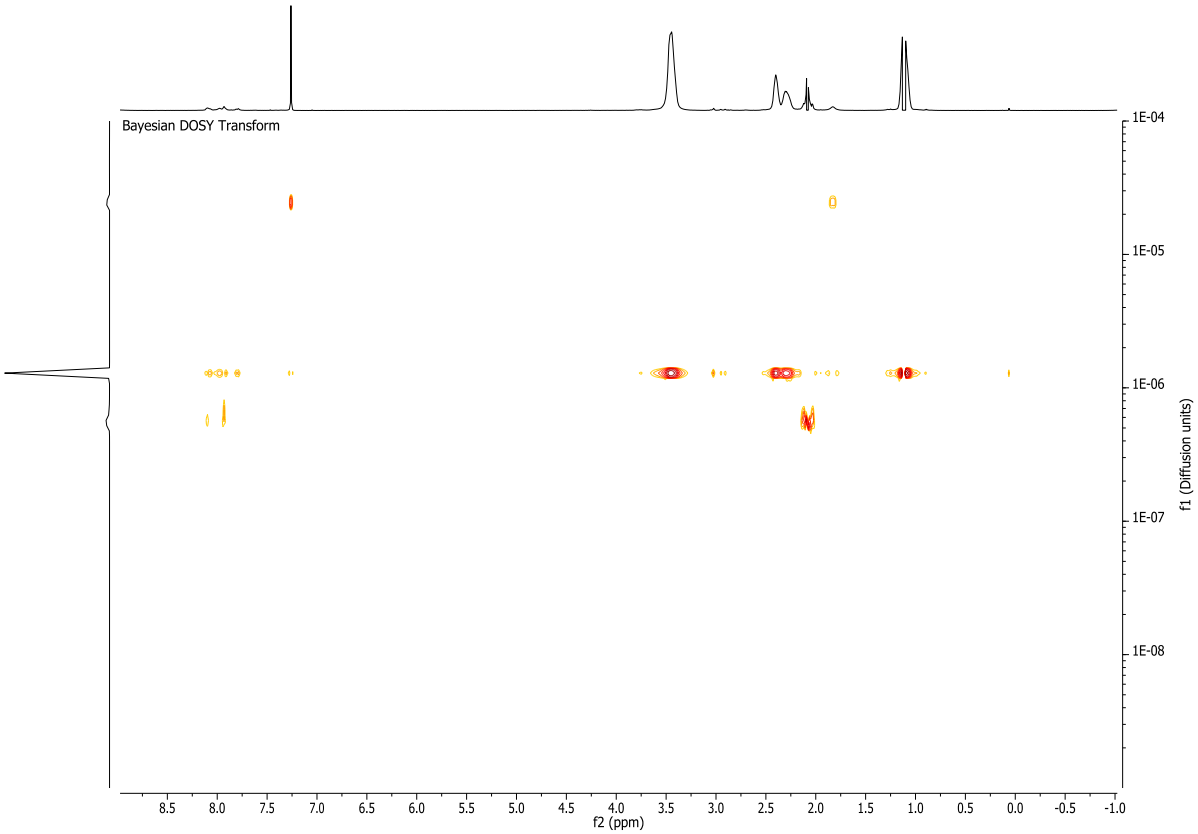
Appendix Figure 44 DOSY-NMR of **DNFBT-20%** and PEG mixture (d-DMSO)



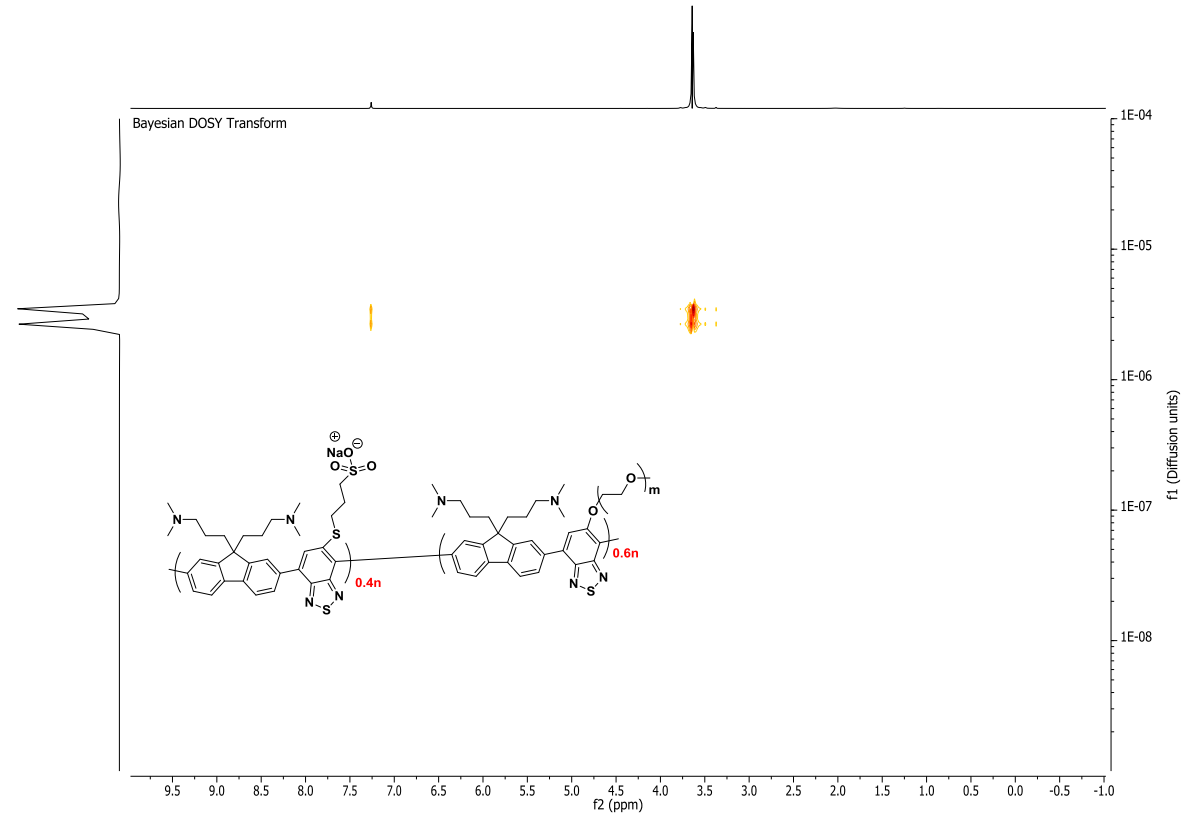
Appendix Figure 45 DOSY-NMR of **DNBT-20%-80%** ($CDCl_3$)



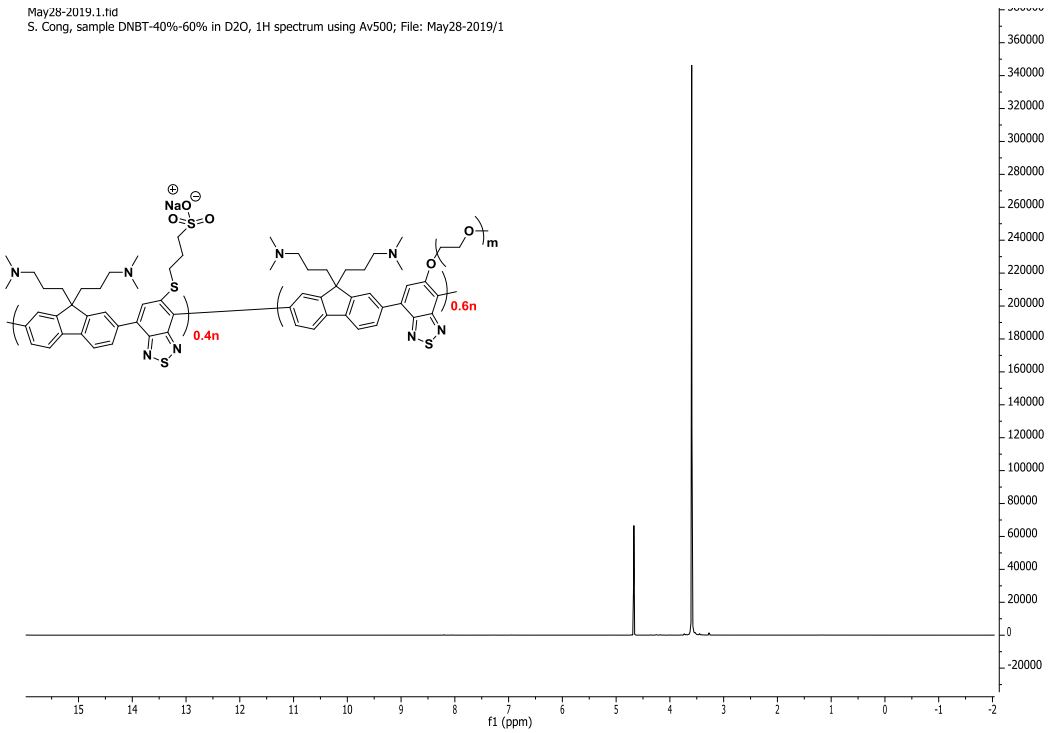
Appendix Figure 46 ^{1}H-NMR of **DNBT-20%-80%** ($CDCl_3$)



Appendix Figure 47 DOSY-NMR of **DNFBT-40%** and PEG mixture (d-DMSO)



Appendix Figure 48 DOSY-NMR of **DNBT-40%-60%** ($CDCl_3$)



Appendix Figure 49 ^{1}H-NMR of **DNBT-40%-60%** (D_2O)

9 Permissions

Permission to reproduce **Figure 6** (section **1.5**):

OHN WILEY AND SONS LICENSE TERMS AND CONDITIONS
Jun 14, 2019

This Agreement between Imperial College London -- shengyu cong ("You") and John Wiley and Sons ("John Wiley and Sons") consists of your license details and the terms and conditions provided by John Wiley and Sons and Copyright Clearance Center.

License Number
4607630133467
License date
Jun 14, 2019
Licensed Content Publisher
John Wiley and Sons
Licensed Content Publication
Journal of Polymer Science Part A: Polymer Chemistry
Licensed Content Title
Standing on the shoulders of Hermann Staudinger: Post-polymerization modification from past to present
Licensed Content Author
Kemal Arda Günay, Patrick Theato, Harm-Anton Klok
Licensed Content Date
Oct 29, 2012
Licensed Content Volume
51
Licensed Content Issue
1
Licensed Content Pages
28
Type of use
Dissertation/Thesis
Requestor type
University/Academic
Format
Print and electronic
Portion
Figure/table
Number of figures/tables
1
Original Wiley figure/table number(s)
It is from paper"Standing on the shoulders of Hermann Staudinger: Post-polymerization modification from past to present" SCHEME 1 Schematic illustration of the main classes of reactions that can be used for the preparation of functionalized polymers via post-polymerization modification.
Will you be translating?
No
Title of your thesis / dissertation
Post-Polymerization Functionalization Of Conjugated Polymer Backbones And Its Applications
Expected completion date
Jun 2019
Expected size (number of pages)
180
Requestor Location

Imperial College London
80 Wood Lane
W12 0BZ
London, london W12 0BZ
United Kingdom
Attn: Imperial College London
Publisher Tax ID
EU826007151
Total
0.00 GBP
Terms and Conditions

TERMS AND CONDITIONS

This copyrighted material is owned by or exclusively licensed to John Wiley & Sons, Inc. or one of its group companies (each a"Wiley Company") or handled on behalf of a society with which a Wiley Company has exclusive publishing rights in relation to a particular work (collectively "WILEY"). By clicking "accept" in connection with completing this licensing transaction, you agree that the following terms and conditions apply to this transaction (along with the billing and payment terms and conditions established by the Copyright Clearance Center Inc., ("CCC's Billing and Payment terms and conditions"), at the time that you opened your RightsLink account (these are available at any time at http://myaccount.copyright.com).

Terms and Conditions

- The materials you have requested permission to reproduce or reuse (the "Wiley Materials") are protected by copyright.

- You are hereby granted a personal, non-exclusive, non-sub licensable (on a stand-alone basis), non-transferable, worldwide, limited license to reproduce the Wiley Materials for the purpose specified in the licensing process. This license, **and any CONTENT (PDF or image file) purchased as part of your order,** is for a one-time use only and limited to any maximum distribution number specified in the license. The first instance of republication or reuse granted by this license must be completed within two years of the date of the grant of this license (although copies prepared before the end date may be distributed thereafter). The Wiley Materials shall not be used in any other manner or for any other purpose, beyond what is granted in the license. Permission is granted subject to an appropriate acknowledgement given to the author, title of the material/book/journal and the publisher. You shall also duplicate the copyright notice that appears in the Wiley publication in your use of the Wiley Material. Permission is also granted on the understanding that nowhere in the text is a previously published source acknowledged for all or part of this Wiley Material. Any third party content is expressly excluded from this permission.

- With respect to the Wiley Materials, all rights are reserved. Except as expressly granted by the terms of the license, no part of the Wiley Materials may be copied, modified, adapted (except for minor reformatting required by the new Publication), translated, reproduced, transferred or distributed, in any form or by any means, and no derivative works may be made based on the Wiley Materials without the prior permission of the respective copyright owner.**For STM Signatory Publishers clearing permission under the terms of the STM Permissions Guidelines only, the terms of the license are extended to include subsequent editions and for editions in other languages, provided such editions are for the work as a whole in situ and does not involve the separate exploitation of the permitted figures or extracts,**You may not alter, remove or suppress in any manner any copyright,

trademark or other notices displayed by the Wiley Materials. You may not license, rent, sell, loan, lease, pledge, offer as security, transfer or assign the Wiley Materials on a stand-alone basis, or any of the rights granted to you hereunder to any other person.

- The Wiley Materials and all of the intellectual property rights therein shall at all times remain the exclusive property of John Wiley & Sons Inc, the Wiley Companies, or their respective licensors, and your interest therein is only that of having possession of and the right to reproduce the Wiley Materials pursuant to Section 2 herein during the continuance of this Agreement. You agree that you own no right, title or interest in or to the Wiley Materials or any of the intellectual property rights therein. You shall have no rights hereunder other than the license as provided for above in Section 2. No right, license or interest to any trademark, trade name, service mark or other branding ("Marks") of WILEY or its licensors is granted hereunder, and you agree that you shall not assert any such right, license or interest with respect thereto

- NEITHER WILEY NOR ITS LICENSORS MAKES ANY WARRANTY OR REPRESENTATION OF ANY KIND TO YOU OR ANY THIRD PARTY, EXPRESS, IMPLIED OR STATUTORY, WITH RESPECT TO THE MATERIALS OR THE ACCURACY OF ANY INFORMATION CONTAINED IN THE MATERIALS, INCLUDING, WITHOUT LIMITATION, ANY IMPLIED WARRANTY OF MERCHANTABILITY, ACCURACY, SATISFACTORY QUALITY, FITNESS FOR A PARTICULAR PURPOSE, USABILITY, INTEGRATION OR NON-INFRINGEMENT AND ALL SUCH WARRANTIES ARE HEREBY EXCLUDED BY WILEY AND ITS LICENSORS AND WAIVED BY YOU.

- WILEY shall have the right to terminate this Agreement immediately upon breach of this Agreement by you.

- You shall indemnify, defend and hold harmless WILEY, its Licensors and their respective directors, officers, agents and employees, from and against any actual or threatened claims, demands, causes of action or proceedings arising from any breach of this Agreement by you.

- IN NO EVENT SHALL WILEY OR ITS LICENSORS BE LIABLE TO YOU OR ANY OTHER PARTY OR ANY OTHER PERSON OR ENTITY FOR ANY SPECIAL, CONSEQUENTIAL, INCIDENTAL, INDIRECT, EXEMPLARY OR PUNITIVE DAMAGES, HOWEVER CAUSED, ARISING OUT OF OR IN CONNECTION WITH THE DOWNLOADING, PROVISIONING, VIEWING OR USE OF THE MATERIALS REGARDLESS OF THE FORM OF ACTION, WHETHER FOR BREACH OF CONTRACT, BREACH OF WARRANTY, TORT, NEGLIGENCE, INFRINGEMENT OR OTHERWISE (INCLUDING, WITHOUT LIMITATION, DAMAGES BASED ON LOSS OF PROFITS, DATA, FILES, USE, BUSINESS OPPORTUNITY OR CLAIMS OF THIRD PARTIES), AND WHETHER OR NOT THE PARTY HAS BEEN ADVISED OF THE POSSIBILITY OF SUCH DAMAGES. THIS LIMITATION SHALL APPLY NOTWITHSTANDING ANY FAILURE OF ESSENTIAL PURPOSE OF ANY LIMITED REMEDY PROVIDED HEREIN.

- Should any provision of this Agreement be held by a court of competent jurisdiction to be illegal, invalid, or unenforceable, that provision shall be deemed amended to achieve as nearly as possible the same economic effect as the original provision, and the legality, validity and enforceability of the remaining provisions of this Agreement shall not be affected or impaired thereby.

- The failure of either party to enforce any term or condition of this Agreement shall not constitute a waiver of either party's right to enforce each and every term and condition of this Agreement. No breach under this agreement shall be deemed waived or excused by either party unless such waiver or consent is in writing signed by the party granting such waiver or consent. The waiver by or consent of a party to a breach of any provision of this Agreement shall not operate or be construed as a waiver of or consent to any other or subsequent breach by such other party.

- This Agreement may not be assigned (including by operation of law or otherwise) by you without WILEY's prior written consent.

- Any fee required for this permission shall be non-refundable after thirty (30) days from receipt by the CCC.

- These terms and conditions together with CCC's Billing and Payment terms and conditions (which are incorporated herein) form the entire agreement between you and WILEY concerning this licensing transaction and (in the absence of fraud) supersedes all prior agreements and representations of the parties, oral or written. This Agreement may not be amended except in writing signed by both parties. This Agreement shall be binding upon and inure to the benefit of the parties' successors, legal representatives, and authorized assigns.

- In the event of any conflict between your obligations established by these terms and conditions and those established by CCC's Billing and Payment terms and conditions, these terms and conditions shall prevail.

- WILEY expressly reserves all rights not specifically granted in the combination of (i) the license details provided by you and accepted in the course of this licensing transaction, (ii) these terms and conditions and (iii) CCC's Billing and Payment terms and conditions.

- This Agreement will be void if the Type of Use, Format, Circulation, or Requestor Type was misrepresented during the licensing process.

- This Agreement shall be governed by and construed in accordance with the laws of the State of New York, USA, without regards to such state's conflict of law rules. Any legal action, suit or proceeding arising out of or relating to these Terms and Conditions or the breach thereof shall be instituted in a court of competent jurisdiction in New York County in the State of New York in the United States of America and each party hereby consents and submits to the personal jurisdiction of such court, waives any objection to venue in such court and consents to service of process by registered or certified mail, return receipt requested, at the last known address of such party.

WILEY OPEN ACCESS TERMS AND CONDITIONS

Wiley Publishes Open Access Articles in fully Open Access Journals and in Subscription journals offering Online Open. Although most of the fully Open Access journals publish open access articles under the terms of the Creative Commons Attribution (CC BY) License only, the subscription journals and a few of the Open Access Journals offer a choice of Creative Commons Licenses. The license type is clearly identified on the article.

The Creative Commons Attribution License

The Creative Commons Attribution License (CC-BY) allows users to copy, distribute and transmit an article, adapt the article and make commercial use of the article. The CC-BY license permits commercial and non-

Creative Commons Attribution Non-Commercial License

The Creative Commons Attribution Non-Commercial (CC-BY-NC)License permits use, distribution and reproduction in any medium, provided the original work is properly cited and is not used for commercial purposes.(see below)

Creative Commons Attribution-Non-Commercial-NoDerivs License

The Creative Commons Attribution Non-Commercial-NoDerivs License (CC-BY-NC-ND) permits use, distribution and reproduction in any medium, provided the original work is properly cited, is not used for commercial purposes and no modifications or adaptations are made. (see below)

Use by commercial "for-profit" organizations

Use of Wiley Open Access articles for commercial, promotional, or marketing purposes requires further explicit permission from Wiley and will be subject to a fee.

Further details can be found on Wiley Online Library http://olabout.wiley.com/WileyCDA/Section/id-410895.html

Other Terms and Conditions:

v1.10 Last updated September 2015

Questions? customercare@copyright.com or +1-855-239-3415 (toll free in the US) or +1-978-646-2777.